UNIVERSITÄT DUISBURG ESSEN

RGD-Receptor with Enhanced Water Solubility

Dissertation

zur Erlangung des akademischen Grades eines Doktors der Naturwissenschaften
– Dr. rer. nat. –

vorgelegt von Diplom-Chemiker

Johannes Hofmann

geboren in Fulda

Institut für Organische Chemie der Universität Duisburg-Essen

Essen 2017

RGD-Receptor with Enhanced Water Solubility

Gutachter:	Prof. Dr. Carsten Schmuck Prof. Dr. Thomas Schrader
Prüfungsvorsitzender:	Prof. Dr. Christian Mayer
Tag der Disputation:	12. Oktober 2017

Die vorliegende Arbeit wurde von August 2009 bis November 2015 an der Universität Duisburg-Essen im Institut für Organische Chemie unter der Anleitung von Herrn Prof. Dr. Carsten Schmuck angefertigt.

Ich erkläre hiermit an Eides statt, dass ich die vorliegende Arbeit selbständig verfasst und mich dabei keiner anderen als der von mir bezeichneten Quellen und Hilfen bedient habe. Die aus fremden Quellen direkt oder indirekt übernommenen Gedanken wurden als solche kenntlich gemacht.

Weiterhin erkläre ich hiermit, dass ich weder an einer anderen Stelle ein Prüfungsverfahren beantragt noch die Dissertation in dieser oder einer anderen Form bereits als Prüfungsarbeit verwendet. Auch wurde diese Dissertation an keiner anderen Fakultät vorgelegt.

Essen, im Juli 2017 .....

Johannes Hofmann

DANKSAGUNG

An erster Stelle möchte ich mich bei meiner Familie bedanken, welche mir den größten Halt und die meiste Unterstützung gegeben hat. Insbesondere in der Bereitschaft meinen Wunsch des Studiums der Chemie zu ermöglichen.

Einen ganz besonderen Dank möchte ich natürlich meinem Doktorvater Prof. Dr. Carsten Schmuck aussprechen, der mir die Gelegenheit gegeben hat mich auf dem Gebiet der Supramolekularen Chemie zu verwirklichen. Ich danke ihm für die Unterstützung bei meinen Aktivitäten im Bereich des Jungchemikerforums der Universität Duisburg-Essen. Vor allem aber auch für die Möglichkeit in seinem Arbeitskreis aktiv mitzuwirken.

Mein weiterer Dank gilt unserem Kooperationspartner dieser Arbeit Prof. Dr. Thomas Schrader sowie Dr. Thomas Gersthagen, die mit vielen neue Ideen und Entwicklungen zu dieser Arbeit beigetragen haben. Bei Prof. Dr. Thomas Schrader bedanke ich mich auch für die Übernahme des zweiten Gutachtens.

Allen meinen Arbeitskollegen möchte ich für ihre Unterstützung und die schönen und abwechslungsreichen Jahre im Arbeitskreis danken. Besonders bedanke ich mich bei Dr. Gerd Gröger, Dr. Barbara Geibel und Dr. Michael Merschky für die besonders nette Aufnahme in den Arbeitskreis. Zusätzlich waren sie mir eine große Hilfe mich mit den analytischen Geräten wie beispielsweise der HPLC vertraut zu machen. Für die große Unterstützung der teilweise doch recht zeitaufwendigen Berechnungen von Molekül-Geometrien bedanke ich mich besonders bei Herrn Wilhelm Sicking. Auch möchte ich mich bei Dr. Julian Oeljeklaus bedanken, der mich während seiner Promotion im Arbeitskreis von Prof. Dr. Markus Kaiser tatkräftig mit HPLC-MS Messungen unterstützt hat.

Ohne die Mithilfe vieler einzelner Personen aus dem eigenen wie auch aus anderen Arbeitskreisen und wissenschaftlichen Abteilungen hätte diese Arbeit nicht fertiggestellt werden können. Daher möchte ich mich bei allen Angestellten in den analytischen Abteilungen, Kollegen aus anderen Arbeitskreisen wie auch der Verwaltung und allen, die mich irgendwann in irgendeiner Form unterstützt haben, bedanken. Jeden einzelnen namentlich zu erwähnen würde wohl den Rahmen der Danksagung sprengen.

CONTENT

1 INTRODUCTION

Finding new efficient therapeutics is the major goal in pharmaceutical chemistry. A lot of efforts are made in understanding how pharmaceuticals interfere in etiopathologies. For example a disease like malignant tumor growth is based on a plurality of single supramolecular processes. Most likely these mechanisms of interaction occur in a reversible equilibrium. Therefore they are dependent on many weak particular intermolecular interactions to form rather stable host-guest systems. Interfering with those supramolecular interactions would permit to treat diseases at their origin instead of curing their symptoms.

Such key could be lying in the interaction of integrins, a family of cell surface receptors. The cornerstone in cancer research was set by *Folkman* et al. in the 1970´s. Based on experiments of *Greene* et al.[1] and *Algire* et al.[2], he assumed that further tumor growth beyond a particular size of 2 mm in diameter necessitates a trigger of formation of new blood vessels. In animal experiments he adduced the evidence of this kind of trigger. He investigated a diffusible substance mediated by tumors. The isolated supernatant fluid caused neovascularization on specially prepared tissue. In a postulate *Folkman* assumed that neovascularization is a consequence of this fluid containing a tumor-angiogenesis-factor (TAF).[3]

Nearly one decade later the hypothesis of *Folkman* received an increased interest among scientific research and number of publications raised exponentially. From there on several angiogenesis factors have been identified and it turned out that *Folkman's* TAF comprised different growth factors,[4] which were identified as receptors of the endothelium tissue. The evidence of upregulation of these cell surface receptors triggered by oncogenes was adduced by *Rak* et al.[5] One important receptor-family promoting cell signaling and adhesion events are the integrins.[6]

Since 1984 it was approved by *Ruoslathi* et al. that contributing glycoproteins like laminin, van Willebrand factor (vWF), osteopontin, vitronectin and fibrinogen have a

particular peptide sequence in common. This specific sequence is eponymous for the sub-family of RGD-integrins (arginine-glycine-aspartic acid).[7,8]

From the origin of *Folkman's* idea of an anti-angiogenesis switch to keep a tumor in a non-vascularized and dormant state[9,10] it took more than three decades to find a suitable and active agent for therapy purposes. Bevacizumab, a monoclonal antibody distributed by *Roche* under the name Avastin® was investigated. The drug is able to inhibit neovascularization by interfering with the vascularization endothelial growth factor (VEGF-A formerly known as VEGF).[11,12]

Realization of an anti-angiogenesis effect based on molecular recognition and inhibition of signaling processes would be a major goal in cancer therapy. Recognition with regard to biological systems is one of the three fundamental functional features of supramolecular species.[13]

A selective intermolecular recognition is based on several interactions including electrostatic, ion-dipole, dipole-dipole interactions and van-der Waals forces. Considered that the RGD-recognition unit combines different intermolecular interaction possibilities it is a suited target for inhibition. The charged residues of RGD-peptides provide electrostatic interactions as well as hydrogen bonding. The rational design of a well-balanced inhibitor with complementary binding sites should help understanding pathological processes on a molecular level. One big advantage of tailor-made active agents would be fewer side effects to organisms. Such benefits are the goal for each therapy. Supramolecular chemistry could help to understand biological active principles. Therefore it is indispensable to understand biological active principles. But before new selective antiangiogenic therapies could be established a better understanding of contribution of single supramolecular interactions need to be generated.

A possible approach is the synthesis of model systems that work in an analogous way but were reduced to the binding sites. These binding sites are most likely relevant for the recognition process. Smaller model-systems can be synthesized more easily than the originally involved particles. Even studies on binding properties can be carried out. Within this work the synthesis of a water-soluble RGD-receptor should be realized. The structure of the receptor should be influenced by the dipolar structure of RGD-peptides. Some previous reported artificial RGD-receptors would provide a poor bioavailability due to an insufficient water-solubility. The purpose of such artificial RGD-receptors is there potential application in biological systems.

2 BACKGROUND

2.1 Focus of this Work

The most important part of this work is the development and evaluation of a water-soluble RGD-receptor. In terms of simplification of a host-guest-system the guest RGD-peptides should be as small as possible. In the model system the receptor should have the function of a ditopic binding motif. In the following chapters some background information about the RGD-integrins, their relevance in biological systems and malfunctions are given.

2.2 Cell Adhesion and Signaling

During the evolution from protozoa (unicellular organisms) to complex metazoa (multicellular organisms) specialized cells for well-defined tasks became a necessity. The organization and survival of higher life organisms is crucially dependent on well-organized organs and individual cells like immune system cells. Therefrom cells cannot arrange themselves randomly. The correct position of a specified cell in order to fulfill its tasks correctly is essential.

A well-structured recognition and signaling system becomes very important in another context too. Threats from bacteria or viruses need to be recognized and combatted by the immune system of an organism. Repelling such threats is only possible, if immune cells can recognize bacteria and viruses specifically. "Communication" of immune cells among each other enables to transfer information about invaders to support a long-term protection, which is mainly accomplished by the adaptive part of the immune system, the effector T cells.[14,15]

Therefore a suitable immune response is dependent on cell adhesion and cell signaling processes. All these phenomena of cellular migration and recognition with their different purposes of wound healing, morphogenic movements and metastasis are crucially dependent on the ability of cell adherence to extracellular matrix (ECM) and mutual recognition. This task is mostly adopted by glycoproteins which act as cell adhesion molecules (CAM). These processes take benefit from high affinity and binding constants towards molecules of the extracellular matrix which also show a remarkable selectivity between different receptors.

Some representatives of these CAMs primarily mediate adherence like cadherins which are calcium dependent glycoproteins.[16] The superfamily of immunoglobulins incorporates a whole set of structures which are involved in simple cell-cell recognition processes including the neural cell adhesion molecule (N-CAM), myelin-associated glycoproteins (MAG). Even immunoglobulin-related molecules are assigned to this family because classification is based on similarities of their peptide sequences.[17]

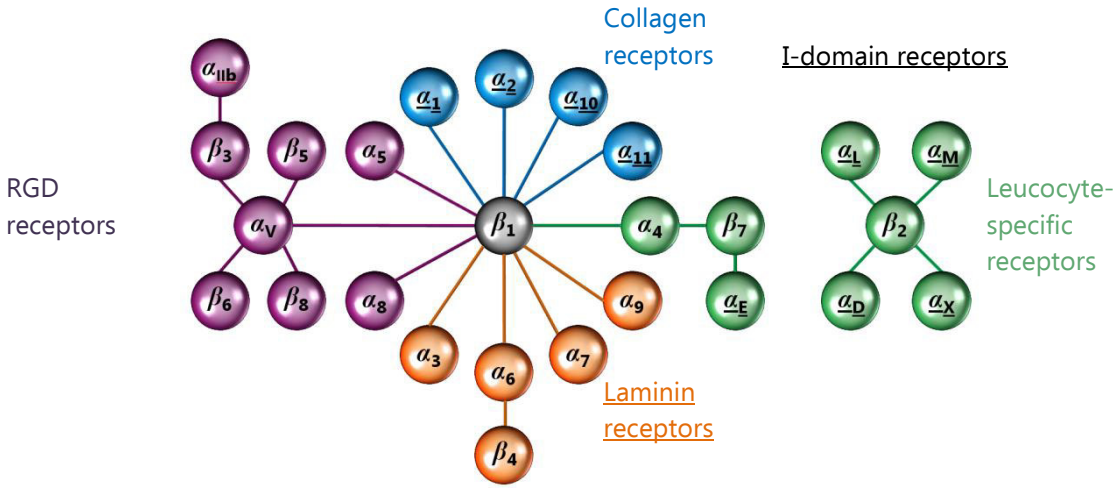

Figure 2-1. Overview of different integrins-subfamilies: A single integrin is represented by a connection line between two subunits. The largest subfamily of RGD-receptors consists of 8 (purple) members (modified graphic in style of *Patterson* and *Sheldrake*[19]).

Among other glycoproteins the integrins represent a class of cell surface receptors mediating adherence as well as signaling. The term integrin was proposed in 1986 by *Tamkun* and *Hynes* to indicate the characteristic of this protein group building a complex with the membrane.[18] Between various other cell surface receptors the integrins represent a superfamily providing communication of cell´s interior with its environment and vice versa.

The family of integrins consists of 24 different transmembrane receptors which are combinations of heterodimeric pairs out of 18 α- and 8 β-subunits (fig. 2-1). The subunits are combined in a non-covalent complex. Based on evolutionary

relationships or restricted expression on specific cells the integrins can be divided into several subfamilies. Some of the α-subunits carry I-domains which allow another subgrouping into the I-domain receptors. For instance leucocyte specific receptors (green) are limited to be expressed on white blood cells.[20] Beside the collagen receptors (blue) and laminin receptors (brown), which are more localized, the RGD-receptors (purple) are exceptional due to their ubiquitous occurrence. They can recognize various ligands from extracellular matrix containing the tripeptide RGD for adhesion phenomena or signal purpose.[21,22] Therefore they appear on many different cell types like cells of the immune system and platelets. Many physiological processes are dependent on proteins with embedded RGD-sequence as recognition criterion which raise the RGD-integrins to a key position.[6]

For this reason the RGD-sequence is an interesting target in terms of investigations on different interfering possibilities. Studies on binding affinities are possible through the use of antagonistic designed receptors. This might be helpful to get a general understanding in these recognition processes.

2.3 Structure and Function of the RGD-Integrins

Generally the structure of an integrin can be divided into three main domains. The ecto-, the transmembrane and the cytoplasmic domain contain different amounts of amino acids respectively (fig. 2-2). The classification is made corresponding to their position whereas a fine fragmentation leads to smaller fragments. These are also called domains and mainly appear in the extracellular region with long peptide chains of around 1100 amino acids. Their names originate from their typical shape or some characteristic feature. For example a certain amount and orientation of β–sheets lead to a particular appearance like propeller shaped unit. Even the embedding of metal ions for functional purpose is eponymous for such domains. The functions of different domains serve primarily the stability of formed complexes. For instance I-domains enclose divalent metal ions which themselves are important to complex acidic side chains of peptides.[23]

A common characteristic of integrins is their heterodimeric composition. The α- and β-subunit are non-covalently associated which makes them flexible and shiftable against each other. Due to the distinct arrangements of subunits' domains like propellers and β-domains integrins can occur in three conformational states, one bent, one extended closed and one extended open conformation. Only the last mentioned conformation is accessible to ligands and called the "ON-state". It needs some trigger to convert the non-active conformations into the ligand accessible

conformation. These three major conformations were suggested by evaluation of a huge quantity of data from EM, SAXS, chrystallographic studies and affinity experiments.[21]

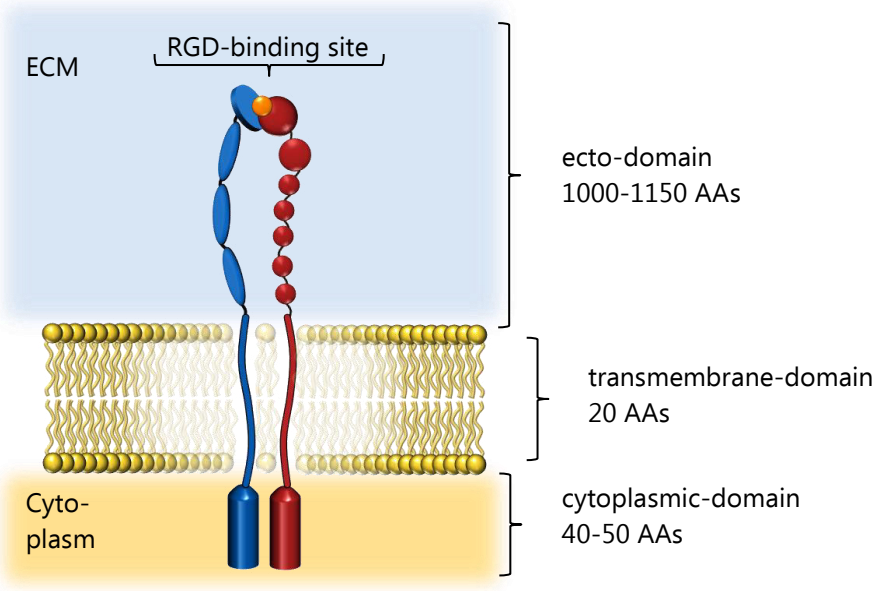

Figure 2-2. Scheme of a heterodimeric transmembrane receptor shows a α_V-subunit (blue) and β_3-subunit (red). Extracellular domains like thigh, calf-1, calf-2 and β-propeller are indicated with red balls (β-subunit) and blue ellipsoids and cylinder (α_V-subunit). The ligand binding site (orange) is located at the interface of both subunits extending in the ECM (modified figure in style of *Sun* and *Springer*).[21,24]

The most interesting part in terms of this work is the binding site for extrinsic ligands like RGD-peptides. It is located in the head region of the integrin (orange ball in fig. 2-2) pointing towards the extracellular matrix (ECM). Integrin $\alpha_V\beta_3$ incorporates the binding site at the interface of the β-propeller of the β-subunit and an I-like-domain at the α-subunit.[25]

The electrostatic potential of $\alpha_V\beta_3$ integrin baring a highly negative charge in the binding pocket of the RGD-sequence is shown in figure 2-3. This high negative charge is needed to attract the guanidinium residue of the arginine. The distances among the central guanidinium carbon atom and the surrounding oxygen atoms of the peptide's residues range between 3.5 to 5.4 Å. This environment provides a suitable binding site with respect to the strength of ion-ion interactions. A characteristic of βI-domains is their incorporated metal-ion-dependent adhesive site (MIDAS) which plays an important role in the attraction of the aspartate residue of the RGD-sequence.[22]

In this case the metal ion is Mn^{2+} which originates from an excess of manganese during preparation process.[26] In the body the divalent cation of βI-domains plays a crucial role in integrin activation. If Ca^{2+} is embedded inside the βI-domain, the

integrin remains in an inactive state. In contrast the ligand binding affinity increases dramatically by an exchange of Ca^{2+} with Mg^{2+}.[28] This exchange triggers the change from the extended closed to the extended open conformation. As well inside-out signaling processes can activate integrins like talin, a major cytoskeletal protein, is doing, if it is overexpressed.[29] In sum there are two strong binding sites to host a RGD-peptide. This facilitates the integrins to a powerful tool for signaling and adhesion processes. An artificial receptor should be designed in a similar way containing two binding sites.

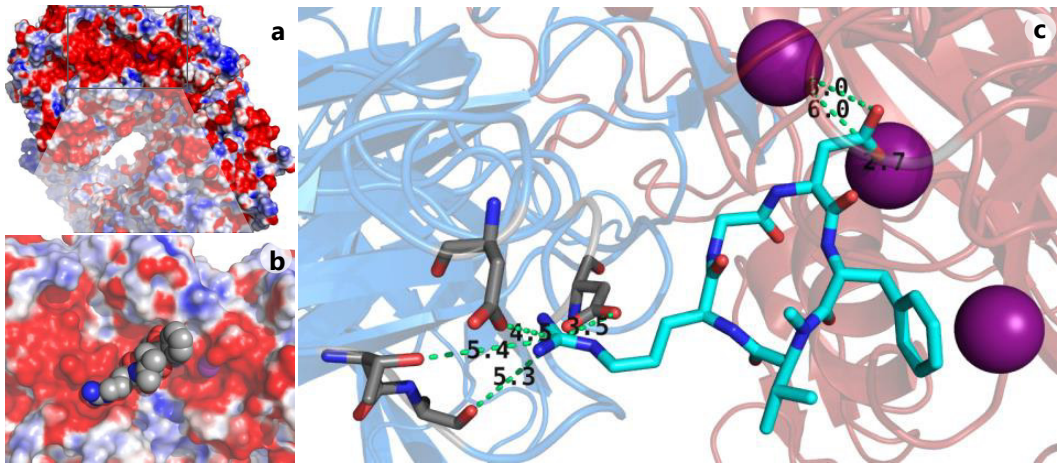

Figure 2-3. Top view of the extracellular part of integrin $\alpha_V\beta_3$ (a) in complex with the antagonist cyclo(-RGDf-N{Me}V-), a cyclic penta-peptide (b). The peptide is bound at the interface of propeller- and βA domain interface. The arginine residue is surrounded by carboxylic residues of the α-subunit (blue) in contrast to the aspartate residue which is mostly complexed by Mn^{2+} (violet spheres) embedded in the β_3-subunit (red). The exchange of Ca^{2+} and Mg^{2+} by Mn^{2+} refers to a buffer solution containing 5 mM $MnCl_2$. The ligand cyclo(RGDf-N(Me)V-) is shown light blue stick model. The glycine residue is positioned at the interface between α- and β-subunits (c). Due to clearness hydrogens are hidden in the scheme. Pictures are derived from the crystal structure (pdb 1L5G).[26,27]

Within the group of RGD-receptors the common binding motif is the tripeptide sequence arginine-glycine-aspartic acid (RGD). The receptors can recognize an overlapping range but distinct set of extracellular ligands. For instance the human integrins $\alpha_V\beta_3$ and $\alpha_{IIb}\beta_3$ attract similar ligands such as fibrinogen, vitronectin, fibronectin, thrombospondin, vWF and others. All of these ligands present the RGD-sequence at a solvent exposed loop. Due to different three dimensional orientation of the RDG sequence presented the ligands can be discriminated by individual integrins specifically. Among the RGD-integrins the functions are diverse. The major platelet receptor is the $\alpha_{IIb}\beta_3$ integrin which is mostly found on mobile platelets. Although the receptor recognizes fibrinogen it is also accessible for ligands like von

Willebrand factor and fibronectin. So the hemostasis needs the activation of $\alpha_{IIb}\beta_3$ integrin to initiate coagulation of blood cells.[30]

The complexity and functional diversity allows the integrins playing a pivotal role in nearly all biological contexts stretching from tissue morphogenesis, regulation of cell growth, wound healing to inflammatory processes. But malfunction in signaling and adhesion processes due to overexpression of integrins or activation triggers can lead to a dysregulation of their functions with severe consequences. Predominantly $\alpha_V\beta_3$, $\alpha_V\beta_5$, $\alpha_V\beta_6$, $\alpha_V\beta_8$, $\alpha_V\beta_1$, and $\alpha_{IIb}\beta_3$, are involved in pathogenesis of a multiplicity of diseases states. In particular malfunction of the platelet receptor $\alpha_{IIb}\beta_3$ cause arterial thrombosis.[31] Others like $\alpha_V\beta_3$ and $\alpha_V\beta_5$ are involved in cancer diseases by contributing in tumor progression and angiogenesis.[32,33] Angiogenic processes induced by basic fibroblast growth factor (bFGF) or tumor necrosis factor α (TNF-α) necessitate integrin $\alpha_V\beta_3$. Any wrong stimulation by vascular endothelial growth factor (VEGF) or transforming growth factor α (TGF-α) is dependent on the function of integrin $\alpha_V\beta_5$.[34] These basic requirements raise the two integrins $\alpha_V\beta_3$ and $\alpha_V\beta_5$, responsible for angiogenic tumor progression, to suitable targets for anticancer therapeutics.[35,36]

2.4 Antagonists of RGD-Integrins and Potential RGD-Receptors

Several glycoproteins that carry the RGD-sequence act as antagonists and regulate integrin-mediated processes like thrombospondin, vitronectin, fibronectin, vWF or fibrinogen. If the growth of tissue starts to get malignant, inhibition of integrins can help to stop signaling processes that cause angiogenesis, promoting tumors, inducing metastasis or obstructing apoptosis of melanoma cells. By blocking either RGD-containing glycoproteins or integrins respectively a purposeful obstruction of signaling or adhesion processes can be performed.[24]

Research for disintegrins that make use of the RGD-sequence as it is a ubiquitous binding motif lead to different approaches. One is the use of monoclonal antibodies as it was mentioned in the introduction. A major problem of this approach is the "overcoming resistance to antiangiogenic therapies" as the title of an article published in 2012 is announcing.[37] Herein the authors denote that treatment of tumors with bevacizumab directed against the growth factor VEGF-A has an unwanted side effect. The authors claim that the dramatic loss of efficacy of the VEGF-A-pathway is caused by alternative angiogenic pathways. The inhibition of neovascularization leads to an increase of tumor invasiveness and metastasis. As a

major response tumors start to spread stem cells to overcome the problem of hypoxia. This fact leads to a high rate of phase III failures in clinical trial.[37,38]

Another promising approach is the development of small molecules with a high affinity towards RGD-integrins. Two promising approaches are concerned with synthesis of non-peptidic integrin ligands[39] and cyclic peptides[40] respectively. Both concepts have a competitive inhibition in common. The interactions of the peptidic structures are mainly based on the binding motif RGD. The non-peptidic diacylhydrazines **3** contain a guanidinium and a carboxylate group at the edges (fig. 2-4). In the last case both groups mimic the functional groups of arginine and aspartic acid as they appear in the RGD-sequence. It was investigated to improve the coating mechanism of implant materials. In an experiment it could be shown that the adhesion of osteoblasts on titanium surfaces could be increased if diacyl-hydrazines (**3**) were incorporated on the titanium surface before. The incorporation was carried out via thiols that were used as residues. The cell adhesion efficiency could be increased up to 40 % compared to material that was not treated before.[39]

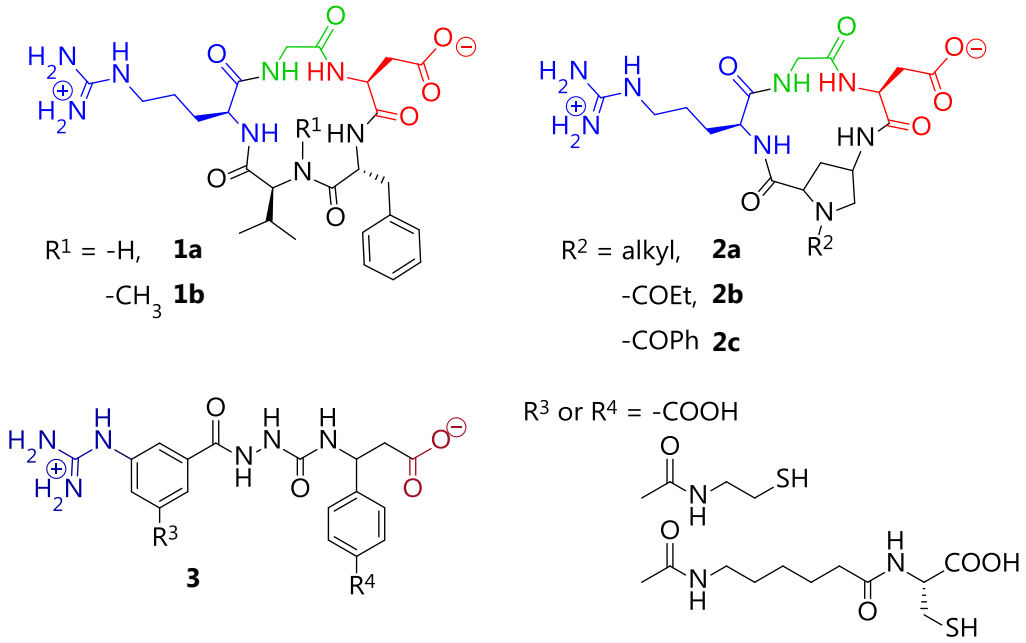

Figure 2-4. RGD-triad (arginine in blue, glycine in green and aspartic in red) in cyclic peptides cyclo(RGDfV) **1a** for R_1=H and cyclo(RGDf-N(Me)V-) **1b** for R_1=CH_3. The α,γ-locked γ-amino-butanoic acid (GABA) supplies highly strained cyclic tetra-peptides **2a-c**.[41] The non-peptidic diacylhydrazines **3** contains a guanidinium (dark blue) and a carboxylate (dark red) group. The residues R_3 and R_4 are possible linker positions for anchoring the molecule to surface (c).[39]

Due to an unknown bioactive conformation of the RGD-sequence in biological systems *Kessler* and coworkers synthesized peptide libraries. By spatial screening they explored a cyclic penta-peptide as lead structure. The cyclic arrangement of the peptides forces the RGD-sequence in a precise orientation so that the peptide's

residues are fixed in a specific orientation to each other. As a most promising candidate the cyclic penta-peptide cyclo(RGDfV) was evaluated. As an intriguing result of the structure-activity studies the existence of the artificial aminoacid D-Phe lead to increased receptor specificity. The reason for such an impact is announced by the authors by a well-defined orientation of the RGD-loop. *Kessler* and coworkers' tried different variations of cyclic polypeptides such as cyclo(RGDfK) or cyclo(RGDf-N(Me)V-) **1b**. The cyclic peptide **1b** with a methylated valine is shown in figure 2-4. Additional to the RGD-triad the best candidates contain the lipophilic amino acid phenylalanine within the cycle. The use of the non-proteinogenic D-configuration of phenylalanine contributes pivotal to the conformation of the cyclic peptide. Inhibitory measurements of vitronectin towards integrins $\alpha_{IIb}\beta_3$ and $\alpha_V\beta_3$ using the peptide cyclo(RGDfV) resulted in IC_{50}-values in nanomolar range. A striking selectivity ratio of 415 to 1 of $\alpha_{IIb}\beta_3$ towards $\alpha_V\beta_3$ integrin could be obtained.[40]

An advanced class of integrin cyclopeptide ligands **2a-c** invented by *Casiraghi* et al. show the highest binding affinity towards integrins at present (fig. 2-4). In competition with echiastin, a viper venom from *Echis carinatus*, some of the developed cyclic tetrapeptides could achieve IC_{50} values in a subnanomolar range. Thereby the venom, which has a low molecular weight, counts as a very potent irreversible $\alpha_V\beta_3$ antagonist with an inhibitory binding constant of K_i= 0.27 nM.[41,42]

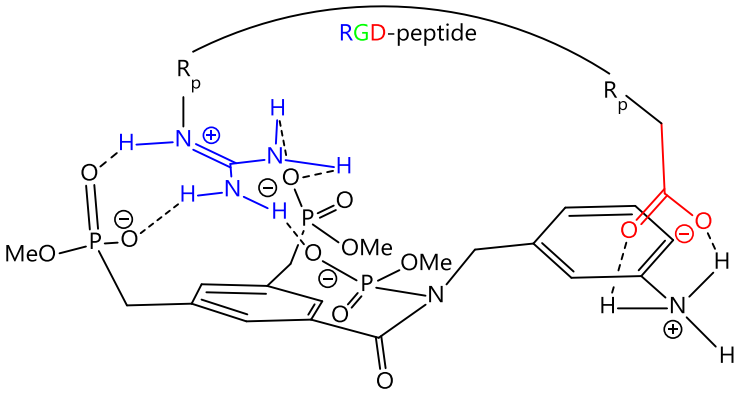

Figure 2-5. Ditopic RGD-receptor in complex with schematic RGD-peptide (due to clearness only residues of amino acids arginine and aspartic are shown).[43]

In a complementary method the capturing of ligand molecules is realized by an artificial receptor. The first class of receptors tailor-made for RGD-sequences is based on a xylylene skeletal structure. The three phosphonate groups attract positively charged ammonium or guanidinium groups by electrostatic, hydrogen bond and π-cation-interactions. With a second binding site composed of a meta substituted aniline residue (fig. 2-5) *Schrader* could obtain a complex stoichiometry of 1:1 with different RGD-substrates. For example binding constants of 700 M^{-1} and 1300 M^{-1} (determined via NMR titration in aqueous solutions) could be obtained with *Kessler's*

peptide cyclo(RGDfV) **1a** and a linear RGD-peptide respectively.[43] In this case the binding pocket of the receptor is mimicked to offer a ditopic binding site for integrin antagonists.[43,44]

The charged residues of the RGD-peptide direct towards the binding sites offered from the receptor. One important aspect is the rigidity of the RGD receptor with its two antagonistic binding sites. The trisphosphonate receptor suffers from a generally high flexibility. In a collaboration of the two working groups *Schrader* and *Schmuck* an enhanced ditopic RGD-receptor was investigated. Through the linkage of the bisphosphonate with a guanidinio carbonylpyrrole a versatile receptor was designed.

The challenging part of finding a suitable linker which provides enough rigidity to prevent intramolecular interactions was synthesized by *Rupprecht* (fig. 2-6). In independent binding studies via UV- and fluorescence titration experiments this enhanced receptor could achieve binding constants of around 2700 M^{-1} against a linear RGD-sequence in aqueous solution. In control experiments it could be shown that peptides enclosing only one charged peptide (arginine or aspartate) no binding affinity could be detected with the enhanced RGD-receptor of *Rupprecht*. One remarkable in this study was the fact that the methyl ester precursor showed a slightly higher binding constant (4700 M^{-1}). Therefore the precursor is only single charged. The authors proposed that the higher charged receptor (fig. 2-6) might be better solvated than the methyl ester protected one.[44]

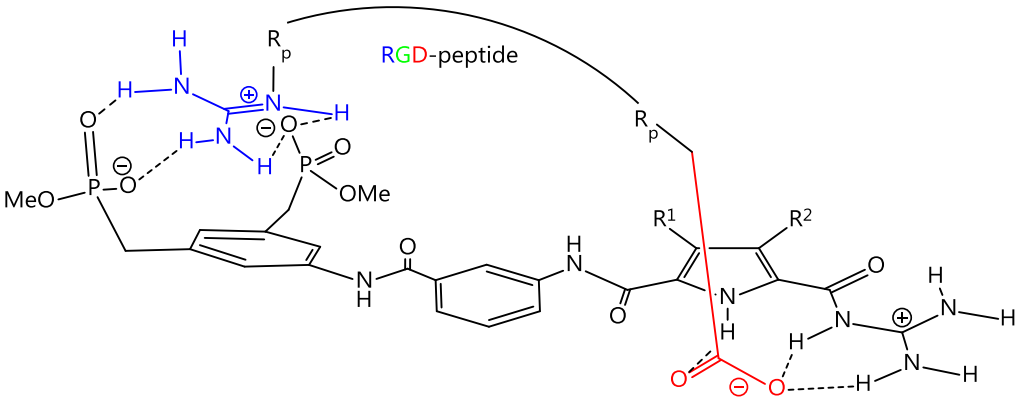

Figure 2-6. Enhanced Ditopic RGD-receptor with rigid aryl linker in complex with schematic RGD-peptide (due to clearness only residues of amino acids arginine and aspartic are shown).[45]

In figure 2-7 a new class of receptor is shown. In a collaborative research of both working groups *Schrader* and *Schmuck* this new type of receptor was developed. It combines the idea of a ditopic RGD-receptor as it was shown before and an additional concept of a cavity which provides a pre-organized binding site. The cage-like structure is provided by a tweezer which has shown before to be a versatile host for cationic guests like lysine and arginine.[46]

Generally the tweezer receptors shown in figure 2-7 suffered from a rather low affinity towards RGD-peptides. In comparative studies they showed the same efficiency like a monotopic tweezer. In proton NMR experiments it could be shown that rather no inclusion of the guest peptides into the cavity occurred. [47] Another inevitable problem deficiency was the low water-solubility especially of the single methyl ester protected receptor. Herewith solutions containing 50 % DMSO were used for the affinity studies.

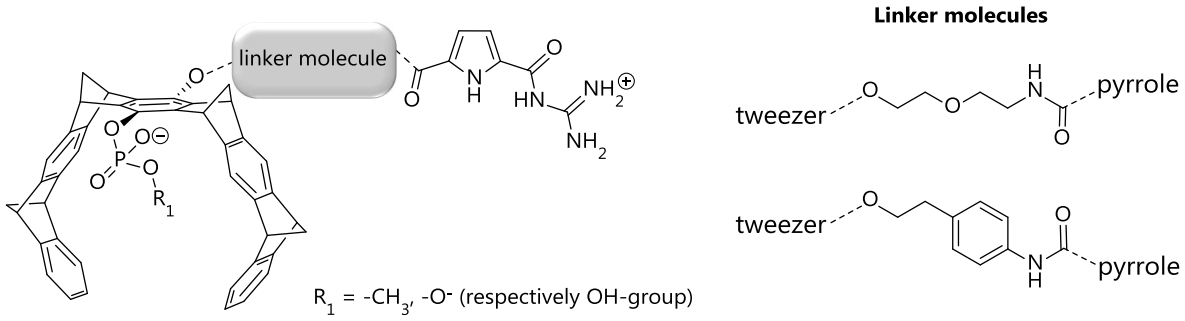

Figure 2-7. New class of ditopic RGD-receptor different linker molecules contains a tweezer as an arginine binding site. Connected via a linker a guanidiniocarbonyle pyrrole is used as aspartate binding site. [47]

Keeping the above mentioned advantages some further improvements in terms of binding affinity and selectivity towards different RGD-peptides can be done. Through the use of a more rigid binding site for the arginine residue like a pre-orientated cavity could enhance binding affinities significantly. The focus should be the development of a water-soluble receptor as this fact is essential with respect to biological systems and a prospective application in such systems. Additionally a ditopic binding site should enhance the binding facilities of the receptor like a chelating effect. Therefore a receptor structure consisting of two individual binding sites for the aspartic acid and the arginine respectively should be considered similar to the integrins and the receptors shown previously. If each binding site is considered to be part of an individual building block a target specific design by the use of different linker molecules could be possible. Due to a well-defined distance of both sites specific RGD-peptides could be preferred in terms of recognition. Further details and the concept of the work will be explained in chapter 3.

3 CONCEPT

3.1 The Principle of Host-Guest-Complexes

The principle of host-guest-systems is originated from receptor theory, which was developed by *Langley* and *Ehrlich* over a period of 30 years beginning from the 1870s.[48] From thereon theory evolved to a subfield of supramolecular chemistry, which was mainly advocated by *Lehn*, *Cram* and *Pedersen* and awarded with the nobel prize in 1987.[49,50] And the field of supramolecular chemistry is still a popular and innovative for research. This is even shown by the current Nobel prize in chemistry (2016) which was awarded to Jean-Pierre Sauvage, Sir J. Fraser Stoddart and Bernard L. Feringa *"for the design and synthesis of molecular machines"*.

"Supramolecular chemistry may be defined as the chemistry 'beyond the molecule', the chemistry of the intermolecular interactions."[51] With this conclusion *Lehn* refers to the fact that supramolecular chemistry concerns itself with non-covalent but rather weak intermolecular interactions. They range from the strongest ion-ion interactions (100 to 300 kJ/mol) over ion-dipole-, dipole-dipole interactions and hydrogen bonding to van der Waals forces and hydrophobic effects (< 5 kJ/mol), which are determined as the weakest ones. But nevertheless combination and accumulation of these interactions facilitates rather strong complex formations. One of the most prominent structures is the DNA double strand which is held together by a multiplicity of base pairs, guanine-cytosine and adenine-thymine. The base pairing itself is driven by supramolecular interactions in a noncovalent fashion. The main interactions that contribute are hydrogen bonds and hydrophobic interactions between the base pairs.[52]

The example of a double-stranded DNA is one of many other self-assembling processes which occur in biological systems. A quick and efficient response to environmental changes is essential for organisms. These responses include

exchanges of information and recognition processes. The formation of complexes between receptor and substrate enables recognition events. The reversibility of such complex formation is an outstanding advantage of supramolecular interactions. The general working mechanism of a host-guest-complex is illustrated in figure 3-1. Due to their specific complementary binding sites only appropriate guests are bound to the receptor or host molecule. Size and shape of the substrate as well as a multiplicity of supramolecular interactions contribute to selectivity in host-guest-systems.

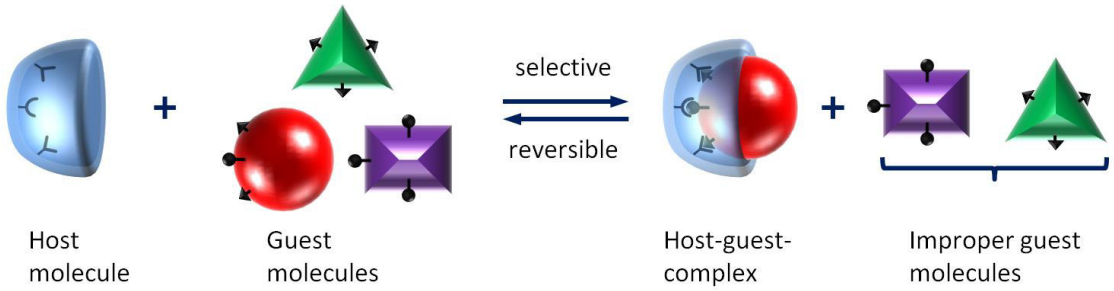

Figure 3-1. The molecular recognition with a high specificity towards different guest molecules is shown by the equilibrium above. Only suitable substrate molecules (guest = red ball) can form a host-guest-system with the receptor (host = blue half-shell). Small black cones and balls define functional groups that act as binding sites.

In the upper graphic only the red ball-shaped guest with a suitable orientation of binding sites is favored to build a complex. Although the other guest molecules have some suitable binding sites they would be less favored. As shown in chapter 2.2 integrin receptors utilize several intermolecular interactions to distinguish between different RGD-peptides in a similar manner. Two prominent representatives are vitronectin and fibronectin. Realizing a biomimetic receptor with similar selectivity necessitates a good balance of conformational flexibility and fixed orientation of binding sites. The form and the orientation of those binding sites of the synthesized RGD-receptor could be used to distinguish between the different RGD-peptides.

Having an increased contact area between guest and host provides more space for supplementary supramolecular interactions. The more attracting binding sites a receptor can offer to a substrate the stronger and more specific the complex should be. Sensing of molecular size, shape and architecture rises with increased number of hydrogen binding, electrostatic and van der Waals interactions.[53]

Even the small binding motif of the RGD-triad incorporates the challenge of selective recognition of complementary binding sites within one molecule. These could lead to self-recognition and self-association. Therefore the composition of the artificial receptor needs to be well-considered. But some principles should be obeyed to obtain a molecular receptor with a high recognition capability. Subsequently two

complementary binding sites for the RGD-sequence are considered. The arginine could be addressed by a negatively charged tweezer, whereas the aspartic acid could be recognized by a guanidiniocarbonyl pyrrole, a carboxylate binder.[54] Small RGD-peptides as analogs of the RGD-peptides as they appear in vivo could be used to validate the binding affinity and the binding selectivity of an artificial RGD-receptor. For example peptides shown in chapter 2.4 could be some useful candidates.

3.2 Concept of the Ditopic Binding Motif for RGD-Peptides

Guanidiniocarbonyl pyrrole carboxylates work as self-complementary systems and form stable dimers. They have been developed by *Schmuck*. The dimerization is mostly based on electrostatic interactions due to opposite charges of functional groups. Additional hydrogen bonds contribute to a strong dimerization constant of an estimated value of 10^{12} M^{-1} in DMSO. Guanidinio and carboxylate function connected via a pyrrole moiety act as complementary binding partners. Due to their rational design the hydrogen donors line up in rather flat molecular geometry (fig. 3-2). This enables guanidiniocarbonyl pyrroles to act as proper oxoanion receptors, especially for carboxylates having a planar structure either. Even in aqueous media complexation constants in the range of 10^{3} M^{-1} could be reached. Therefore the guanidiniocarbonyl pyrrole is a highly efficient carboxylate binder.[54]

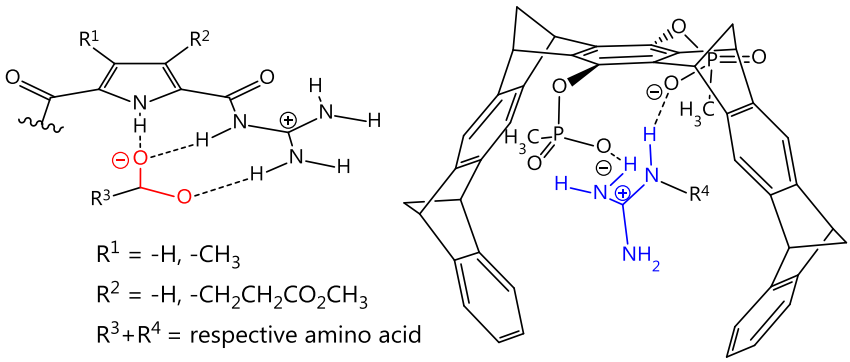

Figure 3-2. Oxoanions such as carboxylates provide an opportune complementary binding partner for guanidiniocarbonyl pyrroles based on their planar orientation (left side). The tweezer's cavity is highly suitable for entrapping positively charged moieties such as arginine or lysine side chain (right side).

As an attractive binding partner for the guanidine moiety of the arginine side chain a molecular tweezer consisting of an aromatic backbone is considered. Invented by *Klärner* and further developed by *Schrader* it is a well-known binding site for primary and secondary alkylammonium guests (fig. 3-2). Due to two attached phosphonate groups at the tweezer's central part, also named as bisphosphonate tweezer, it is sufficiently water soluble. It shows a remarkable affinity towards

N/*C*-protected amino acids like lysine and arginine as guests in aqueous solutions. The bisphosphonate tweezer yielded association constants of around 5000 M^{-1} and 2000 M^{-1} for the protected amino acids lysine and arginine respectively.[46] The affinity towards the arginine residue is supported by the cavity of the tweezer too. In analogy to the guanidiniocarbonyl pyrrole binding site the intermolecular interactions are mainly based on electrostatic interactions. Additionally hydrogen bonds and hydrophobic effects contribute to the association event. The hydrogen bonds are formed between the oxygen atoms of phosphonate groups and guanidinium. Hydrophobic effects arise from the tweezer cavity, which serves as an environment shielded from solvent. The release of water molecules from this hydrophobic environment has a striking entropic advantage.[55,56]

To obtain a molecular receptor with a high recognition efficiency it is recommended to have an increased contact area between guest and host.[53] By addressing both side chains of the RGD-sequence simultaneously a ditopic receptor containing previously introduced binding sites can be designed. The benefit of a ditopic binding motif should be an increased binding affinity towards RGD-peptides. As mentioned before, recognizing the RGD-sequence is challenging due to the complementarity of their binding sites. Guanidinium residue of the guanidinio-carbonyl pyrrole represents a highly suitable guest for the tweezer cavity. Thus intramolecular association would be entropically favored, if both binding sites are allowed to come into contact. An indispensable condition is the use of a suitable linker molecule. On the one hand it needs to provide enough space for RGD-substrates on the other hand intramolecular self-aggregation needs to be prevented.

3.3 Objective of this Work

With the help of computational chemistry appropriate linker molecules to connect the anion and cation binding sites were considered. Methods on a very basic level were used to calculate molecular structures of the desired complexes. With the use of MacroModel simple force field calculations of possible receptors were made to visualize, if intra- or intermolecular interactions are favored. Comparisons of calculations of the receptors with RGD-substrates, e.g. *Kessler's* cyclic RGD-penta-peptides, could give advices for synthetic approaches. Even the kind of the connective groups of the linker molecule needs to be preconceived. For this purpose the guanidiniocarbonyl pyrrole **4** offers three positions (R) for a conjunction with the second binding site (fig. 3-3). A connection of both binding sites providing best preorganization for recognition of the RGD-sequence is required. In principle

attachment of the linker can be carried out as ester or amide function at the carboxyl group at position 5 of the pyrrole **4**.

But nevertheless attaching the linker at the tweezers (**5a** and **6**) will result in a loss of symmetry. Thus synthesis might be challenging in terms of a good yield for a mono-functionalized tweezer. Selectivity control of a mono-functionalization of the tweezer should be achieved by reaction management, e.g. by dilution of reactants or insufficient use of a reagent.

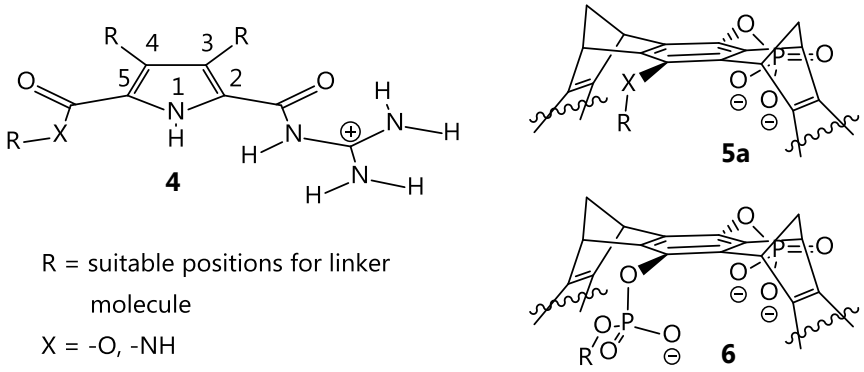

Figure 3-3. Structures of the binding sites pyrrole **4**, monophosphate tweezer **5a** and diphosphate tweezer **6**. Possible positions to connect linker molecule are marked by the residues R.

In figure 3-3 two approaches for an unsymmetrical tweezer are shown. The residue R represents the connected linker molecule. Pre-considerations led to the result that monophosphate tweezer **5a** could originate from an unsymmetrical tweezer central part **5b** (fig. 3-4) thus dissymmetry could be achieved at an early step in syntheses pathway. This might circumvent problems of selectivity and low yield at advanced synthesis steps.

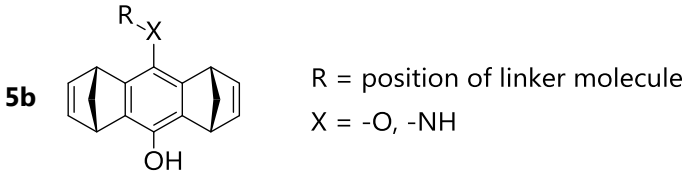

Figure 3-4. Central part **5b** as an appropriate precursor for monophosphate tweezer **5a**.

With regard to possible applications under physiological conditions the receptor needs to be water soluble. As a result the positions of solubility enhancing groups need to be considered as well as pH-stability due to work up at acidic conditions. Therefore the peripheral positions of the guanidiniocarbonyl pyrroles moiety provide some space for such groups. In figure 3-4 possible positions of water solubility enhancing groups are shown. In addition a diphosphate tweezer **6** could be used.[57] In this case the second phosphate group provides an additional negative charge. This

might increase water-solubility in the same manner as attractiveness towards positively charged guest molecules like arginine.

Within this work a basic synthesis strategy taking advantage a convergent synthesis should be applied. Therewith the overall yield should be improved because multistep syntheses will have a negative impact on the yield anyway. A suitable linkage of both binding sites supporting such a convergent synthesis strategy needs to be considered as well. In figure 3-5 the proposed receptor structure is shown in principle. Similar to the receptor shown in figure 2-7 the tweezer should be connected to a guanidiniocarbonyl pyrrole. But beside the functional groups used as binding sites for arginine and aspartic acid solubility enhancing groups should be considered. In general these groups could be attached at the periphery of the guanidiniocarbonyl pyrrole as well as the linker molecule provide space for supplementary solubility enhancing groups.

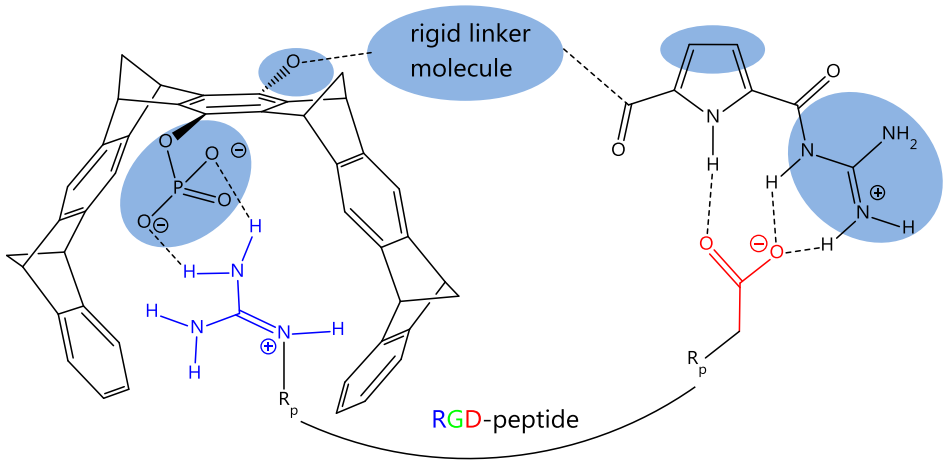

Figure 3-5. Suitable positions for solubility enhancing groups are highlighted in in blue.

In a subsequent step the association constants of the receptor with different RGD-peptides should be determined. To quantify association constants and therefore the affinity towards RGD-peptides different methods can be used depending on the molecular properties of the receptor. Typically titration experiments of the host with guest substrate will be carried out under acquisition of a changing observable.[58,59]

The use of NMR, ITC and UV/VIS are generally suitable methods to evaluate the host-guest-system. With respect to the expected range of binding constant some methods suit better than others. For instance NMR- and UV/Vis-techniques can be used for binding constants smaller than $10^4\ M^{-1}$ and smaller than $10^5\ M^{-1}$ respectively. Measurements that are based on fluorescence and isothermal titration calorimetry (ITC) cover a broad range of binding constants from $10^2\ M^{-1}$ to $10^8\ M^{-1}$. The reason for these ranges is justified by the different concentrations the different

methods require.[60] The used concentration range should be set around the invers of the expected binding constant.[58,61]

Due to the fact that the RGD-receptor is considered to carry chromophore moieties UV/VIS-measurements seem to be highly versatile. Both binding sites, the tweezer as well as the pyrrole contain chromophores nearby the positions of the binding event. Through the association with the substrate the electronic environment within the chromophore should change. As a result the properties of UV-absorption should be influenced too. The change of this observable can be measured and used for a further evaluation. The absorbance maxima of the pyrrole and the tweezer moieties are around 300 nm and 280 nm respectively and will be most suitable as observable. NMR measurements which follow shifts of specific proton signals involved in the binding event might be useful as a second method. The ITC as the third method records the heat change during the stepwise addition of the guest molecule and could be used too, if the contribution of the enthalpy is high enough. As a prerequisite of the binding studies the complex stoichiometry of different host-guest-systems needs to be determined individually. Thereby a correct evaluation of complexation constants is ensured. Determination of complexation stoichiometry could occur via *JOB*-Plot measurements.[62,63] One problem is, that binding constants cannot be obtained directly from such measurements. Therefore non-linear analysis needs to be done with the recorded experimental data. Subsequently results should be reviewed with respect to generally accepted conclusions. In the following chapter all results of syntheses and measurements of this project are discussed.

4 RESULTS AND DISCUSSION

4.1 Projected Synthesis Strategies and First Calculations

The development of artificial receptors reaches its borders in a precise prediction of their binding affinities to substrates. Many different influences like solvent, salt concentration, enthalpic and entropic effects determine the efficiency of formation of a receptor substrate complex. Theoretical calculations can give good evidences for syntheses thus they minimize energies of structures due to conformational changes of the participating molecules. By comparison of the energies and the conformations of differently formed complexes one can propose favored associations. This method was used to get some qualitative hints for the receptor design. Thereby the focus was set on calculated conformations of structures. Due to the charged residues of the peptide sequence and the binding sites unlikely geometries were obtained sometimes. These results were skipped and not presented in this work.

All calculations in this work were carried out with MacroModel 9.6. The structures of molecules were imported with *Maestro*, the molecular modeling interface of Schrödinger software. For comparability all minimizations were executed with OPLS2005 force field, water as solvent and the conjugate gradient minimizer PRCG as minimization method. The value for maximum iterations was set to 10,000. The energies of the RGD-receptor and the substrate alone as well as in a complex were calculated separately. The results of particular calculations were compared to receive an objective quality of the receptor. Because of the low level of the calculations all results were used only as hints for the following receptor syntheses. The structures of the complexes were pre-orientated in order to prevent from local minima, which might entrap some unlikely configuration. Therefore the RGD-recognition unit of the peptide was positioned alongside the supposed binding sites of the receptor.

With the first calculations the focus was set on finding suitable linkers that provide enough rigidity. Such rigid linker should prevent the receptor from an auto-recognition. This is necessary because of the complementarity of the used binding sites. Additionally the positions of both binding sites to each other are determined by the length of the linker. Consequently the linker provides a preorganization of the receptor. Due to the use of a tricarboxylic acid pyrrole building block reasonable linker conjunctions would be an ester or amide group. Depending on the functional group X-H the connection to the monophosphate tweezer **5** could be realized as ether, ester, amine or amide (fig. 3-3).

Based on these ideas different linker molecules, shown in figure 4-1, were designed and computational calculations were carried out. Inter alia a convergent synthesis strategy was planned taking advantage of the click chemistry.

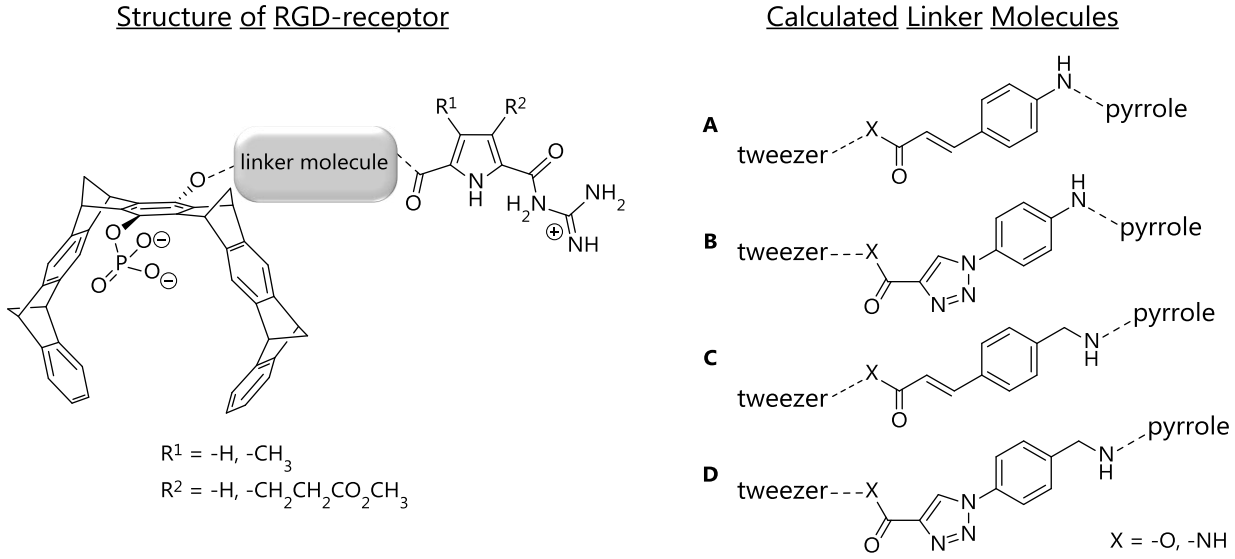

Figure 4-1. Prospective RGD-receptors with various linker molecules. Linker molecules C and D are elongated homologs of A and B respectively.

The click chemistry provides orthogonality towards other functional groups with respect to their reactivity. The functional groups of the receptor, which are necessary for the recognition of the RGD-sequence, should not be influenced by reaction conditions of a copper catalyzed variant of the *Huisgen Cycloaddition*.[64] The pronounced improvement is the separate synthesis of two building blocks, the guanidinium and the aspartic acid binding sites. A comparable linear synthesis strategy often suffers from a very low overall yield. But the efficiency of multi-step synthesis sequence will be enhanced by a convergent approach instead. First receptors were calculated separately without any substrate molecule to check their affinity of auto-recognition. Calculations of receptors with the 4-(aminomethyl) homologues of cinnamic acid and the 1,2,3-triazolyl (linker **C** and **D**) derivative

resulted in too many unfavored conformations (fig. 4-1). Due to the additional methylene group the molecules showed too much flexibility and underwent some self-aggregation. Initially the methylene group was considered to allow a further adjustement of length so that the receptors with different linkers could fit selectively to specific RGD-peptides.

In contrast the calculations of receptors with the linker molecules 4-azidoaniline and 4-aminocinnamic acid (**A** and **B**) led to better results. Their structures and most favored conformation in a complexe with the cyclic RGD-ligand **1a** are illustrated in figure 4-2. Especially their improved pre-orientation of the binding sites revealed reasonably better conformations in complex with the penta-peptide **1a**.

In a direct comparison of receptors **7** and **8** different favored orientations in association with cyclo(-RGDfV-) **1a** could be discovered. Receptor **8** with the 1,2,3-triazolylaniline linker **B** is more twisted than receptor **7** with the 4-aminocinnamic acid linker **A**. Position of the twist is highlighted in green in schemes a and b (fig. 4-2). Although similar starting geometries were used for both structures this remarkable change appeared.

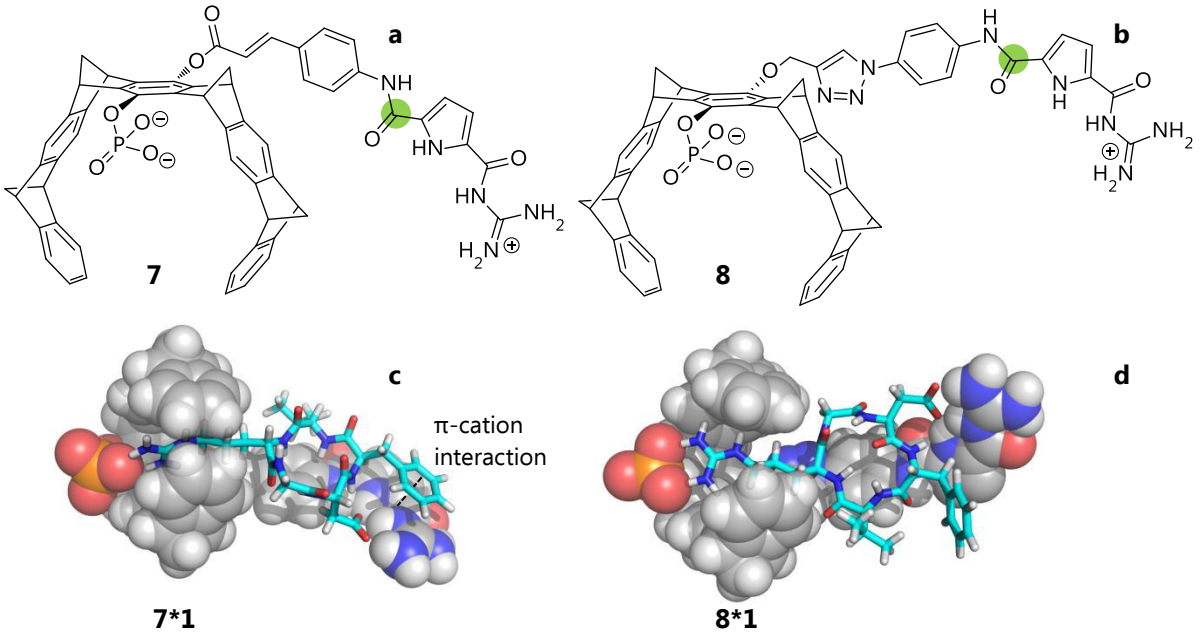

Figure 4-2. Prospective RGD-receptors with two different linker moieties. Receptor **7** contains 4-aminocinnamon acid **A** (a) and receptor **8** comprises the 1,2,3-triazolylaniline linker **B** (b). Pictures c and d reproduce results of calculations of receptors in complex with cyclic peptide **1a**. Pictures were obtained from MacroModel calculations.

The twist occurs along the binding of carbonyl C and pyrrole with a dihedral angle of around 37° for receptor **8**. Receptor **7** shows a twist of 7° only. Due to a longer linker the distance between both binding sites gets larger in a flat receptor geometry. Therefore this increased twist is necessary to form a stable complex with

the substrate. The different orientation and the twist of the receptor resulted in a loss of π-cation interaction (dashed line) between the phenyl group of phenylalanine and the guanidinium of the arginine (fig. 4-2d).

But this is only one of many others contributing intermolecular interactions. According to the principles of *Lehn* enhanced recognition capability for biomimetic receptors comes along with an increased contact area of the receptor and the ligand.[53] In both cases the RGD-receptors revealed conformations with a reasonable contact area. In addition complex of receptor **8** was compared with a complex structure obtained from crystallographic data of integrin $\alpha_V\beta_3$ in association with cyclic peptide **1b**. These data were obtained from the *RCSB protein data bank* (*pdb*).

With the use of *Maestro*[65] both complex structures were compared by their two dimensional projection plot. This function reduces the three dimensions of the examined volume to two dimensions. Of course this feature suffers from a lack of information. But the striking advantage is an easier method to compare contact areas of different complexes.

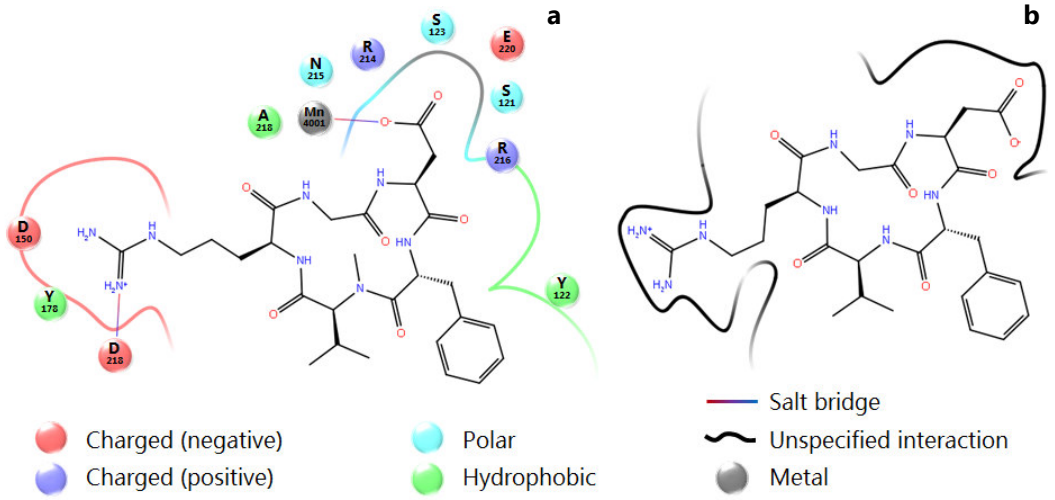

Figure 4-3. Two dimensional scheme of substrate cyclo(-RGDf-N{Me}V-) **1b** in the binding pocket of integrin $\alpha_V\beta_3$ (a) was derived from crystal structure (*pdb* 1L5G).[27] The binding site for guanidinium residue is negatively charged due to two aspartic acids (**D 150** and **D 218**). Binding of carboxylic residue is mostly facilitated by metal ion (**MN 4001**). 2D-plot of cyclo(-RGDfV-) **1a** in the environment of the artificial RGD-receptor **8** (b) was derived from conformational calculations with MacroModel. The black line indicates only unspecified interactions with the artificial receptor in a distance range of ≤ 4 Å. The tool "ligand interaction diagram" of *Maestro* is not able to identify charges of non-peptidic structures like pyrrole and tweezer moieties.[65]

In figure 4-3 the two dimensional plots of previous mentioned complexes are visualized. Left side (a) shows the substrate peptide inside the binding pocket of integrin $\alpha_V\beta_3$. The guanidinium of the arginine residue is nicely buried in a cave that

is negatively charged. The negatively charged environment results from two aspartic acids (D 150 and D 218) of the integrin.

Outstandingly the salt bridge of aspartic acid D 218 contributes to a strong complexation of the guanidinium residue. The aspartic acid of the RGD-triad is mostly attracted by a metal ion-dependent adhesion site (MIDAS). In this case the MIDAS is represented by a divalent manganese cation (Mn^{2+}). This manganese cation (MN 4001) originates from preparation method. During the crystallization process of the extracellular segment it was inserted. But under physiological conditions Mn^{2+} is replaced by Mg^{2+}, if integrin is in the active mode. Although this might bring some changes in association of RGD-substrate the following considerations are based on the integrin structure containing Mn^{2+}. Predominantly positively charged and polar amino acids like arginine, serine and asparagine represent the rest of the binding site.[25] Some additional hydrophobic interactions of the phenylalanine of the cyclic substrate with tyrosine (T 122) are present in this plot.

The second two dimensional plot (right side) shows the result obtained from the calculation of the complex between the receptor **8** and the cyclic substrate **1a**. By a comparison of the two dimensional schemes (fig. 4-3) striking similarities could be revealed. Both plots show a similar contact area between the substrate and the respective receptor. Although the plot derived from the calculated structure reveals unspecified interactions, the plotted contact area is lower or equal to a distance of 4 Å. Especially the functional groups aspartic acid and guanidinium of the RGD-sequence are in an attractive intermolecular contact with the binding sites of the receptor. Indeed the interactions do not seem to be equal to those of the crystal structure but specific interactions like salt bridges or polar interactions are not supported by the program *Maestro* for non-peptidic structures.

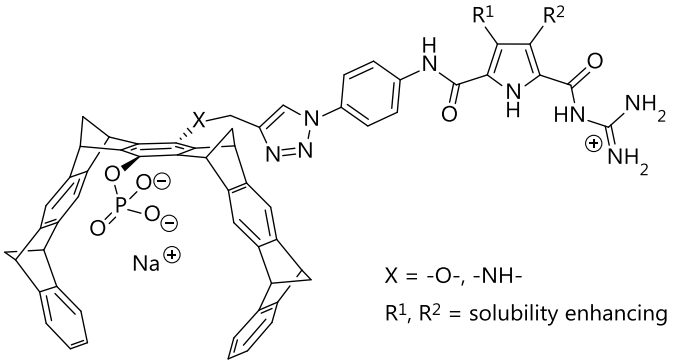

Figure 4-4. The ditopic RGD-receptor containing the 1,2,3-triazolylaniline linker was considered after the evaluation of the theoretical calculations.

Consequently the shape of the binding pocket formed by the receptor is almost similar to the shape of the integrin $\alpha_V\beta_3$ and therefore results were used as starting point for planning the syntheses strategy. In figure 4-4 the projected RGD-receptor is

shown. The positions R^1 and R^2 are considered for an attachment of further groups in order to enhance the water-solubility of the receptor. At the position X different linkage options are possible. Generally the connection between the tweezer and the linker molecule can occur via oxygen or nitrogen atom which needed to be introduced as a hydroxy or amin group respectively. The idea to attach solubility enhancing groups to the linker molecule was dropped. The approach of a suitable guest molecule might be restrained by these groups. Another option could be the introduction of a second phosphate group beside the cavity of the tweezer. The advantage of an additional phosphate at position X is discussed in section 3.3. The synthesis of the artificial ditopic RGD-receptor started with the two building blocks, the pyrrole and the tweezer. Because of the high versatility of click chemistry the approach using 1,2,3-triazolylaniline linker was preferred (receptor **8**, fig. 4-2 b).

4.2 Receptor Syntheses

4.2.1 Syntheses of Basic Building Blocks of the Tweezer

One challenging part of this receptor synthesis is the synthesis of an un-symmetrical tweezer as it was shown in figure 3-3. The critical point is the synthesis of a dissymmetrical tweezer at an advanced step of synthesis pathway.

If one compares the two possibilities of the functional groups next to the linker in molecule **5b** (fig. 3-4) it becomes clear, that a selectivity problem occurs for a central molecule with two hydroxyl groups. Most reactions even protection or deprotection of hydroxyl groups would have the same effect on both positions. A selective reaction of one group or a selective attachment of a linker is not possible in an easy way. Only through suitable reaction conditions the desired mono-functionalization could be obtained.

An appropriate loophole could be the synthesis of un-symmetric tweezer core part. In this case the central part will be designed with two distinguishable functional groups. This slight change could be realized by a replacement of one hydroxyl by an amino group for example. Nucleophilic reactions can be realized much easier with amines than with alcohols for instance.[66] This difference allows a selective protection or further functionalization of the amino function for instance. Thus tweezer **9** (fig. 4-5) was considered carrying a *p*-aminophenol central part instead of a *p*-hydroquinone.

The modification with respect to the overall shape of the receptor compared to receptor **8** should be negligible. Therefore the property of complexation of RGD-

substrates should be similar. The synthesis of un-symmetric tweezer **9** was deliberated in a comparable fashion to synthesis of standard dihydroxy tweezer but with the use of *N*-chloro-*p*-benzoquinoneimine (**13**) instead of quinone.

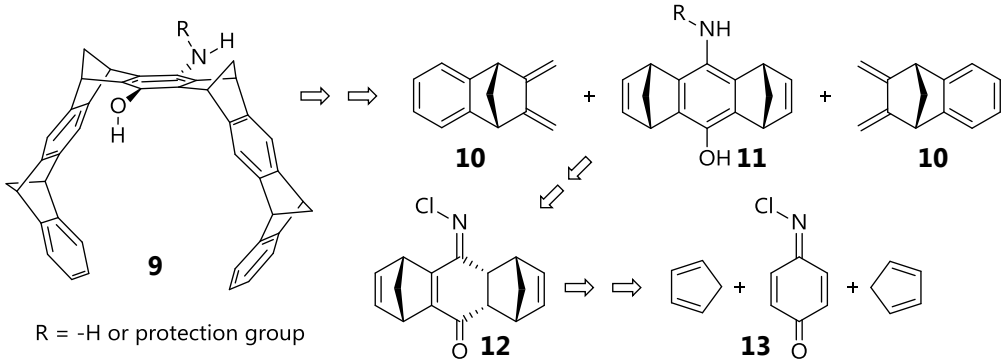

Figure 4-5. Retro-synthesis scheme shows unsymmetric tweezer **9**. The central part was considered to be asymmetric thus using *N*-chloro-*p*-benzoquinoneimine **13** in the first Diels-Alder-reaction step.

After twofold Diels-Alder reaction to the *p*-chloroimino hexahydro-dimethanoantracen-one **12** the chloroimine should be converted into imine by hydrolysis.[67] Subsequent selective protection of the amine followed by tweezer synthesis or vice versa can be performed.

Unfortunately the reaction of *N*-chloro-*p*-benzoquinoneimine and freshly distilled cyclopentadiene was not successful. Neither the desired product nor starting material could be detected in the tarlike mixture. Decomposition took place, although the reaction conditions were kept very mild and the mixture was not heated above 30 °C.

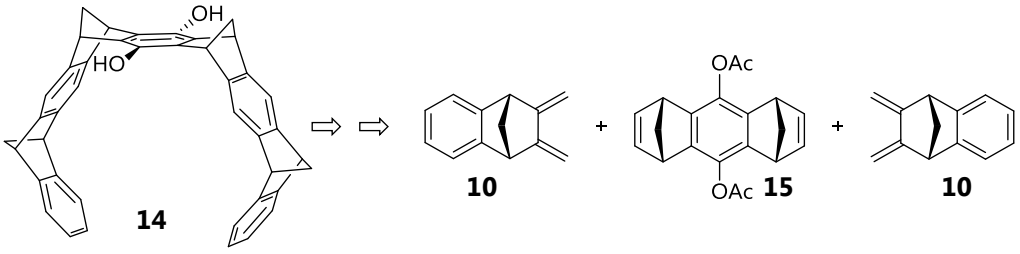

Figure 4-6. Retro-synthesis scheme shows the hydroquinone tweezer **14**. Twofold Diels-Alder-reaction of sidewall **10** with center part **15** followed by an oxidation step leads to the fully aromatized tweezer.

Direct usage of quinoneimine was considered as well. However this reaction already described in literature seems to be an unsuccessful underpinning. The authors described that mostly unwieldy mixtures or cokelike mass were produced. As a reason they assumed a polymerization process.[68] Therefore the synthesis pathway of a dicyclopentadienequinonimine (**11**) and an easy access to an un-symmetrical

tweezer was dropped again. Instead of tweezer **9** the synthesis of dihydroxy tweezer **14** according to well-known synthesis protocol was executed.[46]

The synthesis route was processed via diacetyl protected precursor **15** (fig. 4-6). Most of the steps were executed according to literature described procedures. In the beginning of synthesis pathway the side-wall **10** and core part **15** were synthesized separately. The central molecule was synthesized according to the literature described procedure (fig. 4-7).[46] Synthesis of the tweezers core part started with a Diels-Alder reaction of *p*-benzoquinone and cyclopentadiene. Diketone **16** could be obtained in moderate yield of 56 % due some side reactions of cyclopentadiene. The purified diketone was oxidized with *p*-benzoquinone to benzoquinone **17** subsequently. Purification of quinone **17** occurred via column chromatography and yielded 65 % of desired product.

In a second Diels-Alder reaction molecule **17** was transferred to dimethano-anthracenedion **19a**. The reaction was carried out with one equivalent of cyclopentadiene and resulted in a 1:1 mixture of *syn*- (**19a**) and *anti*-product (**20**). Due to the nonselective synthesis step theoretical yield of the favored *syn*-product was halved. After purification of the mixture *syn*-dimethanoanthracenedion **19a** was obtained in a yield of 47 %.

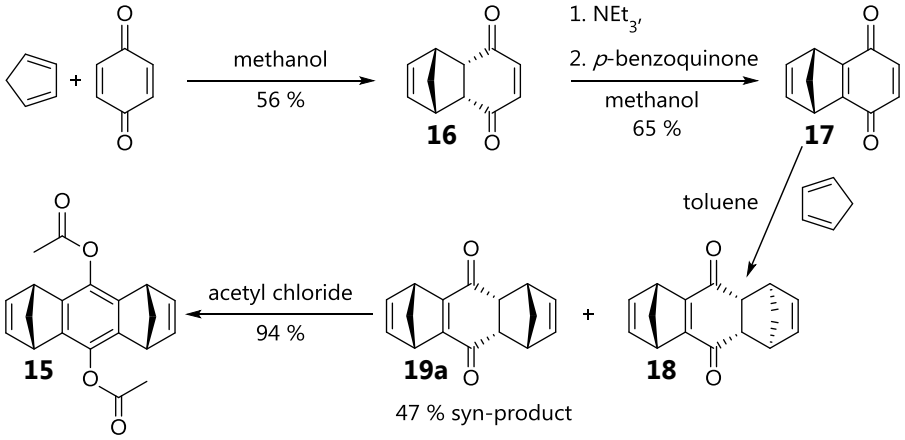

Figure 4-7. Synthesis scheme shows the acetylated central building block **15** of the tweezer. Obtained yields of the core were similar to literature documented ones.[46]

Separation of both products was carried out by repeated crystallization from cyclohexane/ethyl acetate (1/1). Thereby fractions with enriched *syn*- and *anti*-dimethanoanthracenedion were obtained. Purification was pursued until a proportion of 35:1 or higher with respect to the *syn*-product could be realized. The ratio was controlled via ^{1}H NMR (fig 7-4). In a final acetylation step building block **15** was synthesized in a yield of 94 %. Therewith the synthesis of protected core molecule could be executed in similar yields to the literature described synthesis.

In contrast to the synthesis of core building block **15** some improvements could be made for the synthesis of tweezer's sidewall **10** (fig. 4-8). In the initial reaction step the yield could be doubled compared to reported yield.[46] Therewith an increase of more than 25 % could be achieved. Basically this improvement could be accomplished through the change of the polymerization inhibitor. Phenothiazine was used instead of previous used hydroquinone. This inhibitor was applied in catalytic amounts in the first Diels-Alder reaction of maleic anhydride and freshly distilled indene in a slight excess.[69]

By partial crystallization 1,4-methano-1,2,3,4-tetrahydronaphthalene-2,3-dicarbonacid anhydride (**20**) was obtained in a good purity. Even further purification for the next reaction step was not necessary. The following reduction to the tetrahydronaphthalene diol **21** was executed directly according to literature described procedure.[70] Thus the described tweezer synthesis was shortened by two intermediate steps. Those proceeded via opening of anhydride to the di-ester **24** with a consecutive isomerization of the *cis*-tetrahydronaphthalene to the thermodynamically favored *trans*-tetrahydronaphthalene **25** (fig. 4-8, right side).

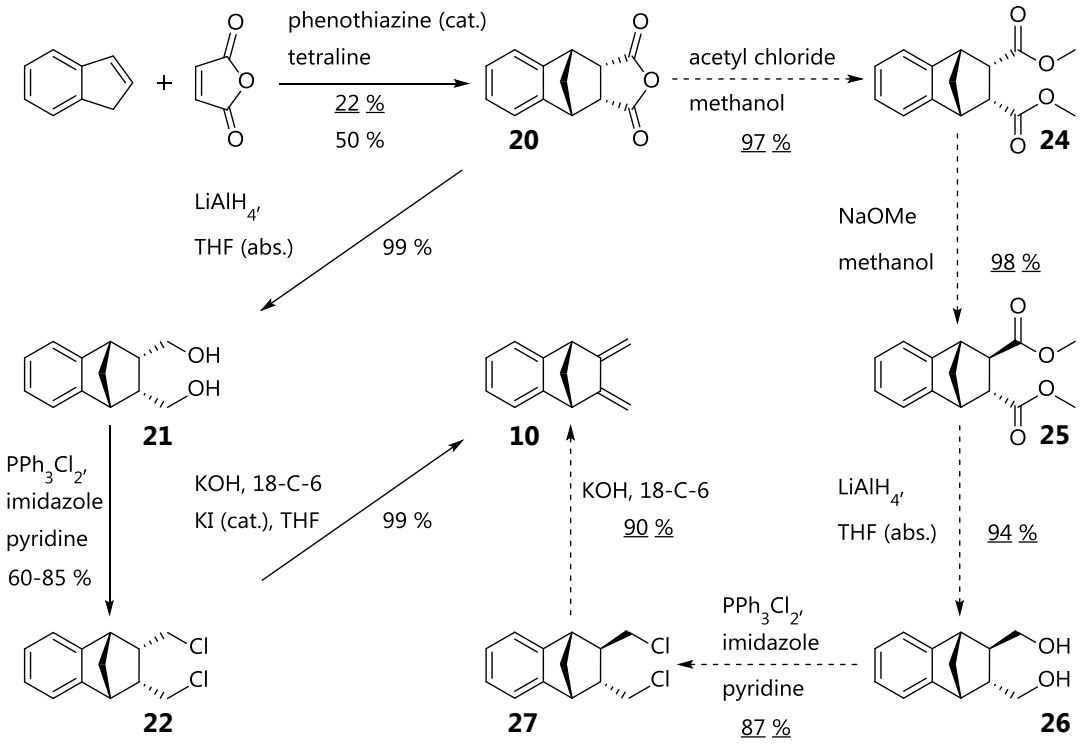

Figure 4-8. Newly investigated synthesis of tweezer's sidewall is shown on left side. Hitherto described synthesis pathway is shown at the right side with dashed arrows. The yields of the previous trail are underlined.[46]

A subsequent reduction to *trans*-diol **26** followed by a transformation to the *trans*-dichloride **27** and a final elimination to diene **10** is described in this synthesis protocol.[46] The overall yield could be increased from 15 % to almost 40 % based on

these changes. In the newly developed synthesis pathway the *cis*-configuration of the anhydride **20** is retained until the elimination step to diene **10**. Tedious purification methods with one exception after the chlorination step were not necessary. Opening of the anhydride **20** with subsequent reduction to *cis*-diol **21** was carried out in a one pot synthesis according to reported reduction reaction of the di-ester **25**.[46]

These shortening allowed a faster proceeding, so that the *cis*-diol **21** could be obtained in two steps less compared to *trans*-diol **26**. One of the most critical steps in this reaction scheme was the transformation from the diol **21** to the dichloro-compound **22**. In various approaches different results with respect to the yield were obtained. At first a difference in the reactivity of nucleophilic substitution at the *cis*-diol compared to *trans*-diol was considered. But in analogous reaction with the *trans*-diol **26** similar problems appeared. Finally it turned out, that different batches of commercially purchased triphenylphosphine dichloride showed significant changes in reactivity. Some batches dropped down yields dramatically, so that only starting material or single chlorinated product could be isolated. Best results of the chlorination to compound **22** varied from 60 to 85 % yield. The highest obtained yield was comparable to the reported yield.[46]

Another circumstance that diminished the yield arose from some practical issues during the workup process. The huge amount of byproduct triphenylphosphine oxide was not easy to remove. Separation problems originated from an excessive use of three equivalents of triphenylphosphine chloride in addition with good solubility of its oxide in the product oil. Dichloride **22** was obtained as colorless oil, which served as a proper solvent for triphenylphosphine oxide. Even filtration of a solution of **22** in DCM over silica did not result in an efficient separation of the favorite product from its side-product. The reason again is the ability of dichloride **22** to act as an eluent for triphenylphosphine oxide. To solve this separation problem a successive precipitation of the oxide was required. By a stepwise removal of DCM from the solution precipitation could be executed repeatedly. The major amount of triphenylphosphine oxide could be removed by this procedure. For a complete removal of this byproduct repeated normal phase chromatography were carried out afterwards. A yield of 85 % could be obtained as best result.

Final elimination to diene **10** revealed the problem of an incomplete elimination. Partially elimination of a single chloride group took place. Again it was considered that the different stereoisomer was responsible for this unpopular result. The incomplete reaction resulted in mixtures of starting material, single elimination and the desired product. Even longer reaction times or slight heating of the mixture did not improve the elimination. To overcome this problem of incomplete reaction some

modifications in reaction auxiliary agents were tried. Potassium *tert*-butoxide, a stronger base, was used instead of potassium hydroxide according to similar reaction described in literature.[71] But elimination of hydrochloric acid on both positions could not be improved unless 18-crown-6 ether in combination with a catalytic amount of potassium iodide was used. Finally a mixture of potassium hydroxide, 18-crown-6 ether and potassium iodide in catalytic amounts led to a full conversion to diene **10** at room temperature. The functional role of potassium iodide might be an inter-halogen exchange. Comparable to a Finkelstein reaction the iodide could attack the dichloride **22** via S_N2-mechanism. Subsequently a faster cleavage of iodide would speed up the elimination because of iodide being a better leaving group than chloride.[66] The obtained product was purified by column chromatography in order to obtain a salt-free product.

Hence the bicyclic diene **10** could be obtained in a yield of 39 % over all four steps. The new developed route is much more economical compared to the published synthesis route with a total yield of 15 % over six steps.

4.2.2 Syntheses of Un-Symmetrical Tweezers

The last two Diels-Alder reactions to build up the tweezer backbone were carried out in a similar fashion to published protocol.[46] During this twofold cyclisation reaction one acetyl group protected core **15** and two diene sidewalls **10** form the tweezer precursor **28**.

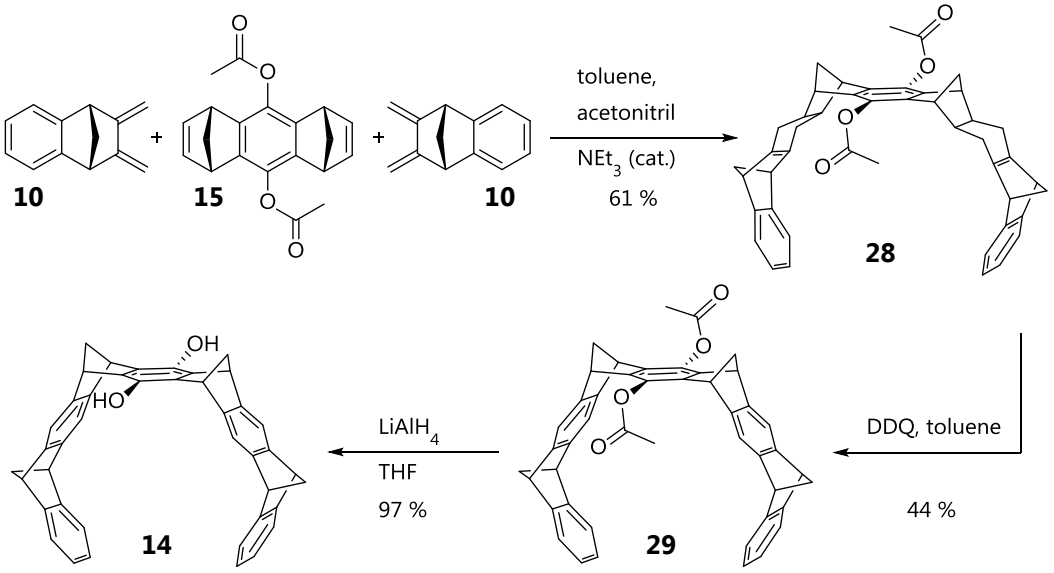

Figure 4-9. Reaction scheme of hydroquinone tweezer **14**.[46] A subsequent DDQ-oxidation of Diels-Alder product **28** lead to the fully aromatic diacetyl tweezer **29**. Final reductive removal of acetyl groups result in hydroquinone tweezer **14**.

One important change was the use of a heavy-walled Schlenk tube with a screw plug as reaction vessel instead of a sealed glass tube for one time usage. The advantage was that the reaction could be carried out under Argon according to Schlenck technique and monitored by TLC and HPLC. Even samples for reaction monitoring were taken under inert gas conditions. Unfortunately the yield of tweezer precursor **28** could not be improved furthermore (fig. 4-9).

After purification via crystallization 61 % of desired product could be obtained. Therewith the achieved yield was comparable to the reported one of 67 %.[72] After subsequent oxidation with an excess of DDQ the acetyl protected tweezer **29** could be obtained. After purification via column chromatography the diacetyl tweezer **29** with an entire aromatic backbone was obtained in 44 % yield.[73] Further byproducts were not determined. Compared to published results (71 %)[72] the yield of this oxidation step was nearly decreased by half. Based on separation problems from oxidation agents DDQ and DDB repeated column chromatography was mandatory. As a consequence the yield was reduced compared to reported results.

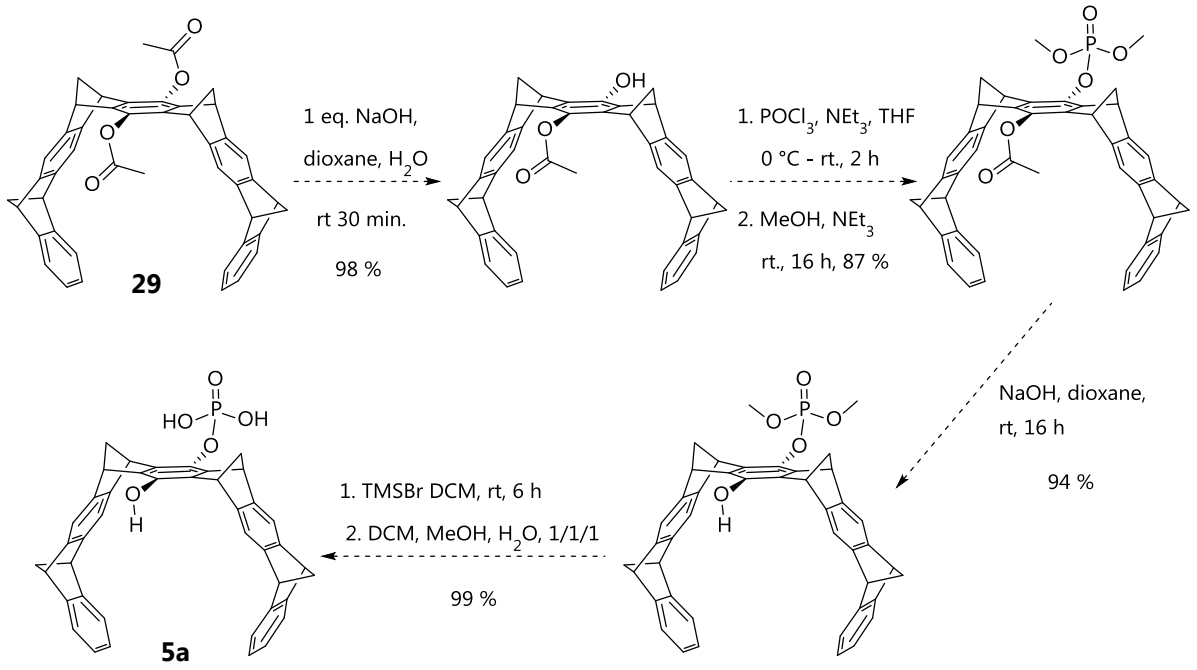

Figure 4-10. Synthesis route to monophosphate tweezer **5a** developed by *Gersthagen*.[47,72]

To obtain an un-symmetrical tweezer **5a** shown in figure 3-3 several approaches are conceivable. One possibility is a partly removal of one acetyl group to obtain a single protected tweezer. This procedure was developed by *Gersthagen*[47,72] and synthesis of tweezer **5a** was carried out via four reaction steps (fig. 4-10). The reaction sequence consists of an initial deprotection reaction to the mono acetyl tweezer followed by a phosphorylation to the intermediate dimethyl phosphate tweezer and finally two deprotection steps of acetyl and methyl groups respectively.

The overall yield of the full sequence is reported with 79 % and seemed to be a promising pathway.

But unfortunately tries to carry out a selective deprotection of one acetyl group failed. Mostly mixtures of mono and double de-acetylated product were obtained and resulted in low yields of the mono-functionalized tweezer.

Due to this dilemma another approach via a fully de-protected hydroquinone tweezer **14** was tested. A direct cleavage of both acetyl groups was performed with 10 eq. of $LiAlH_4$ in THF solution (fig. 4-9). The unprotected molecule **14** could be obtained in quantitative yield nearly. Thereby the overall yield of tweezer **14** could be increased slightly from 8 to 10 % with respect to sidewall synthesis.[46] Mainly this could be achieved by shortening of two steps in the tweezer's sidewall synthesis. The de-symmetrizing step was shifted to the next reaction step.

As it was mentioned before different approaches to an un-symmetrical mono phosphate tweezer **5a** are conceivable. Due to the orthogonality and versatility provided by the click chemistry synthesis strategy was modified with regard to the method *Gersthagen* presented. Insertion of the phosphate group should be subordinated with respect to the linker attachment. This order could prevent undesirable side-reactions of the phosphate group in subsequent reaction steps.

Therefore the attachment of an alkyne function at the tweezer's central position was considered. Different attempts to esterify the dihydroxy tweezer **14** led to mixtures containing mostly starting material. Even the usage of coupling agents like HATU or activated carboxyl functions like acid chlorides were attempted. Unluckily none of the desired esters (**A**-**D**, fig. 4-1) could be obtained in a satisfying amount. This result led to the assumption that access to the hydroxyl positions of the tweezer is sterically hindered. But also reactions with sterically less hindered molecules, e.g. with the truncated tweezer **19b**, did not lead to a positive result either (fig. 4-11). The synthesis of ester **30a** could not be carried out satisfyingly. In this case desired esters suffered from low stability and decomposition took place during work-up and purification processes.

Stability problems of ester functions at the tweezer were already reported by *Gersthagen*.[72] Instead of the esterification reaction an analogous etherification via *Williamson* ether synthesis was considered to connect the tweezer with the linker molecule. For that purpose preliminary test reactions with the hydroquinone **19b**, the tautomeric form of molecule **19a**, were executed (fig. 4-11). The reaction was carried out in a highly diluted acetone solution of **19b**. To the alkaline solution 0.8 eq. of propargyl bromide were added dropwise. The reaction mixture was heated for 24 hours and yielded mono-, di-ethers and diol.

Through a well-considered reaction management the desired core alkyne **30b** could be obtained in a yield of approximately 50 %. Additionally separation by chromatography could be realized easily.

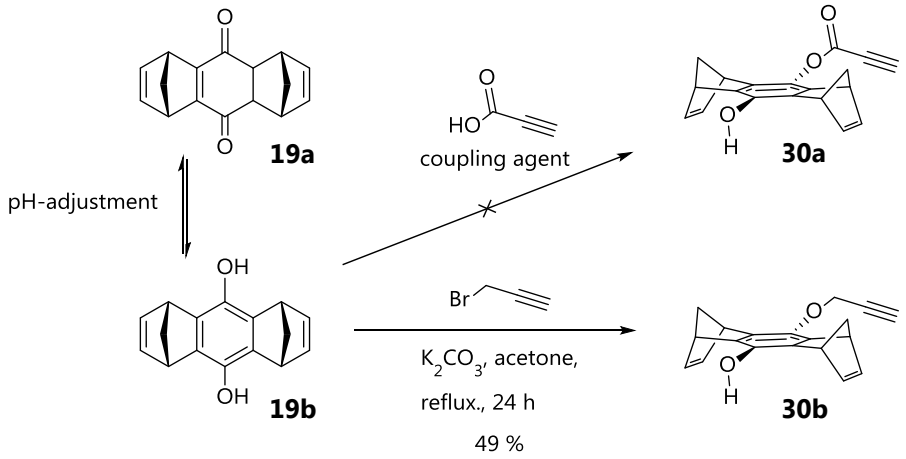

Figure 4-11. Synthesis schemes for esterification and etherification at hydroxyl group of the truncated tweezer **19b**. The mono-alkyne of the core **30b** could be obtained through a *Williamson* ether synthesis.

Unconverted starting material (approx. 10 %) could be recovered by chromatography. A transfer of developed reaction conditions to hydroquinone tweezer **14** led to lower results as expected (fig. 4-12). The corresponding mono-alkyne tweezer **31** could be synthesized in a yield of 15 %. Separation from di-alkyne tweezer and diol-tweezer **14** could be achieved via chromatography. The ratio of bis-alkyne to mono-alkyne changed dramatically from 1/3 for the truncated tweezer **19b** to 2/1 for hydroquinone tweezer **14**. The explanation for this change might be a solubility problem of the tweezer **14** which resulted in a slight suspension. Therefore the concentration of propargyl bromide was slightly higher with respect to dispensed amount of tweezer. In addition the solubility of mono-alkyne tweezer **31** might be considerably better compared to the hydroquinone tweezer **14** so that a second alkynylation could occur easily.

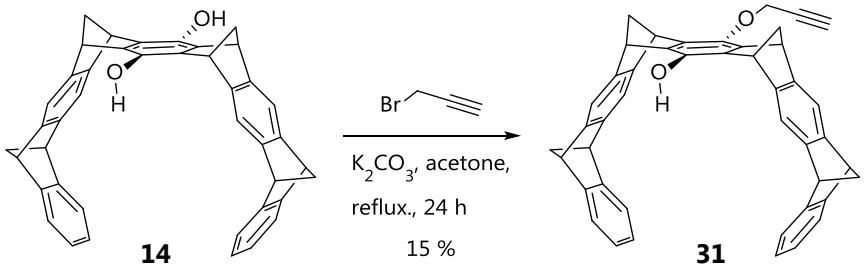

Figure 4-12. Synthesis schemes of un-symmetrical tweezer building block **31** for click chemistry. The mono-alkyne tweezer **31** could be obtained through a *Williamson* ether synthesis.

This reaction nicely showed the difference in reactivity of full versus truncated tweezer. Although the same quantity of equivalents was used, significantly less hydroquinone tweezer **14** was converted to desired mono-alkyne **31**. A supplementary effect might be the sterically unfavored position of the hydroxyl groups towards electrophiles. It was assumed that the hydroxyl groups are more shielded by the extended aromatic skeleton in full tweezer **14** compared to the truncated tweezer **19b**.

Nevertheless the newly discovered access towards unsymmetrical tweezers established a ubiquitous building block for further receptor synthesis. Although the yield of mono-alkyne **31** was pretty low (15 %) unconverted starting material **14** could be regained by chromatography and re-used. Supplementary improvement in reaction management might lead to better ratio of mono-alkyne to bis-alkyne. The big advantage of the mono-alkyne tweezer is its versatility in advanced synthesis route with respect to the orthogonality of click chemistry.

4.2.3 Syntheses of Azido Guanidiniocarbonyl Pyrroles

In figure 4-13 three different azido guanidiniocarbonyl pyrrole building blocks are shown. The guanidiniocarbonyl pyrrole building block **32** is part of receptor **8** used in the previous calculations (fig. 4-2). In this molecule peripheral positions do not facilitate further attaching of solubility enhancing groups.

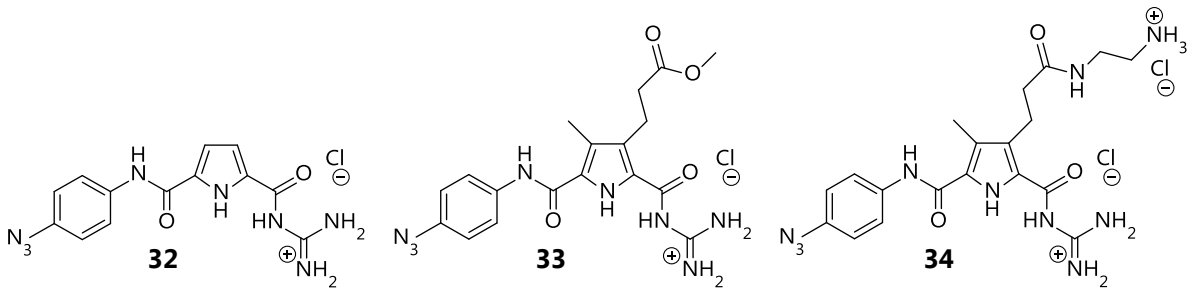

Figure 4-13. Different pyrrole building blocks coupled with linker molecule 4 azido aniline. Guanidiniocarbonyl pyrrole **34** carries additional ethylene diamine in periphery to enhance solubility problems.

Therefore the guanidiniocarbonyl pyrrole **33** was considered as it enables addition of further solubility enhancing groups. In azido guanidiniocarbonyl pyrrole **34** the attachment of an ethylene diamine as an example is given. Due to the possibility of an additional positive charge the water solubility could be increased. This fact becomes very important as receptors should work under physiological conditions. On the other hand sterically overcrowded groups need to be avoided in order to provide substrate peptides an excellent access to their host. Based on these

considerations syntheses of the pyrrole building blocks shown in figure 4-13 were carried out corresponding to literature protocols.[54,74] Only minor changes in work-up and purification processes led to better purities of the desired product in some reactions. By using the alkyne function at the tweezer the azide function needs to be attached at the pyrrole moiety. Therefore the commercially available 4-azido aniline was used to prepare pyrroles **32** to **34**. The use of an azide as an orthogonal protection group to most other reactions expanded the scope of synthesis strategies. The desired click reaction could occur at the final synthesis step.

Initially the synthesis of pyrrole building block **33** was considered to have the opportunity to add further solubility enhancing groups at the backbone of the guanidiniocarbonyl pyrrole, if necessary. Starting from the fully orthogonal protected pyrrole **35** preparation of the azido-pyrrole **37** was carried out (fig. 4-14). Preliminary quantitative deprotection of tertiary butyl ester under standard reaction conditions resulted in the pyrrole **36**.

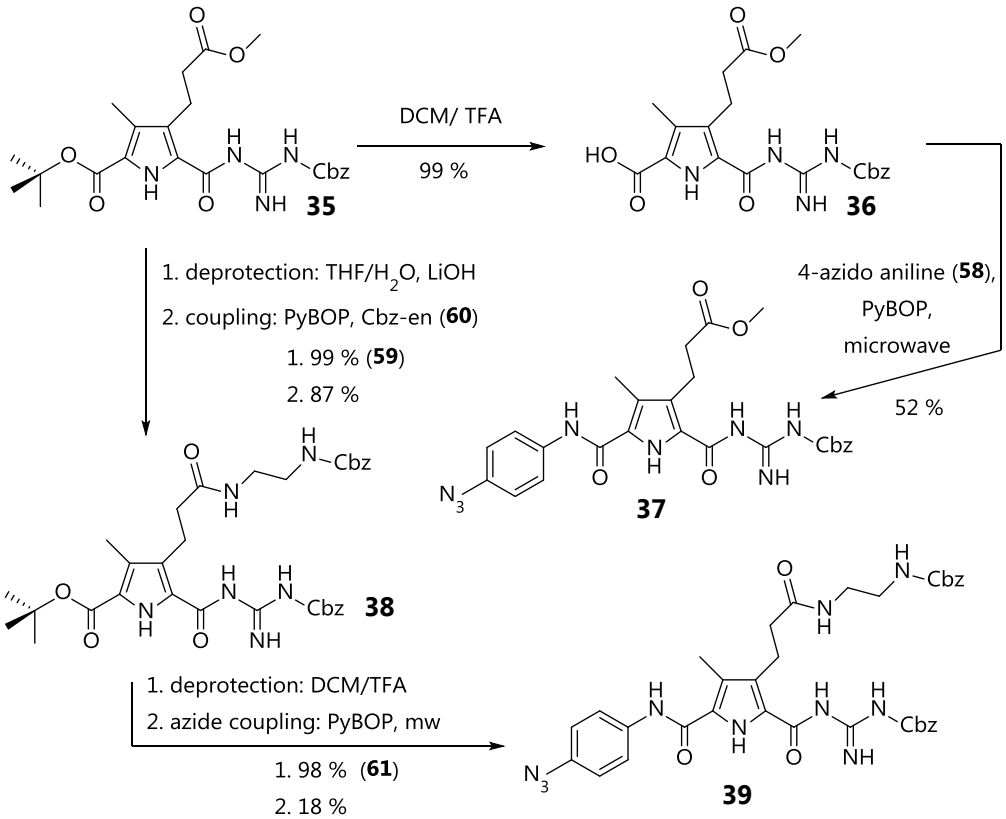

Figure 4-14. Synthesis pathways of pyrroles **37** and **39** starting from fully orthogonal protected Cbz-guanidinocarbonyl pyrrole **35**.

The generated acid function was attached to azide carrying linker molecule. The following formation of amide bonding with 4-azido aniline was evaluated under different reaction conditions due to problems in obtaining the desired product. Therefore different coupling reagents and reaction parameters were tested to obtain at least moderate yields and feasible purities. The coupling reagents HATU, Cl-HOBt

and PyBOP were tried with variation of reaction times and temperature. Reaction progress was controlled via TLC. Mostly mixtures of starting material, product and some indefinite side products were obtained. Final purification via column chromatography of those mixtures led to yields of around 20-30 %. Purification of product was not easy due to many different side products with similar retention time. Even purified material still showed impurities again after TLC check. The reaction time could be identified as a critical parameter with respect to yield. The longer the reaction time was the more side-product was generated. The heat-up phases were considered as a key point to increase the yield. Therefore reaction management was changed and coupling reaction was executed under microwave conditions. The phases of heating the mixtures are much faster compared to conventional ones with oil bath or heating mantle.[75] Therefore the necessary reaction temperature should be reached faster.

The amide formation was carried out via PyBOB as a coupling reagent. With PyBOP best results with respect to the yield could be achieved. Even in conventional reaction management alike in the microwave-assisted coupling reaction. Through reaction control by TLC heat phases could be reduced to a minimum of time. Even cooldown phases were kept as short as possible due to an additional cooling by air stream. During the evaluation of the best conditions the periods of heating did not last longer than 45 min. The temperature controlled by an infrared sensor, was not allowed to exceed above 81 °C. After each heating period the mixture was cooled down with a cooled air stream and TLC control monitored reaction progress. The fast cooling process was used to prevent the product from further decomposition. As a result of changing to microwave conditions the yield of pyrrole **37** increased from 32 % to 52 %. Thereby the yield could be nearly doubled and the amount of unwanted byproducts decreased drastically compared to previous reactions carried out under conventional heating.

Reviewing the purity of azido guanidinocarbonyl pyrrole **37**, analytical HPLC revealed impurities which should have been removed completely by previous purification. The only reason for this phenomenon could be a degradation process of desired product. And indeed decomposition of a purified sample could be proofed with the help of HPLC. A freshly prepared sample of pyrrole **37** with an initial purity of 93 % started to decompose within hours remarkably. A stability check made with HPLC revealed that by keeping samples at room temperature decomposition took place. In a re-check of a freshly prepared sample more than 90 % of initial substance was decomposed after 10 days.

The protected guanidinocarbonyl pyrrole **37** was dissolved in water/methanol (1/1) and stored in a closed HPLC vial at room temperature. Chromatograms of freshly prepared and 10 days old sample are reviewed below (fig. 4-15).

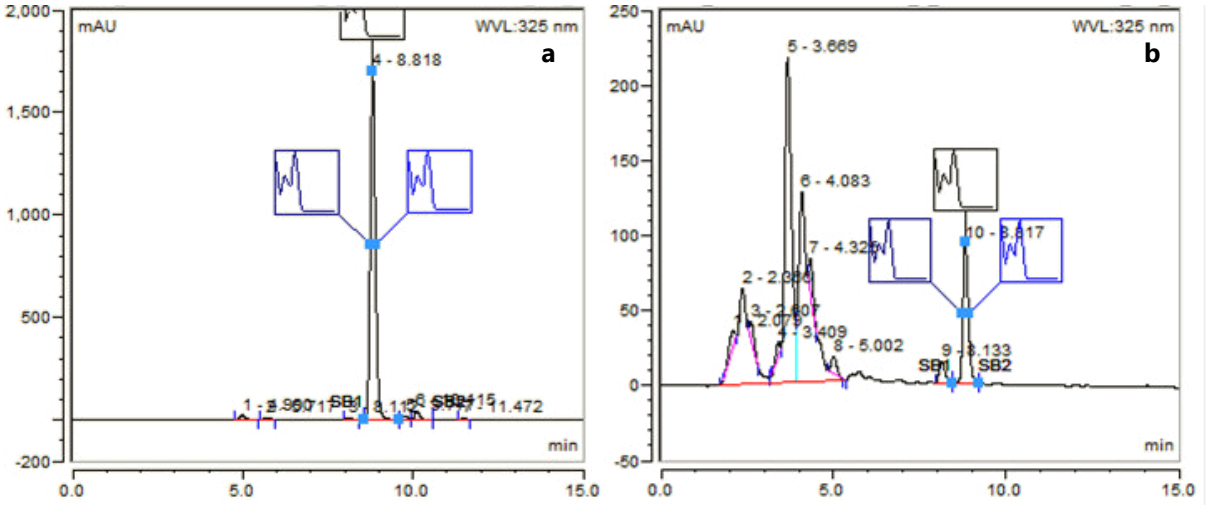

Figure 4-15. HPLC-chromatograms of Cbz-protected 4-azido guanidinocarbonyl pyrrole **37** were prepared under reversed phase conditions. Left side (**a**) shows freshly prepared sample of pyrrole **37** with negligible amounts of impurities. Right side (**b**) reveals a crude mixture after keeping the sample for 10 days.

The chromatogram at the right side shows a crude mixture of different substances. This mixture was obtained after storing the sample for 10 days at room temperature. No further analyzation of this mixture was carried out. Presumably the newly generated impurities originated from derivatization of the azido group. The time-dependent degradation explained synthesis problems of previously described coupling reaction. Trying to raise the yield over 30 % by conventional heating did not lead to successful results due to long reaction times. Through the use of microwave assistance the heat dependent impact on degradation of product could be minimized. The degradation of already purified compound occurred during the solvent evaporation process due to moderate heating probably.

Time dependent ^{1}H NMR-measurements in contrast revealed, that substance **37** dissolved in DMSO-d6 did not show any disintegration for days. But unluckily most of following reactions could not be executed in such inert medium. In consequence of the fast degradation of azido pyrrole **37** all following reactions needed to be faster. Even the heat impact needed to be minimized. To pursue the aim of a convergent synthesis strategy, the triazole formation needs to be last synthesis step of the azido guanidiniocarbonyle pyrrole building block **33**. Removal of Cbz-protection group of pyrrole **37** was tried under various reaction conditions but without success (fig. 4-16).[76]

The most critical point was a selective deprotection at a reasonable time. If the reaction conditions were too mild and reaction time was too short, generally no remarkable conversion took place.

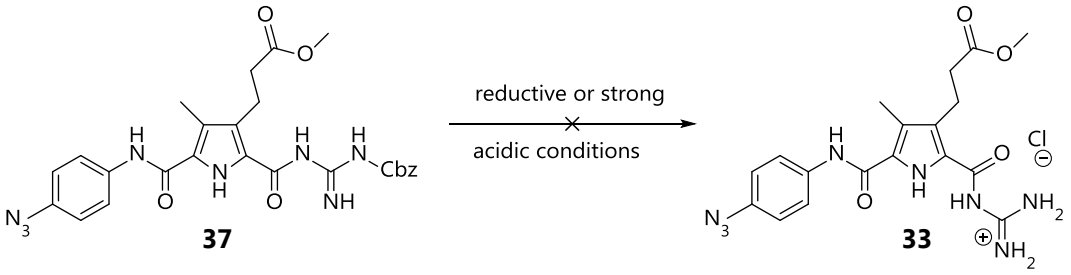

Figure 4-16. Cleavage of Cbz-group of guanidinocarbonyl pyrrole **37** by different conditions did not lead to free guanidine function while keeping an intact azide group.

Longer reaction times under reductive conditions[77] led to typical decomposition of starting material. Even strong acidic conditions usually used to cleave benzyl carbamates led to formation of an amine primarly.[78] Because all attempts of cleaving the Cbz-group were unsuccessful, protected pyrrole **37** was used for cycloaddition with tweezer alkyne. Results of receptor synthesis are described in chapter 4.3.4.

Additionally synthesis of pyrrole building block **34** with an ethylene diamine in the periphery was tried for improved water solubility. Therefore the methyl ester of fully protected guanidinocarbonyl pyrrole **35** was cleaved (fig. 4-14). The cleavage was carried out in aqueous THF solution containing 3 eq LiOH and the product was obtained in a quantitative yield. In an additional approach trimethyltin hydroxide was used to yield 96 % of desired product.[79] Both procedures required final column chromatography to obtain salt-free substance. The introduction of mono-protected ethylene diamine was carried out under standard amide coupling conditions with PyBOP as coupling reagent.[80,81] The coupling product **38** could be obtained in a yield of 87 %. A subsequent cleavage of the tertiary butyl ester yielded guanidinocarbonyl pyrrole with a free acid group in position 5 quantitatively (fig. 4-14).

The successional microwave-assisted coupling of 4–azidoaniline under previous described conditions revealed the double Cbz-protected azido guanidinocarbonyl pyrrole **39** in a poor yield of 18 % after purification via column chromatography. Similarly to the azido guanidinocarbonyl pyrrole **37**, pyrrole building block **39** contained many unidentified byproducts and a rapid decomposition appeared again. The time dependent decay of purified substance in solution was monitored by TLC, which reasonably explained the decreased yield. To circumvent problems in cleavage of the two Cbz functions pyrrole **39** was not used for further receptor synthesis.

Another approach was pursued to overcome the aforementioned stability problems of Cbz-protected azido guanidinocarbonyl pyrroles **37** and **39**. Therefore a new synthesis strategy was considered. The Cbz-protection group should be exchanged with a BOC-group at the guanidine moiety. Cleavage of tertiary butyl carbamate occur under acidic conditions typically.[76] Slightly acidic conditions should result in a free guanidinium moiety in moderate reaction times. For that purpose the smaller pyrrole building block **40** was used and coupled with 4-azidoaniline (fig. 4-17).

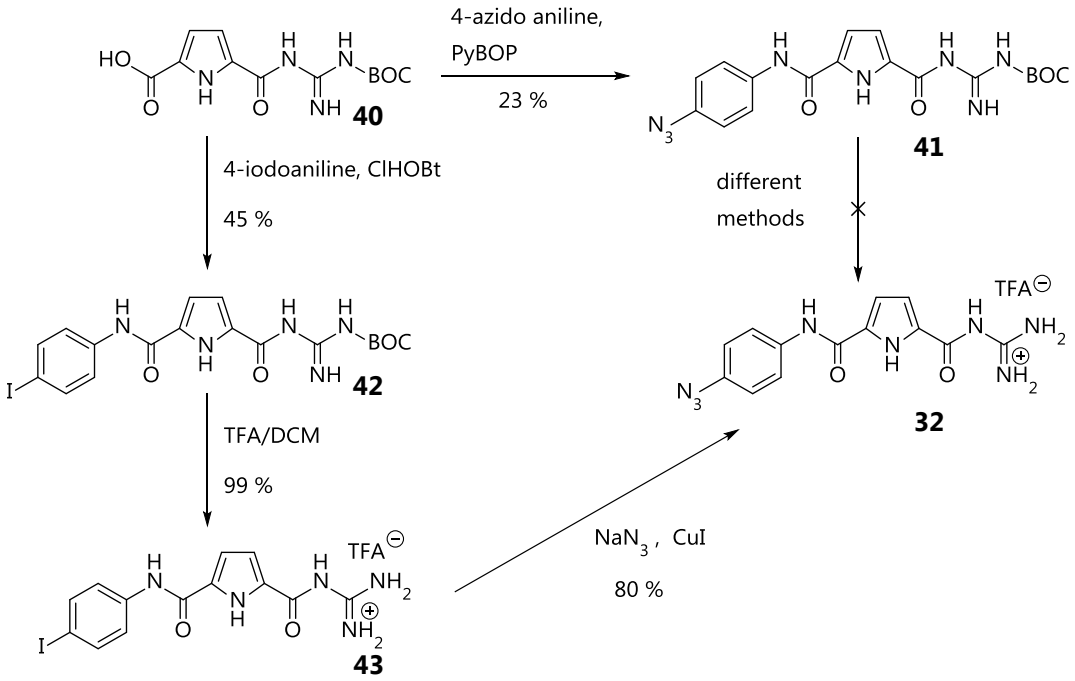

Figure 4-17. Alternative synthesis pathway of the azido pyrrole **32**.

The reaction was carried out with PyBOP at room temperature and yielded only 23 % of the BOC-protected azido pyrrole **41**. A further improvement of the reaction was not attempted due problems in cleaving the BOC-protection group later on. The idea that the BOC-group should be cleaved more easily and much faster than the Cbz-group was a false conclusion. Although different deprotection methods were used the *t*-butyl carbamate could not be cleaved. Instead of desired reaction starting material was reobtained or molecule **41** again started to decompose. This particular BOC protection group was resistant against acidic solutions like TFA in DCM at room temperature. Even cleavage at moderate heating up to 40 °C was tried but the BOC group could not be removed either. In another approach stronger cleavage conditions were tried. Freshly generated HBr-gas or HCl-gas in DCM solution was used in different approaches as cleavage conditions. Under these conditions decomposition of azido pyrrole **41** appeared and therefore no further attempts in deprotection of the BOC group were made.

A new synthesis route starting from pyrrole building block **40** was deliberated to circumvent described deprotection problems of protected azido guanidinocarbonyl pyrrole **41**. Under consideration of the stability problems of pyrrole **37** the insertion of an azide group was planned in a progressed synthesis. Therewith no unexpected side reactions could occur during deprotection step. In the last synthesis step of the receptor the obtained pyrrole building block **32** should be used.

Starting from the BOC protected guanidinocarbonyl pyrrole **40** the aromatic linker 4-iodo aniline was coupled at free acid function by usual amide formation (fig 4-17). The reaction could be carried out at room temperature with the coupling reagent Cl-HOBt in a moderate yield of 45 %. In a subsequent step the BOC-protection of the guanidine moiety was removed before transformation of the iodo-aryl into the azido-aryl residue was executed. In a solution of TFA in DCM the desired iodo-aryl guanidiniocarbonyl pyrrole **43** was obtained quantitatively.

The final synthesis step of pyrrole building block **32** was performed under copper catalysis. This reaction is not affected by free amines or guanidine moieties. A positive influence of previous mentioned functional groups is a stabilizing effect of the catalytic active species Cu(I).[82,83]

The azido guanidiniocarbonyl pyrrole **32** was synthesized by a copper catalyzed nucleophilic aromatic substitution (S_NAr-) reaction. Pyrrole building block **32** could be obtained in a yield of 80 % after its purification from coupling salts. This Ullmann-type coupling reaction is described by several proposed mechanisms found in the literature.[83] The synthesis of 4-azido aniline starting from 4-iodo aniline was carried out successfully according to a reported procedure.[84] This became necessary due to a supply shortfall of the commercially available compound 4-azido aniline hydrochloride. In the previous synthesis pathway of the 1st generation receptor the synthesized 4-azido aniline hydrochloride was used. A common side reaction, the copper promoted azide reduction to amines, which could occur under specific reaction conditions, could be excluded. The reason is that usually electron deficient aromatics are affected by this phenomenon.[85,86]

Luckily the reaction conditions could be transferred to the iodo-aryl guanidiniocarbonyl pyrrole **43**. Thus the insertion of an azide function occurred in the last step of pyrrole building block synthesis in line with a convergent synthesis strategy. The obtained guanidiniocarbonyl pyrrole **32** was used in 2nd generation receptor synthesis, which is described in chapter 4.3.5.

4.2.4 Synthesis of the 1st Generation RGD-Receptor

The RGD-receptor of the 1st generation was synthesized by a copper catalyzed 1,3-dipolar cycloaddition between the mono-alkyne tweezer **31** and the Cbz-protected guanidinocarbonyl pyrrole **37**. (fig. 4-18) The copper (I) catalyzed reaction was set up according to described procedure in literature.[87] Because of a fast conversion of the reagents to the desired triazole **44** no further heating of the reaction mixture was necessary. Reaction monitoring was carried out by TLC and the end of reaction was indicated after one hour of stirring. Purification was executed via filtration of an ethyl acetate solution over silica. The triazole was obtained in a yield of 95 % and purity was checked via normal phase chromatography.

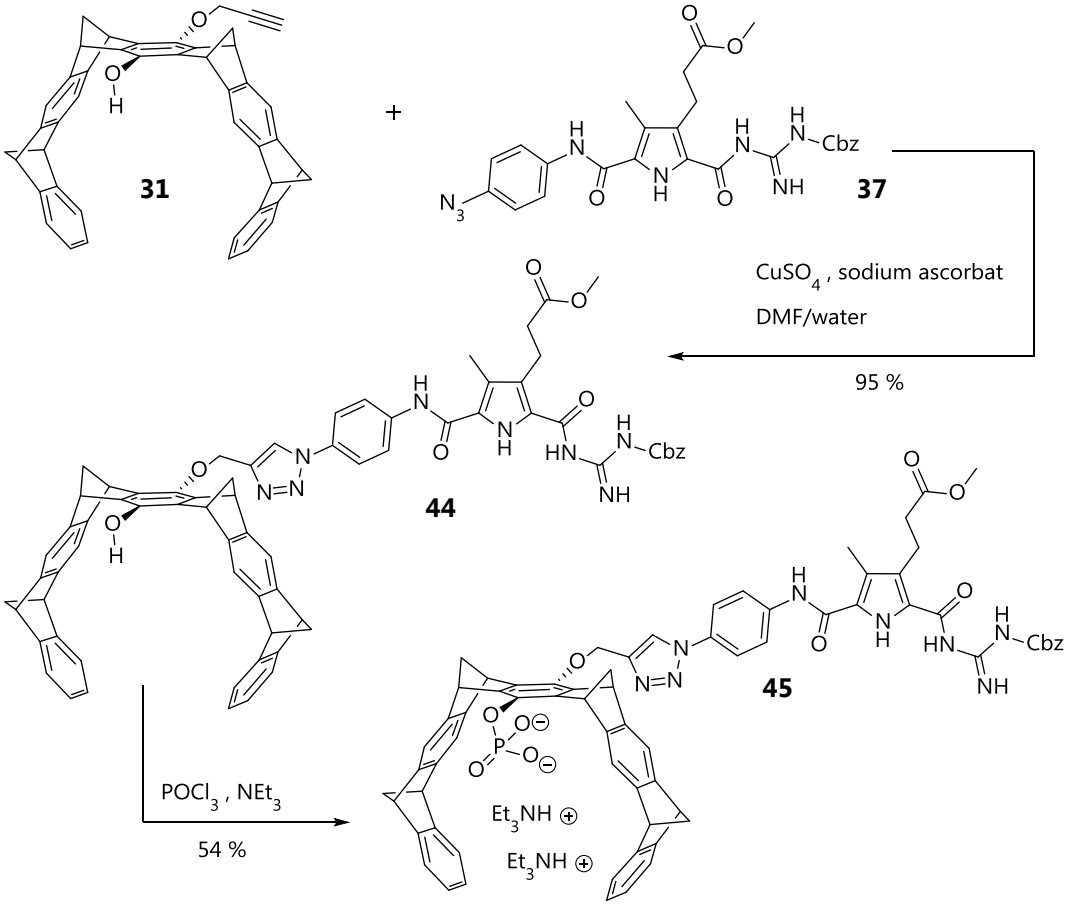

Figure 4-18. Reaction scheme of the precursor **45** of the 1st generation RGD-receptor. A full convergent synthesis strategy was not possible due to problems of Cbz-deprotection of pyrrole **37**.

All ^{1}H NMR signals could be assigned with exception of the nitrogen attached protons. With the help of two dimensional NMR experiments like HMBC and HSQC a distinct assignment could be made. Some proton signals showed overlaying of each other but still they were sharp and distinguishable, so that the molecule could be

identified clearly. A purity check via normal phase HPLC revealed a purity of 99 % at different wavelengths. A subsequent phosphorylation of cyclisation product **44** was carried out similarly to the synthesis described for the tweezer diphosphate.[88] The phosphorylation took place at the free hydroxyl group at the tweezer central position and yielded 54 % of the purified compound **45** (fig. 4-18).

The purification was done by a liquid-liquid extraction with dichloromethane and diethyl ether. Unfortunately some precipitate containing partly product occurred during workup process. Further purification of the precipitate could not be executed satisfyingly. By ^{1}H NMR and mass analysis of the precipitate the amount of desired product was estimated to be around 20 %. Nevertheless receptor synthesis was continued with the purified portion. A full characterization of phosphorylated precursor **45** turned out to be challenging due to peak broadening in the ^{1}H NMR spectrum.

Through the use of hetero single quantum correlation spectroscopy (HSQC) and in comparison with precursor **44** the assignment of the ^{1}H NMR-spectrum could be done properly. In figure 4-19 aromatic regions and methylene groups in neighborhood of phenyl and triazole groups of both molecules **44** and **45** are displayed.

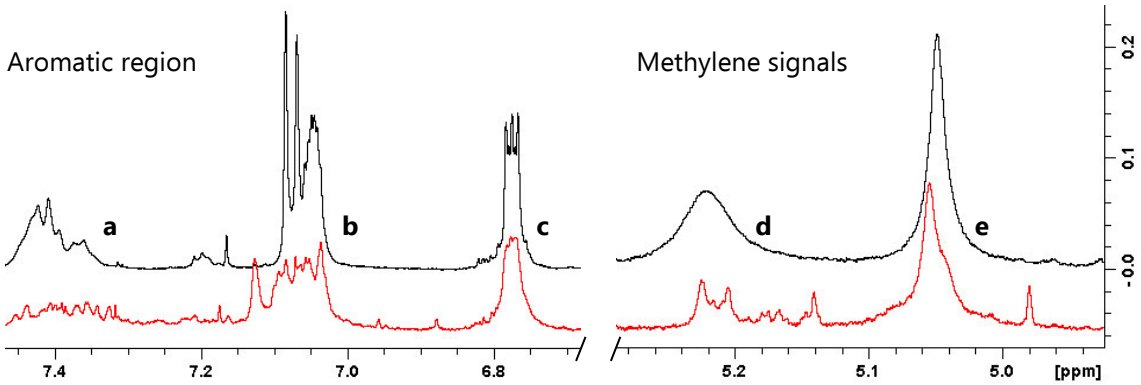

Figure 4-19. Aromatic region (**a**-**c**) of ^{1}H NMR of receptor precursors **44** (black) and **45** (red) on the left-hand side revealed clearly a change in peak widths. The upfield region of the ^{1}H NMR spectra show the methylene groups at 5.24 ppm (**d**) and at 5.04 ppm (**e**) of the Cbz-protection group (**d**) and of the triazole (**e**) respectively.

Both ^{1}H NMR-spectra were measured in DMSO as solvent, so that the signals occurred at comparable positions. Signals of the precursor molecule **44** (black spectrum) appeared clearly. Even the signals of methylene groups exhibit a symmetric shape. But after the phosphorylation reaction was carried out all signals become more diffuse. The red spectrum obtained from the Cbz-protected receptor **45** show a typical peak broadening as it appears due to aggregation. The signals of the Cbz-protection group in the aromatic region at 7.40 ppm (**a**) and at 5.24 ppm (**d**) for the methylene group showed the most significant effect

interestingly. These signals became indistinct so that they nearly disappeared in the noise.

Even the symmetrical shape of triazole methylene group (**e**) is lost after the phosphorylation. All these changes presumably result from partial intermolecular interactions which have a crucial influence on multiplicity and chemical shifts of signals. With the deprotection of guanidine function intermolecular interaction became more important, which was fortified by a further peak broadening in phosphorus NMR.

The ^{31}P NMR was recorded in the proton decoupled mode. Therefore only a singlet peak was expected due to a single phosphate group within the molecule. In figure 4-20 the spectrum of compound **45** (left side) shows a narrow peak at -1.03 ppm and a very broad peak at -5.05 ppm. Initially it was assumed that the origin of the broad peak is caused by some residual phosphorylation side product. But in comparison with ^{31}P NMR of the RGD-receptor **46** it turned out to be an additional signal of the same compound.

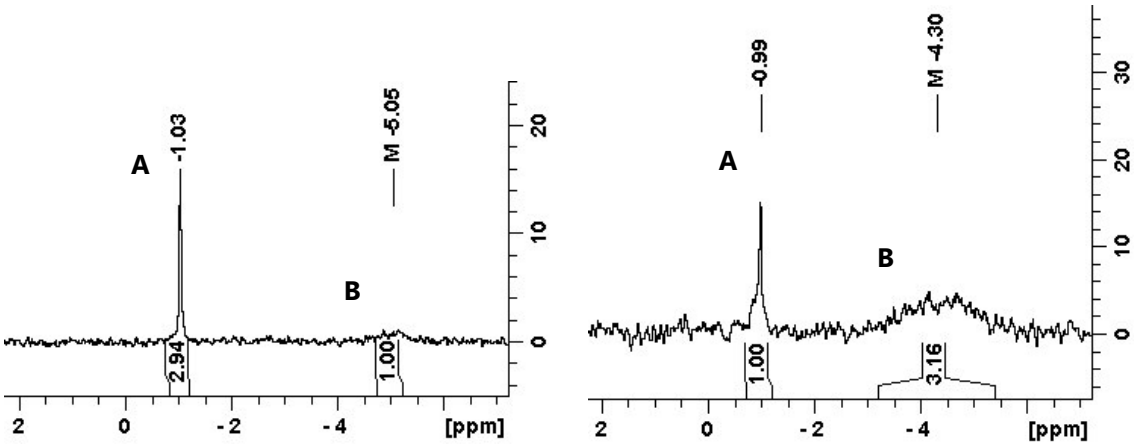

Figure 4-20. ^{31}P NMR spectra of compounds **45** (left) and **46** (right) reveal a shift in the peak proportion. The proportion of peaks A and B became inverse after the deprotection of the guanidine function. This shift indicated some self-aggregation of receptor **46**.

In principle an effect caused by different concentrations could be estimated. But the solutions of both compounds were prepared in the similar concentration range of. The CBZ-protected compound **45** was measured in a concentration of around 4.20 mM whereas the concentration of the DMSO solution of the RGD-receptor **46** was lower (3.00 mM). In comparison the concentration of compound **46** was a bit lower than of precursor **45**. Therefore the beginning of a self-aggregation process was considered. But this will be discussed later in detail. The final Cbz-deprotection of the guanidine function was executed in a THF-solution in the presence of Pd/C under hydrogen atmosphere and yielded 83 % of receptor **46** (fig. 4-21). A TLC control could not be carried out due to solubility problems.

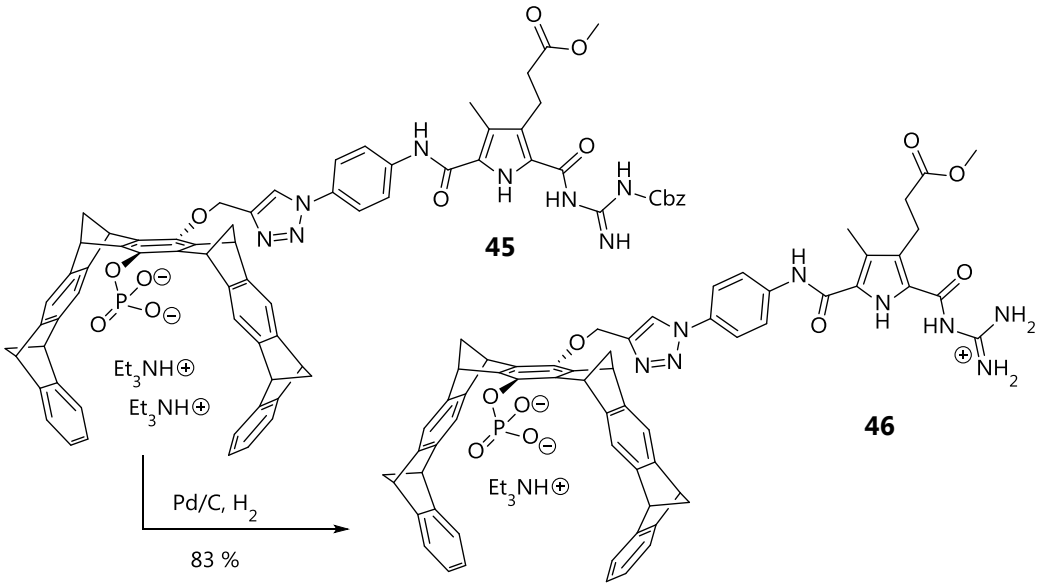

Figure 4-21. Synthesis pathway of 1st generation receptor **46**. Cbz-deprotection was carried out in the last reaction due to previous mentioned problems.

The synthesized compound **46** exhibited extremely bad water solubility. Especially no proper eluent could be found to carry out either normal or reversed phase chromatography. The complete conversion to the final product could be estimated only. Via TLC control no shifts of any substance could be found after the cleavage. The characterization via ^{1}H NMR became even more complicated because of an extreme peak broadening compared to compound **45**. The ^{31}P NMR spectrum (fig. 4-20) shows exemplarily the broadening. Due to this broadening a superposition of signals occurred, which made a distinct assignment impossible.

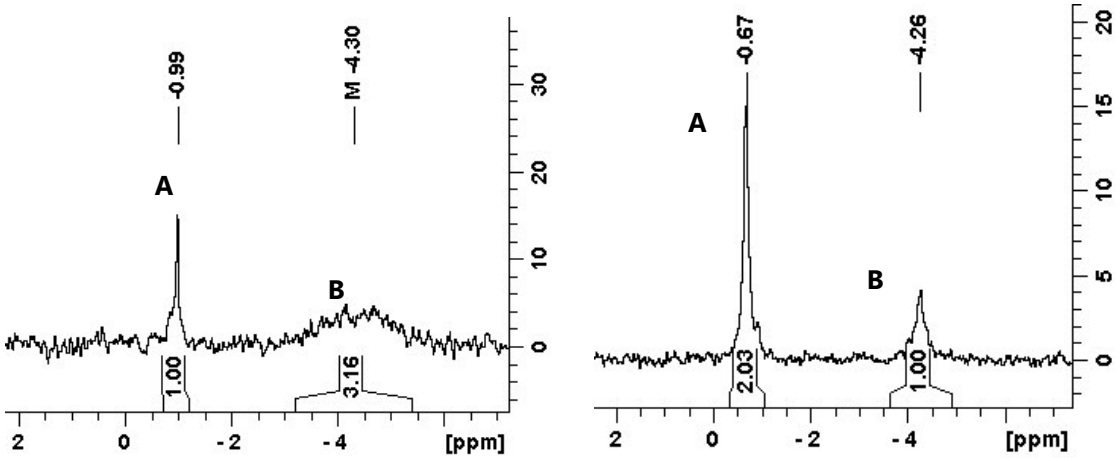

Figure 4-22. ^{31}P NMR of compounds **46** at room temperature (left side) and 90 °C (right side). Proportion of peaks A and B became inverse after deprotection of guanidine function.

But interestingly the ^{31}P NMR spectra at different temperatures of compound **46** revealed a change in the proportions of the sharp signal A and the broadened signal B (fig. 4-22). The temperature dependent NMR experiments of receptor **46** were

carried out at room temperature (left side) and at 90 °C (right side) respectively. Peak B decreased significantly compared to peak A. The integrals exhibit nearly an inversion. The signal ratio A/B changed in favor of signal A from 1:3 to 2:1. The hypothesis is that the deprotection of the guanidine function enabled the molecule to carry a positive charge and therefore facilitated the molecule to form aggregates with the complementary phosphate group. Most interestingly signal B reveals a lower broadening compared to the room temperature spectrum.

This investigation confirmed the hypothesis that compound **46** is able to form aggregates. Even the solubility of the final RGD-receptor in most solvents was too low for any further analysis. DMSO turned out to be the best solvent for molecule **46**. The low solubility in most solvents might be a result of the affinity to undergo self-aggregation. To obtain at least suitable mass spectra from molecule **46** aqueous DMSO solutions with a content of at least 10 % DMSO were necessary to detect the molecule via ESI method. Especially in pure water receptor **46** was nearly insoluble. All other solvent mixtures with lower DMSO content resulted in suspensions even at a µM concentration range. To obtain a proper solution for mass spectrometry a 50 µM DMSO-d6 stock solution was prepared and diluted in the ratio 1 to 10 with methanol. The molecule could be detected as single charged and double charged ion in negative ionization mode.

For further measurements like UV-experiments or AFM-measurements some previous solubility checks were done. A feasible solution of Water/DMSO mixtures were obtained from pure DMSO stock solutions. Thereby the content of DMSO could be minimized to 10 %. Further measurements and binding studies of receptor **46** are described in chapter 4.3.2. Facing the problem of low water solubility of first generation RGD-receptor synthesis of receptor with enhanced water solubility was deliberated. The synthesis of an improved RGD-receptor is described in the following chapter.

4.2.5 Synthesis of the 2nd Generation RGD-Receptor

Additional water solubility enhancing groups at “key-positions” for an improved RGD-receptor were considered. The reduced solubility of receptor **46** in aqueous media is mainly caused by the extended aromatic skeleton of the tweezer. One phosphate group in the vicinity is obviously not enough for compensation. Even the linker molecule, containing a triazole and a benzene ring did not provide any improvement of water solubility.

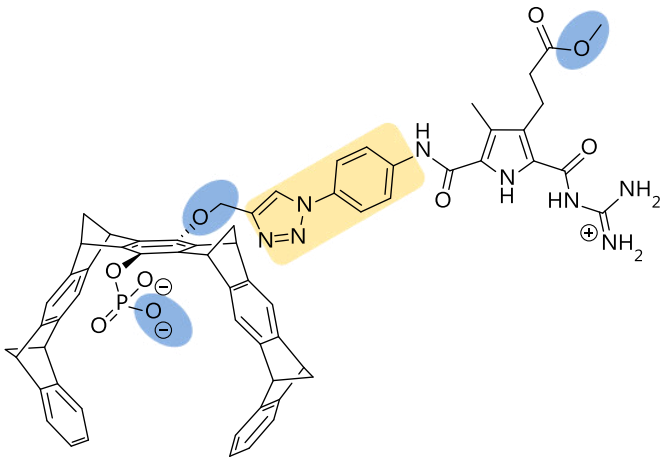

Figure 4-23. Suitable positions for an introduction of a solubility enhancing group are marked in blue. The region of the aromatic linker (beige) needs to remain unsubstituted to avoid any steric hindrance for substrates.

But these unsubstituted aromatics are necessary to prevent intramolecular self-recognition. Any further addition of sterically demanding groups to prevent self-recognition of the binding motif would decrease the ability to recognize RGD-substrates probably. Calculations of substituted aromatics showed indeed a negative influence on the recognition potential, but are not reported in this work. Therefore only the positions highlighted in blue were considered for a reasonable attachment of an additional group (fig. 4-23). A supplementary functional group at the periphery of the pyrrole building block is discussed in chapter 4.3.3. Because of stability problems with azide carrying pyrrole building blocks, the focus was set to the tweezer moiety. Here the bay positions of the tweezer offer suitable possibilities for an insertion of solvent enhancing groups.

As a suitable functional group a second phosphate group was considered. The addition of a second phosphate group in the vicinity to the tweezer skeleton might solve solubility problems as bisphosphonate and bisphosphate tweezers show an inherent better water solubility.[46,89] Furthermore a tweezer moiety containing two phosphate groups might be more attractive to the guanidine residue of arginine. The two most promising positions are right at the central part of the tweezer. Although an additional phosphate attached to the first one like in a pyrophosphate could be obtained via phosphoroimidazolides,[90] the insertion of the second phosphate between aromatic linker and tweezer was favored. The synthesis scheme of an un-symmetrical diphosphate **50** is shown in figure 4-24.

Two different synthesis strategies were developed. As a first idea a synthesis deduced from the normal diphosphate tweezer should lead to the diphosphate tweezer mono-alkyne. The insertion of the alkyne function should occur during the quenching process of the bis(phohoroxydichloride) tweezer **48** (fig. 4-24). The addition of propargyl alcohol to a highly diluted solution of tweezer **48** is important.

Therewith a multiple substitution at the tweezer should be suppressed mostly. Subsequently the diphosphate mono-alkyne tweezer **50** should be generated by a hydrolysis of the residual chlorides.

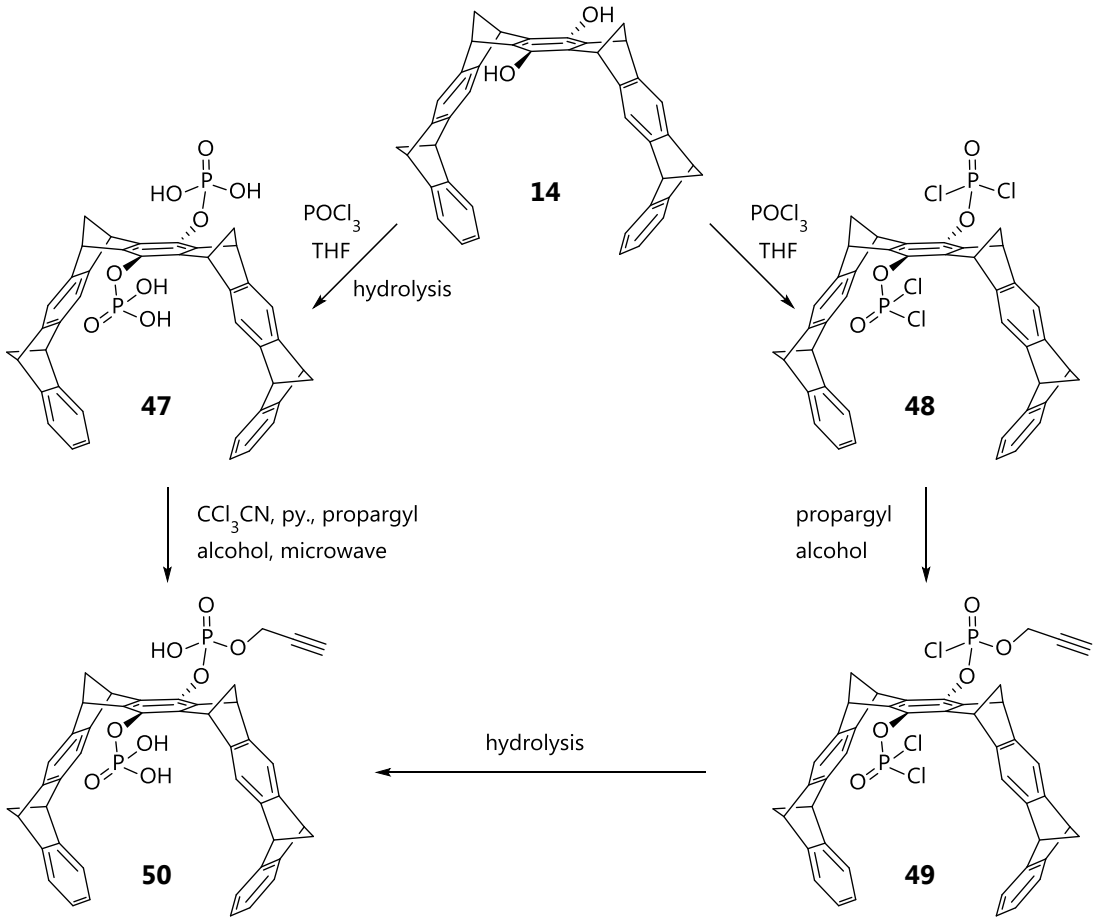

Figure 4-24. The left side shows the analogous pathway of described synthesis protocol.[91] Proposed one-pot synthesis of the mono-alkyne diphosphate tweezer **50** is shown on the right.

The second pathway takes advantage of a selective mono esterification with trichloroacetonitrile as an activating agent (fig. 4-24, left side). The phosphate ester synthesis is described with a monophosphate compound under microwave conditions.[91] Compared to the reported synthesis the pathway via the diphosphate tweezer **47** would suffer from the similar problem of a multiple functionalization.

A supplementary esterification of the second phosphate could not be excluded. After some test reactions in collaboration with *Gersthagen* and *Schrader* on diphosphate aryls this method was skipped due to problems with selectivity of mono functionalization and purification problems. The previous reaction pathway, shown on the right side in figure 4-24, was pursued instead. Therefore the pathway was tried on the truncated tweezer **19b** (fig. 4-25). The results should be used to check the efficiency of the proposed one pot synthesis.

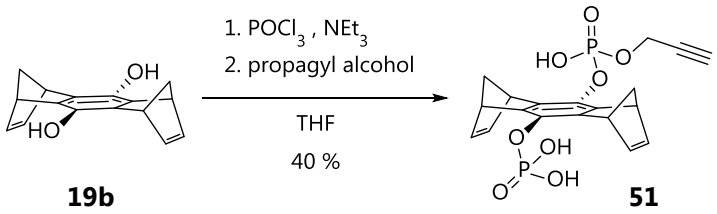

19b **51**

Reaction conditions	Reaction A	Reaction B	Reaction C	Reaction D
Initial concentration of starting material	33 mM	84 mM	84 mM	168 mM
Equivalents of added $POCl_3$	11.0	20.0	10.0	5.00
Equivalents of added propargyl alcohol	0.80	1.00	1.03	1.00
Equivalents of triethylamine	4.40	40.0	x	10.0
Temperature before the addition of propargyl alcohol	only rt	rt, 40 min at 50 °C	1.5 h at 66 °C	30 min at 50 °C
Yields of compound **51** after purification	~10 %	40 %	traces	15 %

Figure 4-25. One-pot synthesis of central diphosphate mono-alkyne **51** worked in moderate yield with respect to the selectivity of a mono functionalization. The table shows different reaction conditions of the parallel synthesis batches.

In parallel synthesis batches single parameters like temperature, concentration of reagents and reaction time were changed. The table in figure 4-25 summarizes the different conditions that were changed between the different reaction batches. Generally all reactions were carried out under argon and started with an ice cold THF-solution of molecule **19b**. As best conditions those of reaction B could be identified in this parallel synthesis approach. It yielded 40 % of the purified mono-alkyne diphosphate **51**. The most critical part seemed to be the temperature control during the reaction process. If the mixture was too cold most of the intermediates were not converted properly. This could be revealed with the conditions of reaction A. With the use of mass spectroscopy some chloric compounds could be detected. If the reaction mixture was treated too hot (more than 60 °C over a period of 1.5 h) most of the intermediates decomposed obviously (Reaction C). As a hint of this assumption only some traces of the desired mono-alkyne diphosphate **51** could be detected. The optimized reaction was carried out under Schlenck technique.

A solution with a concentration of 84 mM of the hydroquinone **19b** in previous dried THF was cooled down to 0 °C. The addition of an excess of phosphorus oxychloride (20 eq.) as well as triethylamine (40 eq.) was done fast by syringe.

The mixture was allowed to warm-up to room temperature for 4 hours. To ensure a full conversion the solution was heated to 50 °C for 40 min. Subsequently solvent and residual phosphorus oxychloride were evaporated in high vacuum. The following addition of 1 equivalent of propargyl alcohol was done very slowly at 0 °C. The final hydrolysis in THF/water solution for 24 h led to the desired product **51**.

Separation of the mono-alkyne **51** from starting material as well from the double alkynylated side product could be achieved via MPLC under reverse phase conditions. As a result from this approach of parallel syntheses some critical points could be figured out. Beside the necessary exclusion from water an excess of 20 eq. of phosphorus oxychloride revealed to be essential. The reaction processes were controlled via mass spectrometry and HPLC. Therefore small amounts of the reaction mixture were treated in a small scale work-up. The crude material was filtered over small syringe filters to remove insoluble parts. The solvent of the filtrate was removed under vacuum and the samples were prepared for analyses.

All attempts to transfer these reaction conditions to dihydroxy tweezer **14** failed. Unluckily all tries resulted in crude mixtures, which did not give any reason of hope to obtain a useful amount of product. Further changes in reaction control by temperature or speed of addition of phosphorus oxychloride and propargyl alcohol did not lead to improved results.

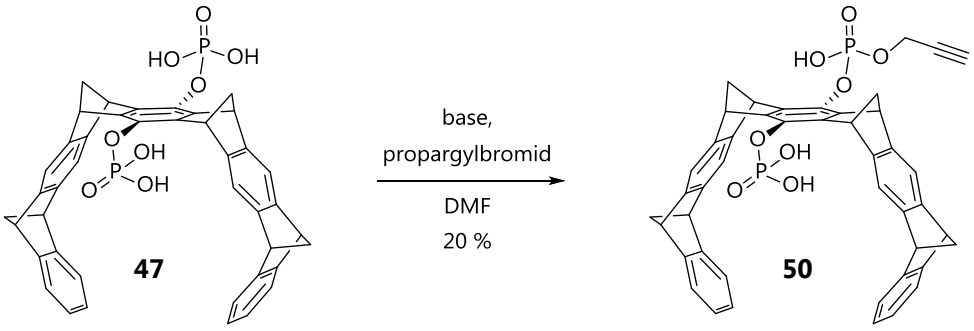

Figure 4-26. Synthesis of mono alkyne diphosphate tweezer **50** via S_N2 reaction with propargyl bromide.

A selective mono alkynylation of the diphosphate tweezer **47** was tried in analogy to *Williamson* ether synthesis in an another approach. The deprotonated phosphate was supposed to react with the propargyl bromide (fig 4-26) in a nucleophilic substitution reaction. A similar reaction was realized before to obtain the mono-alkyne tweezer **31**, which was synthesized for 1st generation RGD-receptor. The desired mono-alkyne diphosphate tweezer could be obtained in a yield of 20% after purification.

Initially a promotion of the S_N2-reaction with potassium carbonate as base was tried. The propargyl bromide was added slowly to the reaction mixture as a

DMF-solution. But no conversion of starting material could be observed with HPLC-MS. In a small-scale reaction with reobtained and purified starting material sodium hydride as a stronger base was used. The stronger base should ensure a full deprotonation of phosphate groups and enhance nucleophilicity consequently.

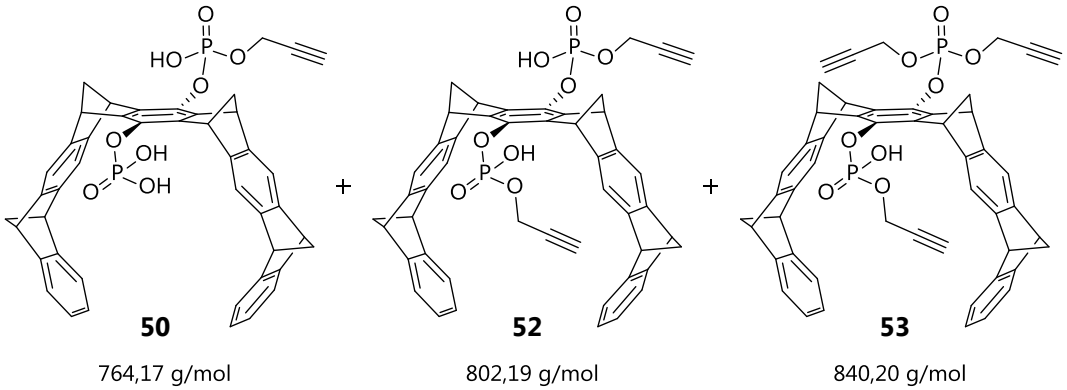

Figure 4-27. Due to 4 hydroxy positions different degree of alkynylation could occur. The exact masses of the three different alkynylation products are given below corresponding molecule.

The small-scale reaction yielded a mixture of mono- (**50**) and di-alkyne (**52**) products (fig 4-27) in a ratio of approximately 2.5:1. All products could be detected via HPLC-MS in an acceptable resolution for a supplementary preparative separation. The tri-alkynylated diphosphate tweezer **53** or even higher alkynylated compound could not be detected.

Using the Schlenck technique the reaction was repeated on a bigger scale. The reaction progress of alkynylation was monitored via HPLC-MS. The addition of a 200 mM propargyl bromide solution to a 35 mM solution of the diphosphate tweezer **47** was carried out stepwise. The previous test reaction revealed that the reagent propargyl bromide was necessary in a large excess in order to obtain a suitable amount of mono-alkynylation product. To control the reaction progress and find the right amount of propargyl bromide, reaction control via HPLC was done after each addition step.

In figure 4-28 the reaction progress after addition of 1.0 equivalent of sodium hydride and 2.4 equivalents of propargyl bromide is shown. The chromatogram of the HPLC-MS analysis reflects the composition of alkynylation products in reaction mixture after stirring the reaction mixture overnight.

The three peaks in UV-chromatogram (a) belong to the starting material **47** at a retention time of 5.63 min, the mono-alkyne diphosphate tweezer **50** at 5.96 min and the di-alkyne diphosphate tweezer (**52**) at 6.24 min. respectively. This assignment could be made by the additional total ion chromatogram shown in figure 4-28 c and the extracted mass spectra at the individual peaks. The masses were obtained via an Ion Trap Mass Spectrometer of *Thermo Fisher* which had a lower performance than

the Q-TOF mass spectrometer from *Bruker*. Therefore the masses were not that exact compared to the high resolution mass spectrometer from *Bruker*. Finally more than 12 equivalents of propargyl bromide were added until a maximum of mono alkynylation could be achieved. It was assumed that the high amount of propargyl bromide was needed due to some internal side-reaction of propargyl bromide by itself. The reaction was stopped at a ratio of 3:5:2 of starting material (**47**), mono alkyne tweezer (**50**) and di alkyne tweezer (**52**) respectively.

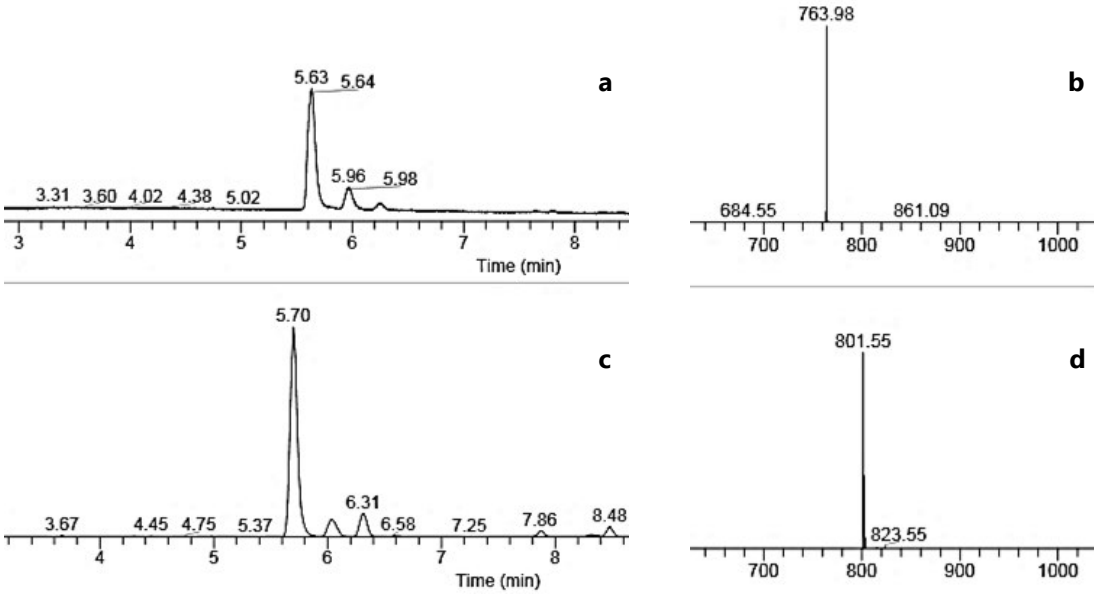

Figure 4-28. The reaction control of the synthesis of the mono alkyne diphosphate tweezer **50** via HPLC-MS carried out on reversed phase revealed three peaks in UV-chromatogram at a wavelength of 210 nm (a). The total ion chromatogram (TIC) (c) shows the same peaks in a time shift compared to the UV-chromatogram (a) due to a delay of the successive measurement technique. The mass spectrum at 6.02 min (b) and 6.31 min (d) pictures represent the mono-alkyne (**50**) and the di-alkynylated compound (**52**) respectively.

The purification of desired mono alkynylated product was executed with preparative HPLC on reversed phase silica. Transferring the separation conditions from analytical HPLC-MS to preparative separation method led to a general problem. The additive ammonium acetate was used to buffer the eluent and guarantee a complete removal via lyophilization afterwards. But unfortunately some blueish complex with the tweezer molecules especially with the alkynylated ones was generated. New separation conditions were investigated with triethylamine to adjust pH-value to slightly basic conditions only.

Additionally a significant decrease of peak resolution occurred with higher amounts of substance, so that only 1-2 mg of raw material could be purified in one run. The chromatograms of the crude mixture (preparative run) as well as of the purified mono-alkyne tweezer **50** are shown in the appendix (fig. 7-24).

The chromatogram of the preparative run revealed the ratio mentioned above. To achieve an improved peak resolution the separation method was adjusted to step gradients. Therewith the desired peaks could be eluted from the column separately. Especially the separation of unconverted starting material from alkynylated products could be enhanced.

Unluckily the purified starting material contained small amounts of the mono- and di-alkyne diphosphate tweezer, although the column was washed carefully after each separation step. This phenomenon could not be explained by problems due to an overloaded column capacity compared to the analytical separation. Rather a possible self-assembly process of the different tweezer species might explain this separation problem.[92] This effect might be more severe at higher concentrations of the tweezer as they were used for a preparative purification process. The purification of the truncated tweezer **51** could be achieved easily via MPLC in contrast. The yield of the diphosphate mono-alkyne tweezer **50** was pretty low. Compared to the small diphosphate mono-alkyne tweezer **51** the yield was only half. Beside the different synthesis procedure the reduced yield originated mostly from problems of separation.

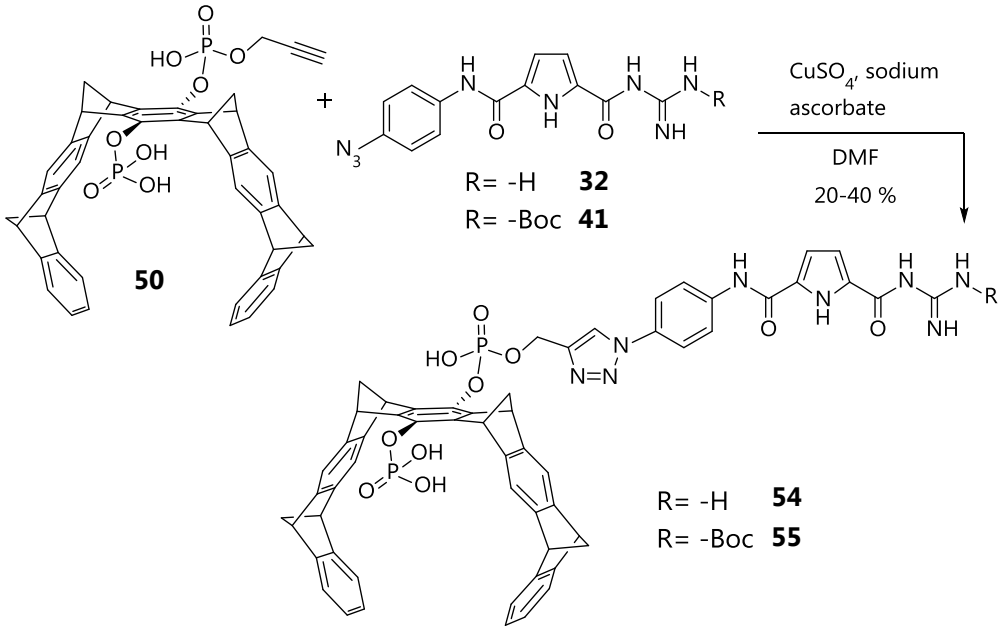

Figure 4-29. A possible access to the water-soluble RGD-receptor **54** or receptor precursor **55** via a cycloaddition of tweezer **50** and azido pyrrole **32** and **41** respectively is shown.

Further formation of the triazoles **55** and **54** by cycloaddition of mono-alkyne tweezer **50** and guanidinocarbonyl pyrroles **41** and **32** were performed in DMF under copper catalysis respectively (fig. 4-29). Under stirring at room temperature a suspension developed in both cases. TLC revealed that initial starting materials were converted completely, but unluckily the obtained product could not be eluted on

solid phase with an appropriate solvent. ^{1}H NMR of precipitate and filtrate showed abnormal signals which were obviously caused by paramagnetic copper(II)-ions which led to unpredictable chemical shifts and modified relaxation times.[93] Therefore no reliable analysis via NMR could be done. The only analytical proof of a successful synthesis could be accomplished via mass spectrometry. Mass samples were prepared as methanol solution of substance containing 5 % TFA. Interestingly the mass could not be found in high performance mass spectrometer but clear evidence could be found in nominal mass spectrometer. Therewith the desired precursor **55** could be detected as a single negativly charged species.

To remove undesired copper salts different attempts were made. The addition of sodium sulfide or the addition of QuadraSil® MP to scavenge the copper did not lead to a good result. The use of QuadraSil® MP led to absorption of most of the product. The silica based scavenger showed the same problems such as other purification methods based on silica like chromatography. Due to additional solubility problems scavenging of copper with sodium sulfide was not reasonable. Elsewise loss of desired product would be too big. Even solubility problems of unprotected receptor **54** might be caused by a strong self-aggregation and inhibited MS-analysis. By reasons of all the problems of insufficient analysis and purity check no further investigations in binding studies of compounds **54** and **55** were made. Because of an easier access and purification of the small tweezer **51** synthesis was progressed according to a fully convergent synthesis method.

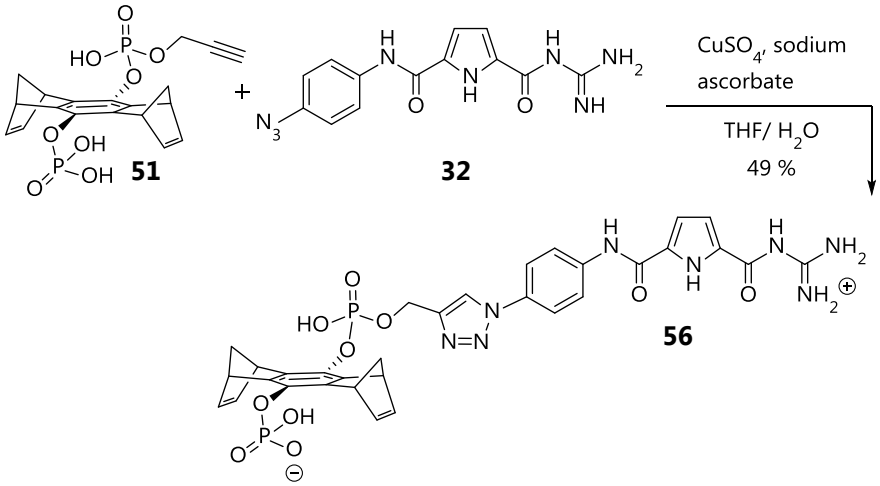

Figure 4-30. Convergent synthesis of the water-soluble RGD-receptor **56** of the truncated tweezer **51** and unprotected pyrrole **32** was realized via copper catalyzed cycloaddition.

The 2nd generation RGD-receptor **56** was assembled in last synthesis step by a cycloaddition of the unprotected azido pyrrole **32** and diphosphate mono-alkyne **51** (fig. 4-30). The reaction was carried out in THF/water solution at room temperature and yielded receptor **56** in 49 %. The initial suspension of azido pyrrole **32** dissolved

with progress of the reaction. The precipitation of copper sulfide from aqueous solution via sodium sulfide did not lead to a sufficient removal of the copper. Chelating agents like EDTA with the purpose to act as a suitable scavenger were also tried unsuccessfully. As a consequence the proton NMR could not be evaluated properly. Again the paramagnetic copper(II) led to a broadening of resonances due to slow relaxation times.[94] Therefore it was tried to remove the copper by precipitation of obtained product. An almost neutral solution of crude mixture was adjusted to pH 2 by addition of 0.1 M solution of hydrochloric acid. The precipitated product could be obtained easily by filtration afterwards. A repeated dissolving and precipitation resulted in a yield of 49 % of purified receptor **56**.

Again ^{1}H NMR suffered from peak broadening, so that evaluation was not easy either. Signal broadening was mostly assumed by intermolecular interactions of free binding sites. But most promising the ^{31}P NMR experiment at neutral pH conditions and at 80 °C showed two distinct signals with similar integrals at 0.98 and -3.39 ppm (fig. 4-31). The 2 different signals could be expected due to different substituted phosphate groups.

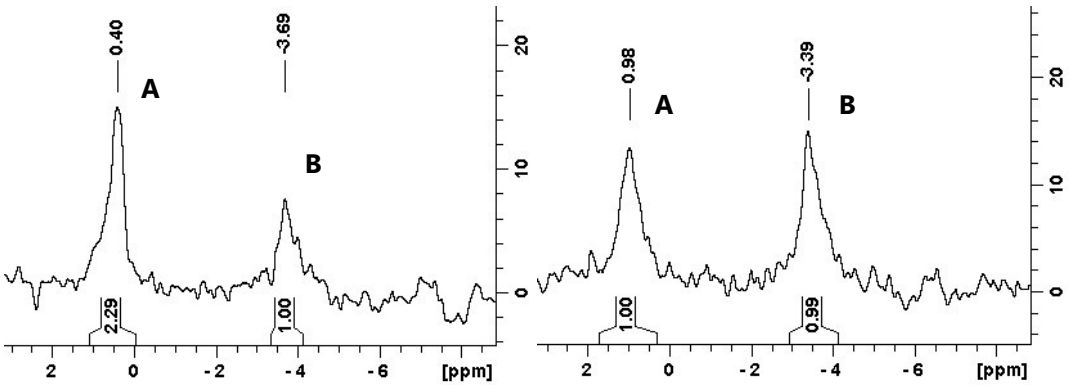

Figure 4-31. ^{31}P NMR of RGD-receptor **56** at 25 °C (left) and at 80 °C (right) showed two different species.

Remarkably the measurement of the ^{31}P-NMR at room temperature led to a down-field shift paired with an increase of signal A. In contrast signal B underwent a high-field shift paired with a decrease of signal. The ratio of signals A and B turned from 1:1 at high temperature to 2:1. This might be a hint for of aggregate formation like a dimerization process. At 80 °C the compound seems to appear monomolecular in solution as the ratio of both signals is 1:1. It could be assumed that the self-aggregation is less distinct compared to the 1st generation RGD-receptor **46**.

The purity control via HPLC failed due to the inapplicability of eluents for the solid phase material. But the TLC check on reversed phase revealed that receptor **56** remained at the starting position while the starting materials could be moved forward. Thus a full conversion was considered. The reduced yield could be explained

by purification method. Through precipitation by pH change some substance still maintained in solution with unwanted copper salts.

Within the last reaction step a convergent synthesis to the ditopic receptor **56** could be investigated. The first approach to a receptor containing a full tweezer did not lead to a water soluble molecule. Unluckily the introduction of a second phosphate to the tweezer to enhance solubility and realize receptor **54** and receptor precursor **55** was unsuccessful due to problems in purification. The most significant problem was a decrease of solubility after the cyclisation to the triazoles. Presumably this was caused by a strong self-aggregation tendency of the obtained molecules.

A clear improvement could be achieved through the truncation of the aromatic skeleton of the tweezer. In combination with a second phosphate group a full water soluble receptor **56** could be synthesized. Additionally the synthesis of the building blocks could be carried out separately to fulfill a convergent synthesis. A significant step was the introduction of the azide at the pyrrole moiety which turned to out as an interim problem with respect to stability (fig. 4-15). Both building blocks the azido guanidiniocarbonyl pyrrole **32**[95] and the truncated diphosphate mono-alkyne tweezer **51** could be synthesized in similar yields of 6.5 %. In particular some unselective reactions like the formation of *syn*-dimethanoanthracenedion **19a** reduced the yield by more than 50 %. Nevertheless the application of a convergent synthesis strategy led to an acceptable overall yield of more than 3 % of the RGD-receptor **56** with respect to each of both building blocks. The new designed receptor **56** with an improved water-solubility was used in UV-binding studies which are described in chapter 4.3.6. The preparation of the guest peptides that were used in these studies is described in the following chapter.

4.2.6 Syntheses of the RGD-Peptides

For binding studies of the developed RGD-receptors **46** and **56** three different RGD-peptides were synthesized, one linear tripeptide and two cyclopeptides containing the RGD-sequence in a fixed conformation (fig. 4-32). The linear tripeptide **P1** has both end positions capped. At the *C*-terminus an amide is obtained after cleavage from resin. The *N*-terminus carries an acetylated amine function, which was synthesized after last deprotection of the Fmoc-group. The capping of both termini was done to prevent from possible interactions of the free functional groups in the binding event with the RGD-receptor. A competition of the free acid position of the *C*-terminus and the acid function of side chain of aspartic acid for guanidiniocarbonyl pyrrole moiety might be the consequence.

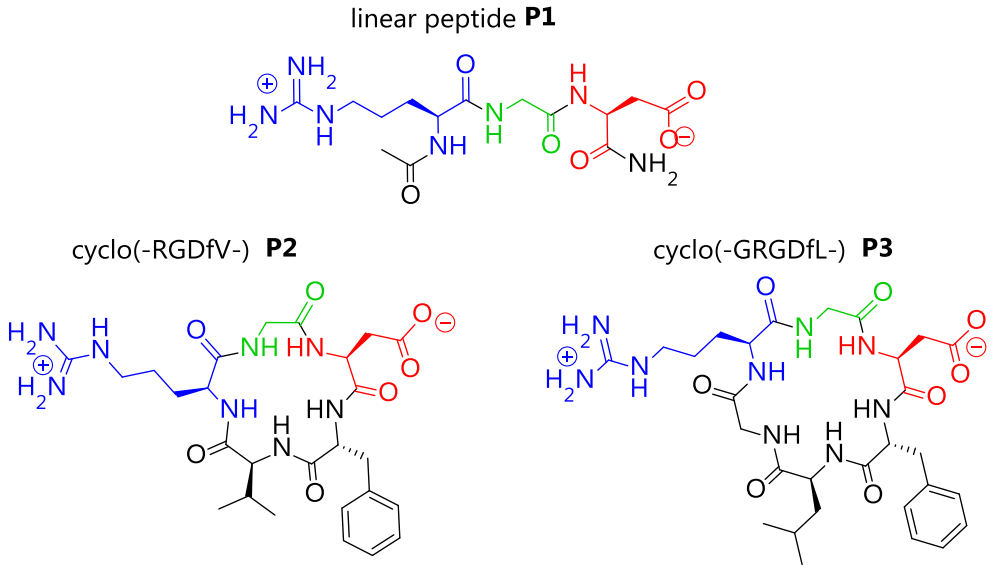

Figure 4-32. Overview of peptides used for receptor evaluation. RGD sequence is more bent in the penta-peptide cyclo(-RGDfV-) (**P2**) than in the hexa-peptide cyclo(-RGDfLG-) (**P3**). Conformation of last one is more closed to conformation of the linear peptide **P1**.

In analogous way a free *N*-terminus might be in a competition with the guanidinium function of the arginine. To eliminate these interaction possibilities enables comparable conditions between linear and cyclic RGD-peptides. Through the cyclisation the latter do not carry any free carboxylate or amino group elsewise than within their side chains.

The main difference between the cyclic peptides **P2** and **P3** is given by the bending of their RGD-sequence. In the hexa-peptide the bending is more relaxed and approximates the fully flexible and linear RGD-tripeptide **P1** whereas the peptide **P2** has a smaller radius because of one amino acid less than in **P3**. This difference should be significantly measureable by checking the association constants with a proper receptor. It is assumed, that a more bent substrate will show a smaller association constant compared to a more relaxed or linear peptide substrate, if receptor's binding sites are stretched by a linker molecule like it is in RGD-receptor **56**.

The peptide syntheses were carried out under standard peptide synthesis on solid phase (SPPS). The progress of each step in peptide synthesis was observed with a *Kaiser* test.[96] All coupling steps were done twice to ensure an enhanced yield. Synthesis of the linear peptide **P1** was executed with Rink Amide MBHA resin followed by an acetylation reaction of the free amine function. Purification was done with MPLC under reversed phase conditions to yield 56 % of **P1**.

The synthesis of the cyclic peptides was carried out with chlorotrityl chloride resin. The resin takes advantage from very mild cleaving conditions. Slight acidic conditions led to cleavage from the resin but spared all side chain protection groups. These

protection groups are essential during the following cyclisation reaction of the linear peptide strand. After cleaving the linear peptide sequence with a solution of DCM, 2,2,2-trifluoroethane (TFE) and acetic acid (3:1:1), cyclisation was done in a very low concentration with the use the coupling agent propylphosphonic anhydride in solution, also known as T3P. The peptide strand synthesis followed by cyclisation was carried out according to literature known synthesis protocol.[97]

In a first purification step the protected cyclic peptides were separated from byproducts of the cyclisation reagent T3P via normal phase chromatography. Further deprotection under classical conditions with DCM/TFA solution was followed by a final purification via MPLC under reversed phase conditions. Purified cyclic RGD-peptides cyclo(RGDfV) (**P2**) and cyclo(GRDGfL) (**P3**) were obtained in yields of 5.2 % and 2.2 % respectively. All peptides were obtained as TFA-salts after purification because 0.05 % TFA was added to the eluent. Due to evaporation of the solvent after purification process the TFA-salt was obtained and considered in yield and preparing of solutions for UV binding studies. Purity checks of obtained peptides were carried out with analytical HPLC. The purity refers to the UV-absorbance and detection was done at different wavelengths due to different absorbance maxima. For the linear peptide **P1** 220 nm was used as an observing wavelength. For the cyclic peptides containing the chromophore phenylalanine the wavelength 258 nm was used additionally.

The linear peptide **P1** could be obtained in a purity of almost 96 % whereas purity check of cyclic peptides discovered particular impurities at 220 nm (fig. 4-33). At a wavelength of 220 nm the cyclic peptides **P2** and **P3** revealed purities of 92 % and 88 % respectively. At a wavelength of 258 nm purity of cyclic peptides looked much better and reached values of 93-95 %.

The low yields of the cyclic peptides were expected due to their longer peptide chain compared to the tripeptide **P1**. In addition their synthesis required a cyclisation step. In general the reaction conditions under high dilution should diminish inter-molecular coupling of the peptide chains and enhance the intramolecular head-to-tail reactions. Although the cyclisation reactions were carried out carefully some peptide chains might have reacted to longer chains or bigger cycles than the desired penta or hexa-cycles. Therefore the obtained yields are in a reasonable yield. For a similar peptide sequence a yield of 79 % with respect to the amount of glycine coupled to the resin.[97] The reported yield sounds rather high with respect to the problems that accompany cyclisation reactions generally.

Consequently the most impurities originated from byproducts of coupling or cyclisation reaction and did not contain aromatic residues like phenylalanine. Even

side-products from cleaved protection groups might be contained. Most probably the impurities did not consist of bigger cycles than the desired one.

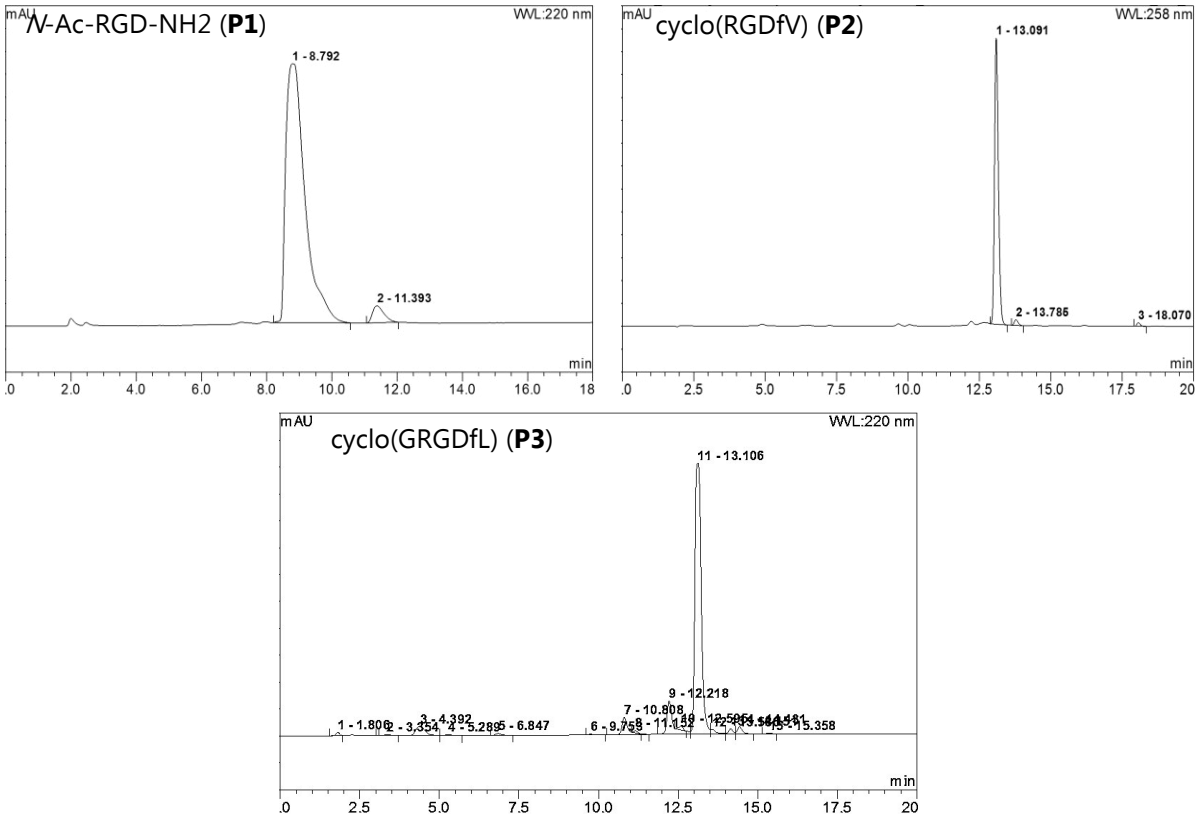

Figure 4-33. The HPLC-Chromatograms of the obtained RGD-peptides showed different purities depending on the observing wavelength. Particularly the purity of the cyclic peptides showed some differences at 220 nm compared to 258 nm.

The Impurities, which could not be removed completely by chromatography, most probably contained coupling agents from linear peptide synthesis and cyclisation reaction. Peptides were stored as TFA salt in freezer at -20 °C.

4.3 Measurements and Results

4.3.1 Determination of Association Constants of Host-Guest-Systems

Determination of the non-covalent association between a host molecule and its guest substrate requires some preliminary consideration. Depending on the expected value of the binding constant K_A the concentration range of initial concentration of the receptor $[R]_i$ is preassigned and given by equation 4.1.

$$\left[R\right]_0 * K_A \leq 1 \tag{4.1}$$

The higher the expected K_A is the lower the chosen starting concentration $[R]_i$ for the receptor needs to be. Within this constraint different measurement methods hold their range of reliability. With NMR technique concentrations of substrate and guest in the low mM range are necessary. Therefore association constants $K_A < 10^4\ M^{-1}$ are reasonable to identify.[59] In contrast to this the UV-Vis spectroscopy can manage concentrations in middle µM range due to a higher sensitivity of this method. Herewith complexation constants K_A up to $10^5\ M^{-1}$ can be determined.

$$k * R + m * S \rightleftharpoons R_k S_m \tag{4.2}$$

$$K_A = \frac{\left[R_k S_m\right]}{\left[R\right]^k * \left[S\right]^m} \xrightarrow{1:1\ complex} K_A = \frac{\left[RS\right]}{\left[R\right] * \left[S\right]} \tag{4.3}$$

A typical element of supramolecular associations is their reversibility which is expressed by the balance equation 4.2. All contributing species reside in an equilibrium state, which allows derivation of association constant via the *law of mass action* (equation. 4.3). Thereby R and $[R]$ indicate the receptor and receptor concentration whereas S and $[S]$ represent substrate and substrate concentration, respectively. Because of a lack of knowledge about the complex concentration $[R_kS_m]$ the association constant K_A could not be determined directly by equation 4.3. Even a determination via correlation of standard-state free energy $\Delta G°$ (equation 4.4) and natural logarithm of association constant requires information about the binding enthalpy $\Delta H°$ and the entropy $\Delta S°$ at the equilibrium of the host-guest-system.

$$\Delta G° = \Delta H° - T * \Delta S° = R * T * \ln K_A \tag{4.4}$$

These parameters could be obtained by isothermal titration calorimetry (ITC) whereas parameters R and T represent ideal gas constant and temperature, respectively. Because of a chromophoric receptor and problems with signal resolution in NMR UV-absorption was used as the preferred method to determine association constants K_A. Due to the fact that this method does not allow any direct access to K_A some mathematical transformations need to be done previously. The formulation of the mathematical model was described in literature in the past so that only a brief version will be recapitulated with annotation to the used literature.[56,59,98]

The problem that association constants could not be derived from equation 4.2 due to an unknown concentration of the host-guest-complex need to be circumvented. For that reason the method of gradually titration of one component (e.g. the guest) to a fixed concentration of the other component (e.g. host) is used. For the following considerations a 1:1 host-guest-system is assumed with the

advantage that the descriptors *k* and *m* get simplified to the value of 1. Thus the complex concentration [*RS*] is given by the difference of total receptor concentration $[R]_t$ and concentration of free receptor [*R*] in equilibrium state equally to the difference of total substance concentration $[S]_t$ and concentration of free substrate [*S*].

$$\left[RS\right] = \left[R\right]_t - \left[R\right] = \left[S\right]_t - \left[S\right] \tag{4.5}$$

$$\left[R\right] = \left[R\right]_t - \left[RS\right] \tag{4.6}$$

$$\left[S\right] = \left[S\right]_t - \left[RS\right] \tag{4.7}$$

Accordingly receptor and substrate concentration within equilibrium are given by difference of their total concentrations and concentration of complex respectively. All above-mentioned relations are expressed by the equations 4.5 to 4.7. Substitution of complex concentration [*RS*], which is given in equation 4.5, in law *of mass action* (formula 4.3) results in equation 4.8. Herein the association constant is only related to the concentrations of the receptor at the beginning labeled by an *i* and the free receptor [*R*] and substrate [*S*] concentrations during the titration experiment.

$$K_A = \frac{\left[R\right]_t - \left[R\right]}{\left[R\right]*\left[S\right]} = \frac{\left[R\right]_t}{\left[R\right]*\left[S\right]} - \frac{1}{\left[S\right]} \tag{4.8}$$

The mathematical approach to obtain K_A takes advantage from the fact that a physical change of an observable, which is correlated to the complex concentration, occurs during the titration steps. Generally this change can be a shift of a NMR signal as well as a change in UV-absorption. Beside the capability of UV-light absorbance the observed substances need to follow the *Beer-Lambert Law* (equation 4.9). The mathematical method is based on this law. This law describes a linear dependency of absorption *A* on concentration *c* at a given layer thickness of cuvette *d*. This dependency is necessary for all participating substances including the complex.

$$A = \varepsilon * c * d \tag{4.9}$$

The observed absorption can exhibit an enforced increase or decrease due to changes in the electrostatic environment of the chromophore. The latter will be influenced by the complexation of substrate molecules because the complexation itself is driven by electrostatic interactions between receptor and substrate. Consequently any difference in the behavior of UV-absorption than the normal

dilution effect has its origin in the formation of a new species, the complex. In UV-titration experiments the observed absorption A_{obs} results from the sum of all absorptions of the single species, which are present in the mixture.

$$A_{obs} = \sum_{x=1}^{3} A_x = \sum_{x=1}^{3} \varepsilon_x * c_x * d \qquad (4.10)$$

This additive behavior of single UV-spectra of individual species (fig. 4-34) can be expressed by equation 4.10. If the necessity of linearity of the absorption behavior for any substance is not fulfilled this mathematical method cannot be applied.

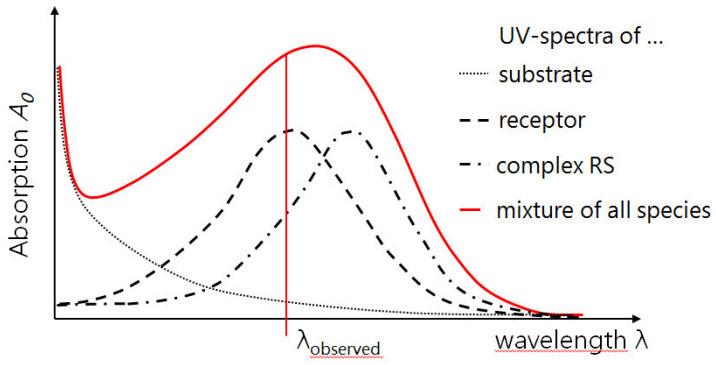

Figure 4-34. Observed spectrum (continuous line) at advanced titration step is a result of addition of single UV-spectra of all present species.

With the premise of a fixed cuvette length of d=1 cm the previous formula is simplified to equation 4.11 containing the three species receptor *R*, substrate *S* and receptor-substrate complex *RS*.[59,58]

$$A_{obs} = A_R + A_S + A_{RS} = \varepsilon_R * [R] + \varepsilon_S * [S] + \varepsilon_{RS} * [RS] \qquad (4.11)$$

For lack of information about the concentrations of the three species receptor [*R*], substrate [*S*] and complex [*RS*] within the equilibrium some transformations and simplifications need to be done to substitute these three unknown parameters by known ones. Further transformations and derivation can be reviewed in literature given by annotations.[56,58,98] As a result one obtains equation 4.12. Therefore unknown parameters will be substituted by known ones and the normal dilution by addition of substrate is taken into acount. This formula requires only initial concentrations of free substrate $[S]_i$ and receptor $[R]_i$ respectively. Initial absorption A_i and absorptivity coefficients ε of pure receptor and substrate solutions could be obtained from pre-measurements.

With aid of the program *origin* this formula enables a determination of K_A via the mathematical method of a non-linear regression. An alternative evaluation could be

executed via a linear regression method. In contrast to previously shown method linear regression methods suffer from unfavorable assumptions due to linearization. Most popular linear regression methods are in particular *Benesi-Hildebrand*, *Lineweaver-Burk* and the *Scatchard* plot. The linear regression approaches suffer from a different weighting of the data. Therefore the results obtained from linear regressions could differ significantly in comparison to non-linear regression analyses.[59]

$$A_{obs} = \frac{A_i}{1+x} - \frac{K_A \cdot \frac{[R]_i}{1+x} \cdot \Delta\varepsilon \cdot \left(\frac{[S]_i \cdot x}{1+x} - \frac{\frac{K_A \cdot [R]_i \cdot [S]_i \cdot x}{(1+x)^2}}{\left(1 + \frac{K_A \cdot [S]_i \cdot x}{1+x}\right)^2 + \frac{K_A \cdot [R]_i}{1+x}} \right)}{K_A \cdot \left(\frac{[S]_i \cdot x}{1+x} - \frac{\frac{K_A \cdot R \cdot [S]_i \cdot x}{(1+x)^2}}{\left(1 + \frac{K_A \cdot [S]_i \cdot x}{1+x}\right)^2 + \frac{K_A \cdot [R]_i}{1+x}} \right) + 1} + \frac{\varepsilon_S \cdot [S]_i \cdot x}{1+x} \qquad (4.12)$$

Equation 4.12 incorporates dilutive effect with the term x/(1+x) caused by gradual titration of substrate to receptor solution. The x represents proportion of added V_a to initial volume V_i per titration step.

As it was mentioned before evaluation according to the presented equation 4.12 is only valid for a complex stoichiometry of 1:1. If another complex stoichiometry or even mixed complexes are existing determination of association constants gets more sophisticated and different computer programs especially made for analysis of spectroscopy data like *SpecFit* need to be used.[60] Nevertheless the stoichiometry of the analyzed complex needed to be determined before. The common technique of continuous variation called the *Job's* method was used.

The method of *Job* uses the corrected absorbance of a single wavelength most likely the maximum of the absorption of the receptor, which is affected by associating the substrate. The corrected absorbance A_{corr} is defined as the observed absorbance reduced by absorbance caused by compounds not being involved in the complexation process [equation 4.13].[62]

$$A_{corr} = A - \left(\varepsilon_S \cdot [S]_t + \varepsilon_R \cdot [R]_t \right) \cdot d \qquad (4.13)$$

$$x_S = \frac{[S]_t}{[R]_t + [S]_t} \tag{4.14}$$

In the *Job* plot the corrected absorbance A_{corr} is plotted as a function of molar fraction of substrate χ_S, which is given by equation 4.14. The molar fraction can range from zero to one (fig. 4-35). Concentrations are used as total ones for all calculations. The maximum of the bell-shaped curve determines stoichiometry by corresponding molar fraction.

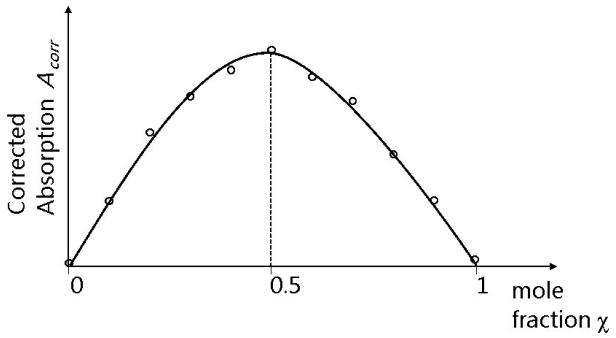

Figure 4-35. Plotting of corrected absorption against molar fraction yields the *Job* plot. The maximum of fitted curve reflects complex stoichiometry. Here the maximum at a molar fraction of 0.5 indicates a 1:1 complex.

Some further conditions need to be fulfilled to carry out *Job's* method correctly. Beside the previous mentioned *Beer-Lambert Law* this method assumes the formation of a single complex predominately. If more than one kind of complex is formed at the same time evaluation of complex stoichiometry gets more sophisticated and needs more assumptions. But the more assumptions are necessary the higher the uncertainty about determined binding constant is.[99] In addition to the previous mentioned requirements pH-value and ionic strength need to be kept constant as well as the total concentration during experiment.

4.3.2 Results of the UV-Titration Experiments with Receptor 46

Preliminary conditions like solubility and *Beer-Lambert* behavior were tested before binding studies were carried out. As mentioned before (chapter 4.2.4) a micro-molar solution of receptor **46** with the addition of 10 % DMSO could be generated. Increasing the proportion of water was always accompanied with precipitation of the receptor at any pH-value. Although a content of 10 % DMSO is not suitable in biological systems first UV measurements were carried out to give some hints for further receptor improvement. Validation of the *Beer-Lambert Law*

was checked with the water/DMSO-solution. The dilution experiment was initiated with a starting concentration of 103 µM of the receptor **46**. The pH was adjusted to pH 6.0 and controlled during the stepwise dilution of the pure receptor solution. For all UV-measurements a Quartz glass cuvette with a maximum volumetric capacity of approximately 1.3 ml was used. The concentrated stock solution was diluted by substitution of 100 µL of the previous solution with 100 µL of clear water/DMSO mixture (9/1) adjusted to pH 6.0 to avoid pH dependent UV-shifts. Under consideration of volume expansion all adjustments of pH were done with 0.1 M hydrochloric acid and sodium hydroxide solution respectively.

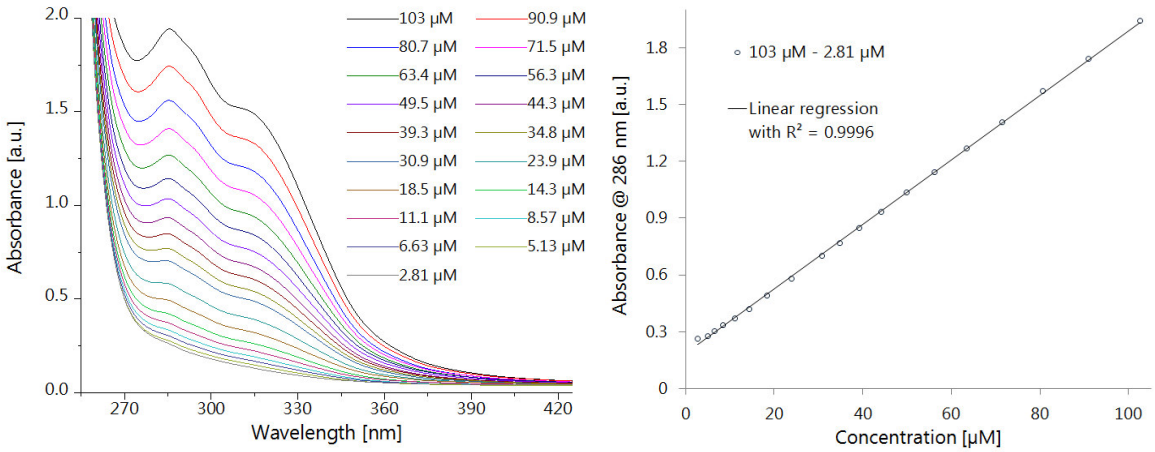

Figure 4-36. Dilution experiment of receptor **46** is shown in left graph. The legend refelects the concentration of sample for each single measurement. The right graph reveals the good accordance to the linear concentration dependent absorbance with 0.9996 as coefficient of determination.

The dilution experiment of receptor **46** (fig. 4-36) revealed a linear dependency of the absorption towards concentration. The screened concentration range reached from 103 µM to 2.81 µM. The analysis was done at the absorption maximum (286 nm) of the receptor, which is corresponding to literature known values for tweezer molecules.[72] As a result of the dilution experiment no concentration dependent UV shifts occurred. The coefficient of the trend line confirmed an almost linear behavior with a value of 0.9996 (fig. 4-36, right side). Only in the low micro-molar region below 10 µM the linear behavior seems to deviate. Therefore no change of aggregation state in the concentration region of interest for binding studies was assumed. This assumption is based on the fact that aggregation of receptor molecules itself will have a significant change in absorption due to changes in electrostatic environment of chromophores. Such systems are crucially influenced by changes of their concentration.

Preliminary binding studies were carried out with the most flexible RGD triad **P1**. The initial concentration of the receptor **46** was 36.8 µM. The pH-value (pH = 6.6) of

the ligand solution was adjusted in same way as for the receptor solution. Although the titration of the ligand peptide was done carefully no distinct and useful UV-shifts were recorded (fig. 4-37). At the left side the overlays of UV-spectra show some unexpected changes. Generally the whole shape of the single UV-spectrum changed during the addition of the quest peptide **P1**. At the right side the change of the absorbance maximum at 286 nm is plotted in dependency of the addition of further substrate.

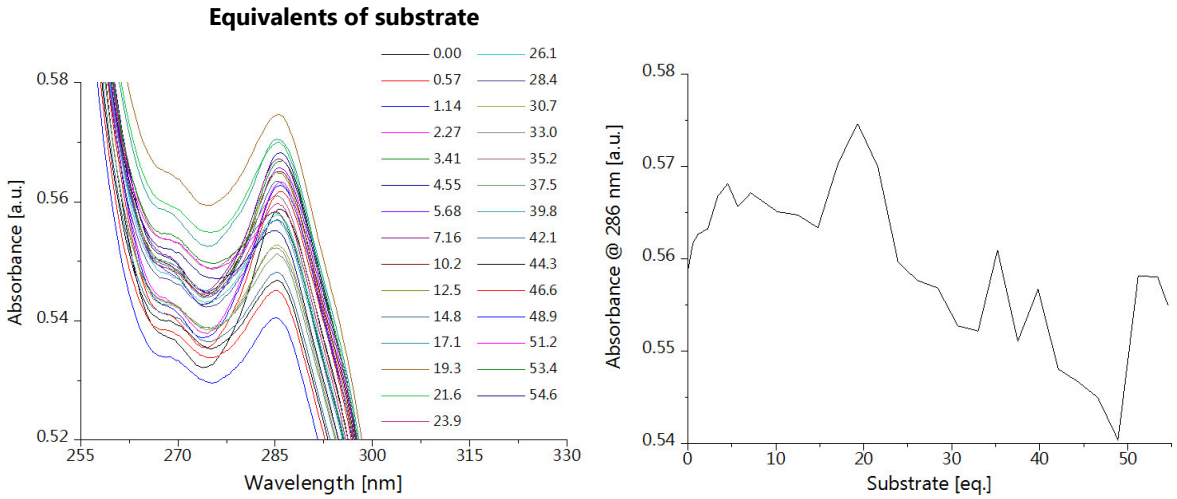

Figure 4-37. On the left side UV titration experiment of receptor **46** with linear RGD-peptide **P1** is shown. Equivalents of added substrate are given in the legend. On the right side absorbance at 286 nm is plotted as a function of added substrate equivalents.

These observed changes were rather unexpected and did not show any clear trend. In principle the absorbance change was rather small so that the significance of these changes is very low. Even a repetition at a higher host concentration of around 50 µM did not yield better results.

In summary the generated data of the first binding studies were not good enough for any continued evaluation. The reason for this phenomenon might be a strong self-association of the RGD-receptor **46**. During the dilution experiment (fig. 4-36) no hint of a self-association could be detected. Within the concentration range that was used to check the validity of the *Beer-Lambert Law* no concentration dependent changes occurred. To get some more information about aggregation behavior of molecule **46** DLS and AFM measurements were executed.

4.3.3 Imaging of Supramolecular Structures with AFM

Imaging structures of solids in sub-nanometer resolution is the power of AFM. The technique is based on investigations of scanning tunneling microscopy (STM)

developed by *Binnig*, *Rohrer*, *Gerber*, and *Weibel* in the early 1980's.[100] From there on AFM developed as a method that extended limitations of STM technique.

Though STM requires conductive samples the material can be non-conductive for measurements with AFM. The operation mode of the AFM is reproduced in figure 4-38 at the left side.

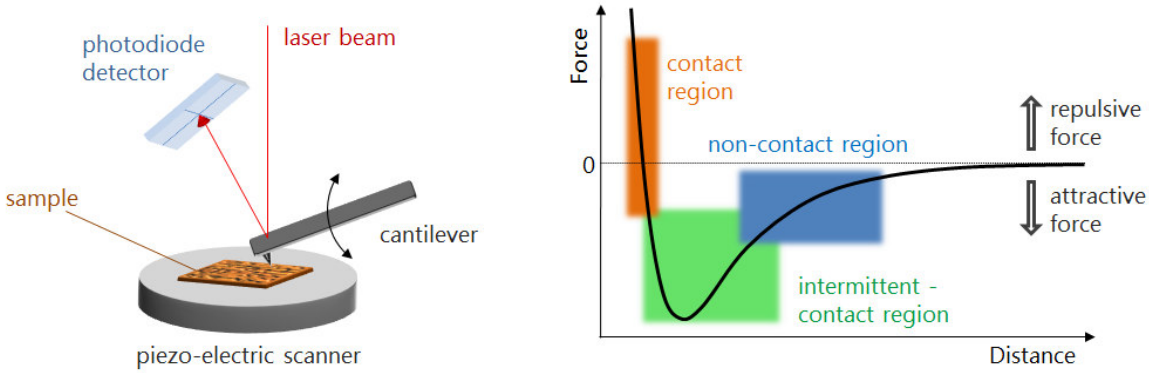

Figure 4-38. On the left side the operation mode of AFM technique is represented. Here an oscillating cantilever is shown, which is used in non-contact and intermittent-contact mode. Right picture shows the *Lennard-Jones-Potential*, which describes the force as a function of distance between probe and sample. (modified graphics in style of *Richter*) [101]

Within this work the intermittent-contact mode also known as tapping mode was used exclusively and will be described briefly. The tip of a cantilever is scanning a sample while the cantilever is oscillating in this mode. The movement of the cantilever is influenced strongly by attractive and repulsive forces caused by the sample. The movement is detected through reflection of a laser beam focused on a photodiode detector. Changes in the oscillation behavior like amplitude or oscillation speed can be recognized by the photodiode detector. The vertical position (called Z-position) of the tip is determined by a feedback signal from detector to the piezo scanner. Consequently the resulting image received by AFM technique is not direct but indirect and computer-assisted. All theoretical descriptions about the intermittent-contact mode including detailed information about the appearing forces can be retrieved from several publications.[102–105]

Compared to measurement techniques that afford recording an observable for further evaluation of association constants atomic force microscopy (AFM) is a visualization method. The usefulness of AFM measurements in this work is limited to visualize possible self-assembly. Unfortunately measurements can only be carried out with samples deposited on a surface. Hence images received by AFM do not reflect conditions in solution. In the case of receptor **46**, which is not capable of being measured in UV-titration experiments, AFM allows getting some insights of

intermolecular interaction behavior. Thus AFM is used to get a better understanding of aggregation affinity.

4.3.4 Results of AFM-Measurements of Receptor 46

All AFM images were recorded with an Innova SPM equipped with an AFM NanoDrive. Evaluation of the obtained pictures was done with the computer program *Gwyddion*. In general samples were dissolved in appropriate solvents and applied to a mica surface via spin coating process. 1 µL of the sample solution was applied with an *Eppendorf* pipette to the target surface. The mica target was rotated at 60 rps during the application. Afterwards the prepared sample was allowed to dry for 1 min at the same rotation speed.

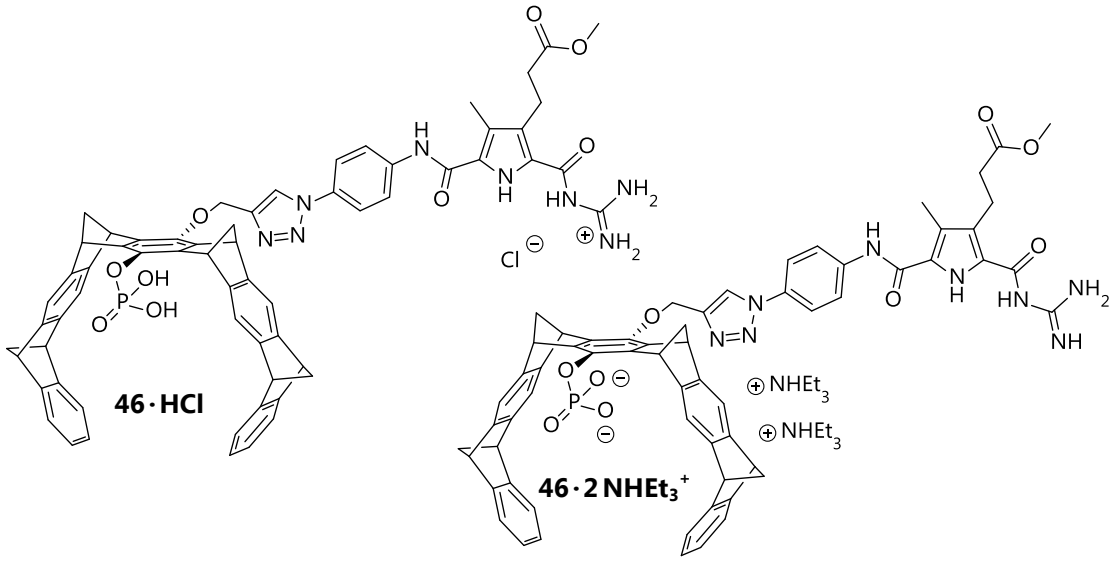

Figure 4-39. The RGD-receptor **46** shown with fully protonated (left side) and deprotonated functional groups (right side) respectively.

To get a better understanding of the aggregation behavior of receptor **46** several AFM images were recorded under basic, neutral and acidic conditions respectively. Because of receptor's tendency to precipitate in acidic aqueous solutions it was dissolved in pure DMSO to ensure comparable concentrations at the different protonation states. The aim was a comparative study on the self-aggregation behavior under diverse protonation states. Especially the contribution of both binding sites depending on the protonation states should be analyzed. Under acidic conditions the phosphate group is supposed to be almost fully protonated and therefore less attractive for guanidinium groups (Fig. 4-39). At basic conditions a fully deprotonated phosphate, which is accessible for positive charged molecules, and a guanidino group are present.

Initially an aqueous suspension of molecule **46** was prepared. Basic and acidic conditions were achieved by addition of triethylamine and hydrochloric acid in slight excess respectively. Slightly acidic conditions as they appear in malignant tissue (pH 6.0) were realized by pH adjustment. A suspension of receptor **46** in water was controlled by a *Hamilton* electrode. The complete removal of water was realized by lyophilization of the suspension afterwards. The residual solids were diluted in pure DMSO to obtain the final solutions of the receptor **46** in desired protonation state for AFM-measurements.

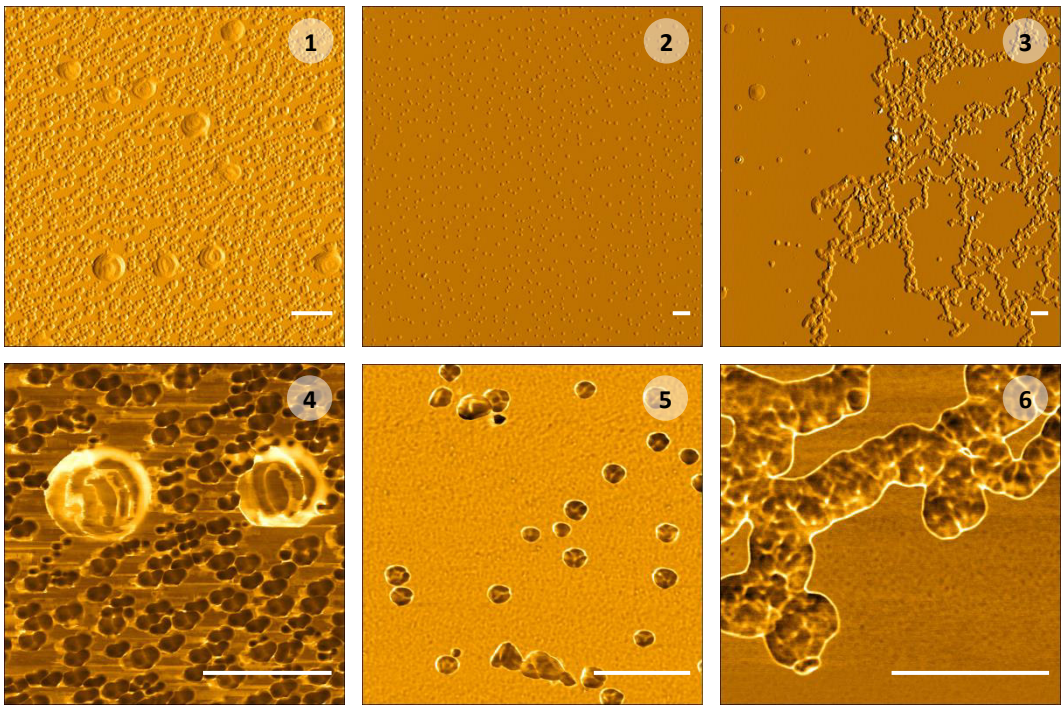

Figure 4-40 AFM-pictures. Tapping amplitude images **1**-**3** give an overview whereas second row phase images **4**-**6** show more detailed receptor **46** under alkaline (**1**, **4**), marginally acidic (**2**, **5**) and acidic (**3**, **6**) conditions respectively. The white scale bars were standardized at 1 µm.

Measurements were repeated at least three times at different positions of a single sample. To ensure regularity of results each sample was prepared two or three times newly and measurements were done repeatedly. An overview of the images at different conditions is given in figure 4-40. Alkaline and neutral DMSO solutions yielded almost similar spherical structures at concentrations up to 829 µM.

Exclusively under strong acidic conditions RGD-receptor **46** showed an inherent affinity to extended branched columnar structures. The images are made from a solution at a concentration of 377 µM (fig. 4-40, picture 3 and 6). In border regions some smaller particles could be found too. But most parts of the samples revealed a network like structure with similar dimensions. Their height varied between 5 to 10 nm and the width between 200 - 500 nm approximately (fig. 4-41). In contrast basic and almost neutral conditions led to significant smaller particles with a

spherical shape and an equally covered surface. The tendency of higher supramolecular aggregates to rods and networks for example could not be found even at higher concentrations.

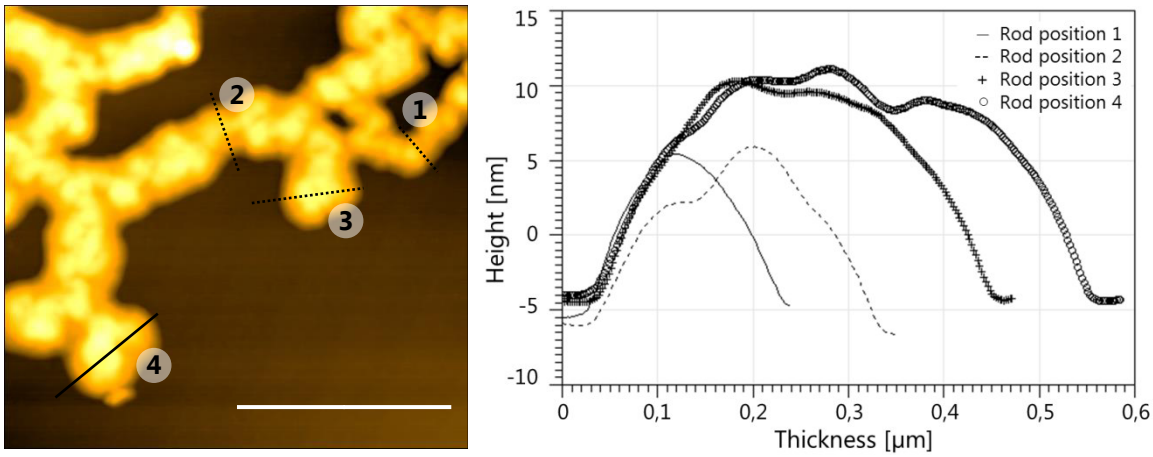

Figure 4-41. AFM-height image of columnar branched network (compare with fig. 4-40, right side) and height profiles of smallest (**1**) and most extended (**4**) parts respectively. The dashed black lines in height image represent the position of measurement. The dimensions are given by white scale bar (1 µm).

Rather a fully covered surface was obtained if the concentration was raised above 900 µM for alkaline and almost neutral environment. In detail at alkaline conditions at a concentration of 637 µM round shaped particles with a height among 10 to 35 nm appeared. Their average diameter was between 200 to 800 nm (fig. 4-42). Due to their halo-like appearance in tapping phase image they seemed to be some kind of vesicles. Beside those spherical structures smaller particles could be found which were determined as impurities originated from triethylamine. This could be verified by comparing AFM-pictures of substance-free triethylamine/DMSO solutions of separate AFM-samples.

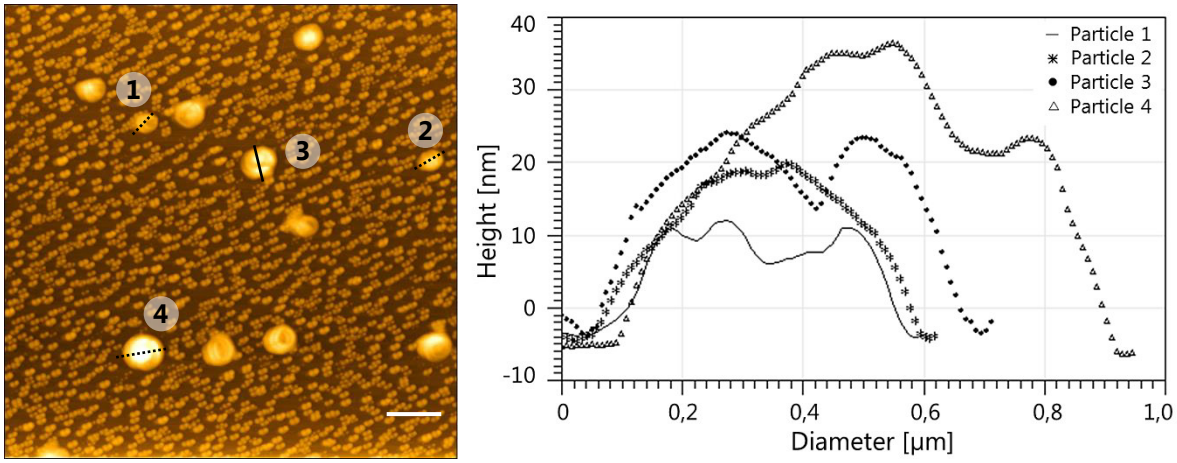

Figure 4-42. AFM-phase image and height profile vesicular particles under alkaline conditions.

A similar behavior of formation of smaller structures was seen under neutral conditions. At a concentration of 829 µM kind of vesicular architecture appeared too. Strikingly the size distribution is narrow compared to other conditions. Heights of particles varied from 10 to 30 nm and particle diameters from 100 to 250 nm could be found. Particles obtained under neutral and alkaline conditions showed a remarkably similarity. Their surface did not appear homogenous but showed kind of a grooved structure. Some of the particles showed a higher degree of engraving than the others. The profile plots extracted from the measurements under neutral and alkaline conditions revealed this characteristical shape of the structures (spherical structure **3** in fig. 4-42 and fig. 4-43).

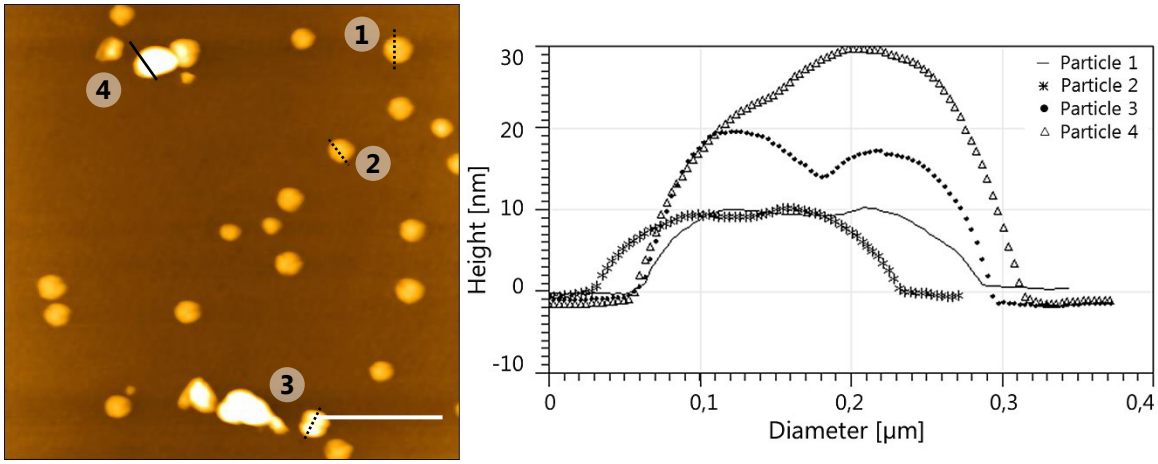

Figure 4-43. AFM-phase image and height profile vesicular particles under almost neutral conditions.

Most probably those smaller structures arose from oligomers building up some accumulated aggregates. Those aggregates could have a more loosely structure to explain the grooved particles. A more detailed and enhanced study via AFM of the aggregates was not made. But AFM-pictures showed impressively, that receptor **46** has the ability to form aggregates. Even though the solvent and concentration is different to those used for UV/ViS-binding studies the results from AFM pictures might explain, why previous binding studies on receptor **46** failed. Because AFM pictures reflected only solidified particles additional method for determination of particle size in solution was considered.

4.3.5 Size Determination of Supramolecular Structures with DLS

Dynamic light scattering (DLS) is most commonly used for the analysis of nanoparticles like colloids. The measurement technique is based on random changes in intensity of laser light scattered from particles in solution. Those changes are

caused by *Brownian* motion, a random thermal motion. "This random movement of particles in a liquid is due to the bombardment by the molecules that surround them".[106]

The *Stokes-Einstein* relation describes the particle size in dependency from diffusion coefficient (equation 4.15).

$$D_h = \frac{k_B T}{3\pi\eta D_t} \tag{4.15}$$

Herein D_h reflects the hydrodynamic diameter of measured particles which is mandatory needed for the size determination. The hydrodynamic diameter is reverse proportional to translational diffusion coefficient D_t and calculated via *Boltzmann`s* constant k_B, thermodynamic temperature T and the dynamic viscosity η. Further information can obtained from appropriate literature.[106]

This technique allows size measurements of aggregates formed in solution and homogenous suspensions. Therewith this technique has an outstanding advantage compared to AFM. To avoid a precipitation of the RGD-receptor **46** a pure DMSO solutions was prepared. To get conditions as close as possible to those to the previous analyses a prior suspension of the receptor in water was set to a pH of 6.0. After lyophilization a 8.59 mM DMSO solution of **46** was prepared. To avoid foreign particles the DMSO was filtered over a nylon filter (pore-size: 200 nm) before. The prepared solution was treated with ultrasonic sound for 30 min to ensure homogeneity of the sample.

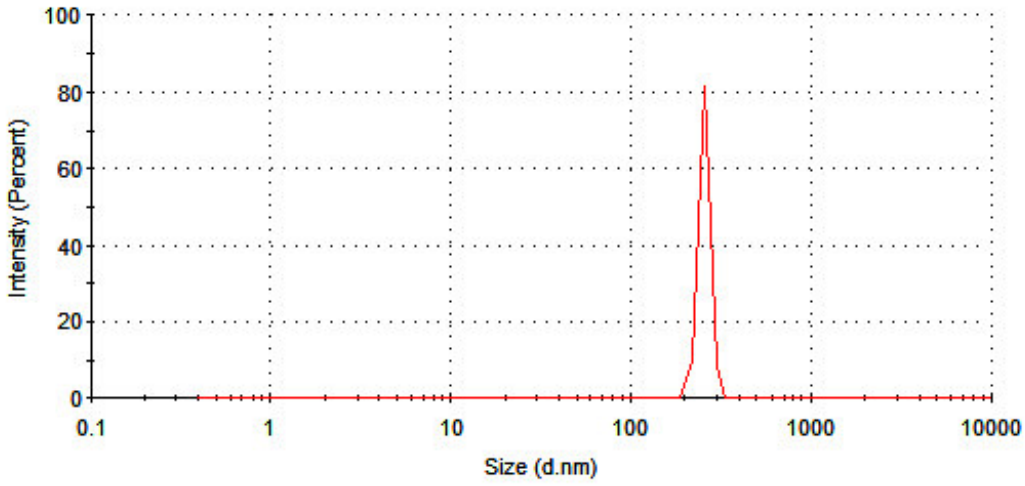

Figure 4-44. Exemplary DLS measurement of 8.59 mM DMSO-solution of **46**. Size distribution is given by intensity.

The DLS measurements revealed particles with an average size of 255 nm (fig. 4-44). Indeed the determined size of the particles match with the results of the

previous AFM experiments. The particles obtained from a neutral solution showed an average size of around 230 nm (fig. 4-43, spherical structure **2**). Coincidental a very high PDI of around 0.8 was calculated by the Zetasizer software. A polydispersity index of 0.7 and higher is equivalent to a very broad size distribution of particles in the measured sample. In contrast to this result the AFM revealed a rather small size distribution at slightly acidic conditions. In comparison of both methods it needs to be considered that DLS measurements were executed on solutions of the receptor. The data of the AFM-measurements were recorded from solid material. With respect to these differences the results of the average size of the particles were similar in a first approximation.

Although the obtained size distribution in figure 4-44 looks promising another source of problem might have some influence on the quality of the measurements. The receptor solution shows some brownish color. The observed color resulted from the chromophore of the spacer molecule azido aniline. Generally the solutions need to be free of suspended particles and colorless to prevent wrong analysis of the software. Further measurements with diluted solutions did not lead to other results. Therefore no additional investigations on DLS-measurements were done.

In combination with results from previous AFM studies the molecule **46** is suggested to undergo self-assembly at even low concentrations. If the receptor molecules tend to build aggregates and did not appear as single species initial UV-titration experiments can be interpreted better. The self-assembly character of receptor **46** might lead to a mixture of different species. During the titration experiment oligomeric aggregates like vesicles, dimers and receptor guest complexes might be in a special mixture. Due to the titration of an antagonistic ligand this previous order becomes imbalanced. Some aggregates would become more favored than others and these changes might lead to a change in UV-absorption and the shape of the single spectrum shown in figure 4-37. Therefore no reliable evaluation of binding constant was possible. To conclude the artificial RGD-receptor **46** turned out to be useless for further binding studies.

4.3.6 Results of the UV-Titration Experiments with Receptor 56

Before the binding studies of the RGD-receptor **56** (fig. 4-45) were carried out the validity of the *Beer-Lambert Law* was checked. At a pH range from 5 to 8 the receptor showed a good water-solubility so that a 5 mM aqueous solution at pH 6.0 could be realized. This stock solution was used for further UV-binding studies. The dilution experiment started with a 228 µM solution of receptor molecule at a pH of

6.0. Buffered solutions during the titration experiments were not used due to possible interactions of buffer salts with the binding sites of receptor or substrate respectively. Phosphate buffers e.g. could be in direct competition with the phosphate groups of the tweezer.

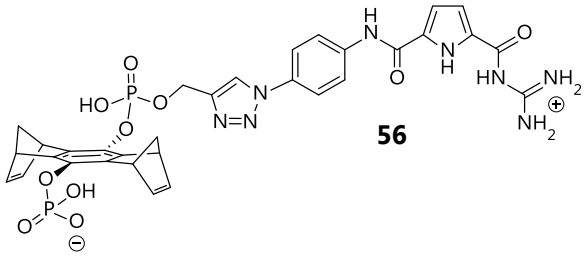

Figure 4-45. Structure of the 2nd generation RGD-receptor **56** showed a significantly better water-solubility compared to the 1st generation receptor.

Therefore the pH value was controlled by a *Hamilton* Minitrode between the single UV-measurements. The concentration of the receptor **56** was reduced stepwise by replacing aliquots of receptor solution with water at pH of 6.0 (fig. 4-46). The limit of a good quality absorbance was reached at a concentration of 11.5 µM. In the second graph the absorbance of each measurement was plotted against the receptor concentration. The coefficient of the linear regression indicated a linear absorption behavior in dependency of the concentration at the maximum of 306 nm.

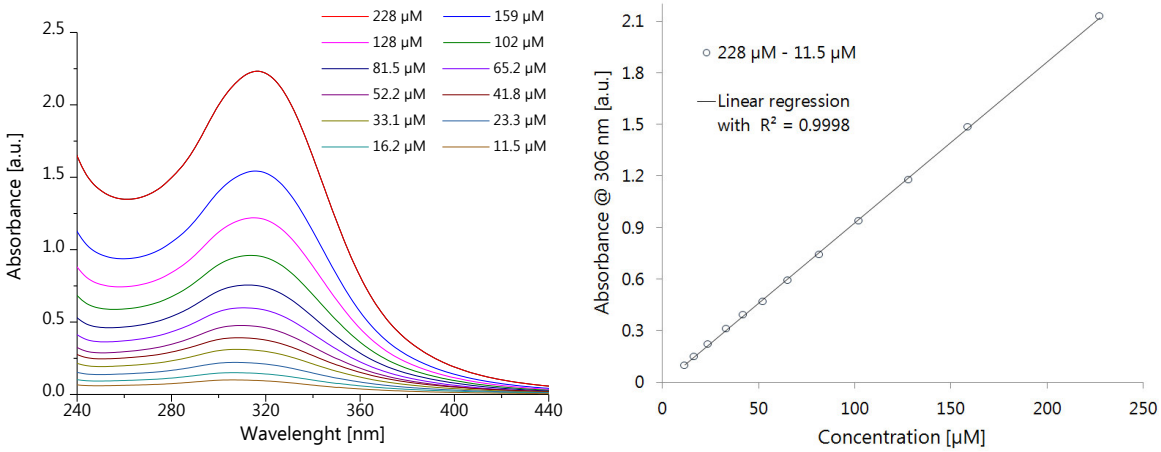

Figure 4-46. Dilution experiment in the range from 228 µM to 11.5 µM. The good quality of linearity of concentration dependent absorbance is given by the coefficient of determination in the right graph.

In a next step the UV-titration experiments of the receptor **56** with the RGD-peptides **P1** to **P3** were carried out respectively. In figure 4-47 the UV-spectra of two titration experiments are shown exemplarily. The spectrum of the linear peptide **P1** at the left side shows only one maximum at 306 nm. This maximum originated from the chromophore of the receptor molecule and decreased during the titration

experiment. All data points of the titration experiment obtained at 306 nm were used for further analysis of the binding constant. The decrease can be explained in parts by the dilution of the receptor. Any further changes referred to additional interfering effects. These effects are supposed to be caused by the interaction of the receptor with the guest substrate.

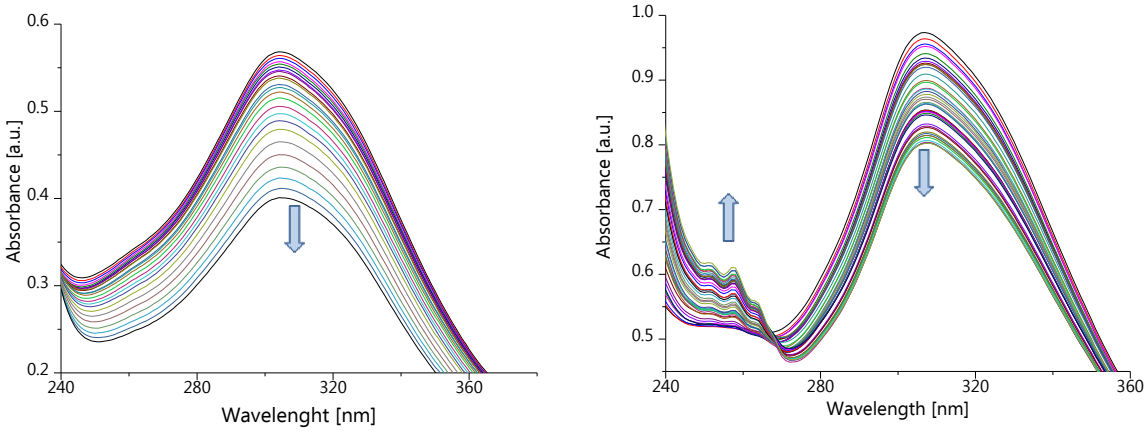

Figure 4-47. UV-spectra from UV-titration experiments of receptor **56** and peptide **P1** (left side) and the cyclic hexa-peptide **P3** (right side). Determination of binding constant occurred at absorbance maximum at 306 nm indicated by arrow pointing downwards. Absorbance increase (arrow pointing upwards) at 260 nm resulted from phenylalanine in the cyclic peptides.

The determination of the binding constants was done in accordance to equation 4.11 which was introduced in chapter 4.4.1. Therefore the intensity at the absorbance maximum is plotted versus the equivalents of substrate that were added. These equivalents are represented by the ratio of volumes of substrate to receptor (V(S)/V(R)) (fig. 4-48).

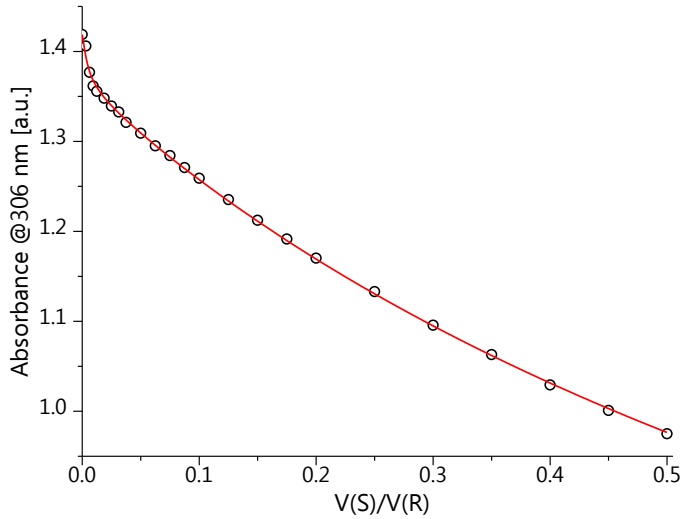

Figure 4-48. The decrease of absorbance is observed at 306 nm and plotted against the ratio of volumes of substrate to receptor [V(S)/V(R)]. The diagramm displays the fitted binding isotherm (red line).

In the first experiment the total amount of the added peptide **P1** was 73.2 equivalents with respect to the used quantity of the receptor. With the assumption of a 1:1 complex formed by the receptor and the guest peptide this experiment yielded a binding constant of 34,300 ± 4,900 M^{-1}. All repetitions of this titration experiment resulted in an averaged binding constant of 33,700 M^{-1} with a standard error of 5,280 M^{-1}. The same procedure was done with the circular peptides **P2** and **P3**. With an average binding constant of 12,700 ± 5,960 M^{-1} the interaction of the hexa-peptide **P3** was three times stronger than with the penta-peptide **P2**. With the guest peptide **P2** an average binding constant of 4,300 ± 980 M^{-1} could be determined.

In comparison the titration experiment of the guest peptide **P3** showed the highest relative standard error compared to the other peptides. The relative error is nearly 50% of the evaluated binding constant K_A. For both cyclic peptides the relative error showed the highest values. On grounds of this and because of a relative small K_A value of 4,300 M^{-1} the titration experiments of the cyclic peptides were repeated with slightly higher concentrations of the guest peptides. However the repetition of the titration experiment with an increased concentration of guest peptide **P2** led to unexpected shifts in the UV-spectrum compared to peptide **P3**. The used peptide concentration for the repetition was 150°times higher than the receptor concentrations.

In figure 4-49 the irregular shifting is shown. The increase of the maximum at 258 nm and the decrease of the maximum at 306 nm showed an abnormal strong shifting in the beginning and after addition of around 8 equivalents of substrate. The magnification of the UV-spectrum (right spectrum) showed the clear aberration of the expected shifting (blue arrow in the left spectrum).

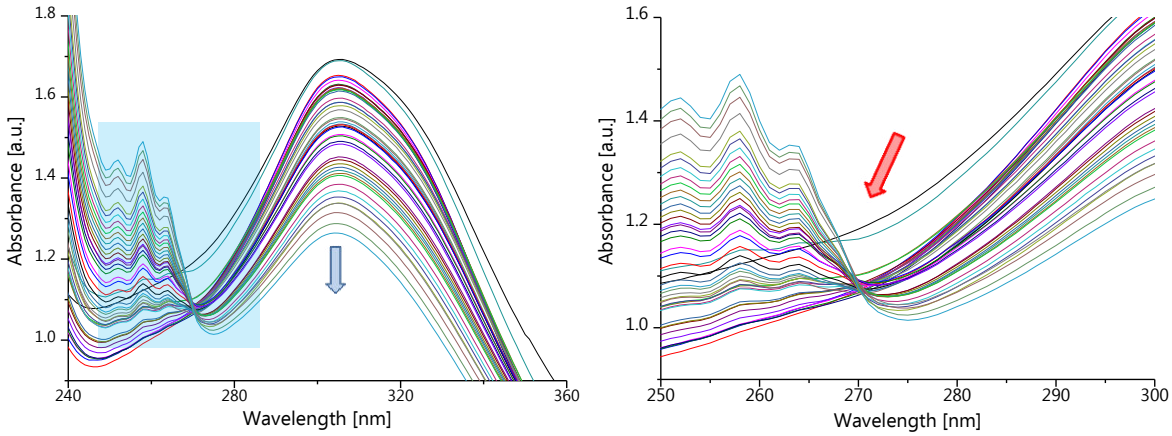

Figure 4-49. UV-titration experiment of penta-peptide **P2** and RGD-receptor **56** with an increased peptide concentration showed some divergences of UV-shifts during the titration. The enlargement (light blue area) in right picture revealed some unusual increase of absorption (red arrow).

The red arrow in figure 4-49 indicates the regions that reveal these unexpected strong shifts. Most strikingly some UV-measurements showed some complete different spectra. Due to these shifts the non-linear regression analysis could not be carried out. Even with disregarding those measurements the regression analysis could not be carried out normally. The observed shifts were similar to those that were found with receptor **46** and peptide **P1** (fig. 4-37). It is assumed that additional interactions than the desired complex formation occurred. For the circular peptide **P3** these affects did not appear and same binding constants were found as before.

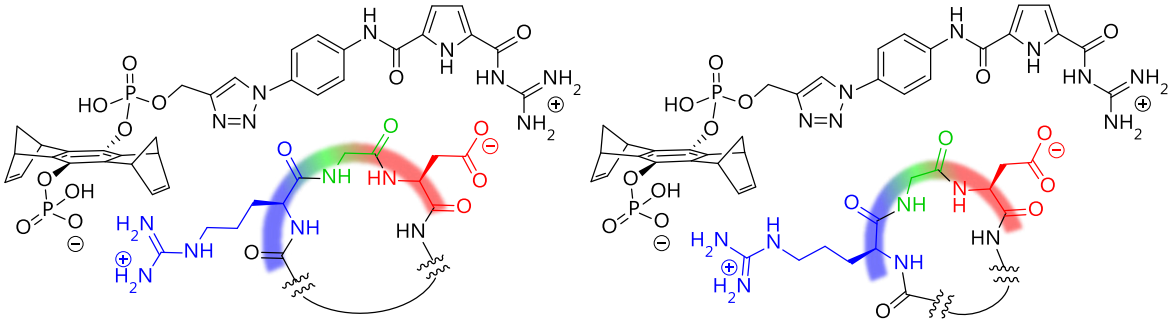

56 · P3 **56 · P2**

Figure 4-50. Scheme of assumed 1:1 complexes of receptor **56** with peptide **P3** (left side) and **P2** (right side) revealed that shown complex geometry with **P2** seemed to be less favored.

Another effect might be an unfavored geometry of the penta-peptide **P2** which might lead to a lower affinity towards the RGD-receptor **56**. This effect might increases the tendency to form aggregates with other peptide molecules. As it was mentioned in chapter 4.3.6 the RGD-sequence of **P2** is even more curved than in the cyclic hexa-peptide **P3** (fig. 4-50). Additionally it needs to be considered as well that the water-soluble receptor **56** carried one phosphate group more than the previous calculated receptor **8** in chapter 4.1. Obviously the additional phosphate group changed the geometry of binding sites to each other so that a 1:1 complex formation like shown above could be less favored.

To validate the complex stoichiometry of the previous receptor-substrate-systems the *Job's* method of continuous variation was executed. *Job* plots were carried out at least two times on each RGD-peptide receptor system. To fulfill the conditions of the used method of continuous variation small amounts of initial receptor solutions were replaced by peptide solution of the same concentration. Thereby the stoichiometry of complex at equilibrium could be obtained from the inflection point of the curve. Under consideration of a dilution effect the net change in UV-absorption at the maximum of 306 nm was used and plotted against the molar fraction.

In figure 4-51 the *Job* plot of the linear RGD-peptide **P1** is displayed. The differential absorbance $\Delta A = A_{obs}-A_R-A_S$ is plotted against the molar fraction x_s of the substrate. Unfortunately the recorded data did not give a clear evidence of the complex stoichiometry. The maximum of the absorbance difference is located at a molar fraction of around 0.38. Therefore a complex stoichiometry of 1:2 of guest peptide to host receptor could be assumed. But indeed the complex could have a stoichiometry between 1:1 and 1:2 of guest peptide to host receptor. With respect to some outlying data which are shown in brackets the data in general seems not to be very significant. For example if the data point of the molar fraction $x_s = 0.5$ would be 0.004 units higher the *Job* plot would indicate a 1:1 complex. Even the dimension of values of the differential absorbance is rather small. The full absorbance difference stretches over 0.01 units.

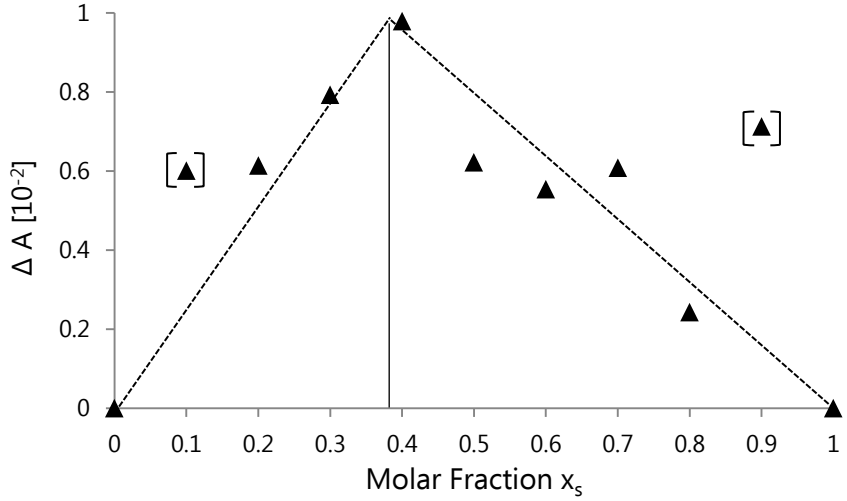

Figure 4-51. The *Job* plot of the linear RGD-peptide **P1** shows the inflection at around 0.38 if some data in brackets were marked as outliers.

Consequently the complex stoichiometry could be between 1:1 and 1:2 with respect to guest peptide to host receptor. The quality of the measurements could not be improved unluckily. Even the repetition of the *Job* plots did not yield better results. Attempts with increased concentrations of the receptor and the substrate yielded even worse distributed data. The *Job* plots of the circular peptides **P2** and **P3** suffer from the same problem of a rather small absorbance difference. In figure 4-52 both plots are shown. Although the inflection point is not pronounced in the *Job* plot of peptide **P2** (left side) a stoichiometry of the peptide-receptor-complex of 2:1 is could be estimated. But the maximum could be located between the molar fractions of 0.5 to 0.7. Again the error is quite high and a rather small shift of a single data point around the proposed maximum could be crucial. For the linear peptide **P3** the *Job* plot gives a rather clear evidence for a 1:2 receptor-substrate-complex.

Thus an analysis with the computer programs *SpecFit* and *ReactLab Equilibria* were tried. The advantage of both programs is that they can carry out the regression analysis with data from multi-wavelength and of competitive complex formation. Inopportunely the algorithms of both programs did not lead to any suitable results due the problem in finding a minimum during the iteration steps.

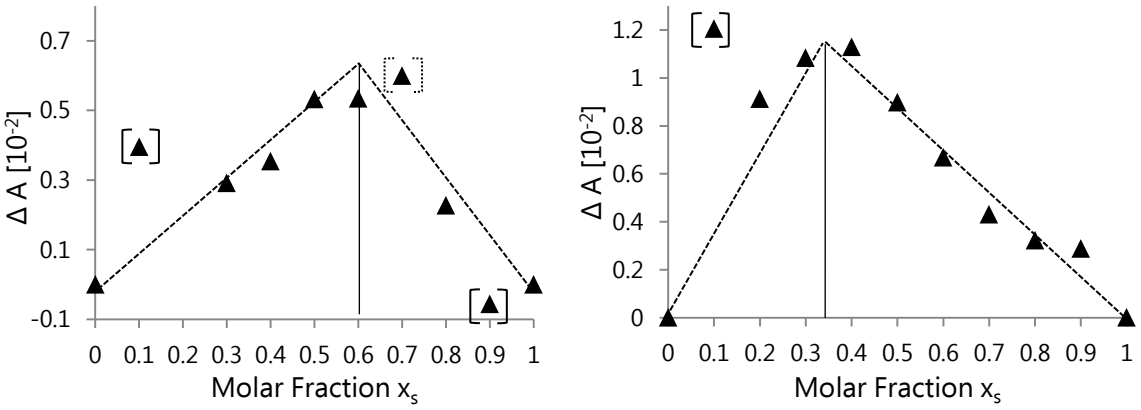

Figure 4-52. *Job* plots of the penta-peptide **P2** (left) revealed a nearly a complex stoichiometry of 2:1 of peptide to receptor whereas the hexa-peptide **P3** (right)

In general it turned out that the obtained data of *Job* plot showed a significance that is too low to obtain trustful results from. The main reason might be that the complex formation did not influence the chromophore of the receptor that much that the UV-absorption is a proper observable. Additionally a mixture of different binding modes that could have a dissimilar complex stoichiometry was assumed to be present at the same time. With the reasonable assumption that the 1:1 complex is one of the main components the previous results of the non-linear regression analyses done with *origin* were considered.

All tries to obtain a higher absorption difference by usage of increased concentrations of the receptor and the substrate did not lead to better results. One problem that accompanied measurements with higher concentrations was the amplified absorption. The absolute absorbance was raised to maximal 2.25 a.u. to keep to the linearity absorbance behavior but without a successful improvement of the obtained *Job* plots. Even more concentrated solutions were not tried. Because the linear absorbance behavior will not be fulfilled anymore with a significant higher absolute absorbance level and the *Beer-Lambert Law* will not be valid anymore. With modern spectrometers a limit is reached at a value of 3 a.u. The limit of a linear relationship between concentration and absorbance is caused by stray light and an asymptotic flattening of the standard curve would occur.[107]

In summary the obtained results from UV-titration experiments with an estimated stoichiometry of a 1:1 complex yielded reasonable binding constants for all 3 RGD-peptides. Due to the unsatisfying results of *Job* plots some additional AFM

measurements of the RGD-receptor **56** were done. These supplementary experiments were executed to investigate the behavior of self-aggregation like receptor **46** showed before.

4.3.7 Results of AFM-Measurements of Receptor 56

The tendency of self-association of receptor **56** was checked via AFM images. To compare the results with previous RGD-receptor **46** they were made in analogous way to the previous ones. But as a most important difference aqueous solutions were made due to a better water solubility of receptor **56**. Three stock solutions at acidic, almost neutral and alkaline conditions were made. As initial concentrations 1.40 mM for alkaline and acidic environments and 821 µM at pH 6.0 were used. Because fully covered surfaces were obtained from these concentrated solutions they were diluted stepwise until feasible AFM scans could be made. In the range of from 140 µM to 8.21 µM of aqueous solutions of receptor **56** moderately covered surfaces could be recorded. Therewith the concentration range was up to 100 times lower in comparison to concentrations of receptor **46**. Due to a lower tendency of aggregate formation the concentration of receptor **56** needed to be lower in order to obtain moderately covered surfaces. At the mentioned concentrations no pronounced aggregation behavior could be observed with exception of alkaline and acidic conditions. In figure 4-53 overview scans show the receptor **56** on mica surface obtained from aqueous media at different pH-ranges. The receptor concentration for alkaline and acidic conditions was 140 µM and under neutral conditions 82.1 µM. Small and medium sized agglomerates could be found mostly for acidic and alkaline conditions interestingly. But especially in a slightly acidic environment (pH = 6.0) they became very small.

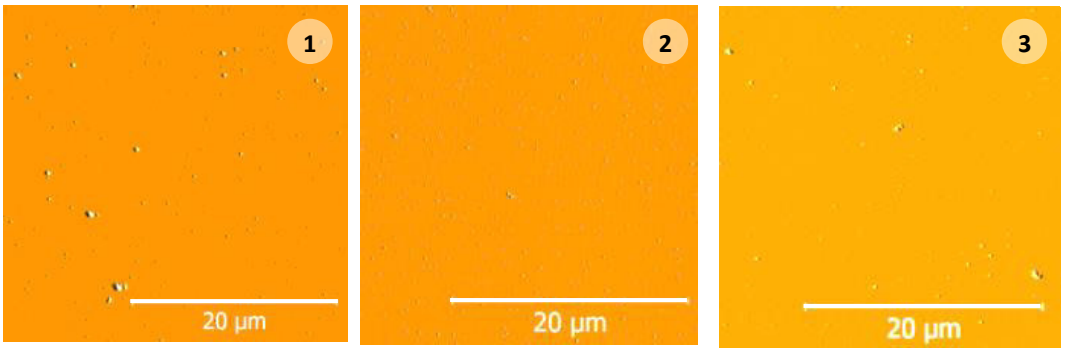

Figure 4-53. The AFM-pictures show different concentrations and environments. The tapping amplitude images **1**-**3** with a scale bar of 20 µm give an overview of alkaline (**1**), slightly acidic (**2**) and acidic (**3**) conditions. Only very small structures could be found.

Higher concentrations at neutral conditions resulted in overcrowded surfaces but the particle size kept the same. Even diluted solutions up to 8.21 µM revealed similar particle sizes. Increased pictures with more detailed scans of figure 4-53 are shown in figures 6-13, 6-14 and 6-15: There are presented in the experimental section in chapter 6.9. Although AFM experiments did not represent molecules in solution results are in accordance to UV-binding studies. Even the tendency of precipitation of molecule **56** can be explained with these results easily. In the previous purification of the prepared **56** this property was used to purify the receptor. And finally the most important result is that RGD-receptor **56** did not show aggregate formation in the desired pH region of pH 6. The first generation RGD-receptor **46** instead revealed those problems.

4.4 Conclusions

Synthesis and evaluation of an artificial RGD-receptor which should be able to recognize RGD-substrates specifically under physiological conditions turned out to be challenging. Although the results of the theoretical calculations looked promising with respect to good binding facilities towards RGD-peptides the receptor **46** was inappropriate (fig. 4-54).

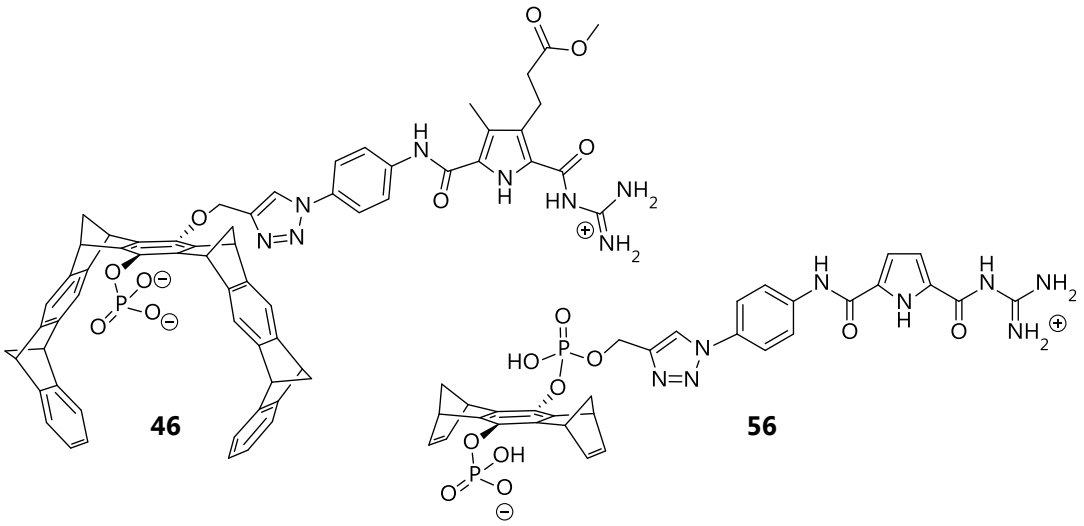

Figure 4-54. Molecule **46** shows the approach to a water-soluble RGD-receptor containing a guanidiniocarbonyl pyrrole and a phosphate tweezer. The development to a fully water soluble and RGD-receptor **56** could be achieved by truncation of the aromatic backbone and the introduction of an additional phosphate group.

First of all the water solubility of the receptor was restricted by the need of additional 10 % DMSO. The tendency to form rather stable aggregates was assumed by the evaluation of the first binding studies via UV-titration experiments. Due to the

irregular increases and decreases of the light absorption a competitive aggregation behavior instead of a defined receptor-substrate-complex formation was considered. The presence of aggregates could be depicted with supplementary AFM measurements. Under alkaline conditions some rod-like structures and more important the presence of spherical particles under acidic and slightly acidic conditions could be visualized. The estimated size of these particles could be found in supplemental DLS measurements.

A fully convergent synthesis route with an improvement of the water-solubility could be developed to yield the ditopic RGD-receptor **56** (fig. 4-54). Secondary the affinity to form aggregates could be reduced. These assumptions were supported by additional AFM experiments which revealed no bigger aggregates like molecule **46** revealed.

The second phosphate group might be seen as most important reason for the improved solubility. But another aspect might be taken into account as well. The binding site for positively charged guanidinium residue was truncated from the first RGD-receptor **46** to the enhanced receptor **56**. Obviously the cavity of the tweezer facilitated strong intermolecular interactions of the RGD-receptor **46** itself.

Although the same problem of auto recognition might be possible with receptor **56** this aspect seemed to play an inferior role. In receptor **46** the backbone of tweezer residue plays another role called the hydrophobic effect. As shown by *Biedermann et al*. the contribution of the hydrophobic effect could not be neglected. The reason is that high energy water hosted by tweezer's cavity is easy to replace by an even more suitable quest. Thus an intermolecular complex with a guanidinium residue is enthalpically and entropically favored.[55]

Unfortunately the guanidinio function of another receptor molecule could be trapped within the cavity so that an exchange of guest molecules could be kinetically hindered. If a kinetical hindrance occurred the exchange with a suitable substrate molecule might be very slow or nearly impossible. It is assumed that different aggregates co-exist in solution. The dilution experiment of first RGD–receptor **46** indicated a linear behavior of absorption against concentration (fig. 4-36). This result could be a false conclusion and rather a stable ratio of different aggregates over a broad concentration range might be thinkable. In general the absorption behavior might be less influenced by aggregation formation.

Structures of the self-association could be dimers as well as oligomers arranged in a head-to-tail arrangement. Last mentioned could be responsible for the rod-like structures (fig. 4-40 and fig. 4-41) formed under acidic conditions. In figure 4-55 the receptor **46** is shown in two ways of imaginable self-aggregation states. In both cases the guanidinio function of the pyrrole residue is hosted by the tweezer. In

solution a mixture of different aggregates containing a various number of molecules **46** is assumed.

The adjusted balance of aggregates in a solution would be in a competition with the binding sites of titrated quest peptides during the UV-binding study. Even if the shifts are not significant the overall shape of the UV absorption spectrum varied unexpectedly (fig. 4-37). This observed behavior could originate from a disturbance in the composition of aggregates in the mixture.

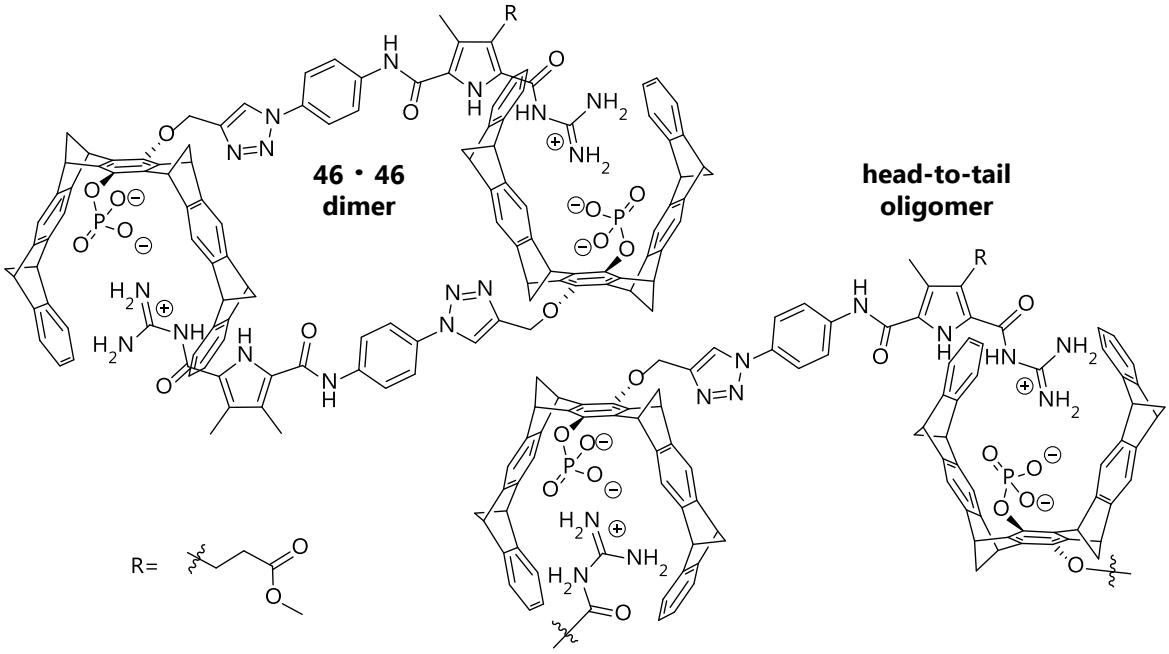

Figure 4-55. Two proposed kind of aggregates of RGD-receptor **46** are shown. A dimer at the left side and an oligomer composed by a head-to-tail aggregation at the right side.

Generally the aggregation behavior could be influenced by variation of conditions like solvent, pH value and competitive guest molecules. Macroscopically the results could be visualized by AFM experiments. Through the change of protonation state of molecule **46** different macroscopic aggregates could be obtained. Thereby it could be shown that receptor **46** was unsuitable for recognition of RGD-sequence.

The improvement of the RGD-receptor showed a striking selectivity towards RGD-substrates with different extensions of their RGD-loops. Due to the low significance of the results of the *Job* plot analyses the evaluation of the data obtained from the UV-binding studies was done with the assumption of 1:1 complexes being formed between the host receptor and the guest peptides correspondingly. Therewith comparisons among the 3 different peptides with respect to their binding affinity towards the receptor could be estimated only. Even attempts to use fluorescence or NMR as an observable failed. No significant change during some test titration experiments could be recorded.

The complexation constant of molecule **56** with the linear peptide was inherently higher than those with cyclic peptides. The constraints of the cyclic peptides forced the RGD-sequence in a specific conformation. The observed selectivity revealed one order of magnitude between the penta-peptide **P2** and the hexa-peptide **P3**. This difference is not really huge compared to other natural receptors. But the obtained results allow further investigations for improvement to obtain target specific RGD-receptors in the end.

5 SUMMARY AND OUTLOOK

The objective of this work was the development of a water-soluble receptor for small molecular weight peptides containing the RDG-sequence as a recognition unit. The focus was set on the synthesis of a receptor with a ditopic binding motif and the evaluation of its binding affinity towards RGD-peptides. Both binding motifs should be designed in a complementary fashion. Therewith it should be possible to recognize the negatively charged side chain of the aspartic acid residue and the positively charged guanidinium group which is part of the arginine amino acid simultaneously.

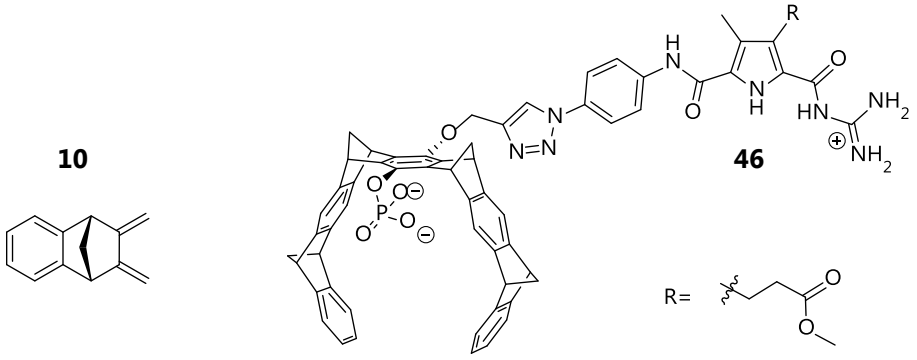

Figure 5-1. Structures of the bicyclic diene **10** and the RGD-receptor **46**.

In a first approach the 1st generation RGD-receptor **46** (fig. 5-1) could be realized in a 22-step-synthesis. Partially the synthesis could be managed via convergent reaction steps like the formation of the tweezer or the triazole. Some further improvements in the tweezer synthesis could be made. Especially a more efficient synthesis strategy of the diene **10** could be developed. The yield of the bicyclic diene **10** could be improved by the change of the polymerization inhibitor in the initial synthesis step significantly. In addition with the shortening from 6 to 4

synthesis steps the overall yield of the diene **10** (fig. 5-1) was improved from 15 % to almost 40 %.

Additionally an easy access to un-symmetrical tweezers could be realized within this work. During the synthesis of the first RGD-receptor **46** the synthesis of the mono-alkyne tweezer **31** (fig. 5-2) could be developed. But unluckily the water solubility of the 1st generation RGD-receptor (fig. 5-1) was too low and unsatisfying for further binding studies with RGD-peptides. Even the characterization of the receptor precursor **45** and of receptor **46** revealed some problems that were related to the poor water-solubility of molecule **46**. Under acidic, slightly acidic and alkaline conditions the molecules trended to form aggregates that could be visualized nicely via AFM. With DLS measurements the size of the aggregates under almost neutral conditions could be confirmed.

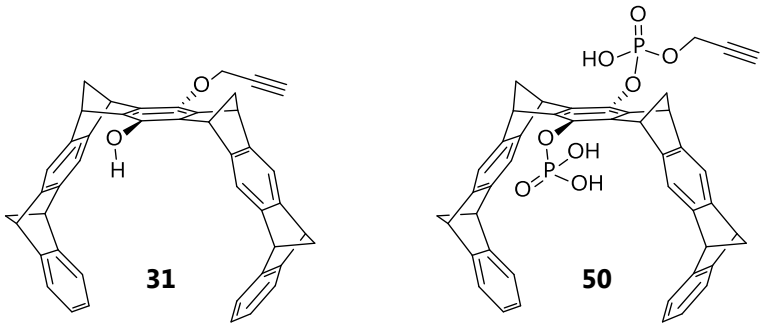

Figure 5-2. Both mono-alkynes the mono-alkyne tweezer **31** and the diphosphate mono-alkyne tweezer **50** were synthesized via a *Williamson* ether synthesis and an analogous *Williamson* ether synthesis respectively.

In a second approach a supplemental water solubility enhancing group in combination with a reduced size of the aromatic backbone of the tweezer was considered. For the realization of a completely water-soluble RGD-receptor an access towards un-symmetrical tweezers and truncated tweezers containing two phosphate groups needed to be developed.

The introduction of a second phosphate group yielded the water-soluble diphosphate mono-alkyne tweezer **50** and the guanidinium binding site **51**. The synthesis of molecule **51** could be realized as a one pot synthesis starting with the diol **19b** (fig. 5-3). In the final synthesis step the RGD-receptor **56** was assembled in a copper-catalyzed cyclisation reaction. This last reaction facilitated a smart linkage of both binding motifs in a convergent syntheses strategy. The low molecular weight RGD-receptor **56** was synthesized in an overall yield of 3 % with respect to the synthesis of molecule **51**.

Generally the syntheses of the basic building blocks followed the standard synthesis protocols. Some improvements with respect to the yield and the efficiency could be made. Especially the synthesis route of the tweezer building block was

shortened by two reaction steps. The synthesis of azido pyrrole **32** revealed some stability problems. The fast decomposition of azido pyrrole **37** during the deprotection step could be circumvented by an introduction of the azide at the unprotected pyrrole **43**.

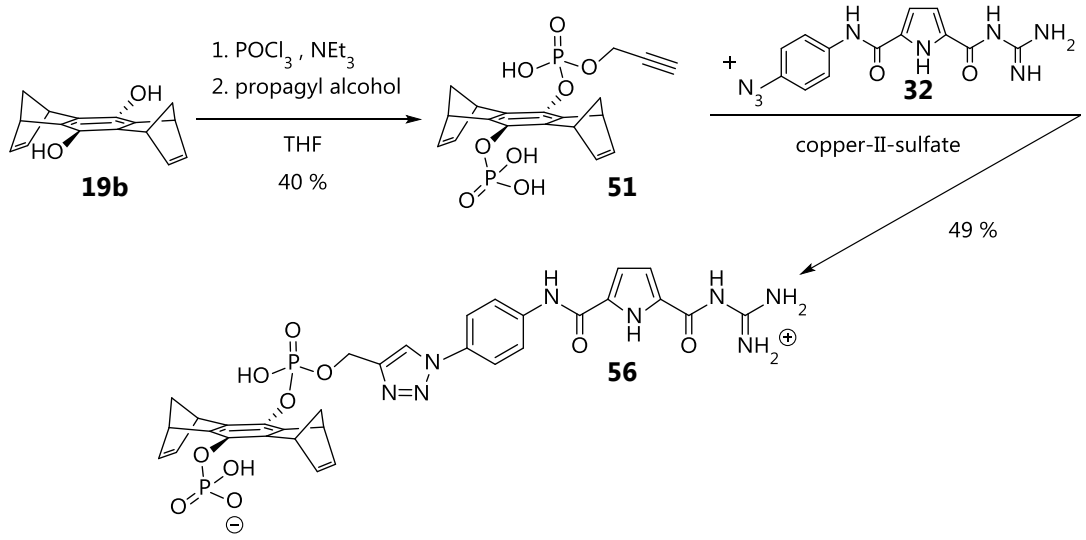

Figure 5-3. The synthesis of the truncated mono alkyne diphosphate tweezer **51** was carried out in a one pot synthesis. The convergent synthesis of the diphosphate mono-alkyne **51** with the pyrrole azide **32** was executed via a 1,3-dipolar cycloaddition.

The characterization of both synthesized RGD-receptors turned out to be complicated. Due to intermolecular interactions caused by processes of self-assembly the NMR spectrum was influenced for example. The more functional groups became unprotected the more distinct the peak broadening appeared in the spectrum. Within the second approach the aim of a totally convergent synthesis strategy could be applied. This allowed an easier characterization of the separated building blocks until the last reaction step.

The UV-binding studies of the receptor **56** under slightly acidic conditions could be carried without further problems. The evaluation of the complex stoichiometry via *Job's* method yielded insignificant results so that host-guest systems with stoichiometry of a 1:1 were assumed. This new receptor showed somehow a specific recognition affinity towards cyclic RGD-peptides. This could be seen by an increase of the association constant from the penta-peptide **P2** towards the hexa-peptide **P3** and the linear RGD-peptide **P1**. The highest binding constants could be recorded using the linear RGD-tripeptide **P1**. Herewith an association constant of $K_A = 3.4*10^4$ M^{-1} was found taking a 1:1 complex into account. Compared to the first synthetic RGD-receptor the K_A -value with linear RGD-peptide could be improved by two orders of magnitude. This first receptor was the trisphosphonate receptor developed by *Schrader* et al. (fig. 2-5). It showed even the same trend to form stronger

complexes with the flexible and linear RGD peptide (K_A = 1300 M^{-1}) compared to the cyclic peptide cyclo(RGDfV) (K_A = 700 M^{-1}).[43]

Last mentioned receptor showed rather marginal affinity difference between the cyclic and the free RGD peptide. Only half an order of magnitude could be achieved in difference of selectivity. Whereas the newly developed water-soluble RGD-receptor **56** showed a slightly higher selectivity between the penta-peptide (K_A = 4,300 M^{-1}) towards linear peptide (K_A = 34,000 M^{-1}).

One big advantage of the newly developed receptor synthesis is the flexibility in the linker length. Based on the concept of separated binding sites connected via a linker and a convergent synthesis this strategy enables a rather fast development of new receptor molecules. This method can be used efficiently to generate different RGD-receptors with dissimilar selectivity and binding properties towards different RGD-peptides more efficiently. Although the objective intended the synthesis of a RGD-receptor containing a full tweezer as binding site for guanidinium residue, it could be shown that a truncated version of the tweezer could afford easier synthesis impressively. Even solubility problems could be circumvented by the diminishment of the tweezer building block.

Nevertheless the results of this work can be used to design tailor-made RGD-receptors by the additional usage of space demanding residues at the linker. Through the truncation of the tweezer and therefore the loss of the hydrophobic aromatic backbone the solubility should not suffer by further residue attachment. The introduction of small residues like methyl or ethyl-side chains for example might have some impact on the selectivity between different RGD-peptide due to their different conformation.

For further research promising results can be expected. Especially when the selectivity of new RGD-receptors can be triggered easily the new receptors could be tested against integrin peptides like vitronectin or fibronectin. This route of research might lead in final application for pharmaceuticals or their evaluation, if they are based on RGD-recognition.

6 EXPERIMENTAL SECTION

6.1 General Procedures of Synthesis and Analysis

Syntheses. All air and moisture sensitive reactions were carried out under argon (purity: 99,996 %) from *Linde*. Obtained solid products were either dried over silica gel (orange) or were freeze dried with an Alpha 1-4 LD Plus lyophilizer from *Christ*. A magnetic stirrer with heating function MR 3001K 800W from *Heidolph* was used for conventional syntheses. High temperature reactions were performed with a heating mantle PILZ® from *Heraeus*. Microwave-assisted syntheses were carried out with a Discover SPS System from *CEM*. Temperature controls of those reactions were performed by infrared sensor. For all vacuum techniques membrane pumps and oil pumps from *Vacuubrand* were used. Removal of solvents from reaction mixtures were performed under reduced pressure with rotary evaporator Laborota 4000 efficient and HB digital water bath from *Heidolph*.

Peptide syntheses were carried out on solid phase. The used synthesis strategy of solid phase peptide synthesis (SPPS) is based on already reported procedure.[60] As main difference the coupling reaction was carried out at room temperature in a Rotamax 120 peptide shaker from *Heidolph*. During the reaction all vessels were flushed with argon to prevent from any side reactions by moisture. As coupling agent PyBOP was used. For cyclic peptides the very labile chlorotrityl chloride resin was used to prevent from loss of sidechain protection of the linear peptide strand.

Solvents. Water was always used as fully desalinated water, which was obtained by Barnstead™ MicroPure™ from *Thermo Fisher* (formerly *TKA*). The electric conductance of the used water was below 0.070 µS. Other used solvents for reactions agreed the specification of American Chemical Society (ACS). If needed pure solvents were obtained by distillation of ACS-grade solvents. Subsequently purified solvents

were stored over molecular sieves and flushed with argon. Water-free solvents were obtained by following procedures[108]:

Diethyl ether was refluxed with sodium and benzophenone as indicator and distilled afterwards. Dichloromethane was heated to reflux with calcium carbonate and distilled subsequently. Dimethylformamide and *tert*-butanol were refluxed with calcium hydride and distilled afterwards.

Solvents used for analytical purpose with HPLC-grade were purchased by *VWR* and *Waters*. Deuterated solvents for NMR-measurements were obtained from *Deutero* and *Sigma Aldrich*.

NMR spectroscopy. ^{1}H-, ^{13}C- and ^{31}P NMR spectra of solutions were recorded with DMX300, DRX500 and an Advance III HD 600 from *Bruker*. If not mentioned elsewise the spectra were recorded at 298 K (corresponding to room temperature). High temperature and two dimensional measurements like DEPT135, COSY90, HSQC and HMBC were recorded with the DRX500 machine respectively. Acquisition of ^{31}P NMR was done in proton decoupled mode except it is mentioned differently. Chemical shifts are given in ppm and refer to the δ-scale were standardized by the following solvent residual peaks: ^{1}H NMR: $CDCl_3$ (δ = 7.26), DMSO-d6 (δ = 2.50), CD_3OD (δ = 3.31), DMF-d7 (δ = 2.75, 2.92, 8.03); ^{13}C NMR: $CDCl_3$ (δ = 77.16), DMSO-d6 (δ = 39.52) and CD_3OD (δ = 49.00), DMF-d7 (δ = 29.76, 34.89, 163.15). The multiplicities of signals are abbreviated as followed: s = singlet, bs = broad singlet, d = duplet, t = triplet, q = quartet, m = multiplet. Evaluation of the spectra was done with the programs TOPSPIN versions 2.1 and 3.0.b.7 and ACD/NMR Processor Academic Edition. The latter one was mainly used to evaluate the *J*-coupling-values of ^{1}H NMR spectra with poor resolution.

High performance liquid chromatography-mass spectrometry (HPLC-MS). HPLC-MS-analyses for reaction control were performed with a combined system of an *Accela* HPLC and a LCQ Fleet™ Ion Trap Mass Spectrometer of *Thermo Fisher*. For chromatography a Zorbax Eclipse XDB-C18 with a length of 150 mm and an inner diameter of 4.6 mm from *phenomenex* was used. Particle size of stationary phase was 5 µm and pore size was 8 nm. UV-detection occurred at 210 nm. For negative ionization mode a standardized gradient run with 5 mM ammonia acetate solutions of water and acetonitrile as eluent was used.

High performance liquid chromatography (HPLC). Analytical reversed phase HPLC-experiments were performed on *Thermo Fisher* (formerly *Dionex*) system consisting of a HPLC-pump, model P680, an auto sampling injection system, model

ASI 100 Automated Sample Injector and an UV detection device, model UVD 340U. Analytical and semi-preparative chromatography was done with columns from *YMC*. Analytical columns had a length of 150 mm and inner diameter of 3.0 mm. The semi-preparative column had a length of 250 mm and an inner diameter of 4.6 mm. Both kinds of columns were filled with RP-18 YMC-Pack ODS-A solid phase with a particle size of 5 µm and a pore size of 12 nm. Evaluation was done with the program Chromeleon 6.80 developed by *Dionex*. Normal phase HPLC was performed on a multicomponent system containing a Hitachi L-6200A Intelligent pump from *Merck*, degasser ERC-3512 from *Erma* and a *Knauer* UV Detector 2600. Assembled by SCPA the HPLC was controlled by the program Chromstar 7 from *SCPA*. For separation a column with a length of 250 mm and an inner diameter of 4 mm filled with NUCLEOSIL® 100-7 with particle size of 7 µm and a pore size of 100 Å from *Macherey-Nagel*.

Preparative HPLC was carried out with two different multicomponent systems. Both systems were assembled by *SCPA* and run under the program PrepCon 5. The first preparative system consisted of a Septech pump from *Merck*, a single UV-detector SPD-10A from *Shimadzu*. The second HPLC system consisted of a HPLC pump Azura P 2.1L from *Knauer*, a UV/VIS diode array detector TIDAS S 500 from *J&M* and a Vario 4000 fraction collector from *LABOCOL*. Both preparative HPLC machines were equipped with a manual injection valve from *Rheodyne*. Columns used for preparative purification were obtained from *YMC* and had same specification of silica like analytical column.

Medium performance liquid chromatography (MPLC). Quantitative MPLC with reversed phase was elaborated on a device from *Armen Instrument*, model Liquid Chromatography Flash. For purifying reusable glass columns ECOPLUS model TAC25/500LS0-SR-2 and TAC25/250LS0-SR-2 from *Kronlab* were used. RP-18 bulk material from *YMC* with particle size of 50 µm or 15 µm and a pore size of 12 nm respectively was used as solid phase.

Thin layer chromatography (TLC). Different sorts of TLC plates from *Macherey-Nagel* were used for reaction control: For normal phase POLYGRAM® SIL G/UV254 (TLC plastic sheets coated with 0.2 mm silica gel and fluorescent indicator, UV-detection at λ = 254 nm) were used. For reversed phase ALUGRAM® RP-18W/UV254 (TLC aluminum sheets coated with 0.15 mm silica gel and fluorescent indicator, UV-detection at λ = 254 nm) were applied. Eluent mixtures are given in volume fractions of the used solvents (v_1/v_2). For UV-detection a Nu-4 KL UV lamp with wavelengths 254 nm and 366 nm from *Benda* was used.

Column chromatography. Quantitative column chromatography was carried out with normal phase silica gel from *Macherey-Nagel*. MN silica gel 60 M, 0.04-0.063 mm / 230-240 mesh ASTM. Mixtures of eluents are specified in volumetric contents of used solvents (v_1/v_2).

Mass spectroscopy. Samples were diluted in a 1 to 10 micro-molar solution of methanol (HPLC-grade) and injected automatically via HPLC-Pump 1100 Series from *Agilent Technologies* and a *Gerstel* CTC-MPS3-auto-sampler (flow injection). The IonTrap mass spectrometer amaZon SL form *Bruker* was used for reaction control. High resolution measurements of purified products were recorded with maXis 4G, a Q-TOF mass spectrometer, or with a BioTOF III from *Bruker*. GC-MS experiments were performed with the quadrupole spectrometer HP 5973N MSD from *Agilent*. Chromatographic separation was supported by a DB5-MS-column with a length of 50 m, an inner diameter of 200 µm and a coating thickness of 330 nm. Masses obtained by GC-MS represent only nominal masses.

IR-infrared spectroscopy. IR-spectra were recorded by a *JASCO*-spectrometer model FT/IR 430 with diamond equipped optics. Absorption bands were given in wave numbers ($\tilde{\nu}$) [cm^{-1}] and intensities with the following abbreviations: vs = very strong, s = strong, m = medium, w = weak, br = broad.

UV-Measurements. To obtain binding constants from UV measurement a V-660 spectrophotometer from *Jasco* was used. Adjustment of pH-values was done with standard solutions of sodium hydroxide (1.0 M and 0.1 M) and hydrochloric acid (1.0 M and 0.1 M). With a calibrated *Hamilton* Minitrode attached to a pH-Meter 766 Calimatic from *Knick* the pH-value was monitored. Transfers of volumes were executed with calibrated pipettes from *Eppendorf*.

AFM-Measurements. AFM-images were obtained by an Innova Scanning Probe Microscope (SPM) equipped with an Atomic Force Microscope (AFM) Nano Drive. The machine is provided by *Veeco* company and acquired by *Bruker*. *N*-doped silicon cantilevers of type AC 160TS from *Olympus* were used as scanning probes. Samples were prepared via spin coating with 60 rps on mica surfaces acquired from *Plano*. Analysis of all images was done with computer program Gwiddion 2.40.

Melting Point. A Melting Point B-540 apparatus from *Büchi* was used to determine melting points with open glass capillaries. All measured melting points are uncorrected.

DLS-Measurements. A Zetasizer Nano ZS from *Malvern* with a 633-nm He-Ne was used. Measurements were performed at an operation angle of 173° with noninvasive back scattering (NIBS) technology. The software used to collect and analyze the data was the Dispersion Technology Software version 7.02 from *Malvern*. Each sample was measured 5 times with automatically selected measurement duration at 20 °C, 25 °C and 40 °C respectively.

6.2 Syntheses of Basic Molecules of the Tweezer

Synthesis of *endo*-1,4-methano-1,2,3,4-tetrahydronaphthalene-2,3-dicarboxylic acid anhydride (**20**)

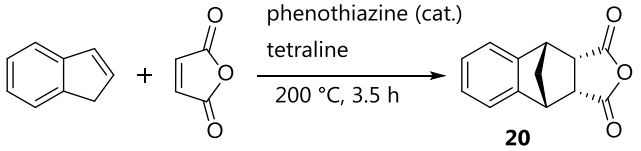

A solution of 50.0 g (430 mmol) of freshly distilled indene and 200 ml tetraline was added to 42.2 g (430 mmol) of maleic anhydride and 748 mg (3.75 mmol) of phenothiacine under inert gas. The reaction mixture was stirred and heated under reflux for 3.5 h with a heating mantle. After cooling down to 100°C the mixture was poured into 200 ml 70 – 80 °C warm toluene under rigorous stirring. The precipitate was filtered off with a G4-frit (pore size 10-16 µm) until a temperature of 40 – 50 °C was reached. The filtrate was kept in the fridge overnight to give a precipitating crystalline solid. The solid was filtered and dried over silica gel. Recrystallization from hexane/ethyl acetate resulted in a colorless crystalline solid (**20**) with a yield of 50% (45.9 g, 214 mmol).

Molecular Weight:	214.22 g/mol.
Formula:	$C_{13}H_{10}O_3$.
Rf-value:	0.74; SiO_2, n-hexane/ethyl acetate (1/1).
Melting point:	187 °C (ethyl acetate).

Spectroscopic data and assignment of molecule positions:

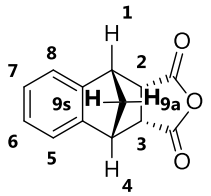

^{1}H NMR: (300.1 MHz, DMSO-d6): δ [ppm] = 1.94 - 1.95 (t, $^{3}J_{H\text{-}9a,H\text{-}9s/H\text{-}1,H\text{-}4}$ = 1.36 Hz, 2 H, H-9a, H-9s), 3.78 (m, 2 H, H-2, H-3), 3.93 (dd, $^{3}J_{H\text{-}1,H\text{-}4/H\text{-}2,H\text{-}3}$ = 3.32 Hz, $^{3}J_{H\text{-}1,H\text{-}4/H\text{-}9a,H\text{-}9s}$ = 1.36 Hz, 2 H, H-1, H-4), 7.14 - 7.22 (m, 4 H, H-5, H-6, H-7, H-8).

HRMS: (ESI pos., methanol/water): m/z = 215.0703 (calculated) for $C_{13}H_{10}O_3 + H^+$, 215.0733 (found), m/z = 269.0784 (calculated) for $C_{14}H_{14}O_4 + Na^+$, 269.0818 (found).*

* Additional mass resulted from nucleophilic opening of anhydride by methanol, which occurred during ionization process probably.

Synthesis of *endo-cis*-2,3-bis(hydroxymethyl)-1,4-methano-1,2,3,4-tetrahydro-naphthalene (**21**)

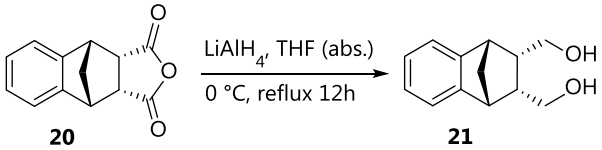

A solution of 38.1 g (178 mmol) of anhydride **20** in 500 ml THF abs. was added to a 0° C cold suspension of 23.1 g (609 mmol) lithium aluminum hydride in 200 ml THF abs. by a syringe under inert gas. The reaction mixture was stirred for 30 min at 0° C and additional 18.5 h under reflux. Afterwards the mixture was cooled down to 0° C again and hydrolyzed by a magnesium sulfate solution of 20 ml slowly. The mixture was heated under reflux for 30 min. The remained solid was separated by filtration and washed with diethyl ether until no product remained in the filtrate (via TLC!) The collected organic layers were evaporated under reduced pressure. The remained solid was lyophilized to yield 99 % (35.8 g, 12 mmol) of diol **21**.

Molecular Weight: 204.27 g/mol.
Formula: $C_{13}H_{16}O_2$.

R_f-value: 0.21; SiO_2, *n*-hexane/ethyl acetate (1/1).
Melting point: 100-102 °C (diethyl ether).

Spectroscopic data and assignment of molecule positions:

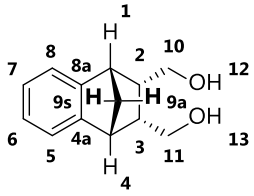

^{1}H NMR: (300.1 MHz, DMSO-d6): δ [ppm] = 1.63 - 1.70 (m, 2 H, H-9a, H-9s), 2.41 - 2.46 (m, 2 H, H-2, H-3), 2.60-2.68 (m, 2 H, H-10, H-11)*, 2.82 - 2.90 (m, 2 H, H-10, H-11)*, 3.29 (m, 2 H, H-1, H-4), 4.33 - 4.36 (m, 2 H, H-12, H-13), 7.01 - 7.06 (m, 2 H, H-6, H-7), 7.13 - 7.18 (m, 2 H, H-5, H-8).

* Double signal set resulted from the diastereotopic protons.

^{13}C NMR: (75.5 MHz, DMSO-d6): δ [ppm] = 42.9 (C-2, C-3), 46.4 (C-1, C-4), 48.7 (C-9), 60.1 (C-10, C-11), 122.6 (C-5, C-8), 125.0 (C-6, C-7), 145 (C-4a, C-8a).

HRMS: (ESI pos., methanol/water):
m/z = 227.1043 (calculated) for $C_{13}H_{16}O_2 + Na^+$, 227.1066 (found),
m/z = 243.0782 (calculated) for $C_{13}H_{16}O_2 + K^+$, 243.0714 (found).

Synthesis of *endo-cis*-2,3-bis(chloromethyl)-1,4-methano-1,2,3,4-tetrahydro-naphthalene (**22**)

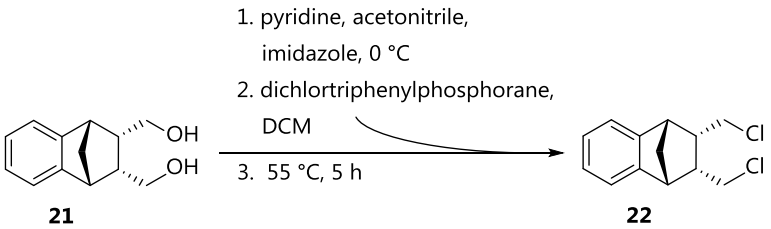

Under inert gas 64.2 g (193 mmol) triphenylphosphine dichloride were dissolved in 150 ml DCM. The mixture was added dropwise to a solution of 27.8 g (408 mmol) imidazole dissolved in 75 ml acetonitrile and 78 ml pyridine. During the addition the

temperature was kept at 0 °C. After 20 min of further stirring at room temperature a solution of 10.5 g (51.4 mmol) of the diol **21** in 8 ml DCM was added. The addition occurred in small portions within 10 min. Afterwards the reaction mixture was heated to 55 °C for 5 h. The end of the reaction was indicated by TLC-control. The reaction mixture was cooled to room temperature and hydrolyzed with a mixture of 200 ml of half conc. HCL and ice water in a 1:1 ratio. The different phases were separated after further addition of 150 ml DCM. The aqueous phase was extracted 5 times with 150 ml DCM. The combined organic phases were washed one time with 150 ml of 2 M HCl-solution, water and saturated $NaHCO_3$-solution respectively. Subsequently the organic phases were dried over sodium sulfate and filtrated. The filtrate was kept in a fridge overnight and the precipitate was filtered off. After washing the filtration residue with ice cold DCM the volume of the filtrate was reduced by evaporation under reduced pressure. By repeated crystallization and subsequent washing the amount of the side-product triphenylphosphine oxide could be reduced. After 3 times of repetitive crystallization the solvent was removed and the obtained raw product (15.5 g) was purified by flash chromatography (SiO_2, *n*-hexane/ethyl acetate 3/1). Because of an insufficient purity the chromatography was done repeatedly to yield 82 % (10.2 g, 42.1 mmol) of dichloride **22** as colorless oil.

Molecular Weight: 241.16 g/mol.
Formula: $C_{13}H_{14}Cl_2$.
R_f-value: 0.77; SiO_2, *n*-hexane/ethyl acetate (3/1).
Boiling point: 97-100 °C (0.5 mbar).

Spectroscopic data and assignment of molecule positions:

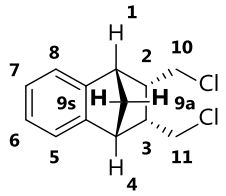

^{1}H NMR: (300.1 MHz, $CDCl_3$): δ [ppm] = 1.83 (dt, $^2J_{H\text{-}9s/H\text{-}9a}$ = 8.79 Hz, $^3J_{H\text{-}9s/H\text{-}1,H\text{-}4}$ = 1.41 Hz, 1 H, H-9s), 1.97 (dt, $^2J_{H\text{-}9a/H\text{-}9s}$ = 8.79 Hz, $^3J_{H\text{-}9a/H\text{-}1,H\text{-}4}$ = 1.41 Hz, 1 H, H-9a), 3.02-3.05 (m, 2 H, H-2, H-3), 3.20-3.27 (m, 4 H, H-10, H-11), 3.32-3.38 (m, 2 H, H-1, H-4), 7.10-7.15 (m, 2 H, H-6, H-7), 7.20-7.23 (m, 2 H, H-5, H-8).

Synthesis of 2,3-dimethylen-1,4-methano-1,2,3,4-tetrahydronaphthalene (**10**)

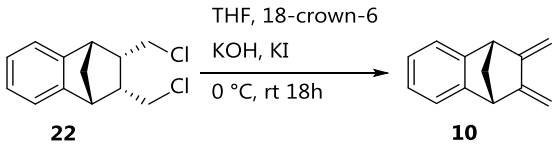

22 **10**

A mixture of 3.72 g (15.4 mmol) of the dichloride **22** and 900 mg (3.40 mmol) of crown ether (18-Crown-6) dissolved in 150 ml of dry THF was cooled to 0 °C. 1.49 g (265 mmol) of powdered potassium hydroxide and 644 mg (3.88 mmol) of potassium iodide were added in one portion and reaction mixture was stirred for 18 h at room temperature. The end of the reaction was indicated by TLC. Subsequently the solvent was evaporated under reduced pressure and the obtained raw product was purified by flash chromatography (SiO_2, *n*-hexane). The diene **10** was obtained as a colorless and crystalline solid in a yield of 99 % (2.56 g, 15.2mmol).

Molecular Weight: 168.24 g/mol.
Formula: C13H12.
Rf-value: 0.43; SiO2, n-hexane.
Melting point: 84 °C (*n*-hexane).

Spectroscopic data and assignment of molecule positions:

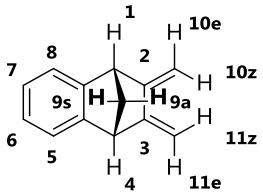

^{1}H NMR: (300.1 MHz, DMSO-d6): δ [ppm] = 1.94 (dt, $^2J_{H\text{-}9s/H\text{-}9a}$ = 8.68 Hz, $^3J_{H\text{-}9s/H\text{-}1,H\text{-}4}$ = 1.57 Hz, 1 H, H-9s), 2.12 (dt, $^2J_{H\text{-}9a/H\text{-}9s}$ = 8.68 Hz, $^3J_{H\text{-}9a/H\text{-}1,H\text{-}4}$ = 1.54 Hz, 1 H, H-9a), 3.84 (t, $^3J_{H\text{-}1,H\text{-}4/H\text{-}9s,H\text{-}9a}$ = 1.54 Hz, 2 H, H-1, H-4), 5.06 (s, 2 H, H-10e, H-11e), 5.20 (s, 2 H, H-10z, H-11z), 7.06-7.09 (m, 2 H, H-6, H-7), 7.20-7.23 (m, 2 H, H-5, H-8).

GC-MS: (EI neg., 70 eV): m/z = 167.23 (calculated) for $C_{13}H_{12}^-$, 167 (found) at a retention time of 35.18 min.

Synthesis of 1,4,4a,8a-tetrahydro-*endo*-1,4-methanonaphthalene-5,8-dione (**16**)

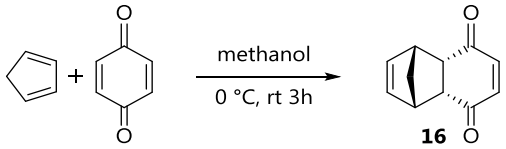

A suspension of 77.7 g (719 mmol) of *p*-benzoquinone in 415 ml methanol was cooled to 0 °C. To this suspension 47.5 g (719 mmol) of freshly distilled cyclopentadiene kept at -78 °C was added slowly via dropping funnel. The reaction mixture was stirred for 3 h at room temperature after addition of the cyclopentadiene. The reaction mixture was stored in a fridge overnight. The precipitate of greenish yellow crystals was filtered by a glass frit G4 (pore size 10-16 µm). Precipitation was done repeatedly with consequent reducing of the volume of previous filtrate by evaporation. The total yield of naphtalene dione **16** was 56 % (70.4 g, 404 mmol).

Molecular Weight: 174.20 g/mol.
Formula: $C_{11}H_{10}O_2$.
R_f-value: 0.41; SiO_2, *n*-hexane/ethyl acetate (2/1).
Melting point: 72-73 °C (methanol).

Spectroscopic data and assignment of molecule positions:

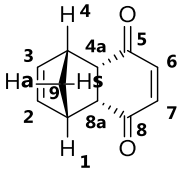

^{1}H NMR: (300.1 MHz, $CDCl_3$): δ [ppm] = 1.35 (dt, $^2J_{H\text{-}9s/H\text{-}9a}$ = 8.45 Hz, $^3J_{H\text{-}9s/H\text{-}1,H\text{-}4}$ = 1.77 Hz, 1 H, H-9s), 1.45 (dm, $^2J_{H\text{-}9a/H\text{-}9s}$ = 8.45 Hz, 1 H, H-9a), 3.27-3.28 (m, 2 H, H-4a, H-8a), 3.34-3.38 (m, 2 H, H-1, H-4), 6.02 (t, $^3J_{H\text{-}2,H\text{-}3/H\text{-}1,H\text{-}4}$ = 1.77 Hz, 2 H, H-2, H-3), 6.62 (s, 2 H, H-6, H-7).

HRMS: (ESI, pos., methanol/water): m/z = 175.0754 (calculated) for $C_{11}H_{10}O_2 + H^+$, 175.0761 (found), m/z = 197.0573 (calculated) for $C_{11}H_{10}O_2 + Na^+$, 197.0589 (found).

Synthesis of (1*R*,4*S*)-1,4-dihydro-1,4-methanonaphthalene-5,8-dione (**17**)

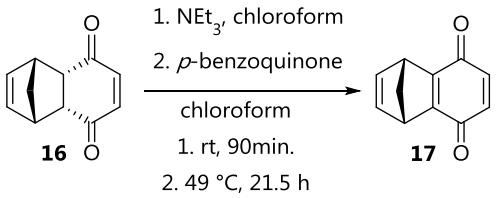

In 85 ml chloroform 12.0 g (68.9 mmol) of dione **16** were dissolved and 135 µl (97.9 mg, 968 µmol) triethylamine were added. After stirring the mixture for 90 min at room temperature 7.45 g (68.9 mmol) of *p*-benzoquinone dissolved in 10 ml chloroform were added. The reaction was heated to 49 °C for 21.5 h. A full conversion was indicated by TLC. The mixture was cooled in a fridge for two hours and the precipitate was filtered. The filtrate was washed once with 100 ml of 1 % sodium hydroxide solution. After additional washing with 40 ml water the remaining organic phase was dried with magnesium sulfate. Afterwards the solvent was evaporated under reduced pressure until brownish oil remained. The purification of the raw product (11.5 g) occurred via flash chromatography (SiO_2, *n*-hexane/ ethyl acetate 2/1) to yield 65 % (7.66 g, 44.5 mmol) of the dione **17**.

Molecular Weight: 172.18 g/mol.
Formula: $C_{11}H_8O_2$.
R_f-value: 0.38; SiO_2, *n*-hexane/ethyl acetate (2/1).
Melting point: 68 °C (ethyl acetate).

Spectroscopic data and assignment of molecule positions:

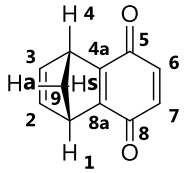

^{1}H NMR: (300.1 MHz, $CDCl_3$): δ [ppm] = 2.26 (dt, $^2J_{H\text{-}9s/H\text{-}9a}$ = 7.09 Hz, $^3J_{H\text{-}9s/H\text{-}1,H\text{-}4}$ = 1.45 Hz, 1 H, H-9s), 2.33 (dt, $^2J_{H\text{-}9a/H\text{-}9s}$ = 7.09 Hz, $^3J_{H\text{-}9a/H\text{-}1,H\text{-}4}$ = 1.49 Hz, 1 H, H-9a), 4.09-4.11 (m, 2 H, H-1, H-4), 6.57 (s, 2 H, H-6, H-7), 6.93 (t, $^3J_{H\text{-}2,H\text{-}3/H\text{-}1,H\text{-}4}$ = 1.92 Hz, 2 H, H-2, H-3).

^{13}C NMR: (75.5 MHz, $CDCl_3$) : δ [ppm] = 48.6 (C-1, C-4), 74.0 (C-9), 135.9 (C-6, C-7), 142.7 (C-2, C-3), 160.9 (C-4a, C-8a), 184.2 (C-5, C-8).

Synthesis of (1R,4S,4aR,5R,8S,9aS)-1,4,4a,5,8,9a-hexahydro-1,4:5,8-dimethano-anthracene-9,10-dione (**19a**)

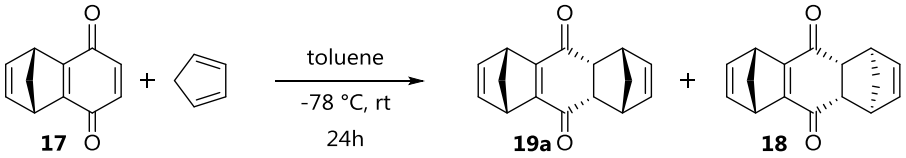

In an argon flushed reaction vessel 6.42 g (37.3 mmol) of *p*-quinone **17** were dissolved in 35 ml toluene and cooled to -78 °C. After dropwise addition of 3.63 ml (2.90 g, 43.9 mmol) of freshly distilled cyclopentadiene the mixture was stirred at room temperature for 24 h. Subsequently the precipitate was filtered and the filtrate was treated separately. Toluene was removed under reduced pressure from filtrate and both solids were dried over silica under reduced pressure. The yield of *syn*- and *anti*-product in total was 99 % (8.82 g, 37.0 mmol). Separation of *syn*-product **19a** from undesired *anti*-product **18** was performed by recrystallization from cyclo-hexane/ethyl acetate (1/1). After five recrystallization processes a *syn*/*anti* ratio of 46.3 : 1 could be obtained from the first precipitate. The second precipitate yielded a *syn*/*anti* ratio of 35.0 : 1. The calculation of the ratio was done by ^{1}H NMR-signal of newly formed double bond (*see appendix*). The obtained yield of the purified *syn*-dione **19a** was 47 % (4.19 g, 17.6 mmol).

Molecular Weight: 238.29 g/mol.
Formula: $C_{16}H_{14}O_2$.
R_f-value: 0.49; SiO_2, *n*-hexane/ethyl acetate (3/1).
Melting point: 155 °C (cyclohexane/ethyl acetate (1/1)).

Spectroscopic data and assignment of molecule positions:

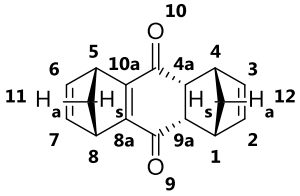

^{1}H NMR: (300 MHz, $CDCl_3$): δ [ppm] = 1.40 (dt, $^{2}J_{H\text{-}12s/H\text{-}12a}$ = 8.77 Hz, $^{3}J_{H\text{-}12s/H\text{-}1,H\text{-}4}$ = 1.35 Hz, 1 H, H-12s), 1.49 (dt, $^{2}J_{H\text{-}12a/H\text{-}12s}$ = 8.77 Hz, $^{3}J_{H\text{-}12a/H\text{-}1,H\text{-}4}$ = 1.79 Hz, 1 H, H-12a), 2.14 (dt, $^{2}J_{H\text{-}11s/H\text{-}11a}$ = 7.25 Hz, $^{3}J_{H\text{-}11s/H\text{-}5,H\text{-}8}$ = 1.46 Hz, 1 H, H-11s), 2.22 (dt, $^{2}J_{H\text{-}11a/H\text{-}11s}$ = 7.25 Hz, $^{3}J_{H\text{-}11a/H\text{-}5,H\text{-}8}$ = 1.43 Hz, 1 H, H-11a), 3.22-3.27 (m, 2 H, H-4a, H-9a), 3.45-3.49 (m, 2 H, H-1, H-4), 3.96-3.99 (m, 2 H, H-5, H-8),

5.79 (t, $^{3}J_{H\text{-}2,H\text{-}3/H\text{-}1,H\text{-}4}$ = 1.76 Hz, 2 H, H-2, H-3), 6.77 (t, $^{3}J_{H\text{-}6,H\text{-}7/H\text{-}5,H\text{-}8}$ = 1.91 Hz, 2 H, H-6, H-7).

Synthesis of (1R,4S,5R,8S)-1,4,5,8-tetrahydro-1,4:5,8-dimethanoanthracene-9,10-diol (**19b**)

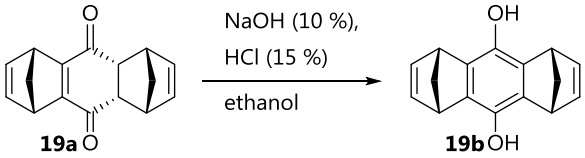

Under argon 2.43 g (10.2 mmol) of *syn*-dione **19a** were dissolved in 250 ml dried ethanol. The solution was degassed and 50 ml of sodium hydroxide solution (10 %) were added. By stirring for 10 min at room temperature the mixture changed the colour from colorless to an intense orange. The color changed to colorless again after addition of 45 ml of hydrochloric acid (15 %) and stirring for 5 min. Subsequently reaction mixture was poured on 150 g ice. The precipitate was filtered over a G4-glass frit (pore size 10-16 µm) and washed with 30 ml cold water. Because of very fine crystals of the precipitate it was dissolved in THF and solvent was evaporated to yield 94 % (2.28 g, 9.06 mmol) of diol **19b**.

Molecular Weight: 238.29 g/mol.
Formula: $C_{16}H_{14}O_2$.
R_f-value: 0.35; SiO_2, *n*-hexane/ethyl acetate (3/1).
Melting point: 260 °C (decomposition).

Spectroscopic data and assignment of molecule positions:

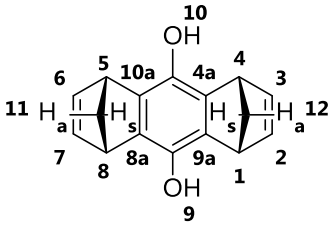

^{1}H NMR: (300.1 MHz, DMOS-d6): δ [ppm] = 1.96 (dt, $^{2}J_{H\text{-}11s,H\text{-}12s/H\text{-}11a,H\text{-}12a}$ = 6.53 Hz, $^{3}J_{H\text{-}11s,H\text{-}12s/H\text{-}1,H\text{-}4,H\text{-}5,H\text{-}8}$ = 1.35 Hz, 2 H, H-12s), 2.26 (dt, $^{2}J_{H\text{-}11a,H\text{-}12a/H\text{-}11a,H\text{-}12s}$ = 6.53 Hz, $^{3}J_{H\text{-}11a,H\text{-}12a/\ H\text{-}1,H\text{-}4,H\text{-}5,H\text{-}8}$= 1.51 Hz, 2 H, H-11a, H-12a), 3.97-3.99 (m, 4 H, H-1, H-4, H-5, H-8), 6.75 (t,

$^{3}J_{H\text{-}2,H\text{-}3,H\text{-}6,H\text{-}7/H\text{-}1,H\text{-}4,H\text{-}5,H\text{-}8}$ = 1.67 Hz, 4 H, H-2, H-3, H-6, H-7), 8.03 (s, 2 H, H-9, H-10).

^{13}C NMR: (75.5 MHz, DMSO-d6) : δ [ppm] = 46.2 (C-1, C-4, C-5, C-8), 69.3 (C-11, C-12), 135.2 (C-4a, C-8a, C-9a, C-10a), 139.7 (C-9, C-10), 142.7 (C-2, C-3, C-6, C-7).

Synthesis of (1R,4S,5R,8S)-1,4,5,8-tetrahydro-1,4:5,8-dimethanoanthracene-9,10-diyl acetate (**15**)

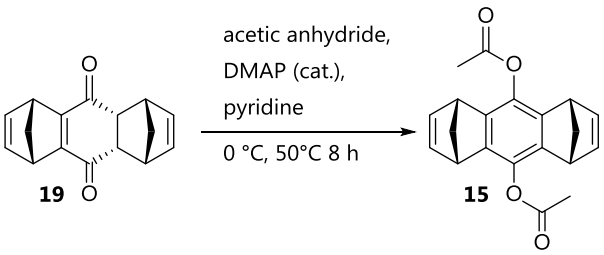

A suspension of 3.50 g (14.7 mmol) of *syn*-dione **19a**, 180 mg (1.47 mmol) DMAP and 25 ml of dry pyridine was cooled to 0 °C. Under inert gas 9 ml (9.72 g, 95.2 mmol, 6.5 eq) of acetic anhydride were added dropwise to the previous suspension. The reaction mixture was stirred for 2 h at room temperature and further 8 h at 50 °C. The reaction was quenched by pouring the mixture into 70 ml of a mixture of ice and water. The precipitate was filtered by a G4-frit (pore size 10-16 µm). The obtained solid was washed with ice cold water until a neutral pH-value could be reached. The solid was dried over silica under reduced pressure. The recrystallization was carried out with chloroform/ethanol (1/4) to yield 94 % (4.40 g, 13.8 mmol) of diacetoxy anthracene **15**.

Molecular Weight: 322.36 g/mol.

Formula: $C_{20}H_{18}O_4$.

R_f-value: 0.32; SiO_2, *n*-hexane/ethyl acetate (3/1).

Spectroscopic data and assignment of molecule positions:

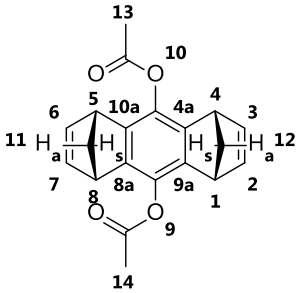

^{1}H NMR: (300.1 MHz, $CDCl_3$): δ [ppm] = 2.21 (dt, $^2J_{H\text{-}11s,H\text{-}12s/\ H\text{-}11a,H\text{-}12a}$ = 7.10 Hz, $^3J_{H\text{-}11s,H\text{-}12s/H\text{-}1,H\text{-}4,H\text{-}5,H\text{-}8}$ = 1.47 Hz, 2 H, H-11s, H-12s), 2.26 (dt, $^2J_{H\text{-}11a,H\text{-}12a/H\text{-}11s,H\text{-}12s}$ = 7.10 Hz, $^3J_{H\text{-}11a,H\text{-}12a/H\text{-}1,H\text{-}4,H\text{-}5,H\text{-}8}$ = 1.34 Hz, 2 H, H-11a, H-12a), 2.34 (s, 6 H, H-13, H-14), 3.80-3.82 (m, 4 H, H-1, H-4, H-5, H-8), 6.75 (t, $^3J_{H\text{-}2,H\text{-}3,H\text{-}6,H\text{-}7/H\text{-}1,H\text{-}4,H\text{-}5,H\text{-}8}$ = 1.81 Hz, 4 H, H-2, H-3, H-6, H-7).

6.3 Syntheses of Guanidiniocarbonyl Pyrroles

Syntheses of fully orthogonal protected guanidinocarbonyl pyrrole **35** have been described before in diploma thesis in 2009. Therefore it will not be described here again. The initial synthesis steps of guanidinocarbonyl pyrrole **40** will not be explained either because the BOC-protected precursor was mainly synthesized by supervised apprentices and regular laboratory staff. Therefore only further modifications of the guanidinocarbonyl pyrroles will be explained in following syntheses.

Synthesis of 5-((*N*-((benzyloxy)carbonyl)carbamimidoyl)carbamoyl)-4-(3-methoxy-3-oxopropyl)-3-methyl-1*H*-pyrrole-2-carboxylic acid (**36**)

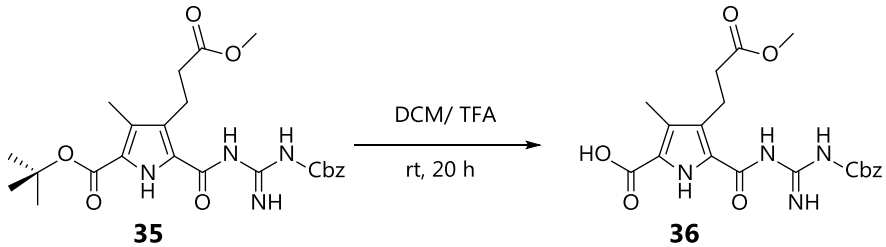

35 **36**

A solution of the orthogonal protected pyrrole **35** (900 mg, 1.85 mmol) in DCM (14.0 ml) and TFA (4.50 ml) was stirred for 20 h at room temperature. The reaction was quenched through the addition of 10 ml of water. The product started to precipitate as a colorless solid immediately. The volatile solvent was evaporated under reduced pressure subsequently. The remaining suspension was lyophilized to yield the pyrrole **36**. Without supplementary purification a yield of 94 % (750 mg, 1.74 mmol) could be obtained.

Molecular Weight: 430.42 g/mol.
Formula: $C_{20}H_{22}O_7N_4$.

R_f-value: 0.00; SiO_2, *n*-hexane/ethyl acetate (1/1).
Melting point: 270 °C (decomposition).

Spectroscopic data and assignment of molecule positions:

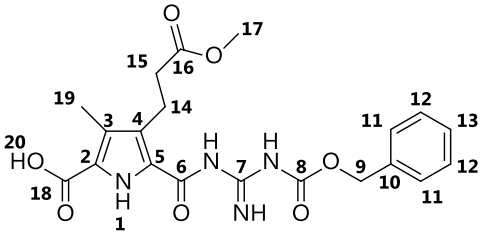

^{1}H NMR: (300.1 MHz, DMOS-d6): δ [ppm] = 2.20 (s, 3 H, H-19), 2.48 (t, $^3J_{H\text{-}15/\ H\text{-}14}$ = 7.50 Hz, 2 H, H-15), 2.96 (t, $^3J_{H\text{-}14/\ H\text{-}15}$ = 7.50 Hz, 2 H, H-14), 3.56 (s, 3 H, H-17), 5.16 (s, 2 H, H-9), 7.34-7.41 (m, 5 H, H-11, H-12, H-13), 8.21 (bs, 1 H, gua-N*H*), 8.70 (bs, 1 H, gua-N*H*), 9.50 (bs, 1 H, gua-N*H*), 11.03 (s, 1 H, N*H*, H-1), 11.96 (s, 1 H, H-20).

FT-IR: (ATR): $\tilde{\nu}$ [cm^{-1}] = 3359 (w), 3184 (w), 1733 (w), 1675 (m), 1614 (m), 1452 (w), 1341 (m), 1249 (m), 1222 (m), 1155 (m), 1091 (m), 960 (m), 771 (m), 733 (m).

HRMS: (ESI, pos., methanol/water): *m/z* $[M]^+$ calcd for $C_{20}H_{23}N_4O_7^+$: 431.1561; found: 431.1561.

Synthesis of 4-azidoaniline hydrochloride (**57**)

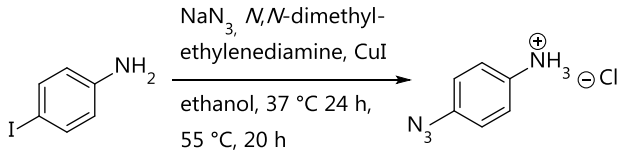

Under inert gas 4.38 g (20.0 mmol) of 4-iodo aniline were dissolved in 50 ml ethanol. After an iterative addition of 318µl (260 mg, 2.95 mmol, 0.15 eq) of *N,N*-Dimethylethylenediamine, 9 drops of a 1 M sodium hydroxide solution, 226 mg, (1.14 mmol, 0.06 eq) of sodium ascorbate, 2.60 g (40.0 mmol, 2.0 eq) of sodium azide and 499 mg (2.62 mmol, 0.13 eq) of copper(I) iodide the mixture was stirred for 24 h at 37 °C. The mixture was stirred for further 20 h at 55 °C. Via TLC control the reaction progress was observed until a full conversion was indicated. The reaction

was quenched by pouring the mixture on 200 ml of brine/ethyl acetate mixture (1/1). The organic phase was separated and the aqueous phase was extracted trice with 50 ml ethyl acetate respectively. The combined organic phases were dried over magnesium sulfate. The separation by filtration and subsequent evaporation of the solvent under reduced pressure led to a brown oil which was filtrated over normal phase silica with ethyl acetate. The final addition of aqueous hydrochloric and subsequent lyophilization yielded 92 % (3.14 g, 18.5 mmol) of 4-azidoaniline hydrochloride (**57**). The purity of the synthesized 4-azidoaniline hydrochloride was similar to that which was purchased by *Sigma-Aldrich*.

Molecular Weight: 170.06 g/mol.
Formula: $C_6H_7ClN_4$.
R_f-value: 0.47; SiO_2, *n*-hexane/ethyl acetate (3/2).
Melting point: 163 °C (ethyl acetate).

Spectroscopic data and assignment of molecule positions:

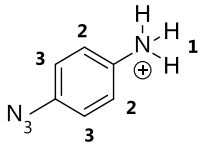

^{1}H NMR: (300 MHz, DMOS-d6): δ [ppm] = 7.18-7.23 (m, 2 H, H-2), 7.36-7.38 (m, 2 H, H-3), 9.64 (br. s, 3 H, H-1).

Synthesis of 4-azidoaniline (salt free) (**58**)

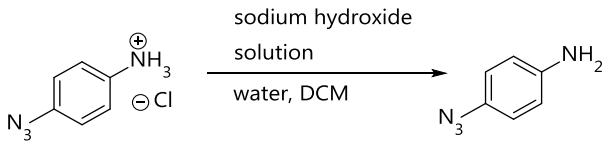

920 mg (5.39 mmol) of 4-azidoanilline hydrochloride were dissolved in water (5 ml) and cooled to 3 C with an ice bath. A dropwise addition of a sodium hydroxide solution (10 %, 1.20 ml) led to a slightly yellowish precipitate which was filtered over G4-glass frit (pore size 10-16 µm). The precipitate was washed with ice-cold water (10 ml) and transferred to a flask by dissolving the residue in DCM (10-15 ml). After evaporation of the solvent under reduced pressure the remained solid was lyophilized to yield 92 % (665 mg, 4.96 mmol) of a yellow powder. The obtained 4-azidoanilline (**58**) was used in the next synthesis step directly after lyophilization.

Molecular Weight: 134.14 g/mol.
Formula: $C_6H_6N_4$.

Spectroscopic data and assignment of molecule positions:

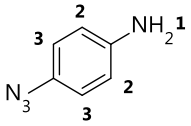

^{1}H NMR: (300 MHz, DMOS-d6): δ [ppm] = 5.13 (br. s, 2 H, H-1), 6.56-6.61 (m, 2 H, H-2), 6.74-6.79 (m, 2 H, H-3).

Synthesis of 2-(*N*-(4-azidophenyl)carbamoyl)-5-((*N*-((benzyloxy)carbonyl)carbamimidoyl)carbamoyl)-4-(3-methoxy-3-oxopropyl)-3-methyl-1*H*-pyrrole (**37**)

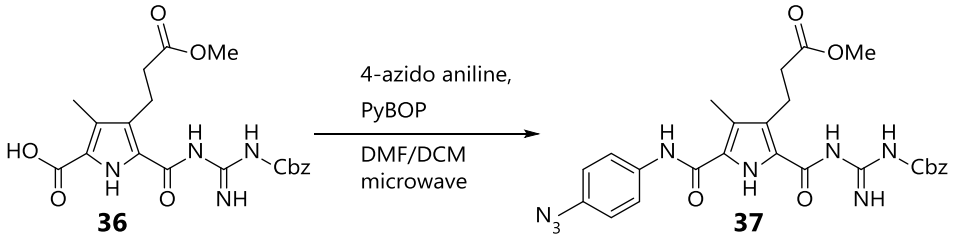

The synthesis of azido pyrrole **37** was carried out in an argon flushed flask under microwave-assistance according to the following synthesis protocol:

Under inert gas 1.61 g (3.74 mmol) of pyrrole **36**, 650 mg (4.85 mmol) of freshly prepared 4-azidoanilline (**58**) (according to the procedure mentioned before) and 3.78 g, (7.26 mmol, 1.9 eq) PyBOP were suspended in 40 ml of a DCM/DMF mixture (1/1). The addition of 1.90 ml (1.75 g, 17.3 mmol, 4.6 eq) NMM was carried out with a subsequent degassing of the mixture. After an initial stirring of the reaction mixture the heating program was started. In a pre-heating step the mixture was heated to 50°C with maximum power (300 W) max. for 2 min under stirring at the highest speed level. In the next step the reaction mixture was heated to 80 C with a power of 250 W for 35 min. Subsequently the mixture was cooled to room temperature. The previous mentioned procedure was carried out 3 times. Reaction control via TLC showed maximum conversion to the desired product after a reaction time of almost 2 h. The solvent was reduced by evaporation. After addition of further 3 ml of DCM the mixture was stored in a fridge over night for crystallization. A repeated precipitation yielded 52% (1.06 g, 1.95 mmol) of pyrrole **37** as a pale brown powder.

Molecular Weight: 546.54 g/mol.

Formula: $C_{26}H_{26}O_6N_8$.

R_f-value: 0.67; SiO_2, *n*-hexane/ethyl acetate (3/2).

Spectroscopic data and assignment of molecule positions:

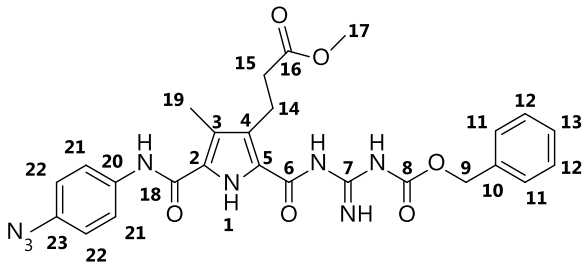

^{1}H NMR: (500.1 MHz, DMOS-d6): δ [ppm] = 2.24 (s, 3 H, H-19), 2.48* (m, 2 H, H-15), 3.07 (br. s, 2 H, H-14), 3.56 (s, 3 H, H-17), 5.21 (br. s, 2 H, H-9), 7.11 (d, $^3J_{H\text{-}21/\ H\text{-}22}$ = 9.14 Hz, 2 H, H-21), 7.30 - 7.52 (m, 5 H, H-11, H-12, H-13), 7.74 (d, $^3J_{H\text{-}22/\ H\text{-}21}$ = 9.14 Hz, 2 H, H-22), 8.58 (br. s, 1 H, N*H*), 9.61 (br. s, 1 H, N*H*), 10.04 (s, 1 H, N*H*), 10.82 (s, 1 H, N*H*), 11.27 (br. s, 1 H, N*H*, H-1).

* (peak showed an overlay with solvent-residual peak at 2.50 ppm; high temperature NMR was used to shift signals and calculate coupling constants as well)

^{13}C NMR: (125.8 MHz, DMSO-d6) δ = 9.9 (1 C, C-19), 19.8 (1 C, C-14), 34.7 (1 C, C-15), 51.1 (1 C, C-17), 66.9 (1 C, C-9), 119.4 (2 C, C-21), 121.2 (2 C, C-22), 128.2, 128.5 (5 C, C-11, C-12, C-13), 133.9, 136.4, 158.0, 159.2 (4 C, C_q), 173.2 (C-16).

The assignment of the carbon atoms was done by two dimensional NMR spectroscopy (HSQC). The correct number of quaternary carbon atoms could not be determined.

HRMS: (ESI, pos., methanol/water): *m/z* $[M]^+$ calcd for $C_{26}H_{26}O_6N_8^+$: 545.1892; found: 545.1830.

Synthesis of *tert*-butyl 5-((*N*-((benzyloxy)carbonyl)carbamimidoyl)carbamoyl)-4-(3-carboxypropyl)-3-methyl-1*H*-pyrrole-2-carboxylate (**59**)

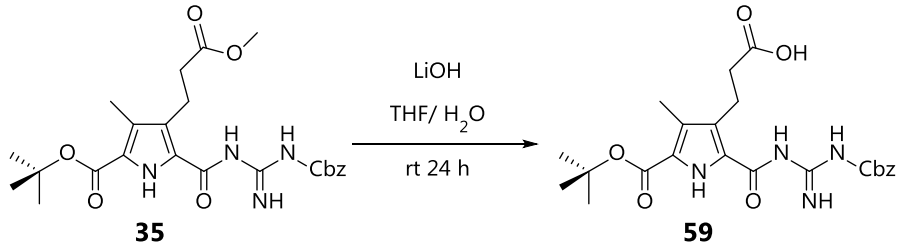

35 **59**

52.0 mg (2.17 mmol) LiOH were added to a solution of 350 mg (719 µmol) of pyrrole **35** in 15 ml of THF/H_2O (2/1). The mixture was stirred for 6 h at room temperature. The volatile solvent was removed by evaporation under reduced pressure and the remaining suspension was lyophilized. The obtained raw product was purified via column chromatography (SiO_2, n-*h*exane/ethyl acetate (1/1) to yield 99 % (339 mg, 717 µmol) of pyrrole **59**.

Molecular Weight: 472.50 g/mol.
Formula: $C_{23}H_{28}O_4N_7$.
R_f-value: 0.22; SiO_2, *n*-hexane/ethyl acetate (1/1).

Spectroscopic data and assignment of molecule positions:

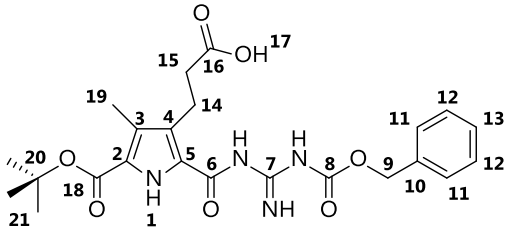

^{1}H NMR: (300.2 MHz, DMOS-d6): δ [ppm] = 1.52 (s, 9 H, H-21), 2.17 (s, 3 H, H-19), 2.32 (t, 2 H, $^3J_{H\text{-}15/\ H\text{-}14}$ = 7.24 Hz, H-15), 2.88 (t, 2 H, $^3J_{H\text{-}14/\ H\text{-}15}$ = 7.24 Hz, H-14), 5.14 (s, 2 H, H-9), 7.35 - 7.40 (m, 5 H, H-11, H-12, H-13), 8.71 (br. s, 1 H, N*H*), 9.46 (br. s, 1 H, N*H*), 10.91 (s, 1 H, N*H*, H-1).

The hydrogen of the carboxylic acid and one of the hydrogens of the guanidinium function could not be assigned but an extremely broadened water signal could be revealed. Therefore a fast exchange with water protons was assumed at least with the acidic proton.

FT-IR: (ATR): $\tilde{\nu}$ [cm^{-1}] = 2927 (w), 1691 (s), 1632 (m), 1556 (m), 1454 (m), 1367 (m), 1254 (s), 1214 (s), 1134 (s), 909 (w).

HRMS: (ESI, pos., methanol/water): *m/z* $[M]^+$ calcd for $C_{23}H_{29}O_4N_7^+$: 473.2031; found: 473.2031; calcd for $C_{23}H_{28}O_4N_7Na^+$: 495.1872; found: 495.1850.

Synthesis of benzyl (2-aminoethyl)carbamate (**60**)[109]

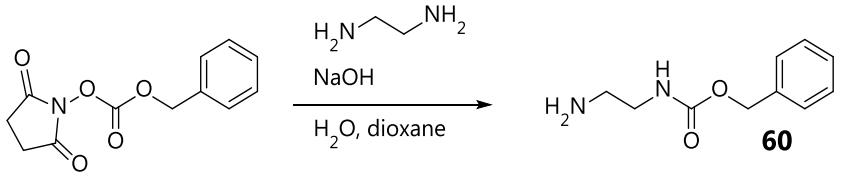

A solution of 6.00 g (24.1 mmol) of *N*-(Benzyloxycarbonyloxy)succinimide in 40 ml $CHCl_3$ was cooled to 0 °C and added to an ice cooled solution of 40 ml (36.0 g, 598) ethylene diamine in 300 ml $CHCl_3$. The addition was carried out under inert gas over a period of 8 h. After stirring for further 8 h under room temperature the mixture was three times washed with 70 ml of brine. The obtained aqueous phase was washed with 40 ml $CHCl_3$. All organic phases were washed three times with 70 ml of saturated $NaHCO_3$-solution and three times with 70 ml of water. Subsequently the solvent was evaporated under reduced pressure. The raw product was purified via MPLC (RP-18-silica, MeOH/H_2O/TFA) to yield 45 % (2.11 g, 10.9 mmol) of **60**.

Molecular Weight: 194.23 g/mol.
Formula: $C_{10}H_{14}O_2N_2$.
R_f-value: 0.22; SiO_2, *n*-hexane/ethyl acetate (1/1).

Spectroscopic data and assignment of molecule positions:

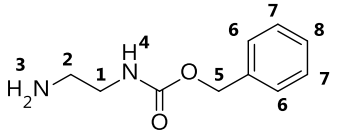

^{1}H NMR: (300.2 MHz, DMOS-d6): δ [ppm] = 2.54 (t, 2 H, $^3J_{H\text{-}2/\,H\text{-}1}$ = 6.72 Hz, H-2), 2.99 (t, 2 H, $^3J_{H\text{-}1/\,H\text{-}2}$ = 6.72 Hz, H-1), 4.99 (s, 2 H, H-5), 6.64 (br. s, 1 H, N*H*), 7.18 (br. s, 1 H, N*H*), 7.29 - 7.35 (m, 5 H, H-6, H-7, H-8), 8.30 (br. s, 1 H, N*H*).

Synthesis of *tert*-butyl 4-(3-((2-(((benzyloxy)carbonyl)amino)ethyl)amino)-3-oxopropyl)-5-((N-((benzyloxy)carbonyl)carbamimidoyl)carbamoyl)-3-methyl-1H-pyrrole-2-carboxylate (**38**)

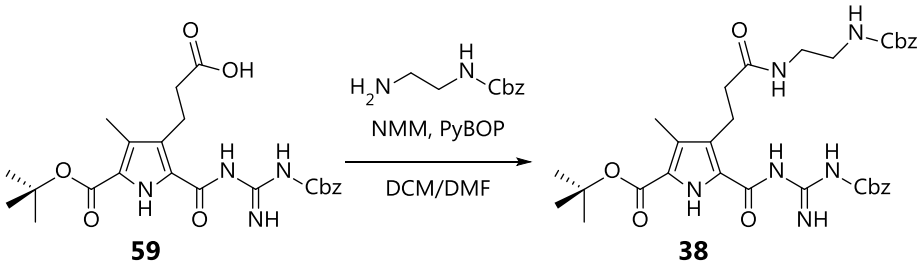

A solution of 27.0 mg (57.0 µmol) of **59**, 13.4 mg (69.0 µmol) of **60** and 39.4 mg (75.7 µmol) of PyBOP were dissolved in 4 ml DCM/DMF (1/1). The reaction mixture was stirred under inert gas and 15 µL (13.8 mg, 136.0 µmol) of NMM were added by syringe in two portions. TLC control showed a full conversion after stirring for 12 h at room temperature. The solvent was removed under reduced pressure to yield the raw product which was further purified via column chromatography (SiO_2, *n*-hexane/ethyl acetate (1/1). After purification 87 % (32.2 mg, 49.6 µmol) of **38** could be obtained.

Molecular Weight: 648.29 g/mol
Formula: $C_{33}H_{40}O_8N_6$
R_f-value: 0.17; SiO_2, *n*-hexane/ethyl acetate (1/1).

Spectroscopic data and assignment of molecule positions:

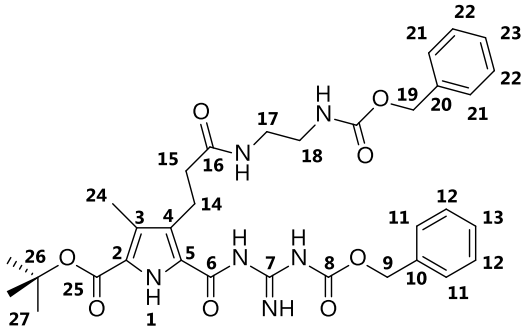

^{1}H NMR: (500.1 MHz, DMOS-d6): δ [ppm] = 1.52 (s, 9 H, H-27), 2.16 (s, 3 H, H-24), 2.23 (t, 2 H, $^3J_{H\text{-}15/\ H\text{-}14}$ = 7.80 Hz, H-15), 2.93 (t, 2 H, $^3J_{H\text{-}14/\ H\text{-}15}$ = 7.80 Hz, H-14), 2.99 - 3.09 (m, 4 H, H-17, H-18), 5.00 (s, 2 H, H-19), 5.17 (br. s, 2 H, H-9), 7.23 (t, 1 H, N*H*), 7.30 - 7.35 (m, 5 H, H-21, H-22, H-23), 7.37 - 7.42 (m, 5 H, H-11, H-12, H-13),

7.80 (t, 1 H, N*H*), 8.65 (br. s, 1 H, N*H*), 9.48 (br. s, 1 H, N*H*), 11.07 (br. s, 1 H, N*H*, H-1).

Not all amine and amide protons could be assigned.

^{13}C NMR: (125.8 MHz, DMSO-d6) δ = 9.8 (1 C, C-24), 20.5 (1 C, C-14), 28.0 (3 C, C-27), 36.9 (1 C, C-15), 38.5 (1 C, C-17), 40.0 (1 C, C-18), 65.2 (2 C, C-9, C-19), 80.8 (1 C, C-26), 125.3 (2 C, C_q), 127.7, 128.1, 128.4 (10 C, C-11, C-12, C-13, C-21, C-22, C-23), 137.1 (2 C, C-10, C-20), 156.1, 160.2 (2 C, C_q), 172.1 (1 C, C-16).

The correct number of quaternary carbon atoms could not be assigned.

HRMS: (ESI, pos., methanol/water): *m/z* $[M]^+$ calcd for $C_{33}H_{40}O_8N_6Na^+$: 671.2800; found: 671.2791; calcd for $(C_{33}H_{40}O_8N_6)_2Na^+$: 1319.5707; found: 1319.5687.

Synthesis of *tert*-butyl 4-(3-((2-(((benzyloxy)carbonyl)amino)ethyl)amino)-3-oxopropyl)-5-((N-((benzyloxy)carbonyl)carbamimidoyl)carbamoyl)-3-methyl-1H-pyrrole-2-carboxylic acid (**61**)

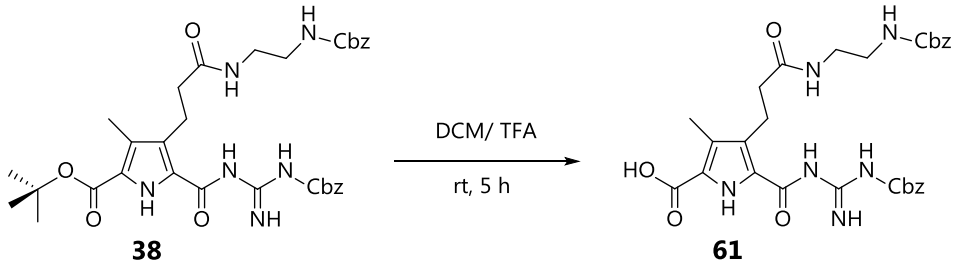

38 **61**

28.1 mg (43.3 µmol) of **38** were dissolved in 4 ml of DCM/TFA (1/1). The reaction mixture was stirred for 5 h at room temperature. The solvent was removed under reduced pressure and the residue was lyophilized to yield 98 % (25.2 mg, 42.5 µmol) of **38** could be obtained.

Molecular Weight: 592.60 g/mol
Formula: $C_{29}H_{32}O_8N_6$
R_f-value: 0.82; RP-18 silica, acetonitrile/water (1/1).

Spectroscopic data and assignment of molecule positions:

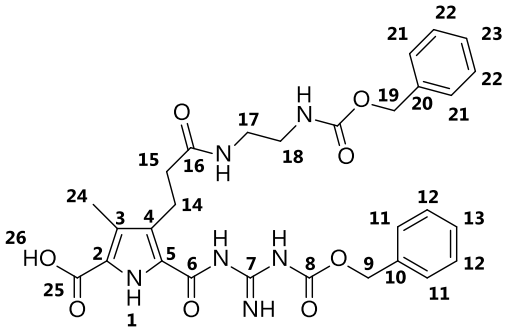

^{1}H NMR: (500.1 MHz, DMOS-d6): δ [ppm] = 2.19 (s, 3 H, H-24), 2.24 (t, 2 H, $^{3}J_{H\text{-}15/\ H\text{-}14}$ = 7.77 Hz, H-15), 2.93 (t, 2 H, $^{3}J_{H\text{-}14/\ H\text{-}15}$ = 7.77 Hz, H-14), 3.00 - 3.09 (m, 4 H, H-17, H-18), 5.00 (s, 2 H, H-19), 5.16 (br. s, 2 H, H-9), 7.23 (t, 1 H, N*H*), 7.30 - 7.35 (m, 5 H, H-21, H-22, H-23), 7.37 - 7.40 (m, 5 H, H-11, H-12, H-13), 7.79 (t, 1 H, N*H*), 7.68 (br. s, 1 H, N*H*, H-1), 8.66 (br. s, 1 H, N*H*), 9.48 (br. s, 1 H, N*H*).

^{13}C NMR: (125.8 MHz, DMSO-d6) δ = 9.6 (1 C, C-24), 20.5 (1 C, C-14), 36.4 (1 C, C-15), 38.5 (1 C, C-17), 40.0 (1 C, C-18), 65.2 (2 C, C-9, C-19), 125.3 (2 C, C_q), 127.7, 128.1, 128.4 (10 C, C-11, C-12, C-13, C-21, C-22, C-23), 137.1 (2 C, C-10, C-20), 156.1, 160.2 (2 C, C_q), 172.1 (1 C, C-16).

Not all quaternary carbon atoms could be assigned.

Synthesis of 4-(3-((2-(((benzyloxy)carbonyl)amino)ethyl)amino)-3-oxopropyl)-5-((n-((benzyloxy)carbonyl)carbamimidoyl)carbamoyl)-3-methyl-1h-pyrrole-2-amido-(*para*-phenyl) azide (**39**)

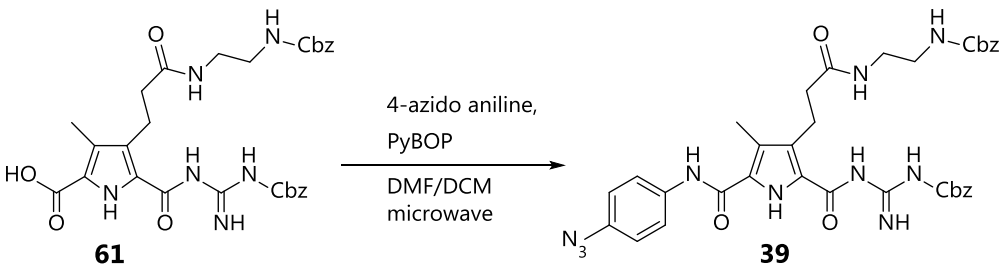

61 **39**

The synthesis of azido pyrrole **37** was executed in an argon flushed flask under microwave-assistance according to the following synthesis protocol:

A solution of 23.0 mg (39.0 µmol) of **61** and 11.0 mg (82.0 µmol) of freshly prepared 4-azidoaniline (**58**) in 5 ml DCM/DMF (1/1) was degassed and stirred at room temperature. Under inert gas 38.5 mg (74.0 µmol) of PyBOP and 15.0 µl (13.8 mg 136 µmol) of NMM were added to the solution. After an initial stirring of the reaction mixture the heating program was started. With a maximum power of 60 W the reaction mixture was heated to 90 °C for 30 min. in intervals of 10 min. intermediate reaction control via TLC was made. The reaction was stopped via evaporation of the solvent reduced pressure. After lyophilization the crude was purified via chromatography (SiO_2, *n*-hexane/ ethyl acetate (2/1)) and yielded 18 % (5.00 mg, 7.06 µmol) of **39**.

Molecular Weight: 708.28 g/mol
Formula: $C_{35}H_{36}O_7N_{10}$
R_f-value: 0.17; SiO_2, *n*-hexane/ethyl acetate (1/1).

Spectroscopic data and assignment of molecule positions:

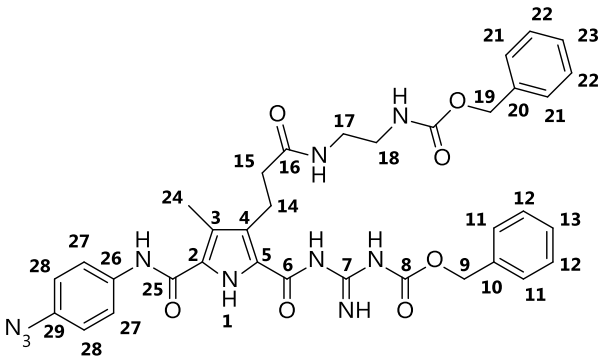

^{1}H NMR: (600.1 MHz, DMOS-d6): δ [ppm] = 2.25 (s, 3 H, H-24), 2.30 (m, 2 H, H-15), 3.02 (m, 4 H, H-14, H-18), 3.09 - 3.11 (m, 2 H, H-17), 5.00 (s, 2 H, H-19), 5.20 (br. s, 2 H, H-9), 7.11 (d, $^3J_{H\text{-}27/\ H\text{-}28}$ = 8.84 Hz, 2 H, H-27), 7.23 (t, 1 H, N*H*), 7.30 - 7.36 (m, 5 H, H-21, H-22, H-23), 7.38 - 7.46 (m, 5 H, H-11, H-12, H-13), 7.74 (d, $^3J_{H\text{-}28/\ H\text{-}27}$ = 8.84 Hz, 2 H, H-28), 7.95 (m, 1 H, N*H*), 8.60 (br. s, 1 H, N*H*), 9.51 (br. s, 1 H, N*H*), 10.03 (s, 1 H, N*H*), 10.96 (br. s, 1 H, N*H*), 11.46 (s, 1 H, N*H*, H-1).

^{13}C NMR: (150.9 MHz, DMSO-d6) δ = 9.7 (1 C, C-24), 20.8 (1 C, C-14), 36.6 (1 C, C-15), 38.4 (1 C, C-17), 39.7 (1 C, C-18), 65.0 – 66.5 (2 C, C-9, C-19), 118.9 (2 C, C_q), 119.1 – 120.9 (4 C, C-27, C-28), 125.3 (2 C, C_q), 127.5, 127.9, 128.1, 128.2 (10 C, C-11, C-12, C-13, C-21, C-22,

C-23), 133.8 (C_q), 137.1 (2 C, C-10, C-20), 142.8 (C_q), 156.1, 159.1 (2 C, C_q), 172.9, 174.3, 206.5 (3 C, C_q).

The correct number of quaternary carbon atoms could not be assigned.

HRMS: (ESI, pos., methanol/water): *m/z* $[M]^+$ calcd for $C_{35}H_{36}O_7N_{10}Na^+$: 731.2661; found: 731.2672; calcd for $(C_{35}H_{36}O_7N_{10})_2Na^+$: 1439.5429; found: 1319.5466.

Synthesis of 5-((*N*-(*tert*-butoxycarbonyl)carbamimidoyl)carbamoyl)-1*H*-pyrrole-2-amido-*para*-phenyl azide (**41**)

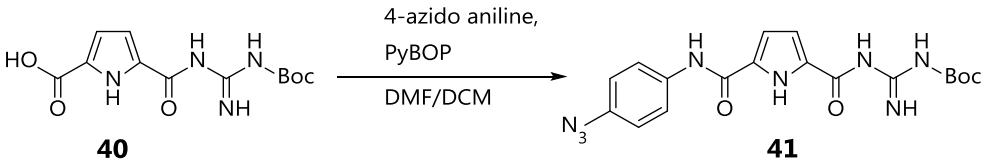

40 **41**

In an inert gas atmosphere 266.0 mg (670 µmol) of **40**, 90.0 mg (671 µmol) of 4-azidoanilline and 430 mg (826 µmol) of PyBOP were dissolved in 15 ml DCM/DMF (1/2). After addition of 70 µL (52.0 mg, 402 µmol) of DIPEA via syringe the reaction mixture was stirred for 14 h at room temperature. The solvent was evaporated under reduced pressure until a residual amount of 7 ml remained. After addition of 15 ml of water the precipitate was filtered and washed with ice water. The crude was dried over silica and purified via column chromatography (SiO_2, *n*-hexane/ ethyl acetate (2/1)) to yield 23 % (62.7 mg, 152 µmol) of **41**.

Molecular Weight: 412.41 g/mol
Formula: $C_{18}H_{20}O_4N_8$
R_f-value: 0.68; SiO_2, *n*-hexane/ethyl acetate (1/1).

Spectroscopic data and assignment of molecule positions:

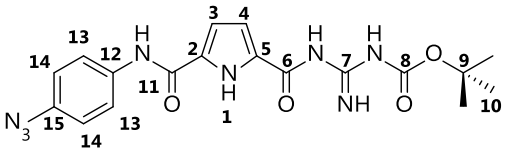

^{1}H NMR: (600.1 MHz, DMOS-d6): δ [ppm] = 1.47 (s, 9 H, H-10), 6.86 (br. s, 1 H, H-3), 7.01 (s, 1 H, H-4), 7.13 (d, $^3J_{H\text{-}13/\ H\text{-}14}$ = 8.87 Hz, 2 H,

H-13), 7.78 (d, $^{3}J_{H\text{-}14/\ H\text{-}13}$ = 8.87 Hz, 2 H, H-14), 8.58 (br. s, 1 H, N*H*), 9.37 (br. s, 1 H, N*H*), 10.16 (s, 1 H, N*H*, H-1), 10.84 (br. s, 1 H, N*H*), 11.36 (br. s, 1 H, N*H*).

^{13}C NMR: (150.9 MHz, DMSO-d6) δ = 27.7 (3 C, C-10), 113.2 (1 C, C-9), 119.4 – 121.4 (4 C, C-13, C-14), 134.1, 136.1 (2 C, C-3, C-4), 158.0, 158.4 (2 C, C_q).

The correct number of quaternary carbon atoms could not be assigned.

HRMS: (ESI, pos., methanol/water): *m/z* $[M]^+$ calcd for $C_{18}H_{21}O_4N_8^+$: 413.1678; found: 413.1680.

Synthesis of 5-((*N*-(*tert*-butoxycarbonyl)carbamimidoyl)carbamoyl)-1*H*-pyrrole-2-amido-*para*-phenyl iodide (**42**)

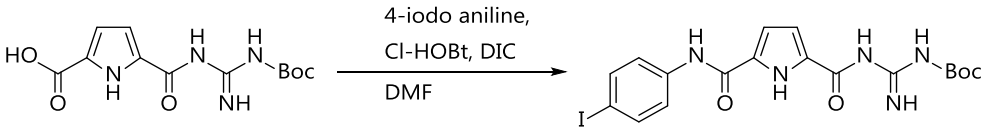

40 **42**

In an inert gas atmosphere 95.4 mg (240 µmol) of **40**, 57.9 mg (246 µmol) of 4-iodoanilline and 47.0 mg (277 µmol) of CI-HOBt were dissolved in 5 ml DMF. After the addition of 40 µL (32.8 mg, 260 µmol) of DIC via syringe the reaction mixture was stirred for 24 h at room temperature. After addition of 15 ml of water the precipitate was filtered and washed with ice water. The crude was dried over silica and purified via column chromatography (SiO_2, *n*-hexane/ ethyl acetate (3/2)) to yield 45 % (51.7 mg, 108 µmol) of **42**.

Molecular Weight: 497.29 g/mol
Formula: $C_{18}H_{20}O_4N_5I$
R_f-value: 0.47; SiO_2, *n*-hexane/ethyl acetate (3/2).

Spectroscopic data and assignment of molecule positions:

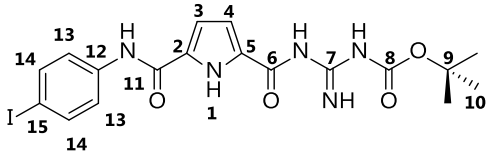

^{1}H NMR: (300.2 MHz, DMOS-d6): δ [ppm] = 1.47 (s, 9 H, H-10), 6.85 (br. s, 1 H, H-3), 7.01 (s, 1 H, H-4), 7.57 (d, $^3J_{H\text{-}13/\ H\text{-}14}$ = 8.99 Hz, 2 H, H-13), 7.69 (d, $^3J_{H\text{-}14/\ H\text{-}13}$ = 8.99 Hz, 2 H, H-14), 8.58 (br. s, 1 H, N*H*), 9.36 (br. s, 1 H, N*H*), 10.15 (s, 1 H, N*H*, H-1), 10.82 (br. s, 1 H, N*H*), 11.39 (br. s, 1 H, N*H*).

MS: (ESI, neg., methanol/water): *m/z* $[M]^-$ calcd for $C_{18}H_{20}O_4N_8I^-$: 496.0493; found: 496.18.

Synthesis of the TFA salt of 5-((*N*-carbamimidoyl)carbamoyl)-1*H*-pyrrole-2-amido-*para*-phenyl iodide (**43**)

42 **43**

50.0 mg (100 µmol) of pyrrole **42** were dissolved in 5 ml DCM. After addition of 1 mL TFA the reaction mixture was stirred for 1 h at room temperature. The solvent was evaporated under reduced pressure to yield 99 % (49.3 mg, 99 µmol) of **43**.

Molecular Weight: 397.18 g/mol
Formula: $C_{13}H_{12}O_2N_5I$
R_f-value: 0.54; SiO_2, ethyl acetate/*iso*-propanol (2/1).

Spectroscopic data and assignment of molecule positions:

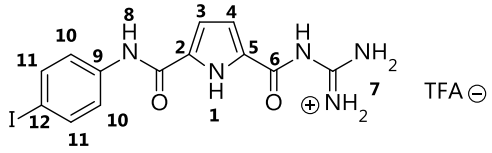

^{1}H NMR: (600.1 MHz, DMOS-d6): δ [ppm] = 7.10 (m, 1 H, H-3), 7.13 (br. s, 1 H, H-4), 7.57 (d, $^3J_{H\text{-}10/\ H\text{-}11}$ = 8.83 Hz, 2 H, H-10), 7.71 (d, $^3J_{H\text{-}11/\ H\text{-}10}$ = 8.83 Hz, 2 H, H-11), 8.32 (br. s, 4 H, N*H*, H-7), 10.27 (s, 1 H, H-8), 11.20 (s, 1 H, N*H*,), 12.62 (br. s, 1 H, N*H*, H-1).

Proton H-8 could be identified via selective NOESY-, HSQC- and HMBCexperiments. See detailed spectrum in the appendix.

^{13}C NMR: (150.9 MHz, DMSO-d6) δ = 87.5 (1 C, C-12), 113.6 (1 C, C-3), 115.3 (1 C, C-4), 122.1 (2 C, C-10), 126.3, 132.1 (2 C, C-2, C-5), 137.4 (2 C, C-11), 138.4 (1 C, C-9), 154.9, 157.7, 159.5 (3 C, C_q).

HRMS: (ESI, pos., methanol/water): *m/z* $[M]^+$ calcd for $C_{13}H_{13}O_2N_5I^+$: 398.0108; found: 398.0121; calcd for $(C_{13}H_{12}O_2N_5I)_2H^+$: 795.0144; found: 795.0128.

Synthesis of 5-((*N*-carbamimidoyl) carbamoyl)-1*H*-pyrrole-2-amido-*para*-phenyl azide (**32**)

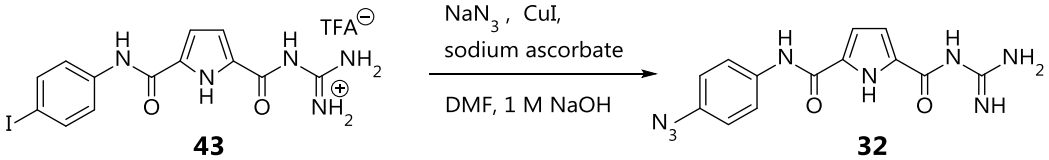

43 **32**

In an inert gas atmosphere 48.0 mg (97.3 µmol) of **43**, 14.5 mg (223 µmol) of sodium azide, 3.32 mg (16.8 µmol) of sodium ascorbate and 2 µL mg (1.64 mg, 18.6 µmol) of 1,2-*N*,*N*-dimethylen diamine were dissolved in 2.5 ml DCM. After addition of 2 drops of 1 M sodium hydroxide solution and 6.00 mg (31.5 µmol) of copper iodide the reaction mixture was stirred at room temperature. The mixture was heated to 40 °C after addition of 4 µL mg (3.28 mg, 37.2 µmol) of 1,2-*N*,*N*-dimethylen diamine, 6.00 mg (31.5 µmol) of sodium azide, 2.20 mg (11.1 µmol) of sodium ascorbate and 3.30 mg (17.3 µmol) of copper iodide the mixture was stirred 16 h at 40 °C and 4 h at 50 °C. The reaction control was carried out via TLC. The crude product was precipitated with 15 ml of water. The precipitate was separated by filtration and dissolved in 25 ml ethyl acetate afterwards. The organic phase was washed successively with of saturated sodium sulfide solution (5 ml), water (5 ml) and brine (5 ml). The solvent was evaporated under reduced pressure and the remaining residue was lyophilized. The azide **32** was obtained in a yield of 80 % (24.2 mg, 77.4 µmol).

Molecular Weight: 312.29 g/mol
Formula: $C_{12}H_{12}O_2N_5$
R_f-value: 0.65; SiO_2, ethyl acetate/*iso*-propanol (2/1).

Spectroscopic data and assignment of molecule positions:

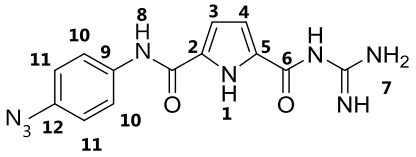

^{1}H NMR: (600.1 MHz, DMOS-d6): δ [ppm] = 6.63 (d, $^{3}J_{H\text{-}3/\ H\text{-}4}$ = 3.49 Hz, 1 H, H-3), 6.93 (d, $^{3}J_{H\text{-}4/\ H\text{-}3}$ = 3.49 Hz, 1 H, H-4), 7.11 (d, $^{3}J_{H\text{-}11/\ H\text{-}10}$ = 8.83 Hz, 2 H, H-11), 7,21 (s, 1 H, N*H*), 7.78 (d, $^{3}J_{H\text{-}10/\ H\text{-}11}$ = 8.83 Hz, 2 H, H-10), 8.32 (br. s, 3 H, N*H*, H-7), 10.16 (s, 1 H, H-8), 11.16 (s, 1 H, N*H*, H-1).

Proton H-8 could be identified via selective NOESY-, HSQC- and HMBCexperiments. See detailed spectrum in the appendix.

^{13}C NMR: (150.9 MHz, DMSO-d6) δ = 111.7 (1 C, C-3), 113.5 (1 C, C-4), 119.4 (2 C, C-11), 121.2 (2 C, C-10), 133.9 (1 C, C-9), 127.2, 135 (2 C, C-2, C-5) 136.4 (1 C, C-12), 158.1, 162.7, 169.7 (3 C, C_q).

HRMS: (ESI, pos., methanol/water): *m/z* $[M]^+$ calcd for $C_{12}H_{13}O_2N_8^+$: 313.1156; found: 313.1159.

6.4 Syntheses of Un-Symmetrical Tweezer Building Blocks

This section describes the syntheses of unsymmetrical building blocks of the tweezer **14** as well as of the truncated tweezer **19b**. Starting with the synthesis of the hydroquinone tweezer **14** the syntheses of the unsymmetrical tweezers **31** and **50** will be shown first.

The synthesis of the hydroquinone tweezer **14** was done in style of reported procedure. The formation of the tweezer skeleton via a twofold Diels-Alder reaction was carried out in reusable Schlenk vessels. In the reported procedure capsuled glass ampullae were used. The advantage compared to the described version was the possibility of reaction monitoring via TLC and mass spectroscopy.

Synthesis of 8,19-Diacetoxy-5,6,6a,7,9,10,11,16,17,17a,18,20,21,22-hexadeca-hydro-5,22:7,20:9,18:11,16-tetramethanononacene (**28**)

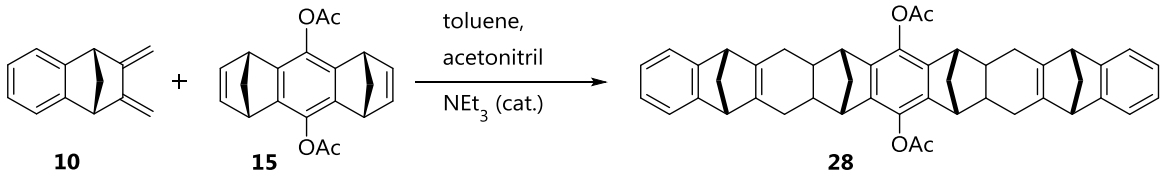

In an inert gas atmosphere 501.0 mg (1.55 mmol) of diyl acetate **15**, 1.01 g (5.97 mmol) of diene **10** were dissolved in 10 ml of toluene and 5 ml of acetonitrile. After stirring for 5 min. 200 µl (145.2 mg, 1.43 mmol) of triethylamine were added via syringe and the mixture was slowly degassed and cooled to -196 °C. The vacuumed Schlenk vessel was heated up to 190 °C in an oil bath. The reaction was monitored via TLC and mass spectroscopy. After 65 h the reaction mixture was cooled to room temperature and the solvent was reduced to 5 ml. The slight suspension was cooled in a fridge to precipitate. After filtration the product **28** was washed with 20 ml of ice-cold cyclohexane and tried to obtain a yield of 61 % (622 mg, 944 µmol).

Molecular Weight: 658.84 g/mol
Formula: $C_{46}H_{42}O_4$
R_f-value: 0.39; SiO_2, *n*-hexan/ethyl acetate (3/1).

Spectroscopic data and assignment of molecule positions:

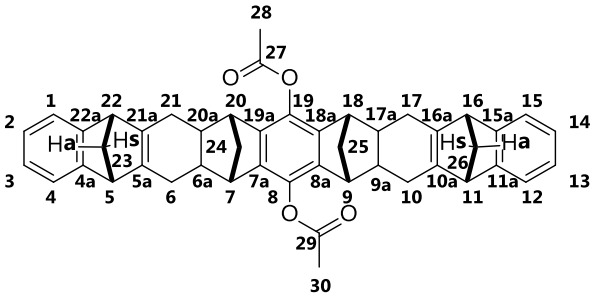

^{1}H NMR: (300.1 MHz, $CDCl_3$): δ [ppm] = 1.65 – 1.68 (m, 4 H, H-24, H-25), 1.95 – 1.98 (m, 2 H, H-23a, H-26a), 2.08 -2.35 (m, 14 H, H-6, H-6a, H-9a, H-10, H-17, H-17a, H-20a, H-21, H-23s, H-26s), 2.29 (s, 6 H, H-28, H-30), 2.83 (s, 4 H, H-7, H-9, H-18, H-20), 3.54 (s, 4 H, H-5, H-11, H-16, H-22), 6.83 (m, 4 H, H-2, H-3, H-13, H-14), 7.11 (m, 4 H, H-1, H-4, H-12, H-15).

^{13}C NMR: (75.5 MHz, $CDCl_3$) δ = 20.9 (2 C, C-28, C-30), 29.8 (4 C, C-6, C-10, C-17, C-21), 38.9 (4 C, C-6a, C-9a, C-17a, C-20a), 45.8 (2 C, C-24,

C-25), 49.9 (4 C, C-7, C-9, C-18, C-20), 53.6 (4 C, C-5, C-11, C-16, C-22), 67.3 (2 C, C-23, C-26), 120.8 (4 C, C-1, C-4, C-12, C-15), 124.1 (4 C, C-2, C-3, C-13, C-14), 135.2 (4 C, C-7a, C-8a, C-18a, C-19a), 139.3 (2 C, C-8, C-19), 147.1 (4 C, C-4a, C-11a, C-15a, C-22a), 152.6 (4 C, C-5a, C-10a, C-16a, C-21a), 169.1 (2 C, C-27, C-29).

MS: (ESI, pos., methanol/water): *m/z* $[M]^+$ calcd for $C_{46}H_{42}O_4Na^+$: 681.2975; found: 681.29.

Synthesis of 8,19-Diacetoxy-5,7,9,11,16,18,20,22-octahydro-5,22:7,20:9,18:11,16-tetramethanononacene (**29**)

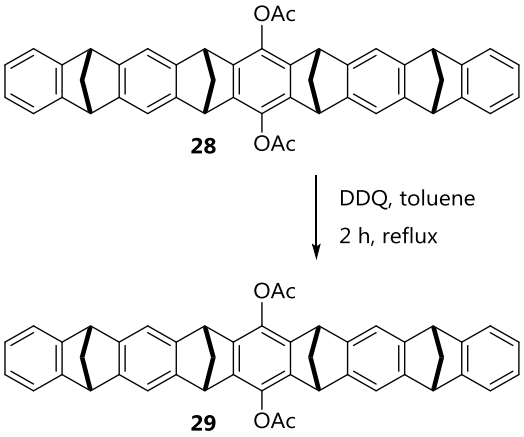

In an inert gas atmosphere 928 mg (1.41 mmol) of **28** and 1.50 g (6.60 mmol) of DDQ were suspended in 30 ml of toluene. The mixture was heated to relux for 2 h. After cooling to 60 °C and an addition of 450 µl (387 mg, 4.83 mmol) of 1,4-cyclohexadiene the mixture was stirred for further 30 min. The red-colored precipitate was filtered and washed with toluene carefully. The obtained crude was lyophilized and purified via column chromatography (SiO_2, *n*-hexane/ ethyl acetate (5/4)) to yield 44 % (399 mg, 613 µmol) of **29**.

Molecular Weight: 650.77 g/mol
Formula: $C_{46}H_{34}O_4$
R_f-value: 0.72; SiO_2, *n*-hexan/ethyl acetate (1/1).

Spectroscopic data and assignment of molecule positions:

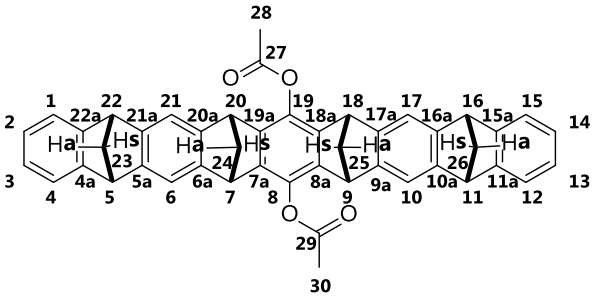

^{1}H NMR: (300.1 MHz, $CDCl_3$): δ [ppm] = 2.45 (m, 2 H, H-24a, H-25a), 2.48 (s, 6 H, H-28, H-30), 2.54 (m, 4 H, H-23, H-26), 2.62 -2.65 (m, 2 H, H-24s, H-25s), 4.11 (s, 4 H, H-7, H-9, H-18, H-20), 4.18 (s, 4 H, H-5, H-11, H-16, H-22), 6.86 - 6.88 (m, 4 H, H-2, H-3, H-13, H-14), 7.18 (m, 4 H, H-1, H-4, H-12, H-15).

^{13}C NMR: (75.5 MHz, $CDCl_3$) δ = 20.9 (2 C, C-28, C-30), 48.8 (4 C, C-7, C-9, C-18, C-20), 51.4 (4 C, C-5, C-11, C-16, C-22), 68.9 (2 C, C-24, C-25), 70.2 (2 C, C-23, C-26), 116.6 (4 C, C-6, C-10, C-17, C-21), 121.5 (4 C, C-1, C-4, C-12, C-15), 124.7 (4 C, C-2, C-3, C-13, C-14), 137.2 (4 C, C-7a, C-8a, C-18a, C-19a), 141.5 (2 C, C-8, C-19), 146.4 (4 C, C-6a, C-9a, C-17a, C-20a), 147.8 (4 C, C-5a, C-10a, C-16a, C-21a), 150.4 (4 C, C-4a, C-11a, C-15a, C-22a), 169.0 (2 C, C-27, C-29).

HRMS: (ESI, pos., methanol/water): *m/z* $[M]^+$ calcd for $C_{46}H_{34}O_4Na^+$: 673.2349; found: 673.2296.

Synthesis of 8,19-Dihydroxy-(5,7,9,11,16,18,20,22)octahydro-5,22:7,20:9,18:11,16-tetramethanononacene (**14**)

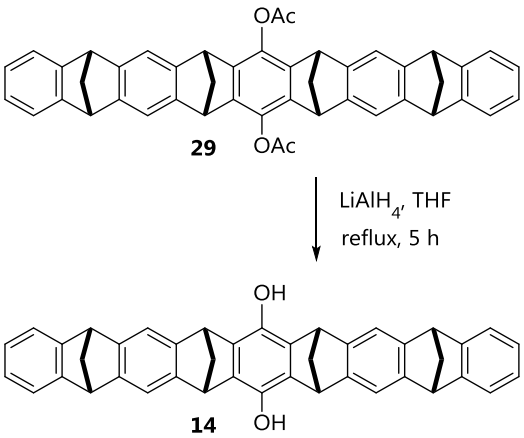

In an argon gas atmosphere 124 mg (3.79 mmol) of $LiAlH_4$ were suspended in 20 ml of THF (abs.) and cooled to -10 °C. Without increasing the temperature above 0 °C a suspension of 255 mg (392 µmol) of **29** in 30 ml THF (abs.) were added dropwise to the previous suspension. The reaction mixture was stirred for 5 h under reflux and cooled to 0 °C afterwards. 22 ml of a saturated NH_4Cl solution were added via syringe and the mixture was stirred for 12 h at room temperature. After adjustment of the pH value to 1 with half conc. HCl the phases were separated and the aqueous phase was extracted twice with $CHCl_3$ (50 ml). The combined organic phases were dried over sodium sulfate and the solvent was evaporated under vacuum. The crude product (300 mg) was lyophilized before purification via MPLC was carried out (SiO_2, *n*-hexane/ ethyl acetate (3/1)). The dihydroxy tweezer **14** was obtained in a yield of 97 % (215 mg, 380 µmol).

Molecular Weight: 566.70 g/mol
Formula: $C_{42}H_{30}O_2$
R_f-value: 0.78; SiO_2, *n*-hexan/ethyl acetate (3/1).

Spectroscopic data and assignment of molecule positions:

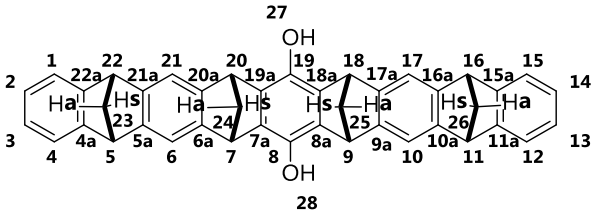

^{1}H NMR: (300.1 MHz, $CDCl_3$): δ [ppm] = 2.37 – 2.43 (dm, 8 H, H-23, H-24, H-25, H-26), 4.06 (br. s, 4 H, H-7, H-9, H-18, H-20), 4.13 (s, 2 H, H-27, H-28), 4.17 (m, 4 H, H-5, H-11, H-16, H-22), 6.73 - 6.76 (m,

4 H, H-2, H-3, H-13, H-14), 7.05 – 7.08 (m, 4 H, H-1, H-4, H-12, H-15), 7.14 (s, 4 H, H-6, H-10, H-17, H-21).

^{13}C NMR: (75.5 MHz, $CDCl_3$) δ = 47.4 (4 C, C-7, C-9, C-18, C-20), 51.3 (4 C, C-5, C-11, C-16, C-22), 68.7 (4 C, C-23, C-24, C-25, C-26), 116.3 (4 C, C-6, C-10, C-17, C-21), 121.5 (4 C, C-1, C-4, C-12, C-15), 124.6 (4 C, C-2, C-3, C-13, C-14), 136.5 (4 C, C-7a, C-8a, C-18a, C-19a), 146.9 (4 C, C-6a, C-9a, C-17a, C-20a), 147.9 (4 C, C-5a, C-10a, C-16a, C-21a), 148.4 (2 C, C-8, C-19), 150.7 (4 C, C-4a, C-11a, C-15a, C-22a).

MS: (ESI, pos., methanol/water): *m/z* $[M]^+$ calcd for $C_{42}H_{30}O_2Na^+$: 689.21; found: 689.22.

Synthesis of 8-prop-2-yn-1-yloxy-19-monohydroxy-(5,7,9,11,16,18,20,22)-octahydro-5,22:7,20:9,18:11,16-tetramethanononacene (**14**)

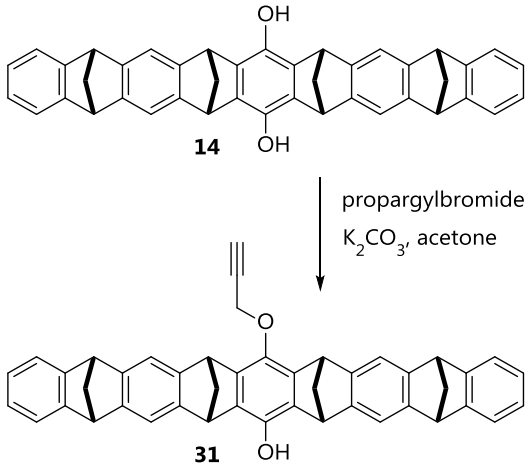

In an atmosphere of argon gas 195 mg (344 µmol) of **14** and 262 mg (1.89 mmol) of K_2CO_3 were suspended in 6 ml of acetone. The mixture was heated to 80 °C for 30 min. and cooled to room temperature afterwards. A solution of propargyl bromide in 264 µl acetone (31.4 mg, 264 µmol, 0.77 eq.) was added dropwise via syringe over a period of 2 h. The reaction was heated to reflux for 12 h. After cooling to room temperature the mixture was filtrated over nylon filter and the precipitate was washed thoroughly with acetone (45 ml). The solvent of the filtrate was evaporated under reduced pressure and the remaining solid was lyophilized. Purification of the crude product (224 mg) via column chromatography (SiO_2,

n-hexane/ ethyl acetate (2/1)) yielded the mono-alkyne tweezer **31** with 15 % (30.4 mg, 50.3 µmol).

Molecular Weight: 604.75 g/mol
Formula: $C_{45}H_{32}O_2$
R_f-value: 0.54; SiO_2, *n*-hexan/ethyl acetate (2/1).

Spectroscopic data and assignment of molecule positions:

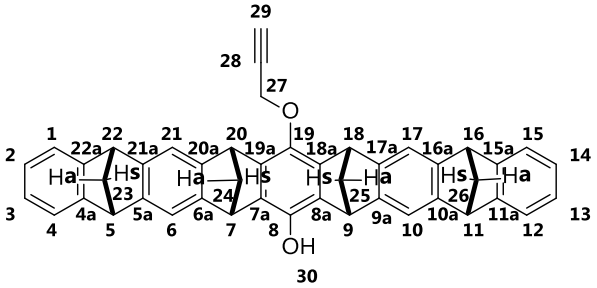

^{1}H NMR: (500.3 MHz, $CDCl_3$): δ [ppm] = 2.25 (t, $^4J_{H\text{-}29/\ H\text{-}27}$ = 2.37 Hz, 1 H, H-29), 2.35 – 2.40 (m, 4 H, H-23, H-26), 2.40 – 2.45 (m, 4 H, H-24, H-25), 4.06 – 4.07 (m, 4 H, H-5, H-11, H-16, H-22), 4.16 – 4.17 (m, 2 H, H-7, H-9), 4.27 (br. s, 1 H, H-30), 4.29 – 4.30 (m, 2 H, H-18, H-20), 4.40 (d, $^4J_{H\text{-}27/\ H\text{-}29}$ = 2.37 Hz, 2 H, H-27), 6.74 - 6.76 (m, 4 H, H-2, H-3, H-13, H-14), 7.06 – 7.08 (m, 4 H, H-1, H-4, H-12, H-15), 7.14 (br. s, 2 H, H-17, H-21), 7.15 (br. s, 2 H, H-6, H-10).

The assignment of unsymmetrical protons could be carried out via selective NOESY- and HSQCexperiments. See detailed spectrum in the appendix.

^{13}C NMR: (125.8 MHz, $CDCl_3$) δ [ppm] = 47.4 (2 C, C-7, C-9), 48.6 (2 C, C-18, C-20), 51.4 (4 C, C-5, C-11, C-16, C-22), 61.7 (1 C, C-27), 69.2 (2 C, C-24, C-25), 70.2 (2 C, C-23, C-26), 75.3 (1 C, C-29), 79.8 (1 C, C-28), 116.3, 116.5 (4 C, C-6, C-10, C-17, C-21), 121.5, 121.6 (4 C, C-1, C-4, C-12, C-15), 124.7, 124.8 (4 C, C-2, C-3, C-13, C-14), 136.5 (2 C, C-7a, C-8a), 140.8 (2 C, C-18a, C-19a), 140.9 (1 C, C-8), 142.2 (1 C, C-19), 146.9, 147.0 (4 C, C-6a, C-9a, C-17a, C-20a), 147.6, 147.7 (4 C, C-5a, C-10a, C-16a, C-21a), 150.5 (4 C, C-4a, C-11a, C-15a, C-22a).

The correct assignment of carbon atoms was executed with COSY-experiment. The double signal sets in the range from

116.3 to 124.8 are caused by the asymmetry of the molecule. See more detailed spectrum in the appendix.

HRMS: (ESI, pos., methanol/water): *m/z* $[M]^+$ calcd for $C_{45}H_{32}O_2Na^+$: 627.2295; found: 627.2309.

Synthesis of (5,7,9,11,16,18,20,22) octahydro-5,22:7,20:9,18:11,16-tetra-methanononacene-8,19-bis-(dihydrogenphosphat) (**47**)

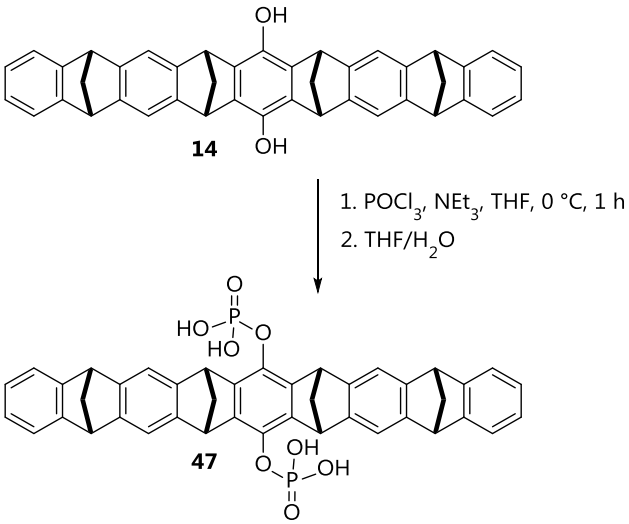

In an argon gas atmosphere 100 mg (176 µmol) of tweezer **14** were dissolved in 10 ml of THF and cooled to 0 °C in an ice bath. Via a syringe 218 µl (365 mg, 2.38 mmol, 13.5 eq) of phosphoryl chloride were added within some minutes. The mixture was stirred for 10 min at 0 °C. Via Hamilton syringe 65.0 µl (47.5 mg, 469 mmol) of triethylamine were added within 15 min and the mixture was stirred for 4 h under room temperature. The yellowish solution revealed some cloudiness. After filtration the filtrate was evaporated under reduced pressure. The remaining residue was suspended in diluted HCl solution and stirred overnight. After lyophilization the purification of the crude via MPLC (RP-18, 50 µm, 12 nm, gradient run: water/acetonitrile with additional 0.05 % NEt_3) yielded the diphosphate **47** in 88 % (112 mg, 154 µmol).

Molecular Weight: 726.16 g/mol
Formula: $C_{42}H_{32}O_8P_2$

Spectroscopic data and assignment of molecule positions:

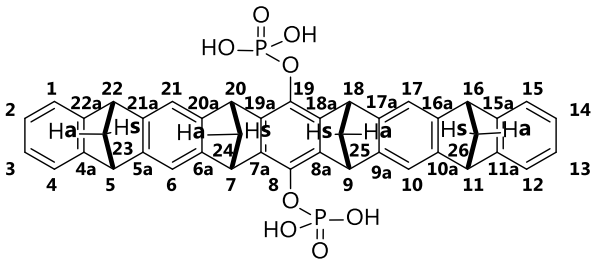

^{1}H NMR: (300.1 MHz, CD_3OD): δ [ppm] = 2.28 – 2.44 (m, 8 H, H-23, H-24, H-25, H-26), 4.03 (s, 4 H, H-5, H-11, H-16, H-22), 4.37 (s, 4 H, H-7, H-9, H-18, H-20), 6.80 – 6.84 (m, 4 H, H-2, H-3, H-13, H-14), 7.02 – 7.05 (m, 4 H, H-1, H-4, H-12, H-15), 7.15 (s, 4 H, H-6, H-10, H-17, H-21).

^{31}P NMR: (121.5 MHz, CD_3OD): δ [ppm] = -3.12 (1 P).

HRMS: (ESI, neg., methanol/water): *m/z* $[M]^+$ calcd for $C_{42}H_{30}O_8P_2^{2-}$: 362.0702; found: 362.0693.

Synthesis of (5,7,9,11,16,18,20,22) octahydro-5,22:7,20:9,18:11,16-tetra-methanononacene-8 (propargylhydrogenphosphat) 19-(dihydrogenphosphat) (**50**)

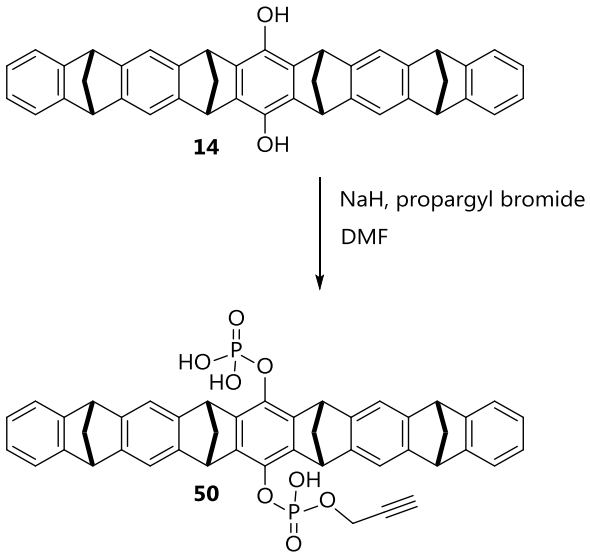

51.0 mg (70.2 µmol) of tweezer **14** were dissolved in 2 ml DMF. A solution of sodium hydride in DMF (0.84 mg, 35.0 µmol per 100 µl solution) was added via

syringe slowly in portions of 100 µl. Via a second syringe a solution of propargyl bromide in DMF (1.80 µl, 2.48 mg, 20.8 µmol per 100 µl solution) was added slowly in small portions. The reaction progress was controlled via HPLC. Therefore a small sample of reaction volume was diluted in a highly diluted hydrochloric solution and lyophilized.

After a total addition of 5 eq. of sodium hydride (350 µmol) and 12 eq. of propargyl bromide (835 µmol) the solvent was evaporated under reduced pressure and the remaining solid was lyophilized 3 times. Purification of raw product was executed via MPLC (RP-18, ACN/ water/NEt_3 (0.01%)) in a gradient run to yield 20 % (10.9 mg) of the diphosphate mono-alkyne **50**.

Molecular Weight: 764.71 g/mol
Formula: $C_{45}H_{34}O_8P_2$

Spectroscopic data and assignment of molecule positions:

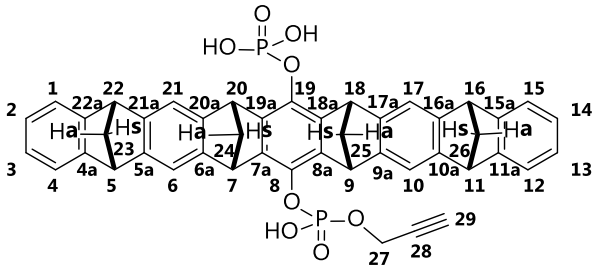

^{1}H NMR: (600.1 MHz, DMSO-d6): δ [ppm] = 2.08 – 2.12, 2.26 – 2.38 (m, 8 H, H-23, H-24, H-25,H-26), 3.47 (d, $^4J_{H\text{-}29/\ H\text{-}27}$ = 2.35 Hz, 1 H, H-29), 4.05 – 4.07 (m, 4 H, H-5, H-11, H-16, H-22), 4.32 – 4.35 (m, 4 H, H-7, H-9, H-18, H-20), 4.44 (d, $^4J_{H\text{-}27/\ H\text{-}29}$ = 2.35 Hz, 2 H, H-27), 6.75 – 6.77 (m, 4 H, H-2, H-3, H-13, H-14), 7.07 – 7.10 (m, 8 H, H-1, H-4, H-6, H-10, H-12, H-15, H-17, H-21), 8.09 (br. s, 3 H, O*H*).

^{13}C NMR: (150.9 MHz, DMSO-d6) δ [ppm] = 46.8 (2 C, C-7, C-9), 48.1 (2 C, C-18, C-20), 50.3, 53.2 (4 C, C-5, C-11, C-16, C-22), 61.7 (1 C, C-27), 71.9 (4 C, C-23, C-24, C-25, C-26), 78.8 (1 C, C-29), 87.8 (1 C, C-28), 114.2, 116.5 (4 C, C-6, C-10, C-17, C-21), 121.5, 122.3 (4 C, C-1, C-4, C-12, C-15), 124.6 (4 C, C-2, C-3, C-13, C-14), 136.5 (2 C, C-7a, C-8a), 140.8 (2 C, C-18a, C-19a), 150.4 (4 C, C-4a, C-11a, C-15a, C-22a).

Not all quaternary carbon atoms could be identified. The intensity of signals of the quaternary carbons was too low to assign them all.

^{31}P NMR: (242.9 MHz, DMSO-d6): δ [ppm] = -4.83 (1 P), -3.93 (1 P).

HRMS: (ESI, neg., methanol/water): *m/z* $[M]^+$ calcd for $C_{45}H_{34}O_8P_2^-$: 763.1645; found: 763.1634; calcd for $C_{45}H_{33}O_8P_2Na^-$: 785.1465; found: 763.1455.

Synthesis of (1R,4S,5R,8S)-1,4,5,8-tetrahydro-1,4:5,8-dimethanoanthracene-9-(propargylhydrogenphosphat)-10-(dihydrogenphosphat) (**51**)

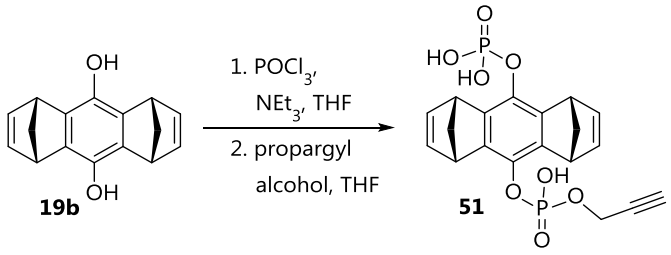

Under an argon gas atmosphere 100 mg (420 µmol) of diol **19b** were dissolved in 5 ml of THF and cooled to 0 °C. Via syringe 782 µl (1.29 g, 8.39 mmol, 20.0 eq) of phosphoryl chloride were added within some minutes. After 10 min 2.33 ml (1.70 g, 16.8mmol) of triethylamine were added within 15 min and the mixture was stirred for 4 h under room temperature. Further stirring at 50 °C for 40 min led to a yellowish color of the mixture. The solvent was removed completely under reduced pressure and the residue was dried for 1 h under reduced pressure. Afterwards the dried residue was suspended in 5 ml of THF and cooled to 0 °C before 24.2 µl (23.5 mg, 420 µmol, 1 eq) of propargylic alcohol was added via syringe over 20 min. The reaction mixture was stirred for 3 h at room temperature. Subsequently the solvent was removed under reduced pressure and the remaining solid was lyophilized to yield 150 mg of raw product. Purification of the crude via MPLC (RP-18, MeOH/ water/TFA (0.05%)) via gradient run yielded 40 % (72.9 mg) of the mono-alkyne **51**.

Molecular Weight: 436.29 g/mol
Formula: $C_{19}H_{18}O_8P_2$

Spectroscopic data and assignment of molecule positions:

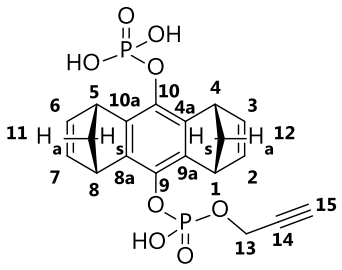

^{1}H NMR: (600.1 MHz, DMSO-d6): δ [ppm] = 2.06 – 2.11 (m, 4 H, H-11, H-12), 3.66 (t, $^{4}J_{\text{H-15/ H-13}}$ = 2.45 Hz, 1 H, H-15), 4.05 – 4.06 (m, 4 H, H-1, H-4, H-5, H-8), 4.67 (dd, $^{3}J_{\text{H-13/ P-9}}$ = 9.08 Hz, $^{2}J_{\text{H-13/ H-15}}$ = 2.45 Hz, 2 H, H-13), 5.04 (br. s. 3 H, O*H*), 6.71 – 6.75 (m, 4 H, H-2, H-3, H-6, H-7).

^{13}C NMR: (150.9 MHz, DMSO-d6) δ [ppm] = 47.5, 47.6 (4 C, C-1, C-4, C-5, C-8), 54.5 (1 C, C-13), 69.1 (2 C, C-11, C-12), 78.3 (1 C, C-15), 78.9 (1 C, C-14), 136.6, 137.3 (4 C, C-4a, C-8a, C-9a, C-10a), 141.6, 142.3 (2 C, C-9, C-10), 142.8, 143.1 (4 C, C-2, C-3, C-6, C-7).

^{31}P NMR: (242.9 MHz, DMSO-d6): δ [ppm] = -5.71 – -5.63 (td, $^{3}J_{\text{P-9/ H-13}}$ = 9.08 Hz, $^{2}J_{\text{P-9/ O}H}$ = 1.94 Hz, 1 P, P-9) -5.39 (d, $^{2}J_{\text{P-9/ O}H}$ = 1.94 Hz, 1 P, P-10)

MS: (ESI, neg., methanol/water): *m/z* $[M]^{+}$ calcd for $C_{19}H_{18}O_8P^{-}$: 435.04; found: 435.12.

Molecule **51** could not be detected with HRMS.

6.5 Synthesis of the 1st Generation RGD-Receptor

Synthesis of receptor precursor **44**

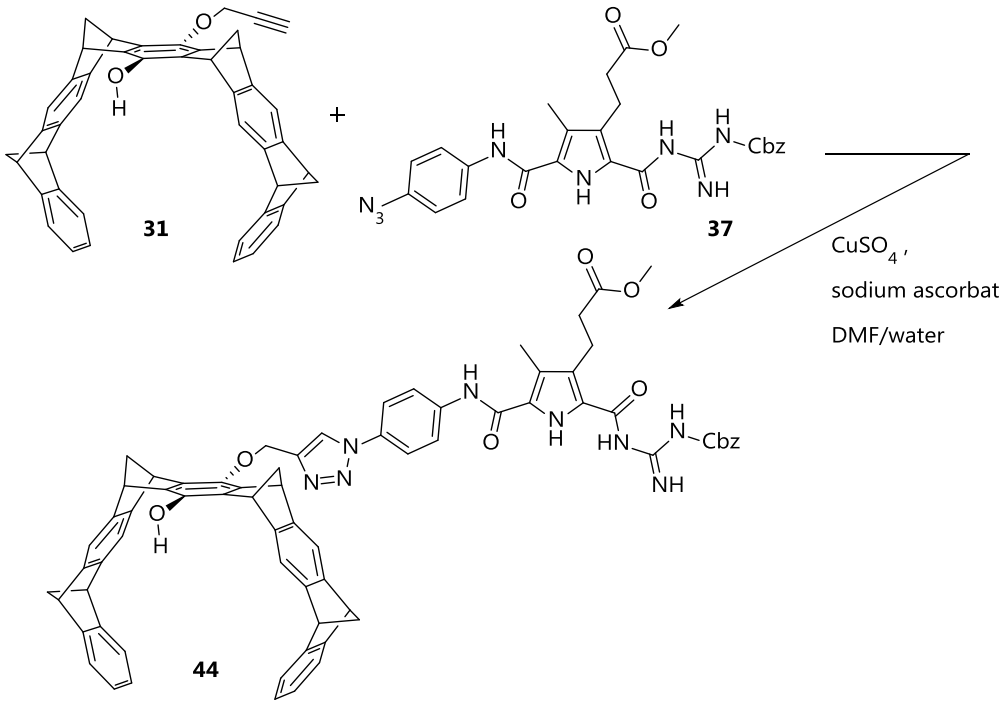

Under inert gas 24.8 mg (41.0 µmol) of **31** and 22.5 mg (41.2 µmol) of **37** were dissolved in 2 ml of DMSO. After 2 min. of steering 2.06 mg (10.4 µmol) of sodium ascorbate and 1.35 mg (5.41 µmol) of copper sulfate pentahydrate ($CuSO_4$ * 5 H_2O) were added. The greenish mixture was stirred at room temperature. After 1 h the mixture turned into a bluewish colour and TLC indicated the complete conversion of starting materials. Addition of 5 ml of water led to a precipitation which was filtrated over a nylon filter. The crude (87.6 mg) was lyophylized and purified via filtration column (SiO_2, ethyl acetate) to yield 95 % (45.5 mg, 39.5 µmol) of precursor **44**.

Molecular Weight: 1151.29 g/mol
Formula: $C_{71}H_{58}O_8N_8$
R_f-value: 0.08; SiO_2, *n*-hexan/ethyl acetate (2/1).

Spectroscopic data and assignment of molecule positions:

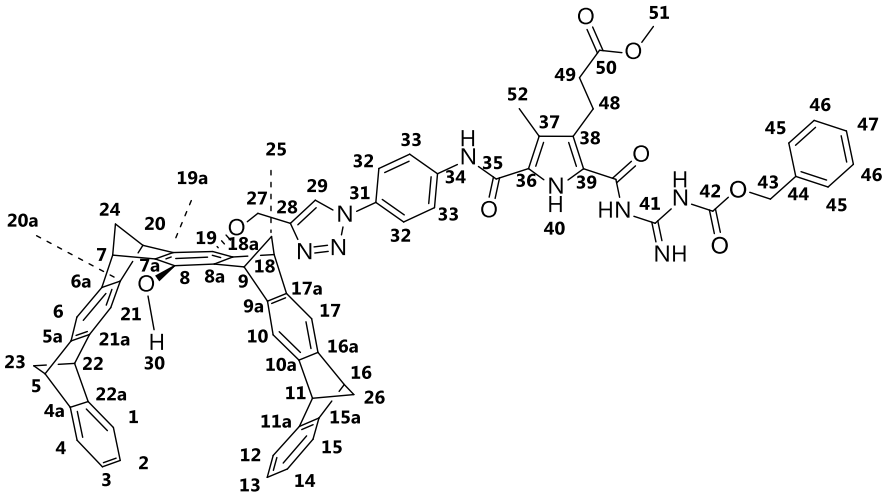

^{1}H NMR: (500.3 MHz, $CDCl_3$): δ [ppm] = 2.34 – 2.39 (m, 4 H, H-23, H-26), 2.39 – 2.43 (m, 4 H, H-24, H-25), 2.46 (s, 3 H, H-52), 2.65* (m, 2 H, H-49), 3.17* (m, 2 H, H-48), 3.47 (s, 1 H, H-30), 3.68 (s, 3 H, H-51), 4.05 – 4.06 (m, 4 H, H-5, H-11, H-16, H-22), 4.20 (br. s, 2 H, H-7, H-9), 4.30 (br. s, 2 H, H-18, H-20), 4.99 (br. s, 2 H, H-27), 5.24 (br. s, 2 H, H-43), 6.74 - 6.76 (m, 4 H, H-2, H-3, H-13, H-14), 7.04 – 7.07 (m, 4 H, H-1, H-4, H-12, H-15), 7.14 (br. s, 2 H, H-17, H-21), 7.15 (br. s, 2 H, H-6, H-10), 7.39 – 7.41 (m, 5 H, H-45, H-46, H-47), 7.71 – 7.74 (m, 4 H, H-32, H-33), 8.01 (br. s, 1 H, N*H*), 8.30 (br. s, 1 H, N*H*), 8.99 (br. s, 1 H, N*H*), 10.14 (s, 1 H, N*H*).

* Peak reveals a multiplicity of a triplet but the resolution was too low to obtain coupling constants.

The triazole proton H-29 and some N*H*-protons could not be identified due to some overlaying of signals.

^{13}C NMR: (125.8 MHz, $CDCl_3$) δ = 10.9 (1 C, C-51), 21.2 (1 C, C-47), 35.4 (1 C, C-48), 47.5 (2 C, C-7, C-9), 48.6 (2 C, C-18, C-20), 51.5 (4 C, C-5, C-11, C-16, C-22), 51.9 (1 C, C-50), 67.88 (1 C, C-27), 68.4 (1 C, C-42), 69.3 (2 C, C-24, C-25), 70.3 (2 C, C-23, C-26), 75.3 (1 C, C-29), 79.8 (1 C, C-28), 116.3, 116.5 (4 C, C-6, C-10, C-17, C-21), 121.1, 121.4 (4 C, C-32, C-33), 121.5, 121.7 (4 C, C-1, C-4, C-12, C-15), 124.7, 124.8 (4 C, C-2, C-3, C-13, C-14), 128.6, 128.9, 129.0 (5 C, C-44, C-45, C-46), 134.8 (1 C, C-43), 135.4 (2 C, C-7a, C-8a), 138.4 (1 C, C_q), 140.5 (2 C, C-18a, C-19a), 140.9 (1 C, C-8), 142.5 (1 C, C-19), 147.0, 147.1 (4 C, C-6a, C-9a, C-17a, C-20a),

147.6, 147.7 (4 C, C-5a, C-10a, C-16a, C-21a), 150.5 (4 C, C-4a, C-11a, C-15a, C-22a), 174.8 (1 C, C-49).

The assignment of carbon atoms was executed with HSQC- and HMBC-experiment. The correct number of quaternary carbon atoms could not be determined.

MS: (ESI, pos., methanol/water): *m/z* $[M]^-$ calcd for $C_{71}H_{57}O_8N_8^-$: 1149.43; found: 1149.55.

Molecule **44** could not be detected with HRMS.

Synthesis of receptor precursor **45**

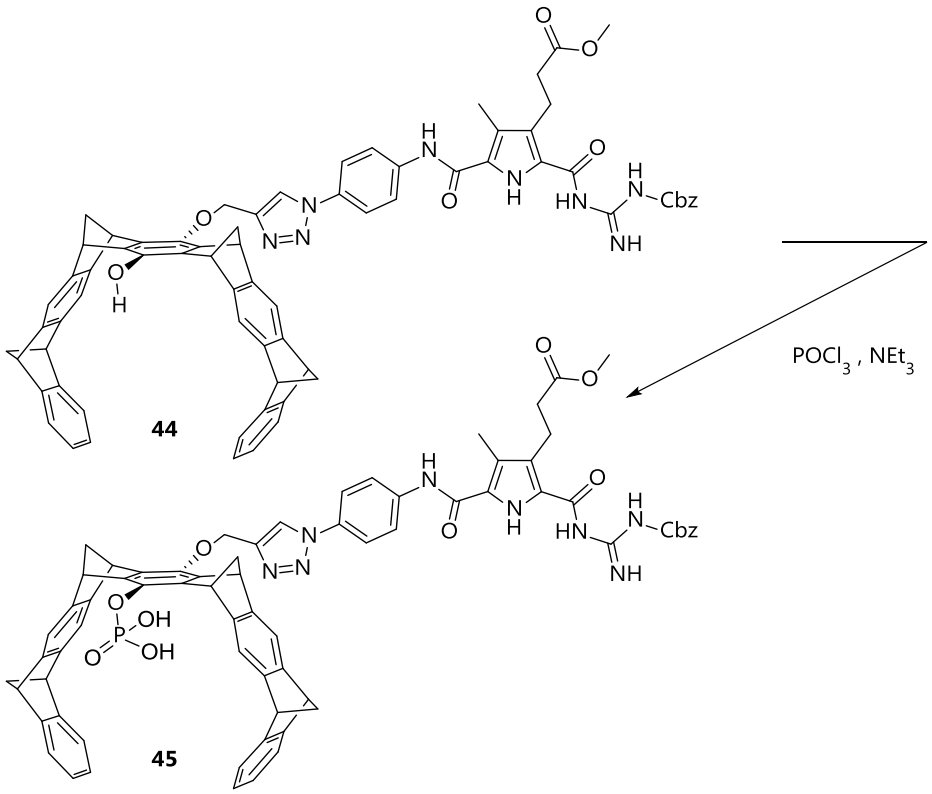

Under inert gas 20.0 mg (17.4 µmol) of **44** were dissolved in 1 ml of DMSO and the mixture was cooled to -3 °C. 50 µl (82. 0 mg, 535 µmol) of phosphorus oxychloride and 50 µl (36.5 mg, 360 µmol) of triethylamine were added via syringe. The reaction mixture was allowed to warm to room temperature and was stirred for 90 min. 1 ml of 1 M hydrochloric acid were added to the reaction mixture. After addition of 10 ml of water the mixture was extracted twice with DCM (20 ml) and twice with diethyl ether (20 ml). The combined organic phases were dried over Na_2SO_4. After filtration the filter residue was washed with further 10 ml of DCM and the solvent of organic

phases was evaporated under reduced pressure to yield 63 % (13.6 mg, 11.0 µmol) of **45**.

Molecular Weight: 1231.27 g/mol
Formula: $C_{71}H_{59}O_{11}N_8P$
R_f-value: 0.00; RP-18, MeOH.

Spectroscopic data and assignment of molecule positions:

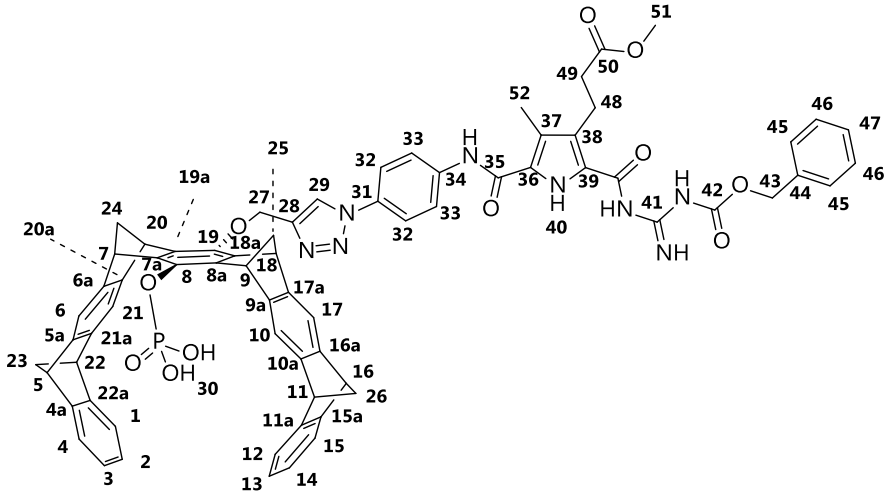

^{1}H NMR: (500.3 MHz, DMSO-d6): δ [ppm] = 2.15 – 2.23 (m, 4 H, H-24, H-25), 2.27 – 2.29 (m, 4 H, H-23, H-26), 2.30 (s, 3 H, H-52), 2.62 – 2.64 (m, 2 H, H-49), 3.15 – 3.17 (m, 2 H, H-48), 3.47 (s, 1 H, H-30), 3.64 (s, 3 H, H-51), 3.99 (br. s, 2 H, H-5, H-11), 4.07 (br. s, 2 H, H-16, H-22), 4.22 (br. s, 2 H, H-7, H-9), 4.34 (br. s, 2 H, H-18, H-20), 5.04 (br. s, 2 H, H-27), 5.19 – 5.21 (m, 2 H, H-42), 6.74 - 6.76 (m, 4 H, H-2, H-3, H-13, H-14), 7.03 – 7.07 (m, 8 H, H-1, H-4, H-6, H-10, H-12, H-15, H-17, H-21), 7.12 (br. s, 1 H, H-29), 7.31 – 7.44 (m, 5 H, H-45, H-46, H-47), 7.97 – 8.05 (m, 4 H, H-32, H-33), 8.09 (br. s, 1 H, N*H*), 8.20 (s, 1 H, N*H*), 8.26 (s, 1 H, N*H*), 8.96 (br. s, 1 H, N*H*), 10.04 (br. s, 2 H, H-30).

Some N*H*-protons could not be assigned due to some overlaying of signals.

^{13}C NMR: (125.8 MHz, $CDCl_3$) δ = 9.9 (1 C, C-51), 21.7 (1 C, C-47), 47.7 (2 C, C-7, C-9), 48.0 (2 C, C-18, C-20), 50.3 (4 C, C-5, C-11, C-16, C-22), 52.0 (1 C, C-50), 64.2 (1 C, C-27), 68.2 (1 C, C-42), 120.6, 121.5 (4 C, C-32, C-33), 128.2, 128.5, 132.5 (5 C, C-44, C-45, C-46), 146.8, 150.2 (C_q).

Not all carbon atoms could be determined especially those carbon atoms of the aromatic backbone of the tweezer. These signals disappeared in the noise. Signals of secondary carbon atoms (CH_2) could be assigned via DEPT-135 experiment.

^{31}P NMR: (202.5 MHz, DMSO-d6): δ [ppm] = -5.05, -1.03.

MS: (ESI, pos., methanol/water): *m/z* $[M]^-$ calcd for $C_{71}H_{59}O_{11}N_8P^-$: 1230.40; found: 1149.55.

Molecule **44** could not be detected via HRMS.

Synthesis of the 1st generation RGD-receptor **46**

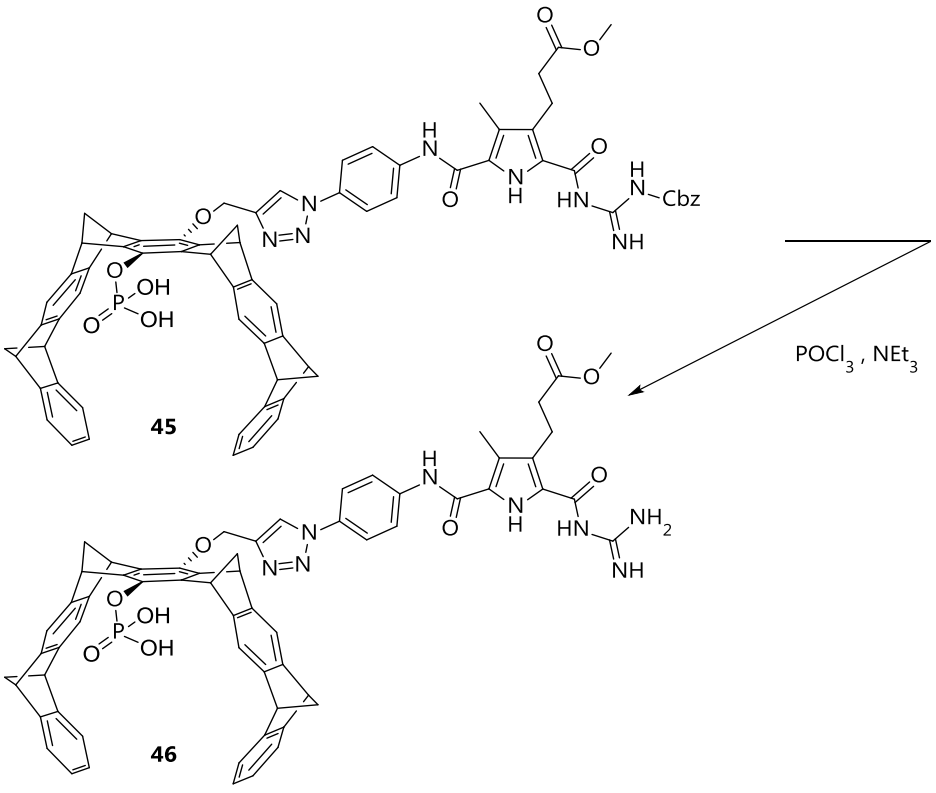

In an argon flushed reaction vessel 11.6 mg (9.42 µmol) of **45** and 1.70 mg (1.60 µmol) Pd/C were suspended in 4 ml of THF. After degassing the argon atmosphere was replaced with hydrogen. The mixture was stirred for 2 d at room temperature under slight overpressure of hydrogen. After separation from Pd/C the filter residue was washed with THF (5 ml) and acetone (5 ml). The solvent of the filtrate was evaporated under reduced pressure and the remaining solid was lyophilized 4 times to yield 83 % (8.58 mg, 7.82 µmol) of receptor **46**.

Molecular Weight: 1097.13 g/mol
Formula: $C_{63}H_{53}O_9N_8P$
R_f-value: 0.92; RP-18, MeOH.

Spectroscopic data and assignment of molecule positions:

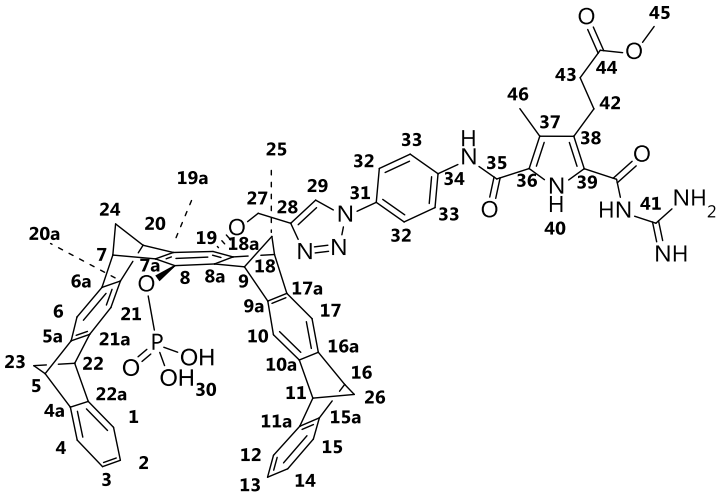

^{1}H NMR: The resolution of proton signals was too low for any assignment.

^{13}C NMR: The resolution of signals of the carbon atoms was too low for a distinct assignment.

^{31}P NMR: (202.5 MHz, DMSO-d6): δ [ppm] = -0.99.

MS: (ESI, pos., methanol/water): *m/z* $[M]^-$ calcd for $C_{63}H_{52}O_9N_8P^-$: 1095.36; found: 1095.47.

Molecule **46** could not be detected with HRMS.

6.6 Synthesis of the 2nd Generation RGD-Receptor

Synthesis of (1R,4S,5R,8S)-10-((((1-(4-(5-(carbamimidoylcarbamoyl)-1H-pyrrole-2-carboxamido)phenyl)-1H-1,2,3-triazol-4-yl)methoxy)(hydroxy)phosphoryl)oxy)-1,4,5,8-tetrahydro-1,4:5,8-dimethanoanthracen-9-yl dihydrogen phosphate **56**

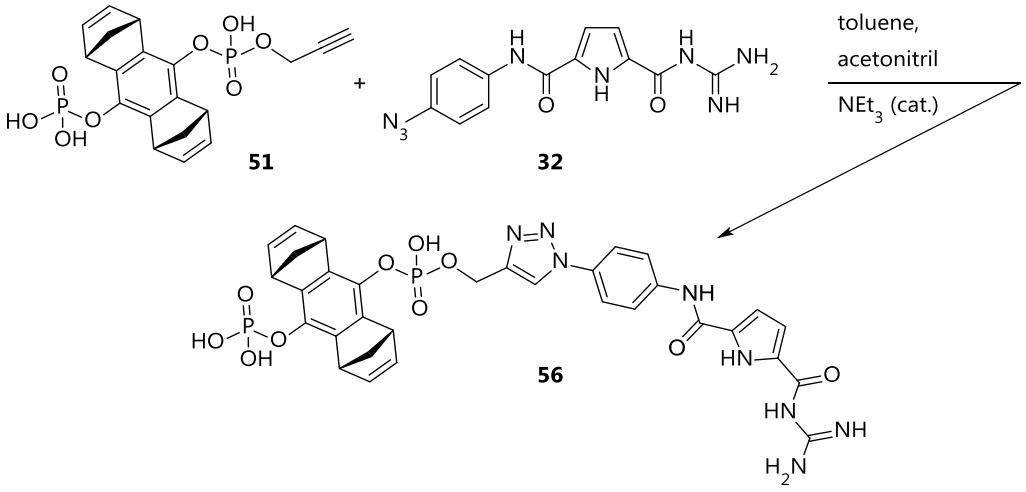

A brownish mixture of 11.4 mg (36.5 µmol) of azido pyrrole **32** in 2 ml THF was stirred in an argon atmosphere. After addition of 16.0 mg (36.7 µmol) of diphosphate mono-alkyne **51**, 1.29 mg (5.16 µmol) of copper sulfate pentahydrate and 1.94 mg (9.79 µmol) of sodium ascorbate dissolved in 4 ml H_2O/THF (1/1) the color of the reaction mixture turned immediately to light brownish and orange. After stirring the mixture for 2.5 d the easily volatile parts were removed by evaporation under reduced pressure. The residual mixture was treated with 2.00 mg (25.6 µmol) of sodium sulfide. The precipitate was filtered over viscose and the filtrate was lyophilized to yield 49.7 mg of raw product. Dissolving the crude in 10 ml of water and treatment with 0.1 M hydrochloric acid led to a precipitation. Only few drops of hydrochloric acid were used until pH 2 was reached. The precipitate was filtered and washed with ice cold water to yield 49 % 13.9 mg (17.7 µmol) of **56** as chloride salt.

Molecular Weight: 748.59 g/mol
Formula: $C_{32}H_{30}O_{10}N_8P_2$
Melting point: 197 °C decomposition (water).

Spectroscopic data and assignment of molecule positions:

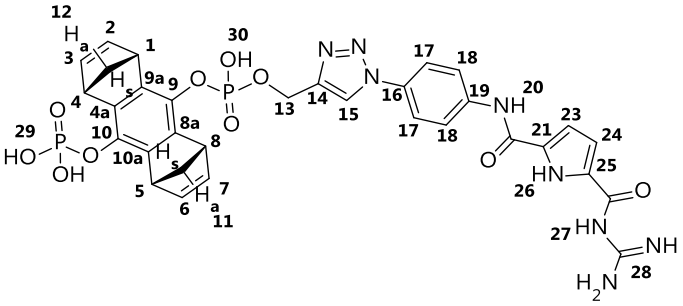

^{1}H NMR: (600.1 MHz, DMF-d7): δ [ppm] = 1.98 (m, 4 H, H-11, H-12), 3.73 (m, 2 H, H-1, H-8), 4.82 (m, 2 H, H-4, H-5), 5.26 (br. s, 2 H, H-13), 7.13 – 7.17 (m, 2 H, H-23, H-24), 7.87 – 7.90 (m, 4 H, H-17, H-18), 8.19 (s, 1 H, H-15), 9.06 (br. s, 2 H, N-*H*), 9.19 (br. s, 2 H, N-*H*), 9.49, 10.65 (2 H, N-*H*), 12.93, 12.95 (3 H, H-29, H-30).

^{13}C NMR: (150.9 MHz, DMF-d7) δ = 64.4 (1 C, C-13), 73.7 (2 C, C-11, C-12), 117.1, 119.9, 121.5 122.2 (4 C, C-17, C-18), 157.6, 160.9 (2 C, C_q).

Most of the carbon atom signals could not be assigned due to extreme peak broadening.

^{31}P NMR: (202.5 MHz, DMF-d7): δ [ppm] = -4.91.

MS: (ESI, pos., methanol/water): *m/z* $[M]^-$ calcd for $C_{63}H_{52}O_9N_8P_2^-$: 747.15; found: 747.24.

Molecule **56** could not be detected with HRMS.

FT-IR: (ATR): $\tilde{\nu}$ [cm^{-1}] = 3307 (w), 2116 (w), 1698 (m), 1542 (m), 1510 (m), 1473 (m), 1312 (m), 1238 (m), 1042 (m).

6.7 Syntheses of Guest RGD-Peptides

All peptide syntheses were carried out on solid phase (SPPS) with a peptide shaker in an inert gas atmosphere. The used solvents in the peptide synthesis were dried, distilled and kept under argon before usage. The used equivalents of reagents refer to the loading of the resin. The synthesis procedure is described as follows. In a first step the resins were swollen with 10 ml DCM for 1.5 h and 6 h for cyclic and linear peptides respectively. Afterwards the resin beads were washed twice with 5 ml DMF.

The deprotection of Fmoc-group was carried out by a twofold treatment of the resin with 5 ml of piperidine for 20 min. After cleavage the resin was washed six times with 5 ml and 10 ml of DMF with respect to linear and cyclic peptides.

The coupling reaction of each amino acid was executed twice with 3 eq of PyBOP, 6 eq of DIPEA and 3 eq of the relevant amino acid. The first coupling was done for 6 h and the second one was carried out overnight (at least for 12 h). Between both coupling steps the resin was washed two times with 5 ml of DMF. Potentially free amine functions of the resins were capped after first coupling step. A full occupation of amine functions was verified via *Kaiser Test*. Before the coupling reaction of the next amino acid was executed the Fmoc-deprotection was carried out twofold with an excess of piperidine. Detailed peptide synthesis procedures will be explained in successional sections.

Synthesis of the linear peptide sequence *N*-Ac-RGD (**P1**)

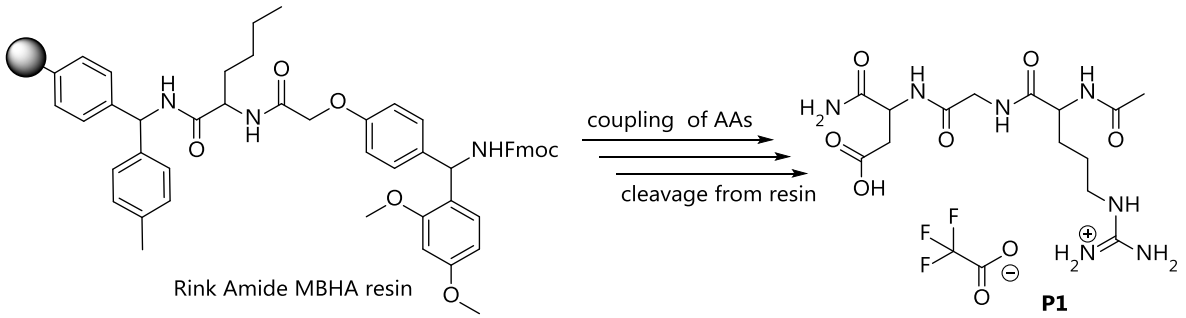

In an argon atmosphere 100 mg of Rink Amide MBHA Resin (loading of the resin: 0.84 mmol·g^{-1}, 84.0 µmol, 1 eq) were pre-treated in accordance to above mentioned procedure. The first coupling step was carried out with 104 mg (252 µmol) Fmoc-L-Asp(OtBu)-OH, 131 mg (252 µmol) PyBOP and 88 µl (65.3 mg, 505 µmol) DIPEA in 5 ml DMF. The end-capping of unreacted amines was executed with 55 µl (59.4 mg, 7 eq) acetic anhydride and 150 µL (138 mg, 16 eq) NMM in 5 ml DMF for 4 h. After a negative result of the *Kaiser Test* the deprotection of the Fmoc protection group was carried out with a twofold excess of piperidine. Afterwards the resin beads were washed for 5 min with 5 ml DMF and the washing procedure was repeated another five times. The coupling reaction of the second amino acid was executed with 75.0 mg (252 µmol) Fmoc-Gly-OH, 131 mg (252 µmol) PyBOP and 88 µl (65.3 mg, 505 µmol) DIPEA in 5 ml DMF. The arginine was coupled as the last amino acid. Therefore 163 mg (252 µmol) Fmoc-Arg-(Pbf)-OH, 131 mg (252 µmol) PyBOP and 88 µl (65.3 mg, 505 µmol) DIPEA in 5 ml DMF were used. Afterwards the Fmoc-group was cleaved and the resin was washed carefully according to the previous described

procedure. The tripeptide sequence was capped by acetylation at the N-terminus before cleavage from the resin was carried out. Thus the resin bounded peptide was treated with a mixture of 55 µl (59.4 mg, 7 eq) of acetic anhydride and 150 µL (138 mg, 16 eq) of NMM in 5 ml DMF. The resin was washed carefully trice with 10 ml of DCM, trice with 10 ml of methanol and trice with 10 ml of DCM in succession. The resin beads were treated for 3 h with 10 ml of a cleaving solution containing TFA/TIS/DCM 95/2.5/2.5. Subsequently the resin was washed with DCM to separate the N-acetylated RGD-peptide **P1** from resin beads several times. The volume of the combined filtrates of peptide solution was diminished under reduced pressure to approximately 3 ml. Through the addition of 25 ml of cold diethyl ether the linear peptide **P1** could be precipitated. The precipitate was filtered over a nylon filter and the obtained crude product was lyophilized. The final purification was done by MPLC (RP-18, 50 µm, 12 nm, gradient run: water/acetonitrile with additional 0.05 % TFA respectively; 100/0 to 98/2 within 18 min) to yield 56 % (22.9 mg, 47.3 µmol) of **P1** as TFA-salt.

Molecular Weight: 387.40 g/mol.

Formula: $C_{14}H_{25}O_6N_7$

Retention time: 8.79 min at HPLC, RP-18, particle size 5 µm, pore size 12 nm, eluent water/methanol with additional 0.05 % TFA respectively; gradient run from 100/0 to 98/2 in 15min.

Spectroscopic data and assignment of molecule positions:

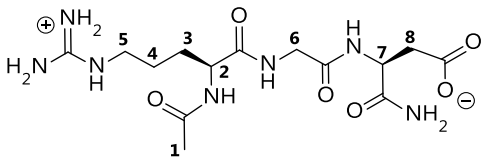

^{1}H NMR: (300.1 MHz, DMSO-d6): δ [ppm] = 1.46 (m, 4 H, H-3, H-4), 1.83 (s, 3 H, H-1), 3.05 – 3.07 (m, 4 H, H-5, H-8), 4.19 (m, 2 H, H-6), 4.37 (m, 1 H, H-2), 4.44 (m, 1 H, H-7), 6.85, 7.14, 7.37, 7.48, 8.09, 8.35 (10 H, N-*H*).

HPLC-purity: 94 % at 220 nm; RP-18, gradient run, methanol/water/TFA.

Synthesis of the penta peptide cyclo(RGDfV) (**P2**)

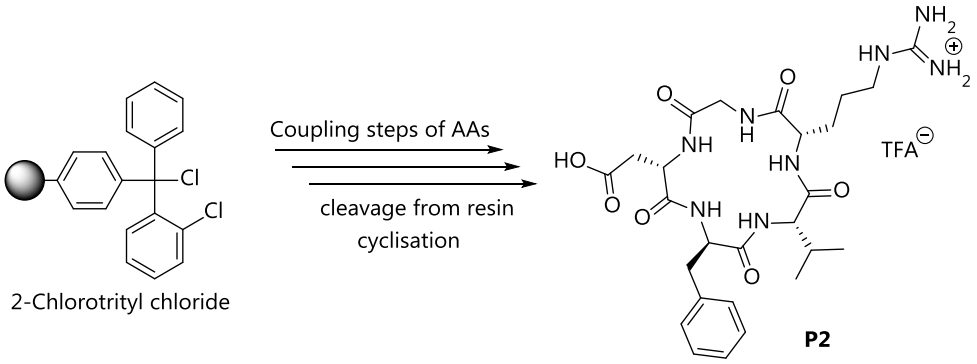

The synthesis of the circular peptide **P2** was performed with the use of *o*-chlorotrityl chloride (loading of the resin: 1.55 mmol·g^{-1}, 406 mg, 630 µmol, 1.00 eq). As in analog to the synthesis of the linear tripeptide the resin was allowed to swell in 10 ml of dichloromethane for 1.5 h and washed two times with 5 ml of dimethylformamide for 15 min afterwards. The incorporation of the first amino acid glycine was done with Fmoc-Gly-OH (562 mg, 1.89 mmol, 3.00 eq), DIPEA (643 µl, 489 mg, 3.78 mmol, 6.00 eq) in 10 ml of dimethylformamide. Afterwards the resin was washed three times with 5 ml of Dimethylformamide. The end capping of free positions at the resin was performed with methanol (1.50 ml, 1.19 g, 37.0 mmol, 58 eq) and DIPEA (643 µl, 489 mg, 3.78 mmol, 6.00 eq) in 8 ml of Dimethylformamide. The mixture was shaken for 16.5 h before the resin was washed thoroughly six times with 5 ml of dimethylformamide. The cleavage of the Fmoc-group was carried out twice with piperidine (2.00 ml) in 8.00 ml of dichloromethane for 20 min followed by a careful washing of the resin with 10 ml of dimethylformamide for six times. These iterative steps were performed after each coupling of the following amino acids L-arginine, L-valine, D-phenylalanine and L-aspartic acid. From the second amino acid on coupling was done twice analog to the linear peptide synthesis to ensure fully covering of free amines. Intermediate checks were done via the *Kaiser Test*. The second coupling step of a particular amino acid was done overnight while the first step lasted for 6-8 h. In the following the amino acids Fmoc-L-Arg(Pbf)-OH (1.23 g, 1.89 mmol, 3.00 eq), Fmoc-L-Val-OH (641 mg, 1.89 mmol, 3.00 eq), Fmoc-D-Phe-OH (731 mg, 1.89 mmol, 3.00 eq) and Fmoc-L-Asp(O*t*Bu)-OH (777 mg, 1.89 mmol, 3.00 eq) were added via the described procedure. All coupling reactions were carried out using PyBOP (984 mg, 1.89 mmol, 3 eq), DIPEA (643 µl, 489 mg, 3.78 mmol, 6 eq) dissolved dichloromethane (10 ml) per coupling step respectively. To release the peptide strand from the resin 10 ml of the cleavage solution 2,2,2-trifuoroethane (TFE)/ acidic acid/ dichloromethane (1/1/3) were added to the resin and the mixture was shaken overnight. After separation of

the peptide solution from the resin beads the residual resin was washed finally three times with dichloromethane (10 ml) for 10 min each time. The combined filtrates were evaporated under reduced pressure to lead to a colorless solid. For the subsequent cyclisation reaction the solid was dissolved in dichloromethane (15 ml). The prepared solution was added dropwise to a second solution of T_3P (1.93 ml, 1.00 g, 3.15 mmol, 5 eq), TEA (2.18 ml, 1.59 mg, 15 mmol, 25 eq), DMAP (7.70 mg, 63.0 µmol, 0.1 eq) in dichloromethane (220 ml) within 20 h. Afterwards the mixture was stirred for 1.5 d at room temperature. Subsequently the solvent was removed by rotary evaporation under reduced pressure yielding a sticky, oily and some orange colored residue.

In a small scale work up 3.00 mg of the raw material were treated with a solution of water/TFA 1/1 (400µl) and stirred for 12 h at room temperature. The analysis via HPLC-MS confirmed the formation of the desired peptide sequence. The remaining crude product was diluted in chloroform (20 ml) and extracted with water (25 ml). The organic phase was dried over sodium sulfate after phase separation. After final filtration and washing with further chloroform (5 ml) the solvent was evaporated and the residual solid was freeze dried. The obtained raw product (319 mg) was purified via column chromatography (SiO_2, dichloromethane/methanol 12/1 and could be obtained as compound protected peptide in a yield of 12 % (41.4 mg, 73.8 µmol).

The cleavage of the protection groups was performed by the addition of water/TFA 1/19 (4.00 ml). The mixture was stirred for 3.5 h at room temperature. The azeotropic distillation with toluene resulted in a colorless solid which was freeze dried to yield compound **P2** in a crude quality (33.2 mg). The final purification was done with chromatography (MPLC, RP-18, 50 g, 12 nm, 15 µm, 25 x 2.5 cm, 220 nm, 25 ml·min^{-1}, gradient run with methanol/water with add on of 0.05 % TFA to yield 5 % (21.8 mg, 31.7 µmol) of **P2**.

Molecular Weight:	574.64 g/mol.
Formula:	$C_{26}H_{38}O_7N_8$
Retention time:	13.10 min at HPLC, RP-18, particle size 5 µm, pore size 12 nm, eluent water/methanol with additional 0.05 % TFA respectively; gradient run from 100/0 to 98/2 in 15min.

Spectroscopic data:

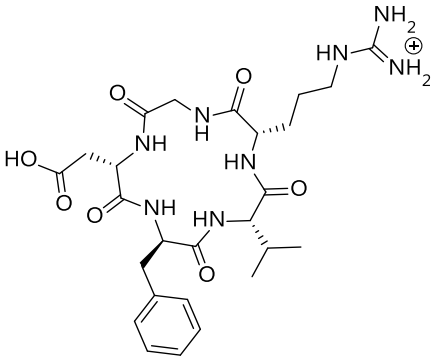

Molecule positions are assigned by standard description of the peptide positions.

^{1}H NMR: (500.3 MHz, DMSO-d6) δ = 0.68* (d, ^{3}J = 6.59 Hz, 3 H, CH_3^{γ}, Val), 0.75* (d, ^{3}J = 6.59 Hz, 3 H, C$H_3^{\gamma'}$, Val), 1.47 – 1.54 (m, 2 H, CH_2^{γ}, Arg), 1.72 (m, 2 H, CH_2^{β}, Arg), 2.36 (m, 1 H, CH_2^{β}, Asp), 2.39 – 2.42 (m, 1 H, CH_2^{β}, Val), 2.46 (m, 1 H, C$H_2^{\beta'}$, Asp), 2.93 (m, 2 H, CH_2^{β}, D-Phe), 3.08 – 3.10 (m, 2 H, CH_2^{δ}, Arg), 3.24 – 3.25 (m, 2 H, CH_2^{α}, Gly), 3.81 (m, 1 H, CH_2^{α}, Val), 4.01 – 4.05 (m, 1 H, CH_2^{α}, Arg), 4.55 (dd, 1 H, CH_2^{α}, Asp), 4.61 (m, 1 H, CH_2^{α}, D-Phe), 7.15 – 7.16 (m, 2 H, C$H_{ar,\ ortho}$, D-Phe), 7.17 – 7.18 (m, 1 H, C$H_{ar,\ para}$, D-Phe), 7.23-7.26 (m, 2 H, C$H_{ar,\ meta}$, D-Phe), 7.44 (br. s, 1 H, N*H*, D-Phe), 7.74 (br. s, 1 H, N*H*, Asp), 7.85 (br. s, 1 H, N*H*, Gly), 8.00 (br. s, 1 H, N*H*, Val), 8.09 (d, ^{3}J = 8.22 Hz, 1 H, N*H*), 8.38 (br. s, 1 H, N*H*, Arg), 12.24 (br. s, 1 H, COO*H*, Asp).

Protons of the guanidine function could not be assigned due to peak broadening.

* Diastereotopic methyl groups of the valine result in different chemical shifts.

HRMS: (ESI, pos., methanol/water): *m/z* $[M]^-$ calcd for $C_{26}H_{38}O_7N_8^-$: 575.2936; found: 575.2933.

Synthesis of hexa peptide cyclo(RGDfLG) (**P3**)

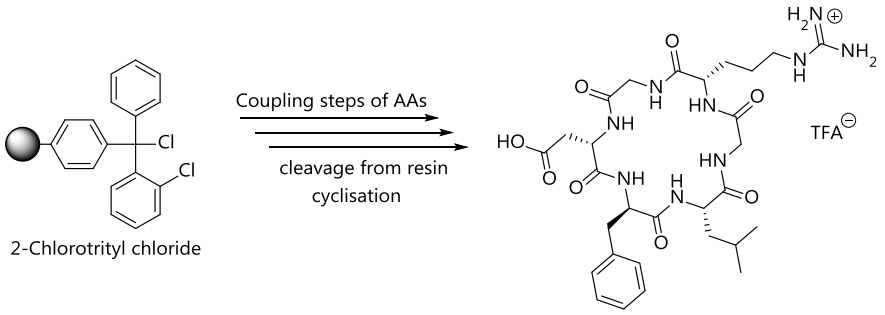

Synthesis of the cyclic peptide **P3** was carried out in analogous manner to the preparation of the cyclic peptide **P2**. The amino acids glycine, L-arginine, glycine, L-leucine, D-phenylalanine and L-aspartic acid were incorporated on *O*-chlorotrityl chloride (loading 1.55 mmol·g^{-1}, 406 mg, 630 µmol, 1.00 eq) iteratively using Fmoc-Gly-OH (562 mg, 1.89 mmol, 3.00 eq), Fmoc-L-Arg(Pbf)-OH (1.23 g, 1.89 mmol, Fmoc-Gly-OH (562 mg, 1.89 mmol, 3.00 eq), 3.00 eq), Fmoc-L-Leu-OH (668 mg, 1.89 mmol, 3.00 eq), Fmoc-D-Phe-OH (731 mg, 1.89 mmol, 3.00 eq) and Fmoc-L-Asp(O*t*Bu)-OH (777 mg, 1.89 mmol, 3.00 eq). Furthermore DIPEA (643 µl, 489 mg, 3.78 mmol, 6.00 eq) in 10 ml dimethylformamide was added to each coupling reaction. The second coupling reaction of each amino acid was done overnight. After washing three times with 5 ml dimethylformamide the end capping of free positions at the resin was performed with methanol (1.50 ml, 1.19 g, 37.0 mmol, 58 eq) and DIPEA (643 µl, 489 mg, 3.78 mmol, 6.00 eq) in 8 ml dimethylformamide shaking for 16.5 h. Subsequently washing the resin six times with 5 ml dimethylformamide cleavage of Fmoc was carried out twice with piperidine (2.00 ml) in 8.00 ml dichloromethane for 20 min followed by a careful washing of the resin six times with 10 ml dimethylformamide. These iterations were performed after each coupling of the following amino acids L-arginine, L-valine, D-phenylalanine and L-aspartic acid. From the second amino acid on coupling was done twice similar to linear peptide synthesis to ensure fully covering of free amines. The second coupling of a particular amino acid was reacted overnight while the first lasted for 6-8 h. Amounts of the used amino acids are announced below. Fmoc-L-Arg(Pbf)-OH (1.23 g, 1.89 mmol, 3.00 eq), Fmoc-L-Leu-OH (668 mg, 1.89 mmol, 3.00 eq), Fmoc-D-Phe-OH (731 mg, 1.89 mmol, 3.00 eq) and Fmoc-L-Asp(O*t*Bu)-OH (777 mg, 1.89 mmol, 3.00 eq). The couplings were carried out using same amounts of PyBOP (984 mg, 1.89 mmol, 3 eq), DIPEA (643 µl, 489 mg, 3.78 mmol, 6 eq) dissolved dichloromethane (10 ml) respectively. To keep the protection groups of the side chains of the peptides for further cyclisation a very mild cleavage method using 10 ml solution of 2,2,2-trifuoroethane (TFE)/ acidic acid/ dichloromethane (1/1/3) was added to the

resin and the mixture was shaken overnight. Washing the resin finally three times with 10 ml dichloromethane for 10 min respectively led to a colorless solid after evaporation of the solvents. A solution of the residue in dichloromethane (15 ml) was added within 20 h to a solution of T_3P (1.93 ml, 1.00 g, 3.15 mmol, 5 eq), TEA (2.18 ml, 1.59 mg, 15 mmol, 25 eq), DMAP (7.70 mg, 63.0 µmol, 0.1 eq) in dichloromethane (220 ml) The mixture was stirred for 1.5 d at room temperature. Subsequently the solvent was removed by rotary evaporation under reduced pressure yielding a sticky, oily and orange colored residue.

In a small scale work up 3.00 mg of the raw material were treated with a solution water/TFA 1/1 (400µl) and stirred for 12 h at room temperature. An analysis via HPLC-MS confirmed the formation of the correct peptide sequence.

The sticky residue was diluted in chloroform (20 ml) and extracted with water (25 ml). Organic phase was dried over sodium sulfate after phase separation. Finally filtrating and washing with further chloroform (5 ml) the solvent was evaporated and the residual solid was freeze dried. The obtained raw product (319 mg) was purified via column chromatography (SiO_2, dichloromethane/methanol 12/1 and could be received as compound **P3** 12 % (41.4 mg, 73.8 µmol).

Cleavage of protection groups were performed by addition of water/TFA 1/19 (4.00 ml) and stirring for 3.5 h at room temperature. Azeotropic distillation with toluene. The remained solid was freeze dried to yield compound xx in a crude quality 33.2 mg. Purification was done with chromatography (MPLC, RP-18, 50 g, 12 nm, 15 µm, 25 x 2.5 cm, 220 nm, 25 ml·min^{-1}, gradient run with methanol/water with add on of 0.05 % TFA. Yield 8.30 mg

Molecular Weight: 645.72 g/mol

Formula: $C_{29}H_{43}O_8N_9$

Retention time: 4.61 min at HPLC, RP-18, particle size 5 µm, pore size 12 nm, eluent water/methanol with additional 0.05 % TFA respectively; gradient run from 40/60 to 0/100 in 15min.

Spectroscopic data:

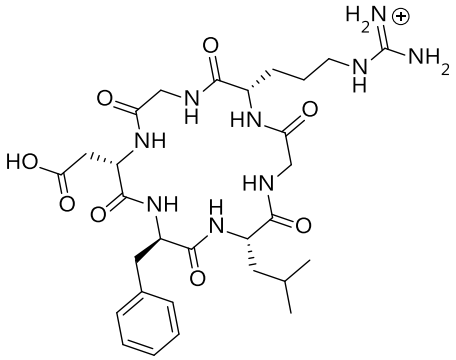

Molecule positions are assigned by standard description of the peptide positions.

^{1}H NMR: (600 MHz, DMSO-d6) δ = 0.63* (m, 3 H, CH_3^{δ}, Leu), 0.72* (m, 3 H, C$H_3^{\delta'}$, Leu), 1.06 (m, 1 H, CH^{γ}, Leu), 1.35* (m, 1 H, CH_2^{β}, Leu), 1.41* (m, 1 H, C$H_2^{\beta'}$, Leu), 1.46 (m, 2 H, CH_2^{γ}, Arg), 1.56* (m, 1 H, CH_2^{β}, Arg), 1.74* (m, 1 H, C$H_2^{\beta'}$, Arg), 2.54 (2 H, CH_2^{β}, Asp), 2.85* (m, 1 H, CH_2^{β}, D-Phe), 3.00* (m, 1 H, C$H_2^{\beta'}$, D-Phe), 3.08 – 3.10 (m, 2 H, CH_2^{δ}, Arg), 3.55-3.56* (d, ^{2}J = 15.2 Hz, 1 H, CH_2^{α}, Gly [A]), 3.63* (m, 1 H, CH_2^{α}, Gly [B]), 3.78-3.80* (d, ^{2}J = 15.2 Hz, 1 H, C$H_2^{\alpha'}$, Gly [A]), 3.91* (m, 1 H, C$H_2^{\alpha'}$, Gly [B]), 3.95 (br. s., 1 H, CH_2^{α}, Arg), 4.07 (1 H, CH^{α}, Leu), 4.37 (br. s. 1 H, CH^{α}, D-Phe), 4.54 (1 H, CH^{α}, Asp), 7.15 – 7.16 (m, 2 H, C$H_{ar,\ ortho}$, D-Phe), 7.18 – 7.19 (m, 1 H, C$H_{ar,\ para}$, D-Phe), 7.22-7.25 (m, 2 H, C$H_{ar,\ meta}$, D-Phe), 7.42 (br. s, 1 H, CH_2^{δ}N*H*, Arg), 7.68 (br. s, 1 H, N*H*, Asp), 7.94 (br. s, 1 H, N*H*, Gly [B]), 8.20 (br. s, 1 H, N*H*, Leu), 8.38 (br. s, 1 H, N*H*, Gly [A]), 8.38 (br. s, 1 H, N*H*, Arg), 8.43 (br. s, 1 H, N*H*, D-Phe), 12.26 (br. s, 1 H, COO*H*, Asp).

* Diastereotopic protons of the corresponding amino acids result in different chemical shifts.

COSY, HMBC and HSQC experiments facilitated assignment of the signals especially to separate signals of the 2 glycine amino acids A and B.

Protons of the guanidine function could not be assigned due to peak broadening.

^{13}C NMR: (150.9 MHz, DMSO-d6) δ = 21.4* (1 C, *C*H_3^{δ}, Leu), 23.6* (1 C, *C*$H_3^{\delta'}$, Leu), 24.2 (1 C, *C*H^{γ}, Leu), 25.6 (1 C, *C*H_2^{γ}, Arg), 27.6 (1 C,

CH_2^{β}, Arg), 36.5, (1 C, CH_2^{β}, Asp), 37.0 (1 C, CH_2^{β}, D-Phe), 40.1 (1 C, CH_2^{β}, Leu), 40.8 (1 C, CH_2^{δ}, Arg), 42.2 (1 C, CH_2^{α}, Gly [B]), 43.2 (1 C, CH_2^{α}, Gly [A]), 49.9 (1 C, CH^{α}, Asp), 51.5 (1 C, CH^{α}, Leu), 53.9 (1 C, CH^{α}, Arg), 55.5 (1 C, CH^{α}, D-Phe), 126.8 (1 C, CH_{para}, D-Phe), 128.6, (2 C, CH_{meta}, D-Phe), 129.6 (2 C, CH_{ortho}, D-Phe), 137.4 (1 C, C_q, D-Phe), 157.0, 158.2, 169.8, 170.7, 172.0, 172.3, 173 (C_q, carbonyle and guanidinium).

* Diastereotopic methyl groups of the amino acids leucine result in different chemical shifts.

The classification of the carbon atoms was completed by two dimensional NMR spectroscopy (HSQC). The correct number of quaternary carbon atoms could not be determined.

HRMS: (ESI, pos., methanol/water): *m/z* $[M]^-$ calcd for $C_{29}H_{42}O_8N_9^-$: 644.3151; found: 644.3134.

6.8 UV-Binding Studies

6.8.1 General Procedure of the Titration Experiments

Solutions of receptor and peptide were prepared according to the following procedure. Desalinated water was adjusted to pH 6.6 with 0.01 M sodium hydroxide and 0.01 M hydrochloric acid solutions. After the preparation of the aqueous solutions of the receptor and the substrate the pH value was controlled again. If necessary the adjustment of pH was done with previous mentioned alkaline and acidic solutions. Thereby the increase of the total volume was considered for the calculation of the final concentration. The UV-measurements were executed in a quartz glass cuvette with a length of 1 cm and a maximum volume of 1200 µL. Each series of measurement was started with an initial volume of 800 µL of pure receptor solution. In the beginning added amounts of the substrate were kept small whereas amounts were increased with progress of the titration experiment.

Thereby it was ensured that strong interactions could be determined in the beginning of experiment. The high substrate concentration was chosen to have the possibility to obtain high ratios of substrate to receptor at the end of the experiment which is mandatory for weaker interactions. In table shown below (figure 6-1) the progress of an exemplary titration experiment is shown.

Step #	V_S [µL]	Substrate [eq]	V_{total} [µL]	Ratio V_S / V_R	A_{obs} at λ_{max}	A_{exp} (dilution)
1	0	0	800	0.000	1.419	1.419
2	5	0.92	805	0.006	1.377	1.410
3	10	1.83	810	0.013	1.356	1.401
4	15	2.75	815	0.019	1.348	1.393
5	20	3.66	820	0.025	1.339	1.384
6	30	5.49	830	0.038	1.321	1.367
7	40	7.32	840	0.050	1.309	1.351
…	…	…	…	…	…	…
21	280	51.25	1080	0.350	1.063	1.051
22	320	58.57	1120	0.400	1.029	1.013
23	360	65.9	1160	0.450	1.001	0.978
24	400	73.22	1200	0.500	0.975	0.946

Figure 6-1. Exemplarily UV-titration experiment of receptor **56** with a peptide substrate. The expected absorption A_{exp} without any effect was calculated considering only the dilution effect of the added receptor solution during the experiment.

After each addition step the solution was mixed by shaking it for 5 to 10 seconds and measurement was carried out after 2 min. During this delay the mixture was allowed to equilibrate. Therefore the sample was tempered at 25°C within the heated thermos-block of the UV-machine. The measurement was carried out with a tempered sample too.

6.8.2 Evaluation of the Binding Constants

All titration experiments started with an initial volume of 700-800 µl of the pure receptor solution in a UV cuvette at a pH of 6.0. The concentration of the receptor solution at the beginning of the experiments varied from $5.575 \cdot 10^{-5}$ M to $1.173 \cdot 10^{-4}$ M. All peptide solutions used in the UV-experiments were approximately 100 to 150°times higher concentrated than the receptor solution. The total amount of added substrate peptides varied from 18 to 80 equivalents. Generally small quantities of 2.5 µl to 5 µl of peptides were added at the beginning of an experiment. With progress of the titration experiment the amounts were increased up to 40 µl per step.

The UV spectrum of the UV-titration experiment of receptor **56** with the linear peptide **P1** is shown in figure 6-2. The single measurements are shown on the left side. The plot of the binding isotherm in figure 4-48 (red line) was obtained from a non-linear regression analysis with the computer program *origin*. The experiment was done with a ligand concentration of $8.16 \cdot 10^{-3}$ M and a receptor concentration of $5.575 \cdot 10^{-5}$ M.

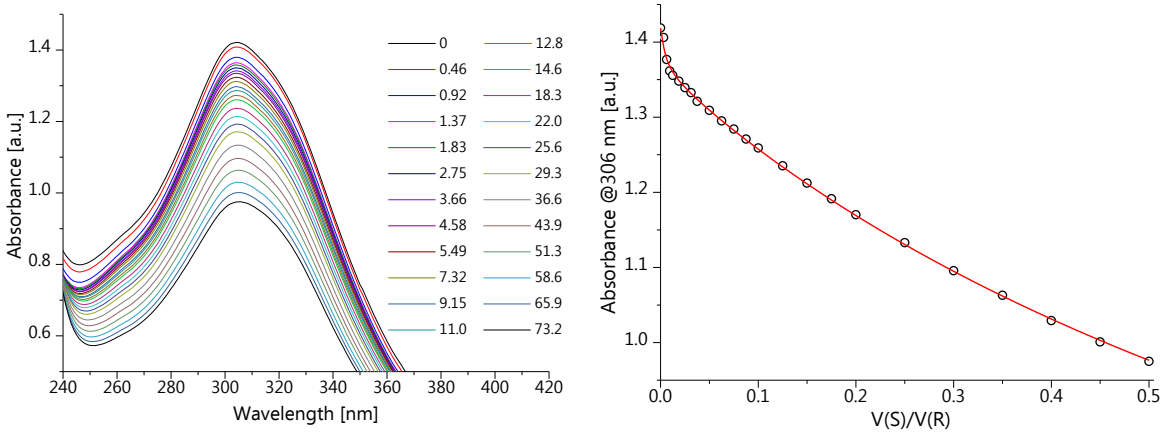

Figure 6-2. UV-measurements of the titration experiment of receptor **56** and ligand **P1**. The added equivalents of substrate are given in the table at the right side.

After the addition of 73.2 equivalents of the substrate peptide the measurement was stopped (fig. 6-1). The effect of the dilution was taken into account for analysis.

Some constraints were made before non-linear regression analysis was started. The variables of substrate concentration [S] and receptor concentration [R] were set to fixed values. Additionally the initial absorption A_i and the extinction coefficient of the receptor **56** were fixed. From the preliminary dilution experiment of receptor **56** an extinction coefficient ε of 2500 $L \cdot mol^{-1} \cdot cm^{-1}$ could be derived via the *Beer-Lambert Law* which was set as constraint too. For the final evaluation the ratio of V_S/V_R, synonymic to equivalents of added substrate, was plotted against observed absorption A_{obs} at maximum wavelength λ_{max}. The non-linear regression analysis revealed an average binding constant of 33.7 10^{-3} M^{-1} for the RGD-peptide **P1** with a standard error of 5.3 10^{-3} M^{-1}. In an analogous way the cyclic peptides **P2** and **P3** were evaluated. Their UV-measurements and binding isotherms are shown in figure 6-3.

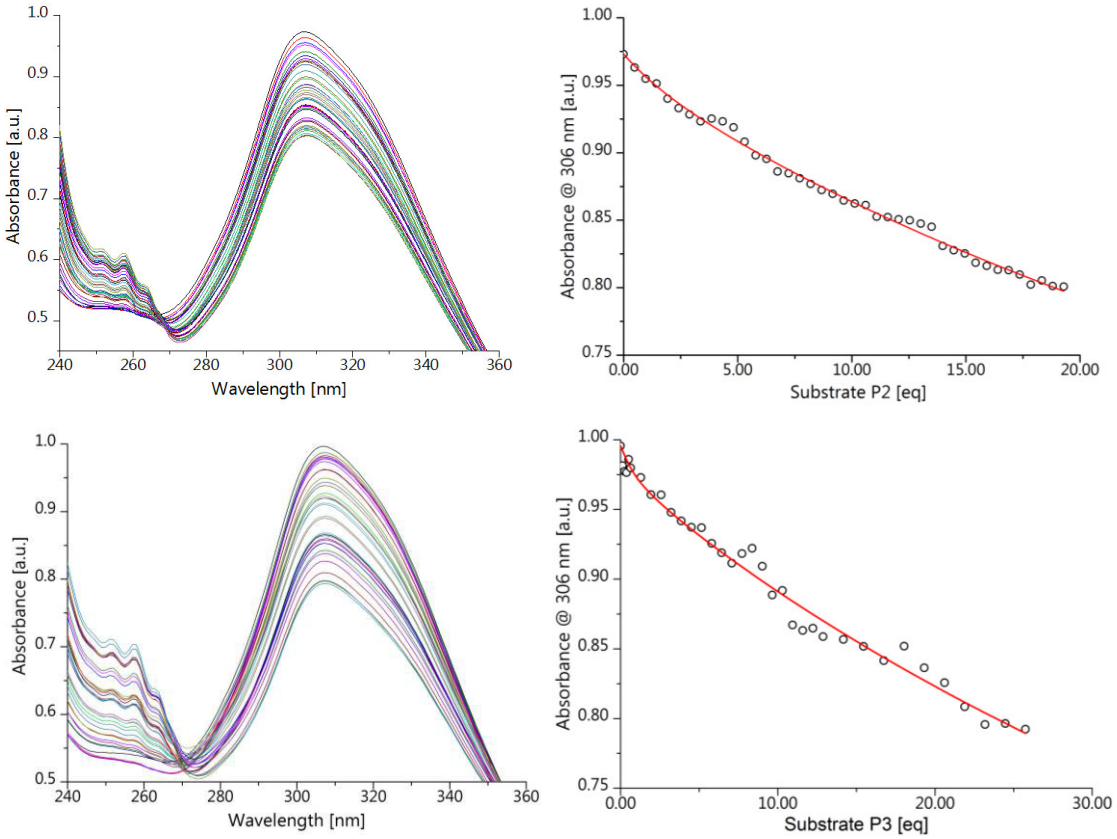

Figure 6-3. Left side: UV-measurements of titration experiment of receptor **56** and cyclic peptide **P2** (top) and **P3** (bottom). Respective binding isotherms are displayed at the right side. The black curls represent the single measurements.

In both cases the receptor concentration was 1.173 $\cdot 10^{-4}$ M. The concentration of the peptide solutions were 7.9 $\cdot 10^{-3}$ M and 1.057 $\cdot 10^{-2}$ M for the penta-peptide (**P2**) and the hexa-peptide (**P3**) respectively. The average binding constants of 13.3 $\cdot 10^{-3}$ M^{-1} for hexa-peptide **P3** and 4.3 $\cdot 10^{3*}$ M^{-1} for penta-peptide **P2** were calculated via non-linear regression analysis. In particular the average values were obtained from at

least 2 different and independent titration experiments. In figure 6-3 UV-spectra and binding isotherms of particular measurements of both cyclic peptides are shown.

The extinction coefficients at a wavelength of 306 nm of the receptor-peptide complexes were estimated at around 2300 $L \cdot mol^{-1} \cdot cm^{-1}$. The estimated values were not obtained from any experimental data. They could only be derived from non-linear curve fitting with *origin*. In figure 6-4 the proposed peptide receptor complex of the hexa-peptide **P3** and receptor **56** is shown. Here the complementary binding sites are positioned in opposite of each other.

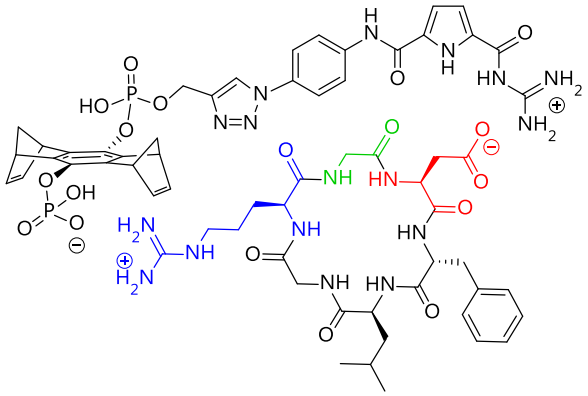

Figure 6-4. Proposed binding motif for a 1:1 association between receptor **56** and peptide **P3**.

The repeated titration experiment of RGD-peptide **P2** at a higher concentration of the substrate revealed some interesting results. In this experiment a peptide concentration 150 times higher than the initial receptor concentration was used. In figure 6-5 the full experiment is shown.

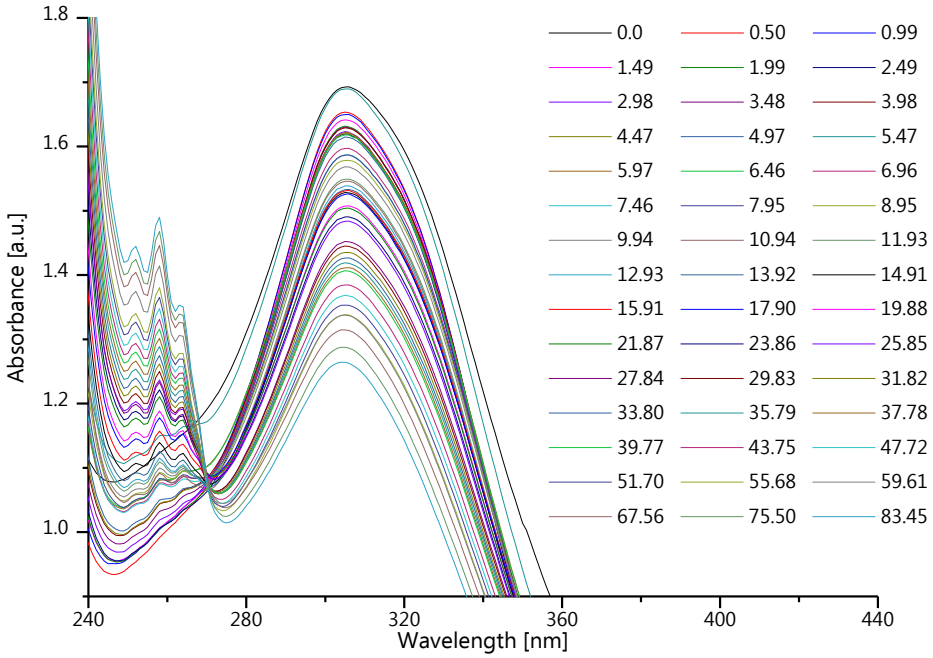

Figure 6-5. UV titration experiment of receptor **56** and peptide **P2** with increased concentration.

The experiment was carried out under same conditions as the previous experiments. Due to the higher concentration of peptide solution 83.45 equivalents were added in total. For the non-linear regression analysis the unfeasible measurements that revealed strange shifts were deleted. The plot of the linear regression analysis with the adjusted data set is shown in figure 6-5.

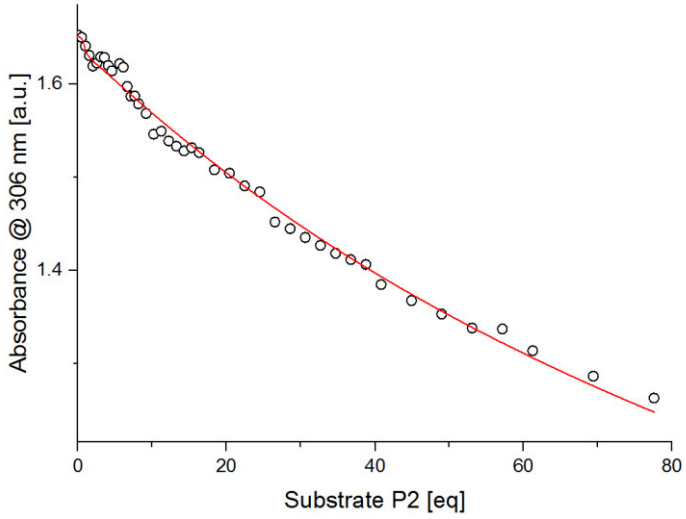

Figure 6-6. Plot of the linear regression after elimination of the most unfeasible measurement data.

Although the plot looked quite acceptable (fig. 6-6) no suitable binding constant could be evaluated from the acquired data. The *Job* plots were carried out with equimolar solutions of receptor and substrate. For the *Job* plots a concentration range between 55.7 µM and 139 µM was used. The adjustment of the molar specific molar fractions occurred via volume exchange. In the initial step the pure receptor solution was measured.

Step #	$V_{exchanged}$ [µL]	Substrate [eq]	V_{total} [µL]	Molar fraction [x_s]	A_{obs} at λ_{max}
1	0	0	800	0	1.434
2	80	0.1	800	0.1	1.282
3	88.9	0.2	800	0.2	1.135
4	100	0.3	800	0.3	0.994
5	114.29	0.4	800	0.4	0.855
6	133.33	0.5	800	0.5	0.719
7	160	0.6	800	0.6	0.570
8	200	0.7	800	0.7	0.433
9	266	0.8	800	0.8	0.293
10	400	0.9	800	0.9	0.156
11	800	1	800	1	0.039

Figure 6-7. Table of an exemplary *Job* plot analysis.

For further steps the adjustment of the molar fraction occurred via exchange of the initial solution. The individual steps are shown in figure 6-7 exemplarily.

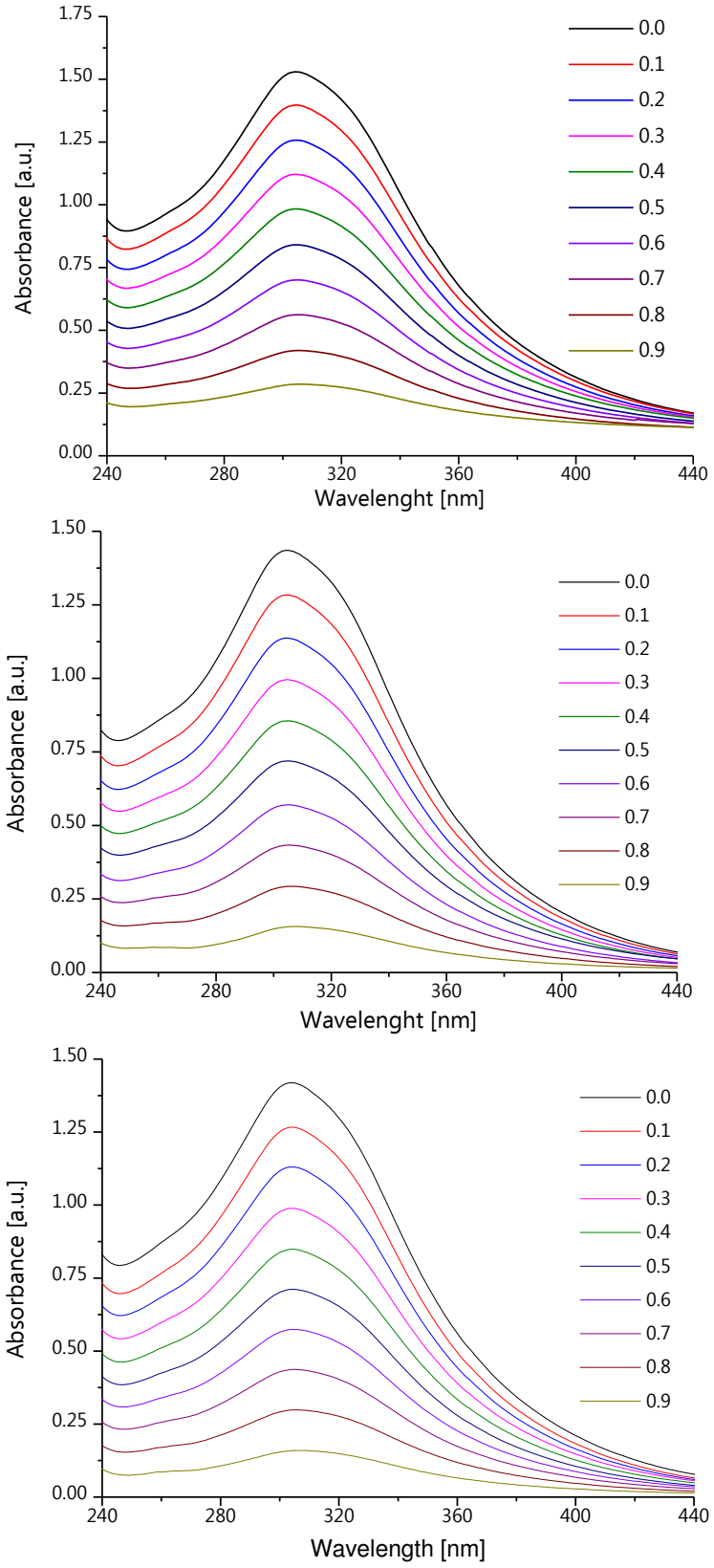

Figure 6-8. Exemplarily the UV-spectrum of the second titration experiment with a higher concentration for *Job* plots of peptide **P1** (top), **P2** (middle) and **P3** (bottom) are shown respectively.

In figure 6-8 the Job plots of the RG-receptor **56** and the 3 respective peptides are shown. The individual curves represent the single measurements at the specific molar fraction given in the legend beside the plot. The data of the maxima at 306 nm were used to calculate the differential absorbance ΔA. The observed absorption of the last step (fig. 6-7) was calculated from previous measurements of the pure peptide solutions. To obtain the *Job* plots shown in chapter 4.3.6 the differential absorbance ΔA was plotted against the molar fraction of the substrate. The results of higher and lower concentrated sample solution were equivalent.

6.9 AFM Images of the Synthesized RGD-Receptors

Generally the preparation of samples was carried out via the spin coating method. Through the spinning process a complete removal of solvent could be guaranteed. Tentatively samples were prepared via drop casting method. But unfortunately they suffered from an incomplete drying of the DMSO solvent. Although the samples were dried carefully under reduced pressure for several days no complete removal of solvent could be obtained. As a consequence no structures or aggregate could be imaged except some droplets of DMSO.

As the best method a spin coating process with a rotation speed of 60 rps could be developed. The duration of one minute of spin coating could be investigated to be sufficient enough for a complete remove of the solvent. The preparation of the solutions was carried from aqueous suspensions initially. With hydrochloric acid and triethylamine the suspensions were adjusted to the acidic (pH 3), neutral (pH 6) and alkaline (pH 11) conditions. After removal of the water via lyophilization the residue was dissolved in DMSO. The DMSO was filtered over a nylon filter with a pore-size of 200 nm to avoid contamination with foreign particles. The same was done with the water before suspensions were prepared.

The samples were measured directly after their preparation. The following AFM images (fig. 6-9) show further results of the previous shown pictures (fig 4-41). Beside the described structures some smaller aggregates could be found. In an experiment to check the purity of the DMSO solvent and DMSO solutions of triethylamine the same small aggregates could be found too. Even in highly diluted DMSO solutions of triethylamine these small aggregates could be found.

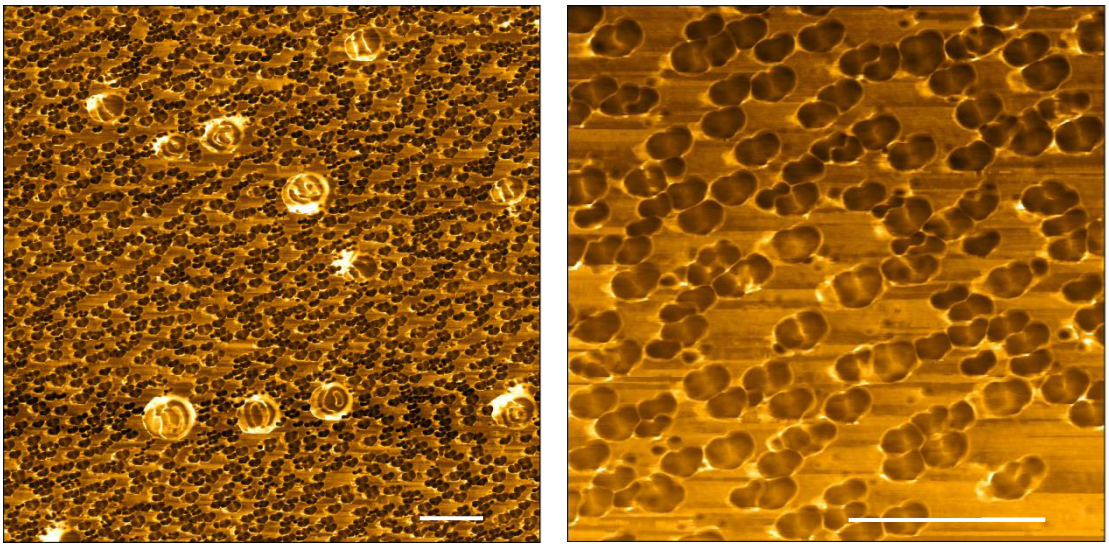

Figure 6-9. Tapping phase pictures show alkaline DMSO solution of receptor **46** on the left side and DMSO solution of pure NEt3 on the right side.

Figure 6-10 shows AFM pictures of a highly diluted DMSO solution of triethylamine. These particles were supposed to result from triethylamine salts that were already in the purchased bottle. At a pH of 6.0 those round shaped and noted particles could be obtained in a rather narrow size distribution (fig. 6-11).

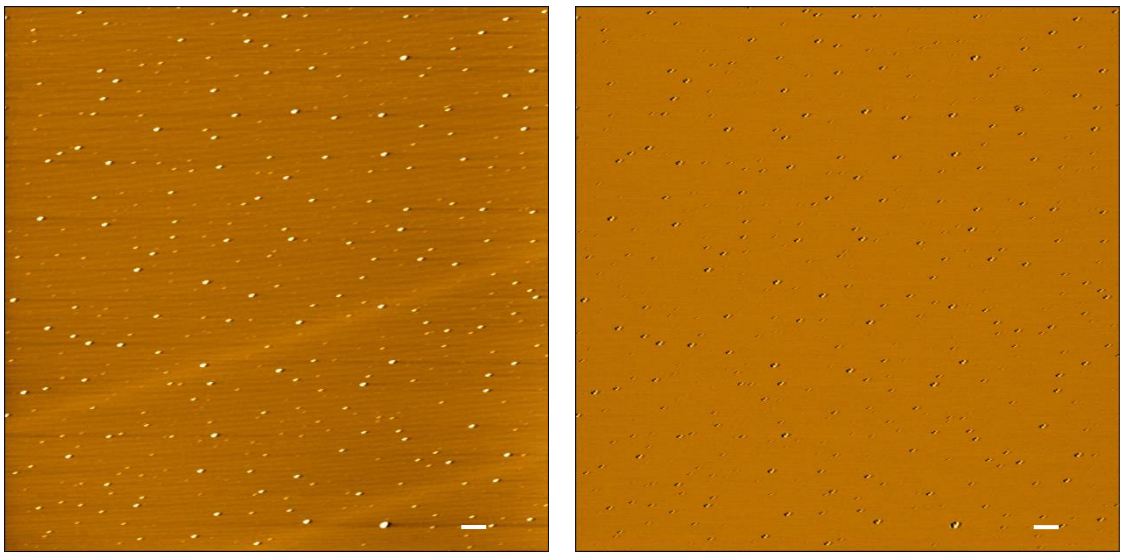

Figure 6-10. Surface covered by small particles obtained from a highly diluted triethylamine solution in DMSO. On the left side height images and on the right side pictures of the tapping phase are represented.

These particles were distributed rather equally over the surface. In some cases bigger conglomerates could be found too. They were assumed to originate from many of these small particles that dominated. Under acidic conditions rarely small agglomerates appeared. Generally these network structures (fig. 4-39) appeared. Only in border regions smaller particles appeared more randomly. The AFM images of height and tapping phase are shown in figure 6-12.

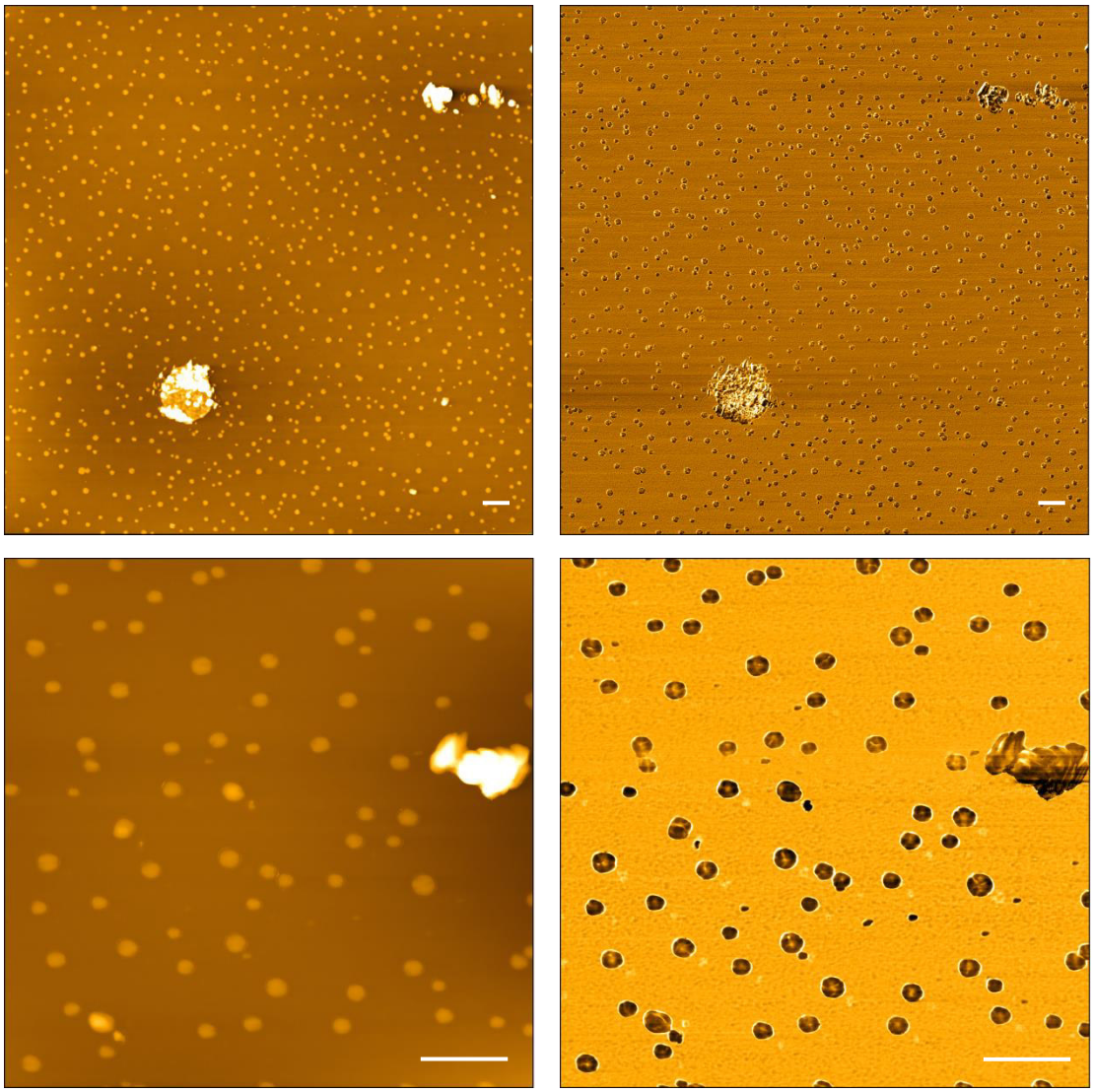

Figure 6-11. Almost neutral DMSO solutions of RGD-receptor **46** led to particles with a spherical shape. The pictures at the top show an overview whereas the pictures below show more details of particles. At the left side the height images revealed some bigger agglomerates, which appear white colored. Strikingly the particles appear in a rather narrow size distribution with exception of some rare bigger agglomerates.

The preparation of AFM-samples of RGD-receptor **56** was done accordingly to previous mentioned method of spin coating. The main difference was that the second generation receptor was prepared in aqueous solution. The AFM images of receptor **56** revealed strikingly smaller aggregates compared to receptor **46**.

Scans of the receptor solutions at different pH-values like they were presented in figure 4-53 were carried out. Further scans of different concentrations of receptor solution at different pH values are given below. Almost neutral solutions with a pH of 6.0 revealed the lowest tendency of self-assembly.

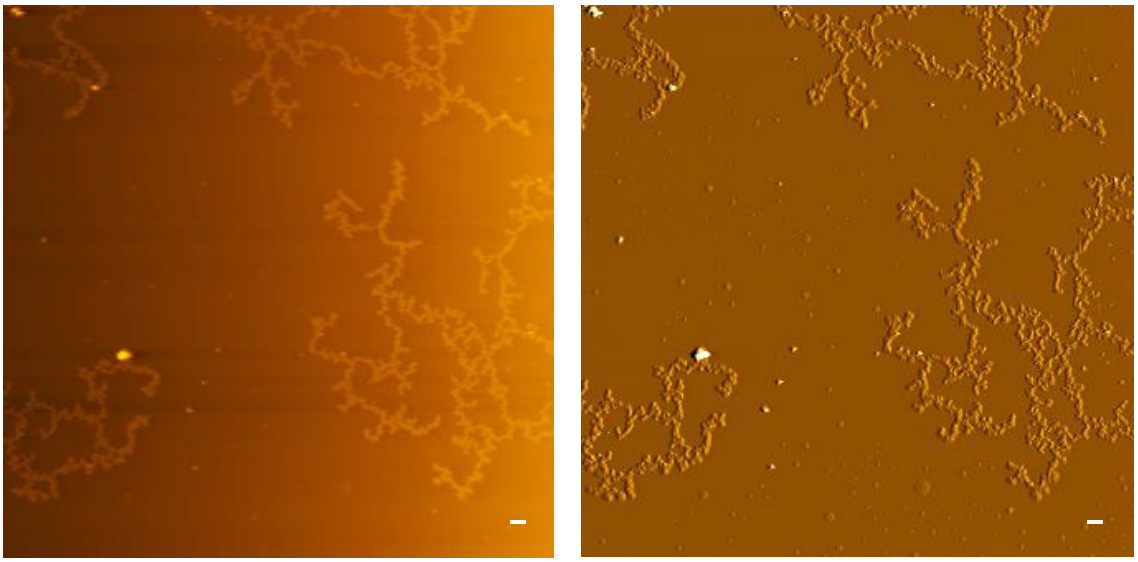

Figure 6-12. Height image at left side and corresponding tapping phase of receptor **46** under acidic conditions. The white scale bar measures 1 µm.

In figure 6-13 almost neutral conditions are shown. The pictures show an overcrowded surface if concentration is too high. The tapping phase image at the left side shows a sample with a concentration of 821 µM. If the concentration is decreased ten times lower some very tiny spots appeared only. The image at the right side shows the tapping phase of a nearly unpopulated mica surface.

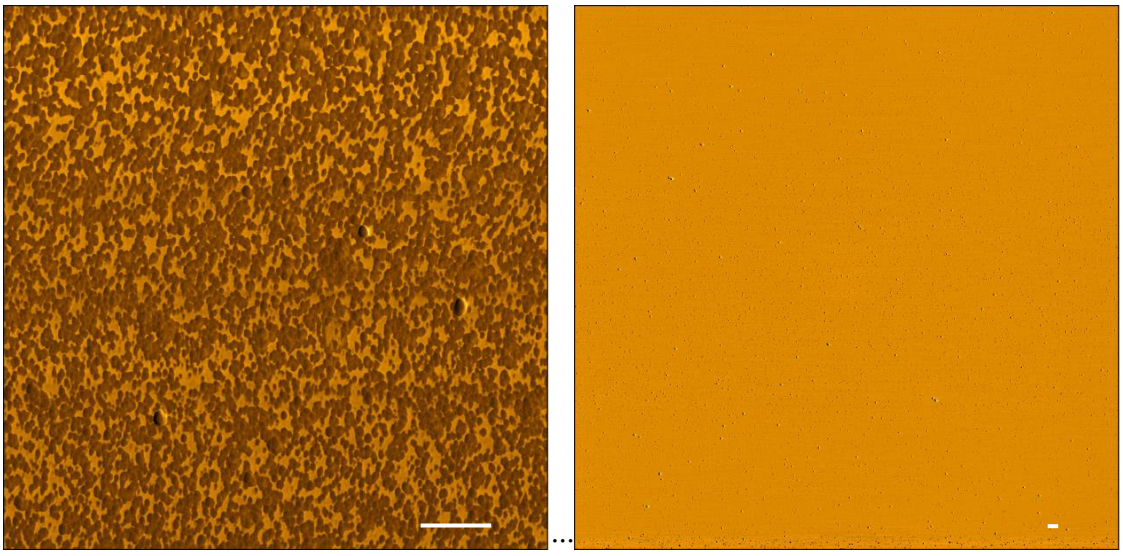

Figure 6-13. Overview scans revealed that receptor **56** did not tend to form aggregates under slightly acidic conditions (pH 6). Tapping phase images of concentrated solution (821 µM) on the left side and diluted solution (82.1 µM) at the right side are displayed. The white scale bar measures 1 µm.

Acidic conditions were obtained via addition of hydrochloric acid until a pH of 3.0 was reached. Alkaline conditions were obtained via addition of triethylamine until a pH value of 11.0 was obtained. In figure 6-14 concentrated and diluted solutions are

shown. In both pictures bigger agglomerates could be found. At lower concentrations they became more scattered over the mica surface as it is shown below.

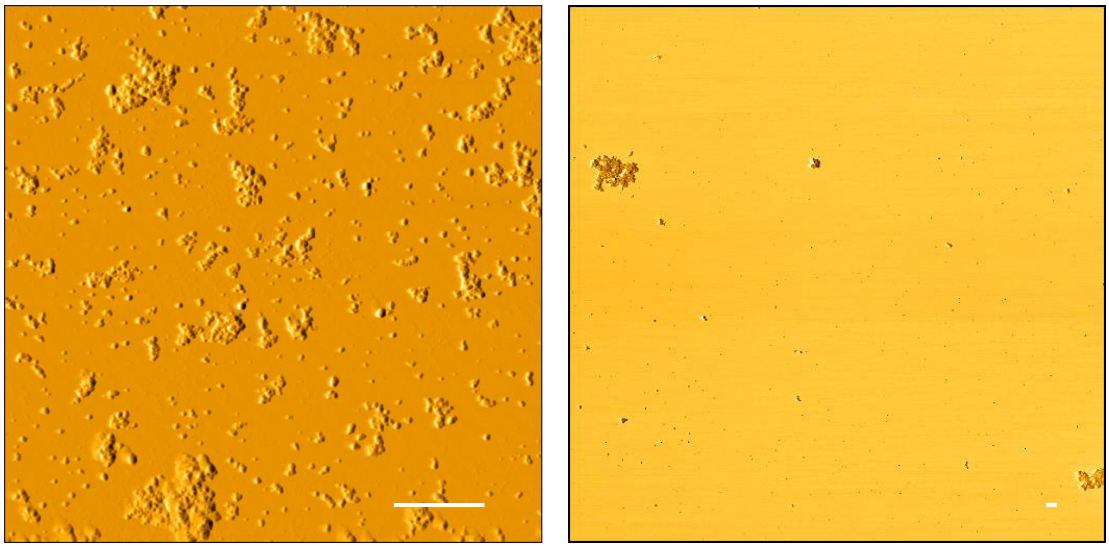

Figure 6-14. Detailed scan at pH 3 exhibited a clear aggregation behavior of receptor **56**. Both pictures show scans of the tapping phase at a concentration of 821 µM at the left and 82.1 µM at the right side. The white scale bar measures 1 µm.

Even at alkaline conditions (ph 11) the tendency to form smaller aggregates increased as it is shown in figure 6-15. Here the tapping phase of receptor **56** at a concentration of 82.1 µM is shown. Compared to the aggregates of the receptor under neutral conditions this picture reveals bigger agglomerates.

Figure 6-15. Tapping phase of receptor **56** at pH 11 with a concentration of 82.1 µM. The white scale bar measures 1 µm.

In summary these AFM study showed impressively that the second generation receptor does not suffer from an enhanced self-assembly as the first generation receptor **46** is did.

7 APPENDIX

7.1 Zusammenfassung und Ausblick

Die Zielsetzung dieser Arbeit war die Entwicklung eines wasserlöslichen Rezeptors zur Erkennung von niedermolekularen Peptiden, welche die RGD-Sequenz als Erkennungseinheit tragen. Im Focus standen die Synthese eines Rezeptors bestehend aus einem doppelten Bindungsmotiv sowie die Bestimmung seiner Bindungsaffinität gegenüber RGD-Peptiden. Beiden Bindungsmotive sollten in einer komplementären Art und Weise gestaltet sein. Dadurch sollte die simultane Erkennung der negativ geladenen Seitenkette der Asparaginsäure sowie die positiv geladene funktionelle Guanidiniumgruppe, die Teil der Aminosäure Arginin ist, ermöglicht werden.

10

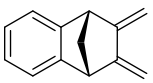

46

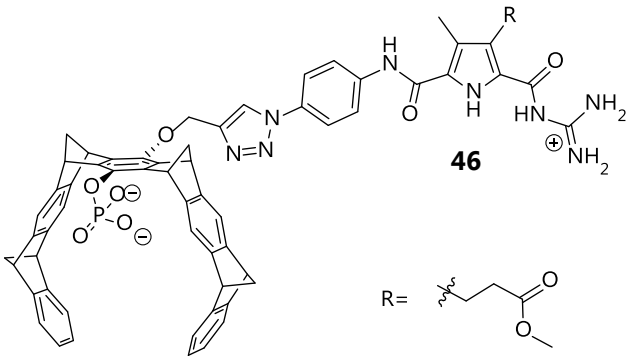

Abbildung 7-1. Struktur des bizyklischen Diens **10** und des RGD-Rezeptors **46**.

In einem ersten Ansatz wurde der RGD-Rezeptor **46** der ersten Generation in einer 22 stufige Synthese dargestellt (Abbildung 7-1). Teilweise konnte die Synthese über konvergente Reaktionen wie beispielsweise die Darstellung des Tweezers oder des Triazols durchgeführt werden. Weiterhin konnten Verbesserungen in der Tweezersynthese etabliert werden. Besonders zu erwähnen ist die effizientere Herstellung des Diens **10**. So konnte die Ausbeute in der ersten Synthesestufe durch den Tausch des Polymerisations-Inhibitors deutlich gesteigert werden.

In Kombination mit einer Syntheseverkürzung von 6 auf 4 Stufen konnte die Ausbeute von 15 % auf nahezu 40 % erhöht werden (Abbildung 7-1). Weiterhin konnte ein einfacher Zugang zu unsymmetrischen Tweezern innerhalb dieser Arbeit entwickelt werden. Während der Synthese des ersten RGD-Rezeptors **46** konnte ein Weg zum Mono-Alkin Tweezer **31** (Abbildung 7-2) gefunden werden.

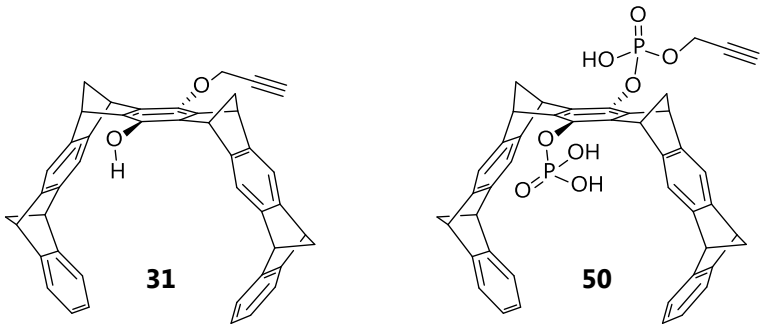

Abbildung 7-2. Beide abgebildeten Mono-Alkine konnten mit Hilfe einer *Williamson Ether Synthese* bzw. einer analogen *Williamson Ether Synthese* hergestellt werden.

Wie sich herausgestellt hatte, war die Wasserlöslichkeit des RGD-Rezeptors der ersten Generation für weitere Bindungsstudien mit RGD-Peptiden ungenügend (Abbildung 7-1). Selbst die Charakterisierung des Rezeptor-Vorgängers **45** und des Rezeptors **46** zeigte einige Probleme, die im Zusammenhang mit der schlechten Löslichkeit im Allgemeinen zu sehen sind. Unter sauren, leicht sauren wie auch basischen Bedingungen zeigte sich, dass Aggregate gebildet wurden. Diese konnten mittels AFM veranschaulicht werden. Mit Hilfe von DLS-Messungen konnte die Größe der gebildeten Aggregate unter nahezu neutralen Bedingungen bestätigt werden.

In einem zweiten Ansatz wurde über eine weitere Phosphatgruppe in Zusammenhang mit einer Größenreduzierung des aromatischen Grundgerüstes des Tweezer-Moleküls nachgedacht. Für die Realisierung eines komplett wasserlöslichen RGD-Rezeptors musste eine Synthese von unsymmetrischen Tweezern wie auch deren kleineren Homologen entwickelt werden. Die Einführung einer zweiten Phosphatgruppe ergab den wasserlöslichen Diphosphat-Tweezer **50** und die Bindungsstelle (**51**) für die Guanidiniumfunktion. Dabei konnte die Synthese des verkürzten Tweezers **51** sogar als Eintopf-Reaktion ausgehend vom Diol **19b** (Abbildung 7-3) durchgeführt werden. Im letzten Syntheseschritt wurde der RGD-Rezeptor **56** durch eine kupfer-katalysierte Cycloadditions-Reaktion zusammengefügt. Dieser letzte Reaktionsschritt ermöglichte eine elegante Verknüpfung beider Bindungsmotive in Verbindung mit einer konvergenten Synthesestrategie. Der niedermolekulare RGD-Rezeptor **56** wurde in einer Gesamtausbeute von 3 % in Bezug auf Molekül **51** synthetisiert.

Im Allgemeinen wurden die Synthesen der Grundbausteine nach den protokollierten Standardsynthesen durchgeführt. Dabei konnten einige

Verbesserungen mit Hinblick auf Ausbeute und Effizienz gemacht werden. Besonders die Synthese des Tweezerbausteines konnte um 2 Reaktionsschritte verkürzt werden. Bei der Synthese des Pyrrolbausteines **32** zeigten sich Stabilitätsprobleme. Eine schnelle Zersetzung des Pyrrols **37** bei der Entschützung der Guanidin-Funktion konnten durch die spätere Einführung des Azides am ungeschützten Pyrrol **43** umgangen werden.

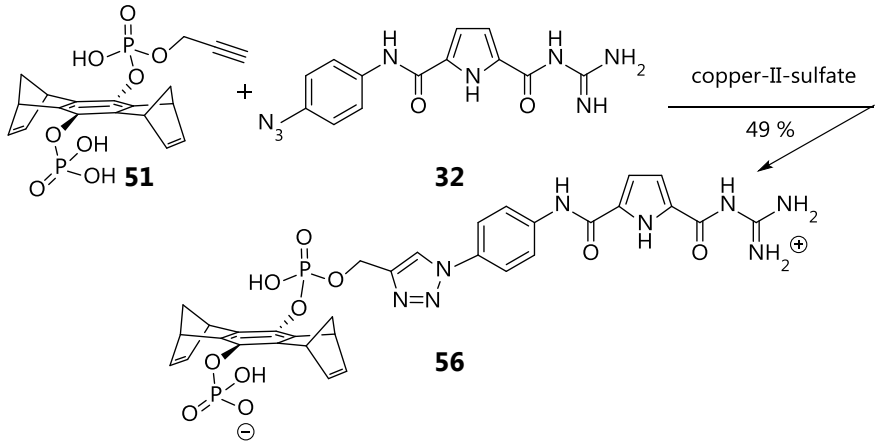

Abbildung 7-3. Die konvergente Synthese zwischen dem Diphosphat Mono-Alkin **51** und dem Pyrrolazid **32** wurde mit Hilfe einer 1,3-dipolaren Cycloaddition durchgeführt.

Eine Charakterisierung beider hergestellten RGD-Rezeptoren stellte sich als schwierig heraus. Aufgrund intermolekularer Wechselwirkungen durch Selbstassemblierungsprozesse wurden beispielsweise NMR-Spektren beeinflusst. Je mehr funktionelle entschützt vorlagen, desto deutlicher war eine Peakverbreiterung in den Spektren zu sehen.

Die UV-Bindungsstudien des RGD-Rezeptor **56** konnten ohne weitere Löslichkeitsprobleme unter leicht sauren Bedingungen durchgeführt werden. Die Ermittlung der Komplexstöchiometrie mittels der Methode nach *Job* lieferte nicht besonders signifikante Ergebnisse. Daher wurden 1:1 Stöchiometrien für die Wirt-Gast-Systeme angenommen. Dieser neue Rezeptor zeigte eindrucksvoll eine spezifische Erkennungsaffinität gegenüber dem linearen RGD-Peptid und zwischen den zyklischen RGD-Peptiden, die von *Kessler* et al. entwickelt wurden. Das konnte durch einen Anstieg der Bindungskonstante vom zyklischen Penta-Peptid **P2** über das zyklische Hexa-Peptid **P3** bis hin zum linearen RGD-Peptid **P1** gezeigt werden. Die größte Bindungskonstante wurde mit dem Peptid **P1** erzielt, mit dem unter Annahme eines 1:1 Komplexes eine Konstante von $K_A = 3.4*10^4$ M^{-1} gefunden werden konnte. Im Vergleich zum ersten synthetischen RGD-Rezeptor konnte die Bindungskonstante mit einem linearen RGD-Peptid um zwei Größenordnungen verbessert werden. Dieser erste Rezeptor war der von *Schrader* et al. entwickelte Triphosphonat-Rezeptor (Abbildung 2-5). Er verdeutlichte den gleichen Trend

stärkere Komplexe mit einem flexibleren und linearen RGD-Peptid (K_A = 1300 M^{-1}) im Vergleich zum zyklischen Peptid cyclo(RGDfV) (K_A = 700 M^{-1}) zu bilden.[43]

Der zuletzt genannte Rezeptor wies einen geringen Affinitätsunterschied zwischen dem zyklischem und dem freiem RGD-Peptid auf. Nur eine halbe Größenordnung an Selektivitätsunterschied wurden damit berichtet. Dagegen zeigte der in dieser Arbeit neue entwickelte wasserlösliche RGD-Rezeptor **56** von Natur aus eine höhere Selektivität zwischen dem Penta-Peptid (K_A = 4,300 M^{-1}) und dem linearen RGD (K_A = 34,000 M^{-1}).

Ein besonders großer Vorteil des neu entwickelten Rezeptors ist seine Flexibilität durch die variable Länge des Linker-Moleküls. Basierend auf dem Konzept von separierten Bindungsstellen, die über ein Linker-Molekül verknüpft sind, und einer konvergenten Synthese können schnell neuen RGD-Rezeptoren entwickelt werden. Diese Methode kann effizient zur Entwicklung verschiedener RGD-Rezeptoren mit unterschiedlichen Selektivitäts- und Bindungseigenschaften gegenüber verschiedenen RGD-Peptiden verwendet werden. Trotz der zuvor angestrebten Zielsetzung, einen RGD-Rezeptor mit einem kompletten Tweezer als Guanidium-Bindungsstelle zu entwickeln, konnte eindrucksvoll gezeigt werden, dass eine verkürzte Version des Tweezers eine einfachere Synthese bedeutet. Besonders die Löslichkeitsproblematik konnte damit umgangen werden. Letztlich können die Ergebnisse dieser Arbeit dazu beitragen maßgeschneiderte RGD-Rezeptoren durch die Verwendung von raumfüllenden Resten am Linker-Molekül zu kreieren. Durch die Verkleinerung des Tweezer-Moleküls und dem damit verbundenen Verlust des hydrophoben aromatischen Grundgerüstes können weitere Reste ohne größeren Einfluss auf die Löslichkeit eingeführt werden. Die Einführung von beispielsweise kleineren Resten wie Methyl oder Ethyl-Seitenketten kann einen Einfluss auf die Selektivität zwischen unterschiedlichen RGD-Peptiden haben.

Für eine weitere Forschung können erfolgreiche Ergebnisse erwartet werden. Besonders wenn eine Einstellung der Selektivität möglich ist, könnten Tests gegenüber größeren Proteinen wie Vitronectin oder Fibronectin durchgeführt werden. Dieser Ansatz ermöglicht dann einmal die Anwendung in Arzneimitteln oder deren Bewertung, wenn diese RGD-basiert sind.

7.2 Purity Control via NMR

^{1}H NMR of the *syn*-dione **19a**

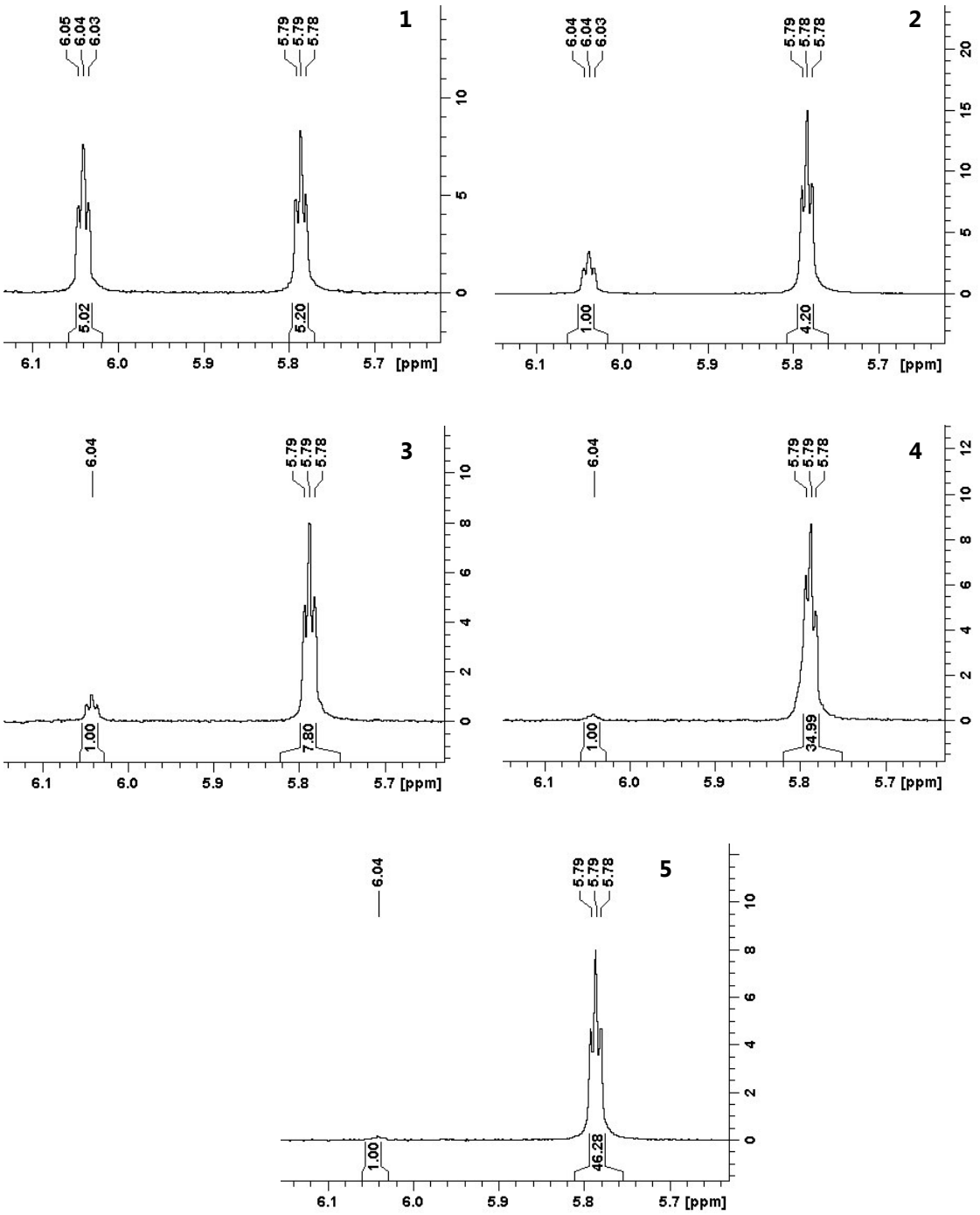

Figure 7-4. The *syn/anti* ratio after Diels-Alder-reaction to molecule **19a** is shown in the proton NMR spectra above. Here the selective crystallization was used for purification. From the first NMR spectrum (**1**) to the last one (**5**) the progress of purification is shown by an increased *syn/anti* ratio. After 5 crystallization steps a ratio of 46:1 of *syn*- (**19a**) to *anti*-dione (**18**) could be obtained.

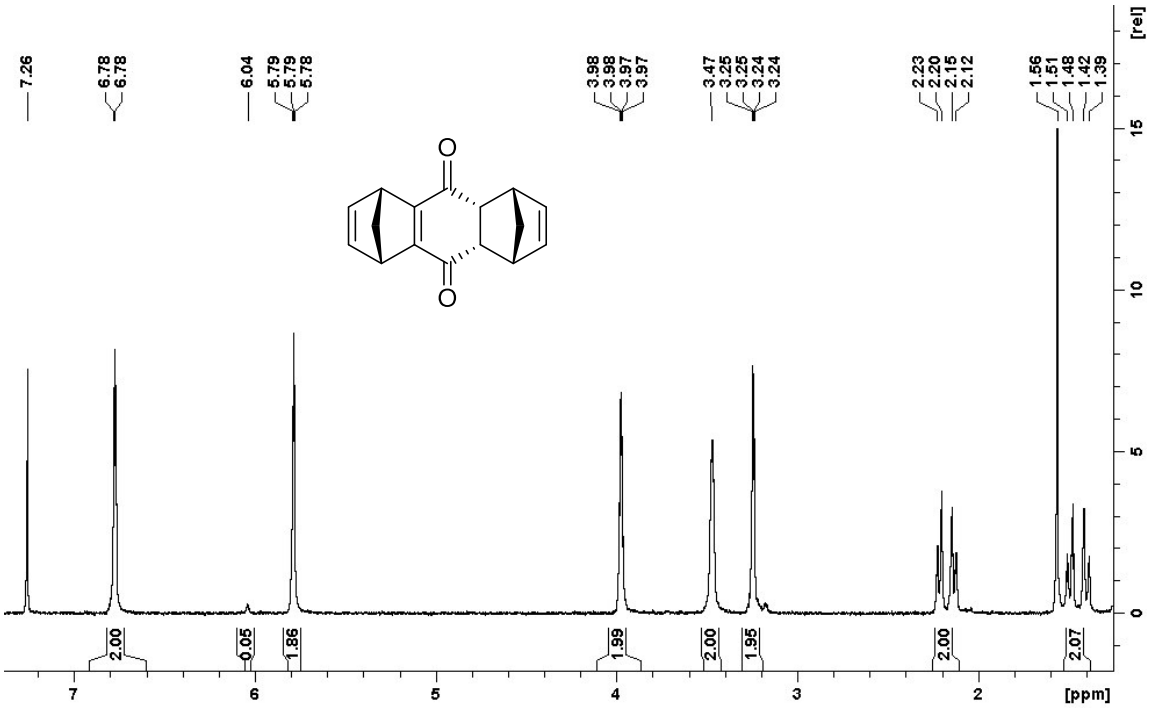

Figure 7-5. Full ^{1}H NMR of the purified *syn*-dione **19a**. The purification process was controlled via ^{1}H NMR shown in figure 7-4. The *syn* to *anti* ratio in this case is almost 1 to 38. The calculation occurred via the ratio of the integrals of the signals at 6.04 (*anti*-dione **18**) and 5.79 (*syn*-dione **19a**).

^{1}H and ^{13}C NMR of the mono-alkyne tweezer **31**

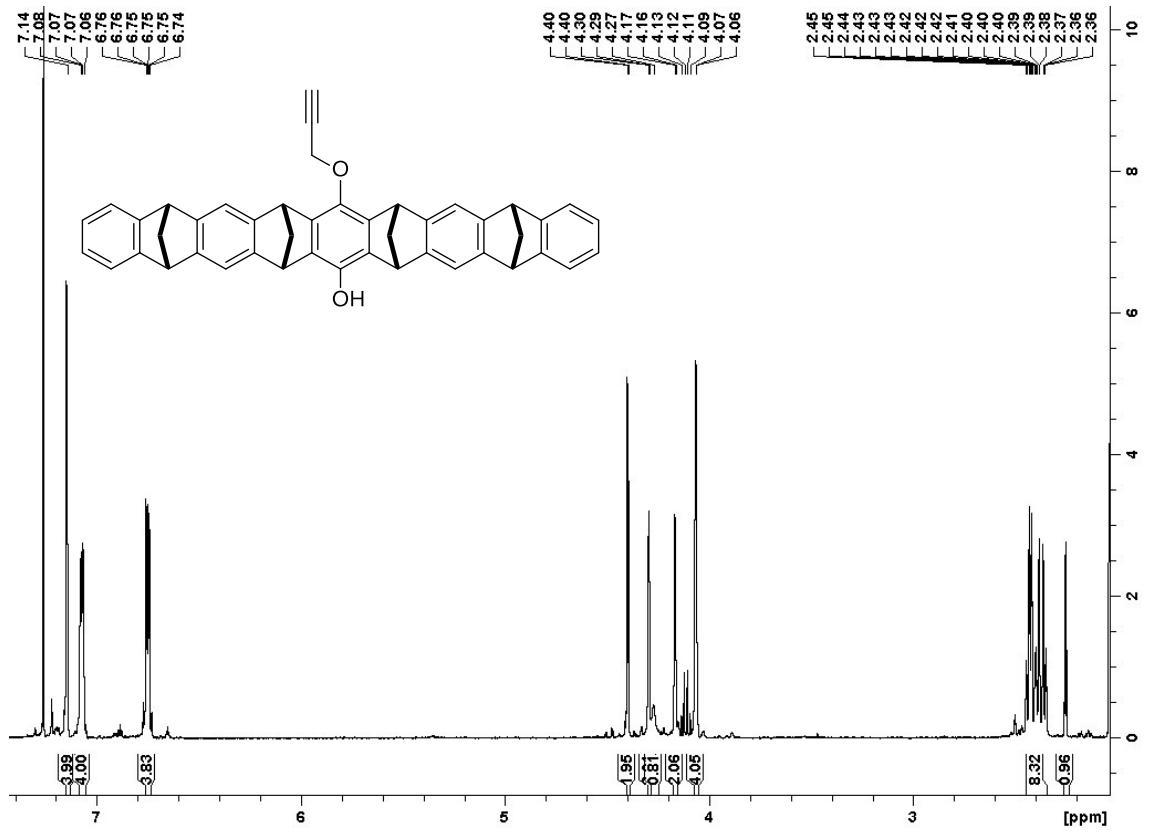

Figure 7-6. ^{1}H NMR of the un-symmetrical mono-alkyne tweezer **31**.

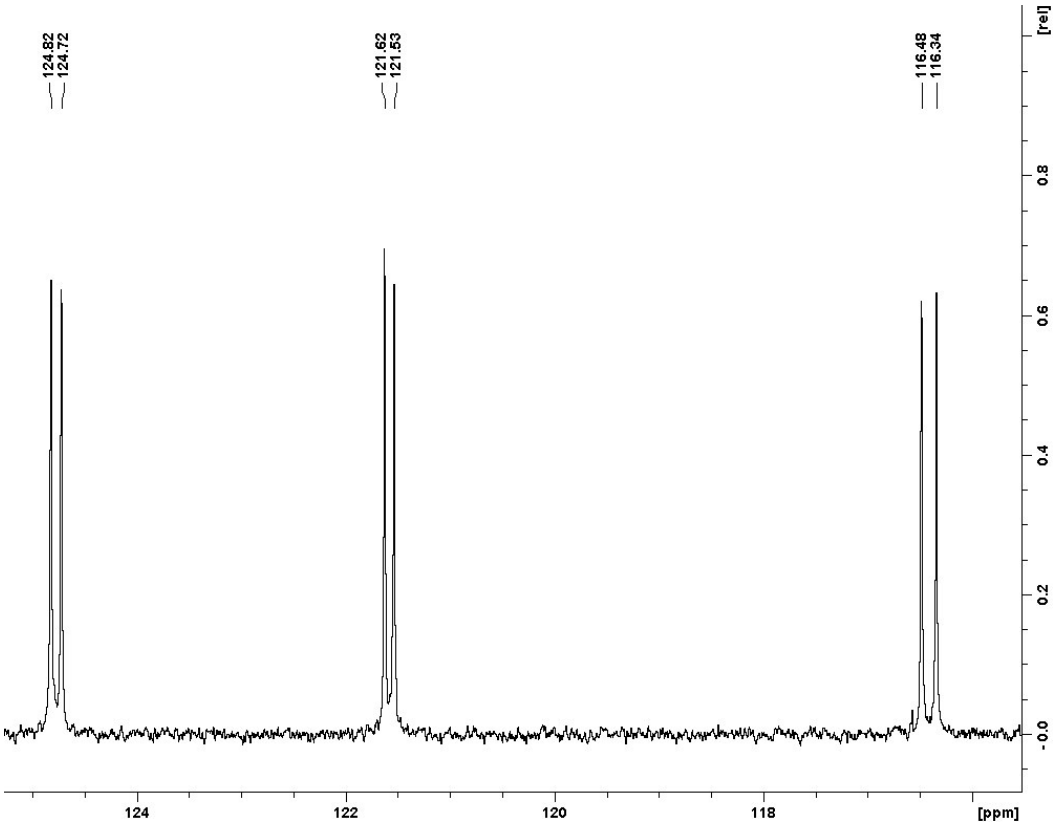

Figure 7-7. Double signal set in the ^{13}C NMR of the un-symmetrical mono-alkyne tweezer **31**.

^{1}H NMR spectra of the azido pyrroles **32** and **37**

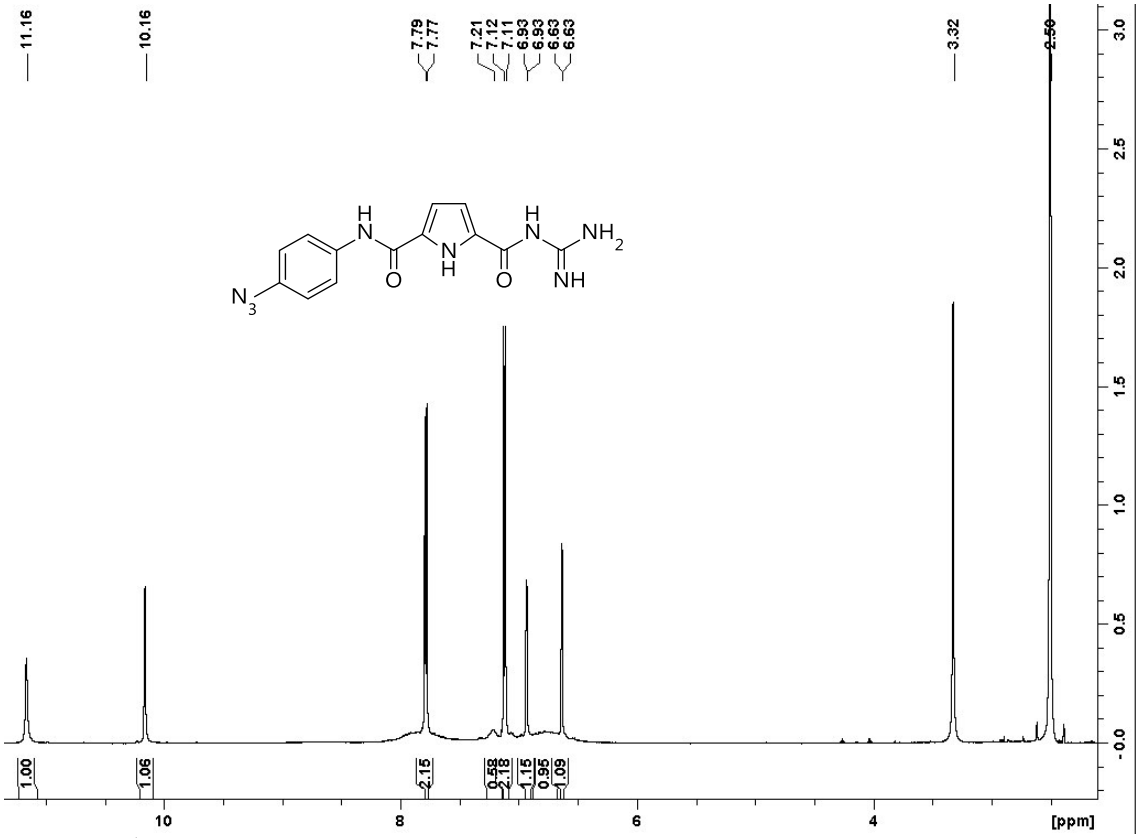

Figure 7-8. ^{1}H NMR of the purified azido pyrrole **32**.

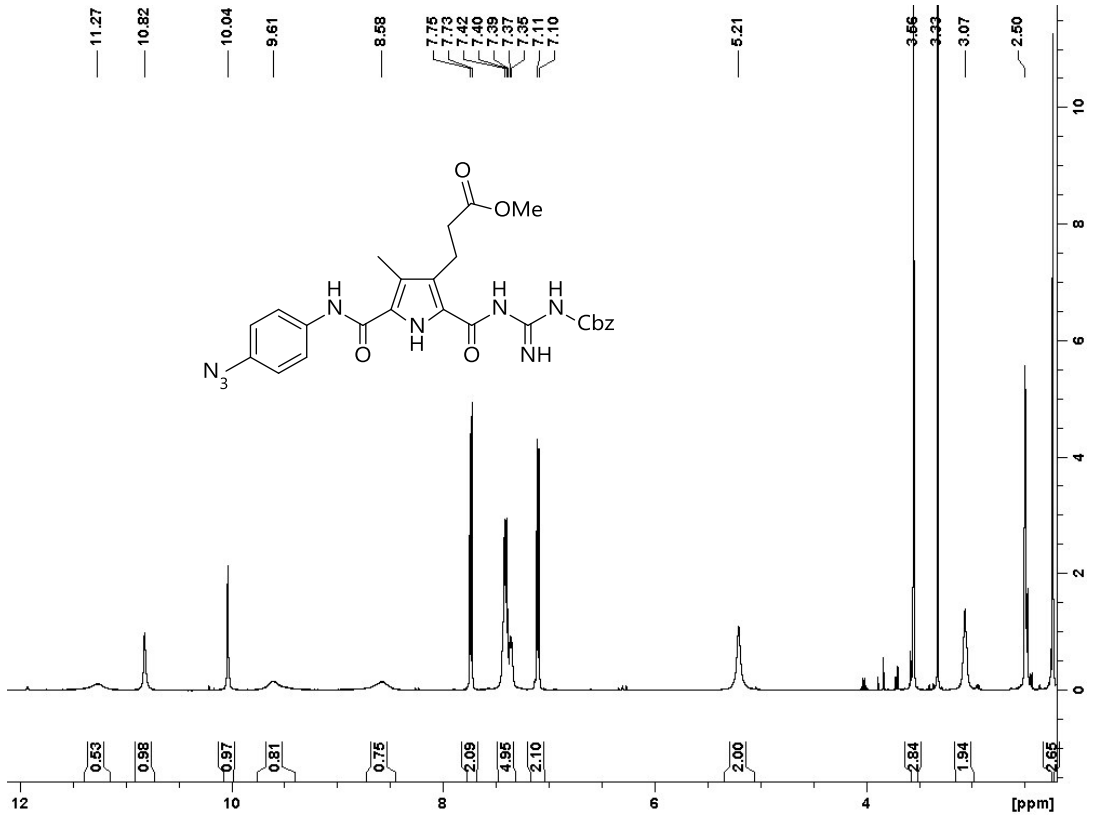

Figure 7-9. ^{1}H NMR of the purified azido pyrrole **37**.

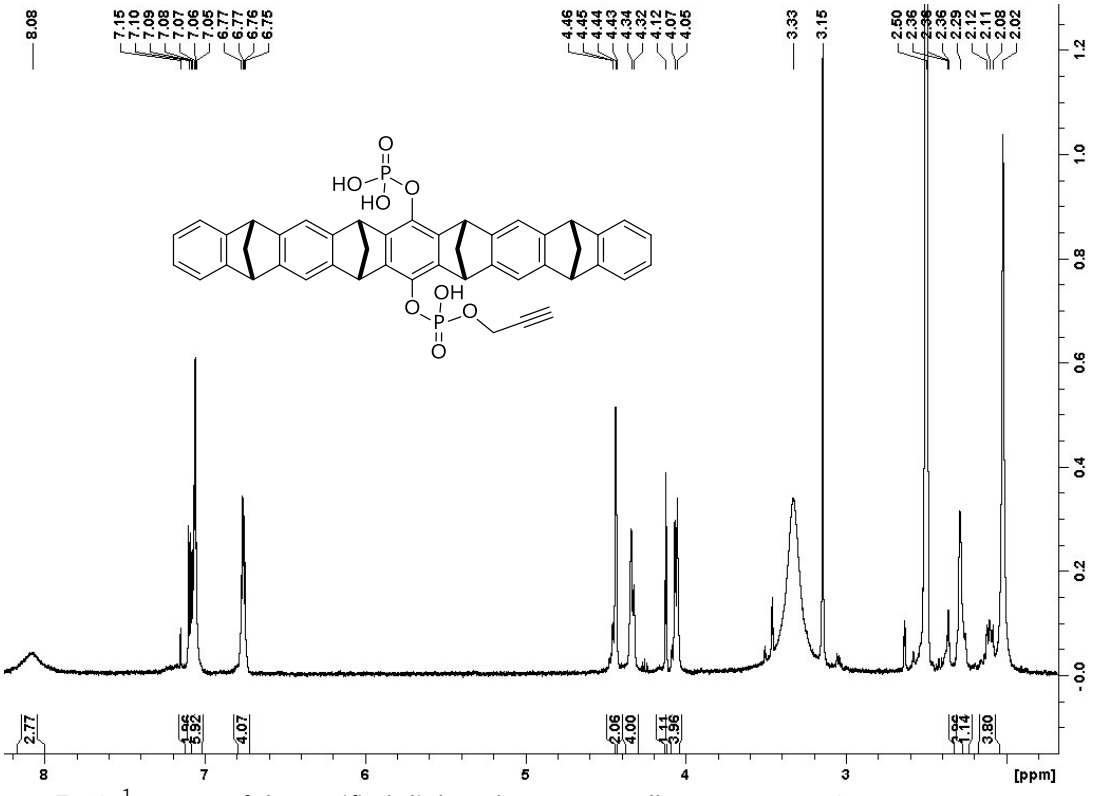

Figure 7-10. ^{1}H NMR of the purified diphosphate mono-alkyne tweezer **50**.

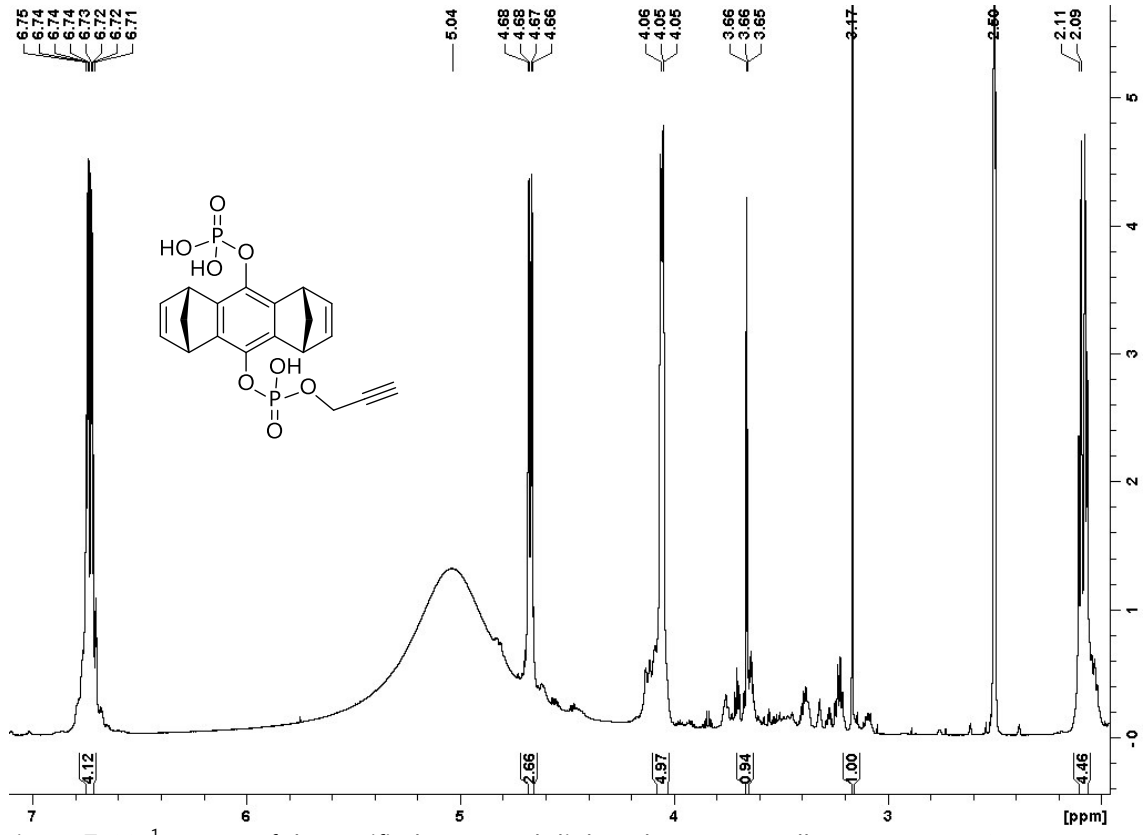

Figure 7-11. ^{1}H NMR of the purified truncated diphosphate mono-alkyne tweezer **51**.

^{31}P NMR of receptor **56** in DMF and DMSO

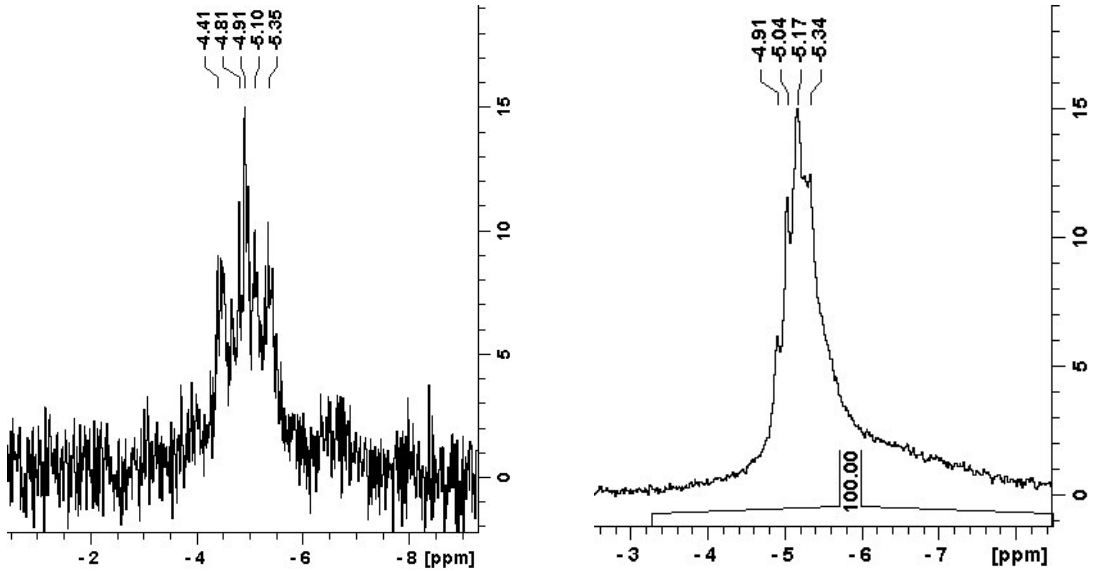

Figure 7-12. In fully deuterated DMF (left side) as well as in DMSO (right side) the ^{31}P-NMR spectra of **56** revealed some broadening. It is assumed that the different signals belong to different species formed by aggregation.

^{1}H NMR of the RGD-receptor **56**

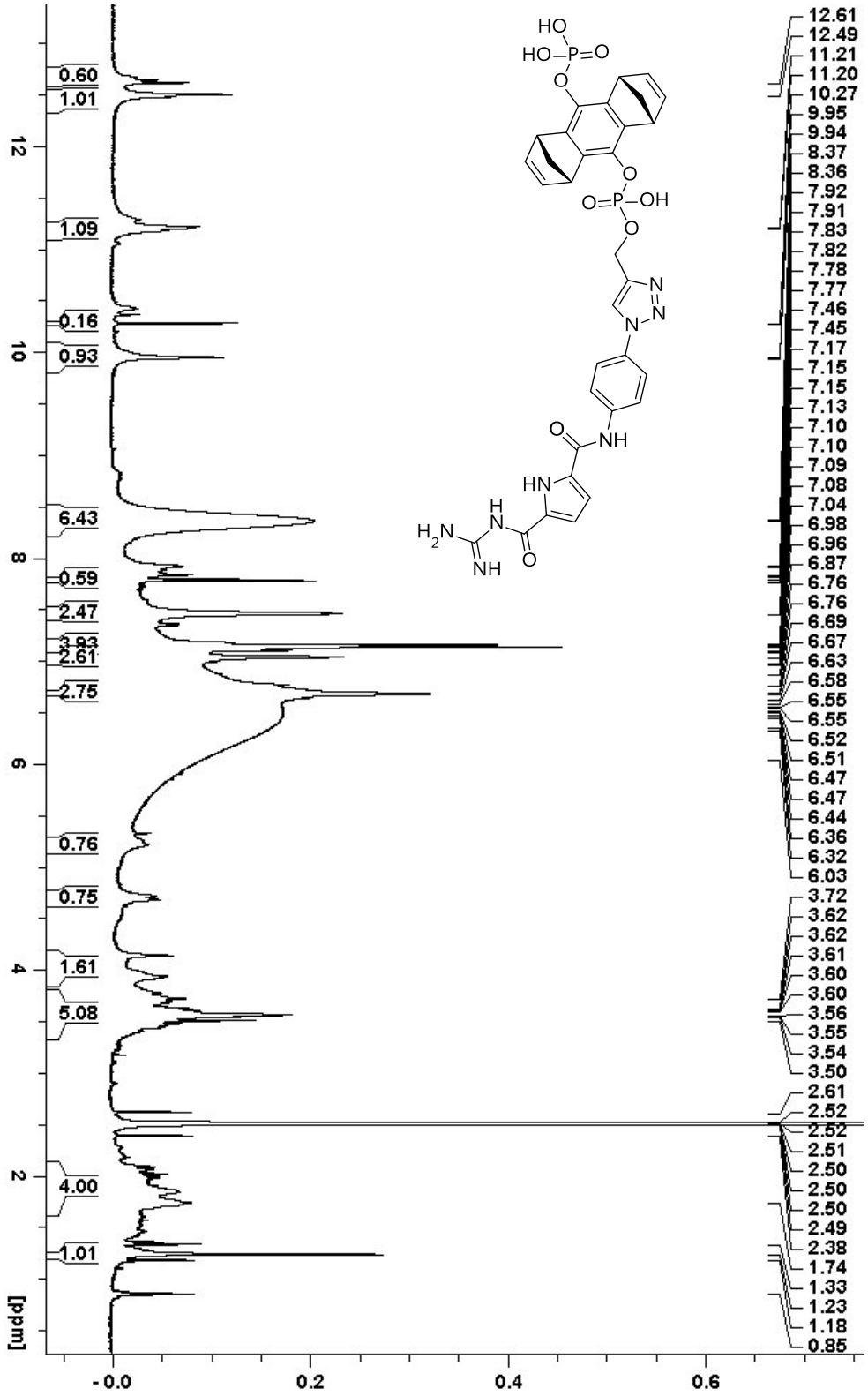

Figure 7-13. The ^{1}H-NMR spectra of molecule **56** showed some huge signal at a chemical shift reaching from 5.70 ppm to 7.70 ppm. The maximum at 6.65 ppm is centered so that the signal appeared rather symmetrical. Due to the missing water signal this signal seems to be the residual water signal in interaction with the negatively charged phosphate groups. All other molecule signals appeared in a moderate resolution. The reason might be some intermolecular interactions of 2 or more receptor molecules.

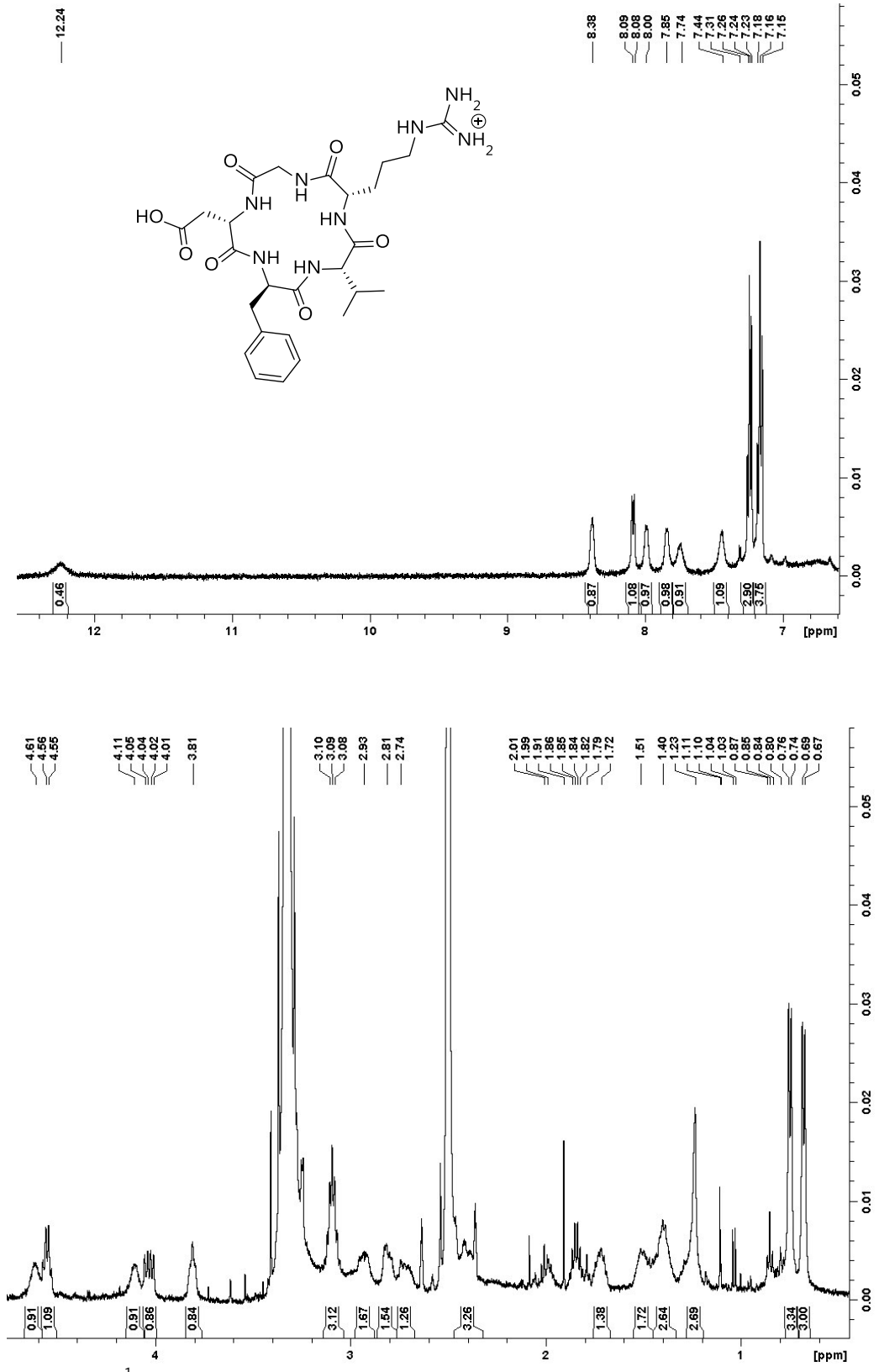

Figure 7-14. Full ^{1}H-NMR spectra of the penta-peptide **P2** in DMSO-d6.

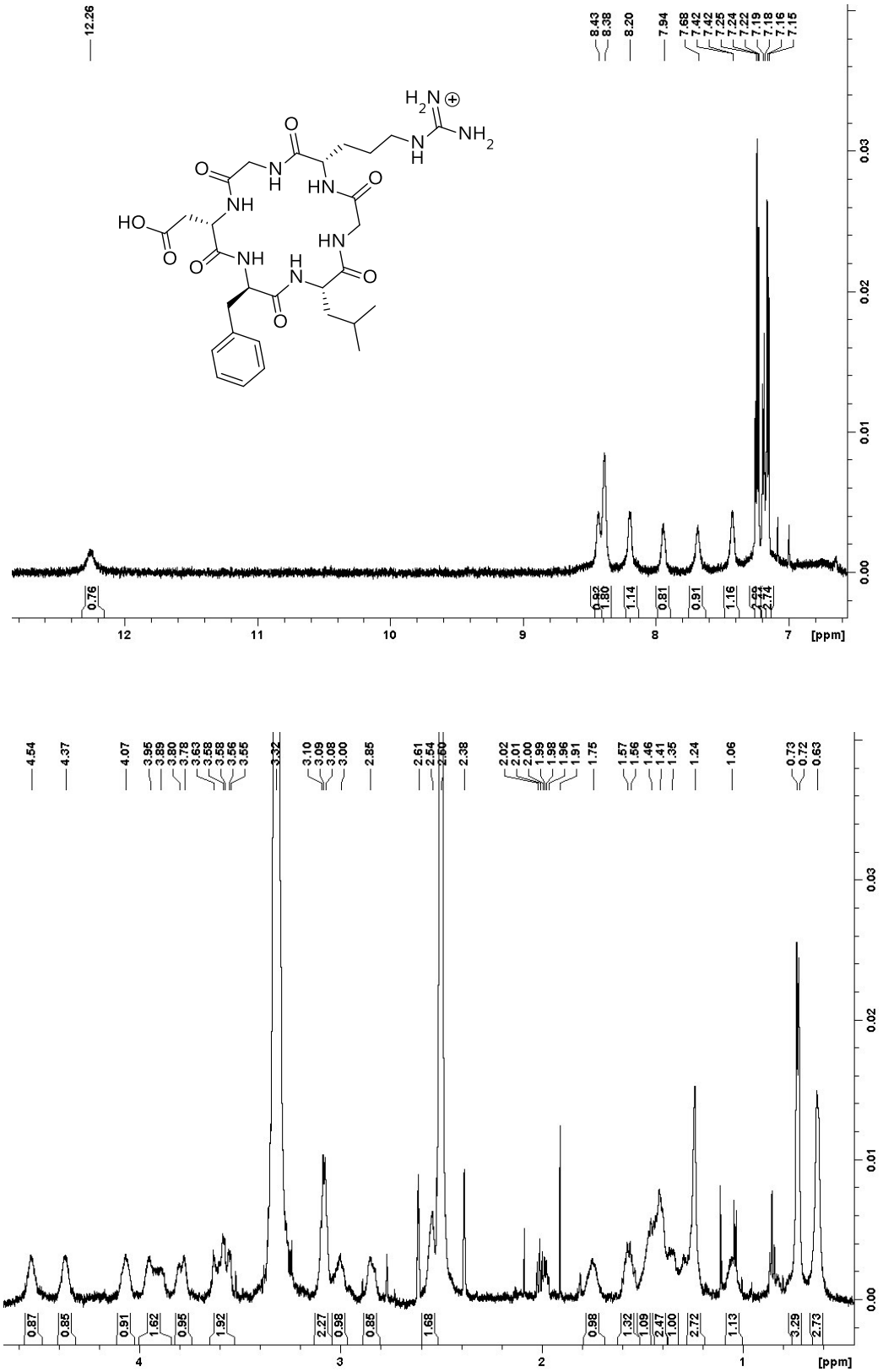

Figure 7-15. Full ^{1}H-NMR spectra of the hexa-peptide **P3** in DMSO-d6.

7.3 2D NMR Spectra

Two dimensional NMR soectra were recorded with a DRX500 and an Advance III HD 600 from *Bruker* for assignment purposes.

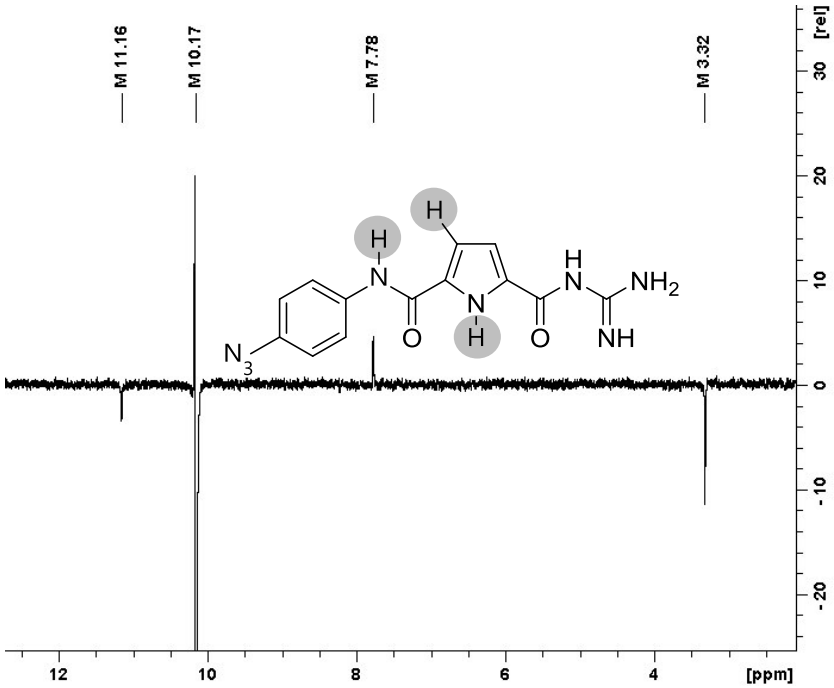

Figure 7-16. Selective NOESY-spectra of guanidiniocarbonyl pyrrole **32** showed the coupling interactions of the aniline proton with the pyrrole N*H* and the pyrrole C*H* proton.

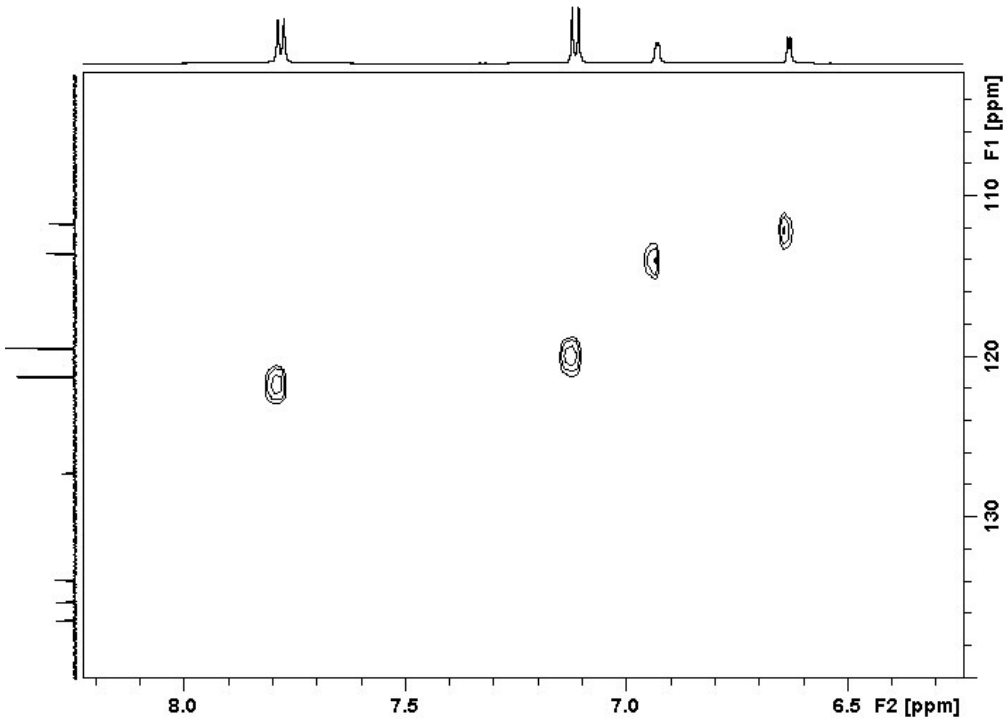

Figure 7-17. HSQC-spectra of the guanidiniocarbonyl pyrrole **32**.

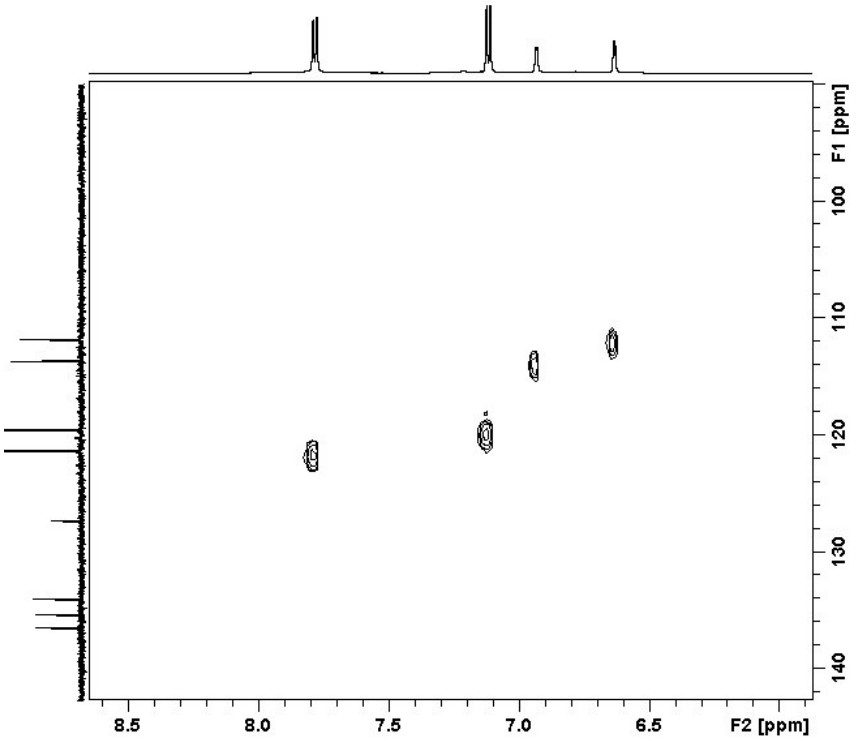

Figure 7-18. HMBC-spectra of the guanidiniocarbonyl pyrrole **32**.

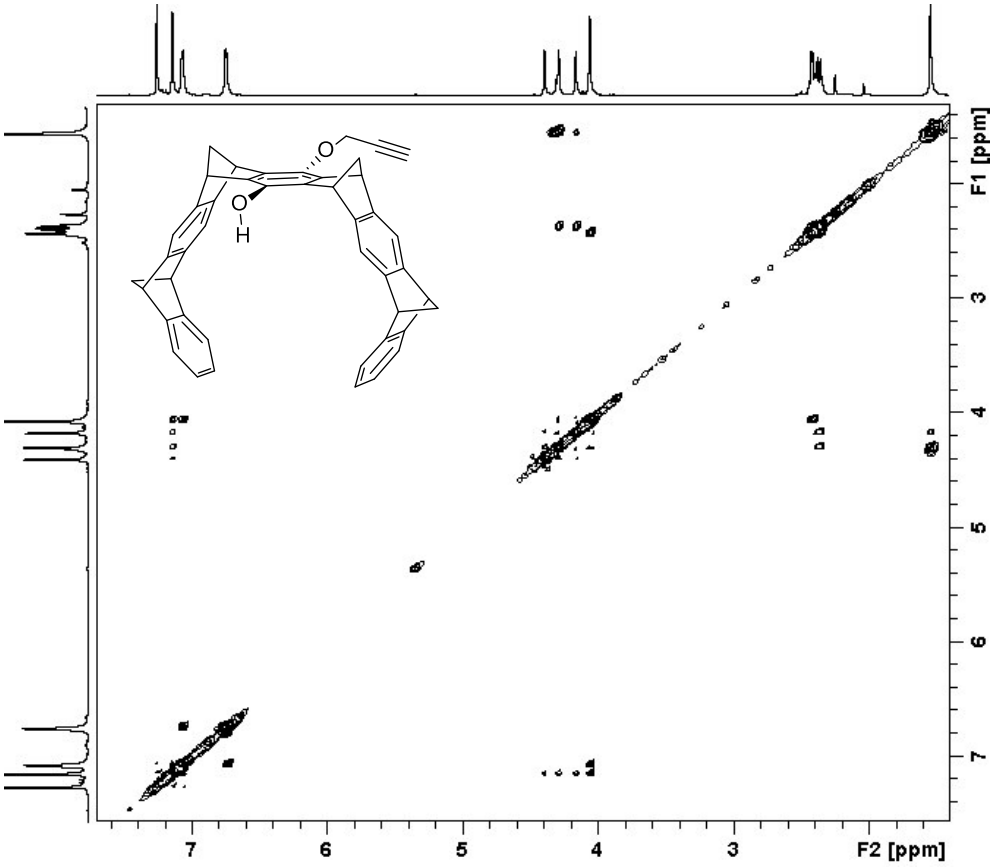

Figure 7-19. Selective NOESY-spectra of the dihydroxy mono-alkyne tweezer **31**.

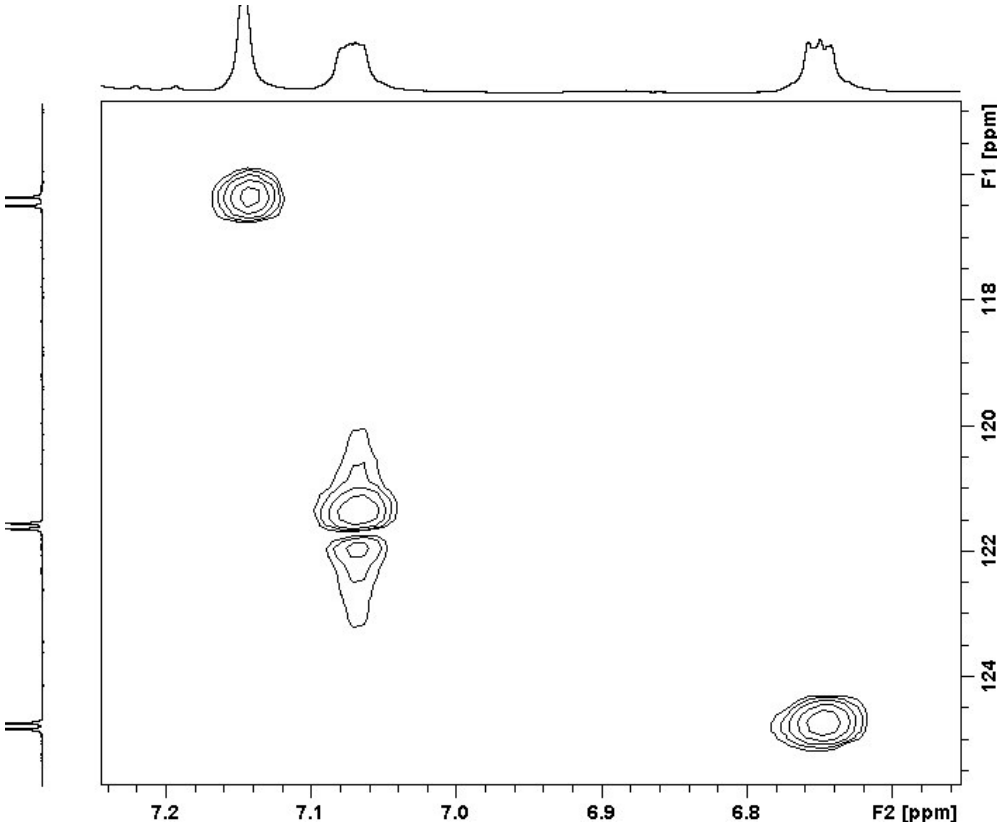

Figure 7-20. HSQC-spectra of the dihydroxy mono-alkyne tweezer **31**.

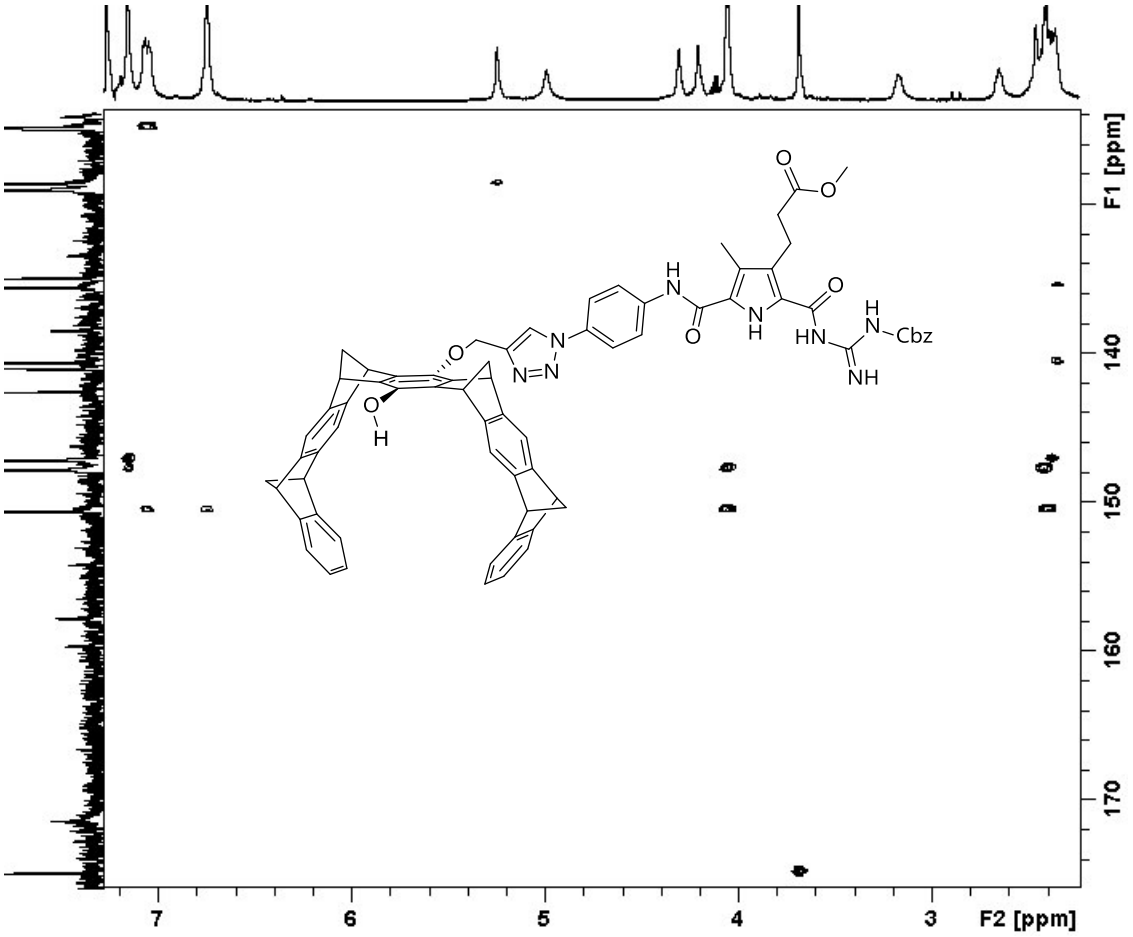

Figure 7-21. HMBC of the RGD-receptor precursor **44**.

7.4 Purity Control via HPLC

The purity of the obtained building blocks was checked with HPLC too. The purity checks were done under either normal phase or reversed phase conditions.

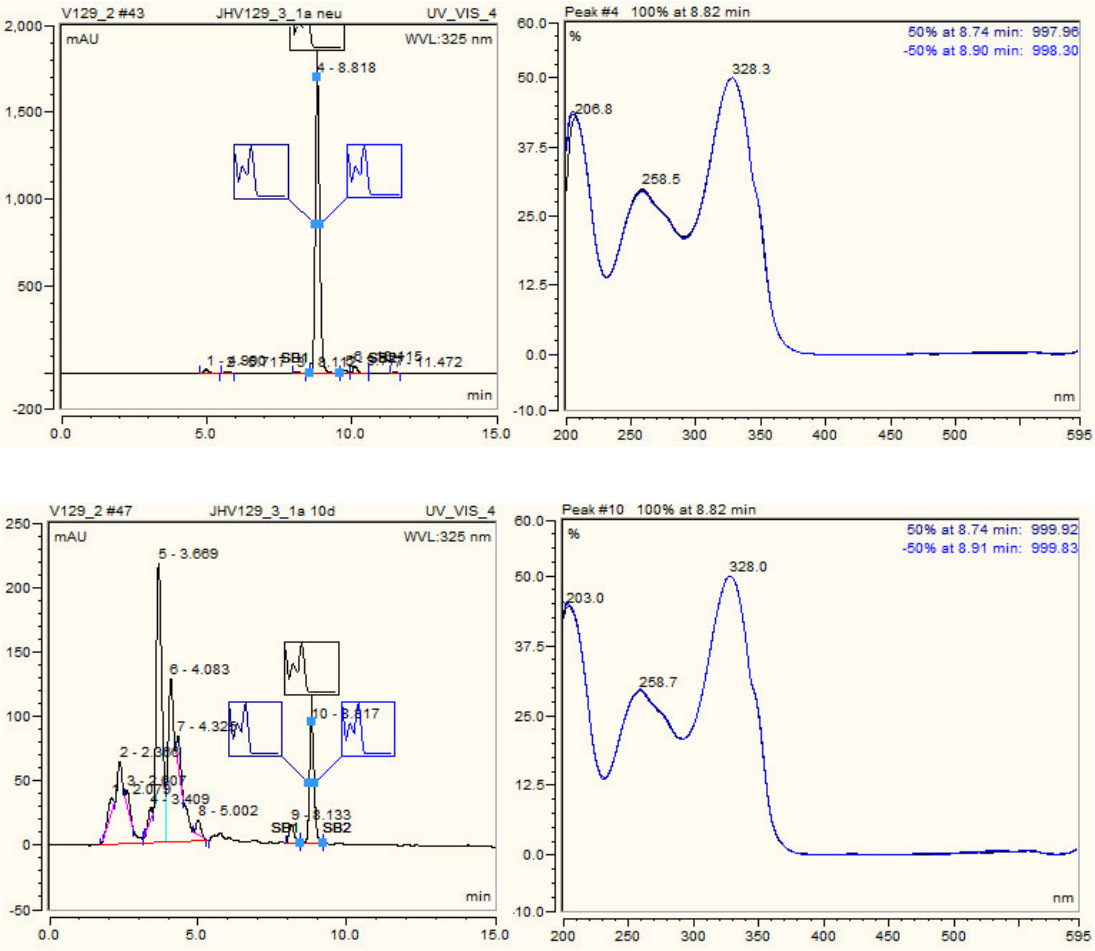

Figure 7-22. HPLC runs of the azido pyrrole **37** were carried out with analytical column (reversed phase) of *YMC*. Chromatograms at the top and bottom show freshly prepared and aged (after 10 days) sample respectively. Gradient runs started from methanol/water 80/20 to 100/0 within 12.5 min. Freshly prepared sample revealed a purity of 93 % whereas aged one contained only 10 % of pyrrole **37**.

The purity check of the RGD-receptor precursor **44** (fig. 7-18) was carried out via HPLC under normal phase conditions. The detection occurred at 4 different wave lengths, 220 nm, 258 nm, 285 nm and 327 nm. At the absorption maximum of the tweezer at 285 nm a purity of 99 % could be found. At 220 nm some impurities were found with an overall purity of more than 92 %. In figure 7-20 the individual chromatograms are shown.

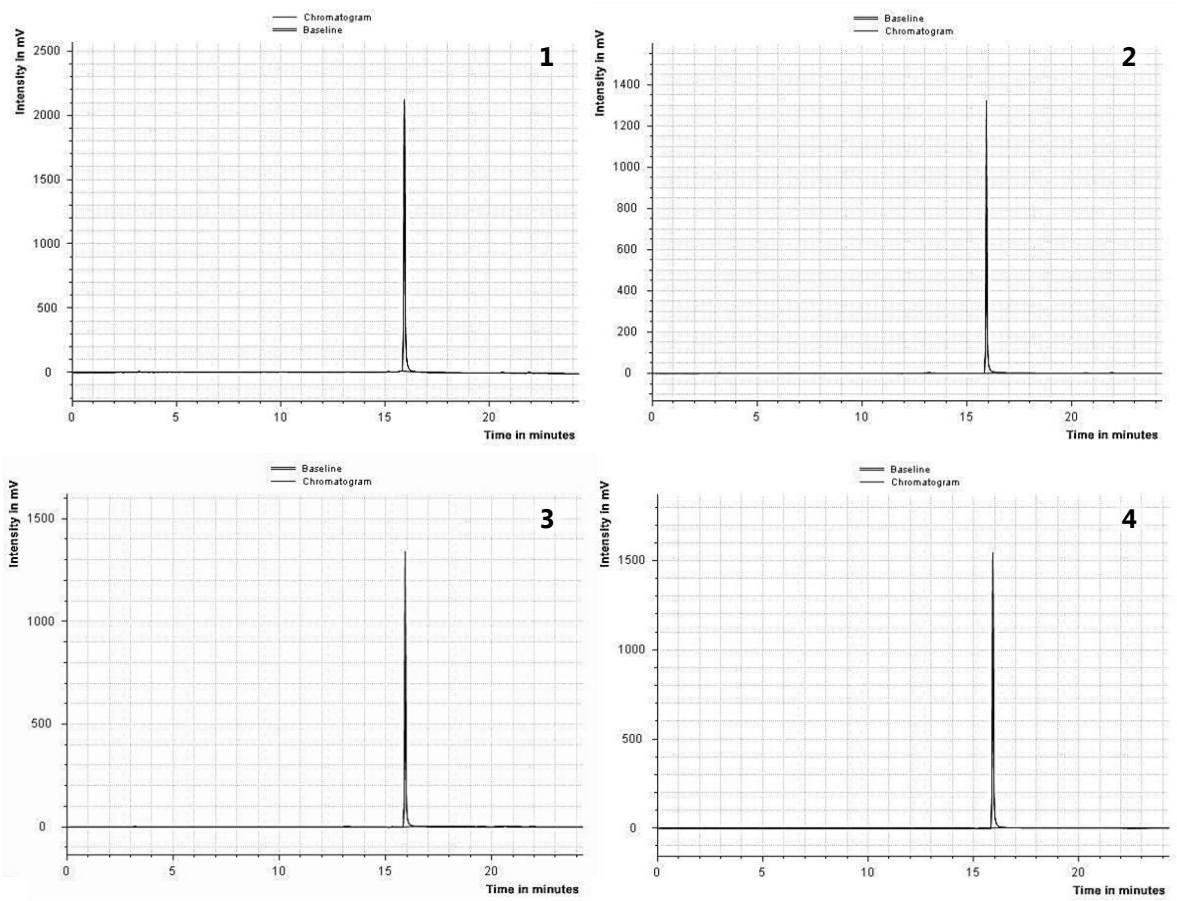

Figure 7-23. The HPLC runs under normal phase conditions revealed a purity of precursor **44** up to 99 % at 258 nm (**2**), 285 nm (**3**) and 327 nm (**4**). At 220 nm (**1**) a purity of around 94 % could be detected.

The mono alkyne tweezer diphosphate **50** (B) was purified with a multicomponent system consisting of the *Merck* Septech pump. In figure 7-24 the preparative run (left side) and the purity check (right side) done with the Dionex system are shown.

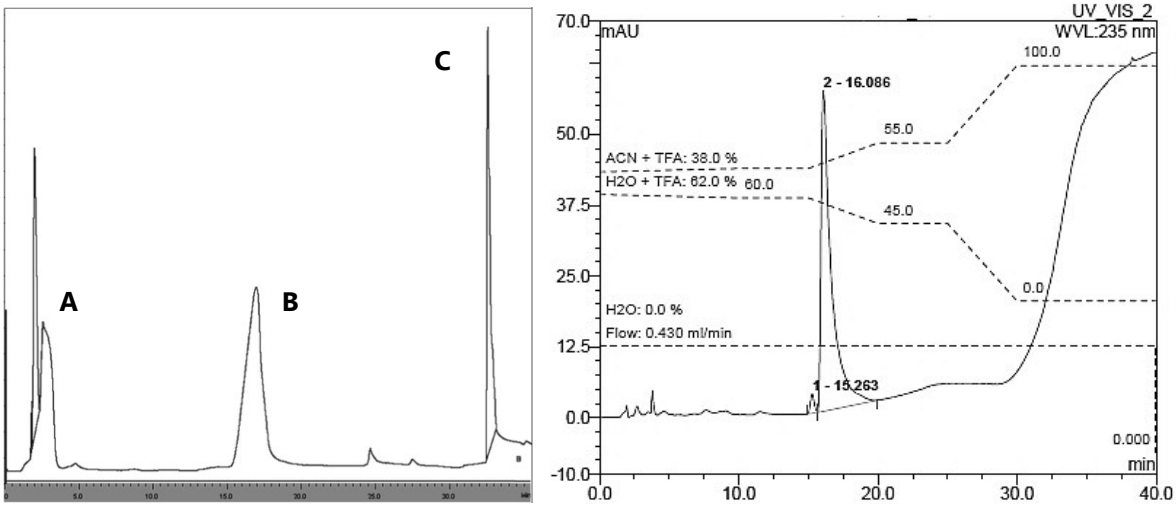

Figure 7-24. The preparative HPLC run (left) reveals a ratio of 3:5:2 of starting material (A), mono alkyne tweezer **50** (B) and bis alkyne tweezer **52** (C). The HPLC purity control (right side) of the mono alkyne tweezer **50** revealed a purity of more than 94 % at 235 nm.

The purity of the RGD-peptides was monitored with analytical HPLC under reversed phase conditions. The obtained purities at a wavelength of 220 nm were 94 % of **P1**, 90 % of **P2** and around 80 % of **P3**. Exemplarily 3 chromatograms of the peptides are shown in figure 7.. The initial peak in the beginning of chromatogram **1** is due to injection of the sample. The second peak at 11.393 minutes could not be identified further. The indicated shoulder of the main peak at 8.792 minutes is assumed to have its origin from an overloading of the column.

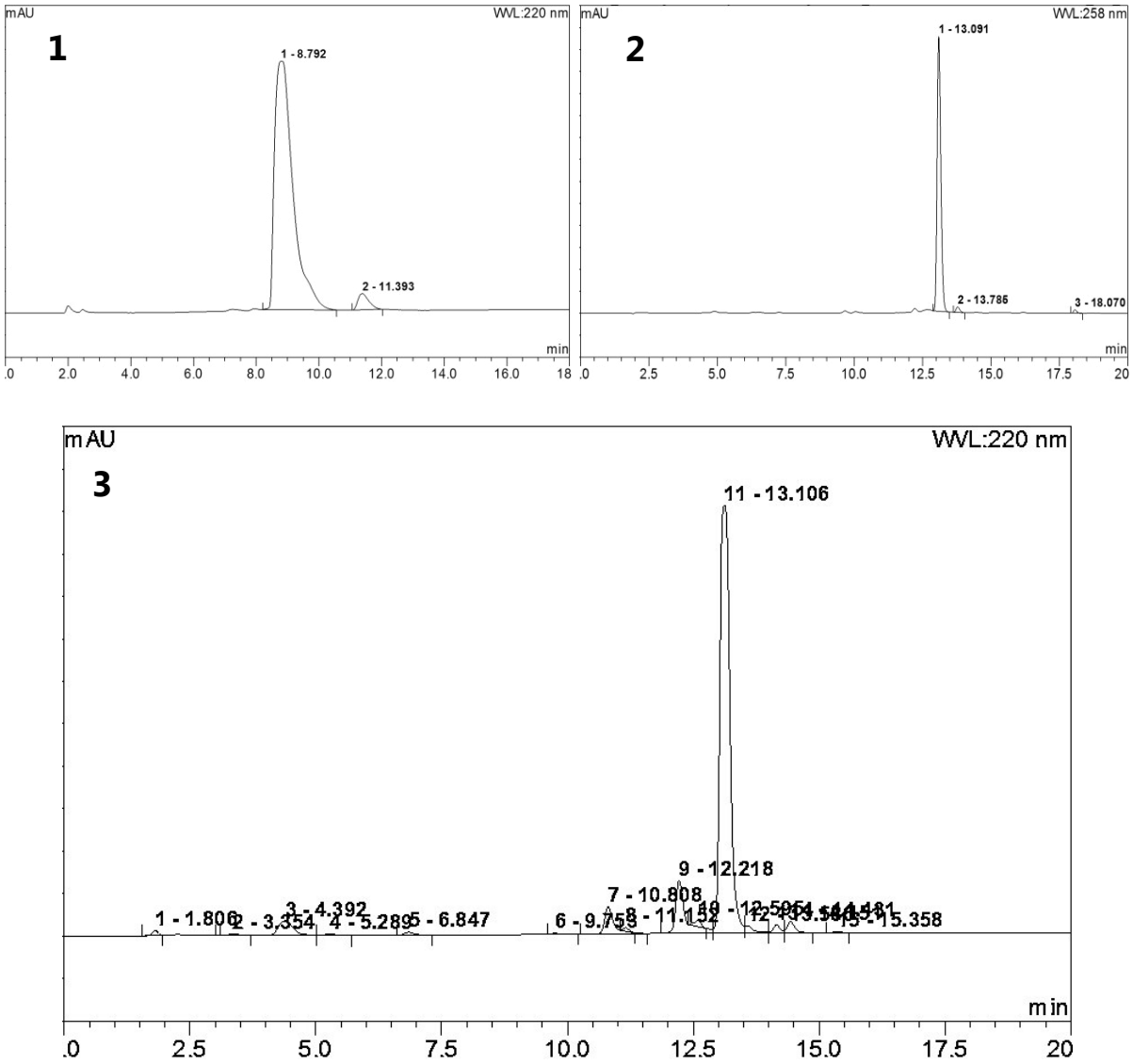

Figure 7-25. The HPLC-Chromatograms of the synthesized RGD-peptides revealed different purities. The linear RGD-peptide **P1** revealed a purity of 94 % (**1**). Particularly the purity of the cyclic peptides showed some differences at 220 nm compared to 258 nm. Peptide **P2** showed a purity of more than 96 % at 258 nm (**2**) but revealed only 90 % at 220 nm. Similarly **P3** revealed a purity of 90 % at 258 nm but only 81 % at 220 nm.

7.5 Table of Abbreviations

α	alpha
AA	amino acid
abs.	absoluted
Ac	acetyl
AFM	atomic force microscopy
AMIDAS	adjacent to MIDAS
approx.	approximately
Ar	aryl
Arg	arginine
arom.	aromatic
Asp	aspartic acid
β	beta
bFGF	basic fibroblast growth factor
br	broad
bs	broad singlet
CAM	cell adhesion molecule
$C_2O_2Cl_2$	oxalyle chloride
ca.	circa
calc.	calculated
cat.	catalytical
Cbz	benzyloxycarbonyl
Cbz-OSu	*N*α-(benzyloxycarbonyl-oxy) succinimide
$CDCl_3$	deuterated chloroform
CF	cyanuric fluoride
conc.	concentrated
Cl-HOBt	6-chloro-1-hydroxy-benzotriazole dihydrate
d	day/days
	duplet
	(ref. to NMR)
DCM	dichloromethane
dd	duplet of duplet
DDQ	2,3-dichloro-5,6-dicyano-benzoquinone
δ	delta
°C	degree Celsius
DIC	N,N′-diisopropylcarbo-diimide
DIPEA	*N,N*-diisopropylethyl-amine
DMAP	*N,N*-dimethylpyridin-4-amine
DMF	dimethyl formamide
DMSO	dimethyl sulfoxide
DMSO-d6	fully deuterated DMSO
ECM	extracellular matrix
e.g.	exempli gratia
EM	electron microscopy
ESI	electrospray ionization
eq	equivalents
f	D-phenylalanine
F	phenylalanine (L-conformation)
Fmoc	9*H*-fluoren-9-yl-methoxycarbonyl
Fmoc-Cl	9*H*-fluoren-9-yl-methoxy-carbonyl chloride
FT	fourier transformation
g	gram
Gly	glycine
gua	guanine
h	hour
HATU	(2-(7-Aza-1*H*-benzo-triazole-1-yl)-1,1,3,3-tetramethyluronium hexafluorophosphate)

HCTU	(2-(6-Chloro-1*H*-benzotriazole-1-yl)-1,1,3,3-tetramethyl-aminium hexafluoro-phosphate)
HPLC	High performance liquid chromatography
HRMS	high resolution mass spectroscopy
HSQC	Heteronuclear Single Quantum Coherence
Hz	hertz
i	iso
Im	imidazole
IR	infra-red
J	coupling constant
K_a	binding constant
l	liter
Leu	leucine
m	medium (ref. to IR)
	multiplet (ref. to NMR)
M	mega
m/z	mass per charge
M^{-1}	1 per mol
MAG	myelin-associated glycoproteins
max	maximum
mbar	millibar
MBHA	4-methylbenzhydrylamine
mg	milligram
MHz	megahertz
MIDAS	metal ion-dependent adhesion site
min	minute
ml	milliliter
mm	millimeter
mmol	millimol
MPLC	medium performance liquid chromatography
MS	mass spectroscopy
µg	microgram
µl	microliter
µm	micrometer
n	normal
N	normality
$NaHCO_3$	sodium bicarbonate
NaOH	sodium hydroxide
N-CAM	neural adhesion molecules
$NEt(iPr)_2$	*N,N*-diisopropylethylamine
NEt_3	triethylamin
nm	nanometer
NMM	4-methylmorpholine
nmol	nanomol
NMR	nuclear magnetic resonance
O*t*Bu	*tert*-butyl ester
Pbf	2,2,4,6,7-pentamethyl-2,3-dihydrobenzofuran-5-ylsulfonyl
pH	negative decade logarithm of oxonium cations
Ph	phenyl
Phe	phenylalanine
ppm	parts per million
py	pyrrole
PyBOP	1-benzotriazolyloxytri-pyrrolidino-phosphonium hexafluorophosphate
pyr	pyridine
q	quaternary (context of labeling carbon atoms)
	quartet (ref. to NMR)
R_f	retention factor

RP-18	reversed phase octadecyl-SiO_2 (octadecyl silica gel)
rps	rounds per second
rt	room temperature
s	singlet (ref. to NMR)
	strong (ref. to IR)
SAXS	small angle X-ray scattering
SiO_2	silica gel
SO_2Cl_2	sulfuric dichloride
$SOCl_2$	thionyl chloride
T	temperature
t	triplet
t, tert	tertiary
TBDMS	*tert*-butyldimethylsilane
TBDMS-Cl	*tert*-butyldimethyl-chlorosilane
TBPP	Tetrabenzylpyrophos-phate
TEA	triethyl amine
TFA	trifluoro acetic acid
TFE	2,2,2-trifuoroethane
TFFH	tetramethylfluoro-form-amidinium hexafluoro-phosphate
TIS	triisopropylsilane
TLC	thin layer chromate-graphy
TNF-α	tumor necrosis factor α
T_3P	propylphosphonic an-hydride
UV	ultra violet
V	valine
VEGF-A	vascular endothelial growth factor
vs	very strong
$\tilde{\nu}$	wave number
W	watt
w	weak

8 BIBLIOGRAPHY

(1) Greene, H. S. N. *J. Exp. Med.* **1941**, *73* (4), 475–486.

(2) Glenn H. Algire, Harold W. Chalkley, Wilton R. Earle, Frances Y. Legallais, Helen D. Park, Emma Shelton, Edward L. Schilling. *JNCI J. Natl. Cancer Inst.* **1950**, *11* (3), 555–579.

(3) Folkman, J. *J. Exp. Med.* **1971**, *133* (2), 275–288.

(4) Plank, M. J.; Sleeman, B. D. *J. Theor. Med.* **2003**, *5* (3-4), 137–153.

(5) Rak, J.; Yu, J. L.; Klement, G.; Kerbel, R. S. *J. Investig. Dermatol. Symp. Proc.* **2000**, *5* (1), 24–33.

(6) Clemetson, K. J. *Cell. Mol. Life Sci. CMLS* **1998**, *54* (6), 499–501.

(7) Wang, F.; Li, Y.; Shen, Y.; Wang, A.; Wang, S.; Xie, T. *Int. J. Mol. Sci.* **2013**, *14* (7), 13447–13462.

(8) Pierschbacher, M. D.; Ruoslahti, E. *Nat. Lond. U. K.* **1984**, *309* (Copyright (C) 2015 American Chemical Society (ACS). All Rights Reserved.), 30–33.

(9) Folkman, J. *Ann. Surg.* **1972**, *175* (3), 409–416.

(10) *Tumor angiogenesis: basic mechanisms and cancer therapy*; Marmé, D., Fusenig, N. E., Eds.; Springer: New York, 2008.

(11) Springer International Publishing. *Drugs R. D.* **2002**, *3* (1), 28–30.

(12) Angiogenese-Hemmer AVASTIN(R) erhält EU-Zulassung - Neues Wirkprinzip gegen Darmkrebs http://www.presseportal.de/pm/7431/637275/angiogenese-hemmer-avastin-r-erh-lt-eu-zulassung-neues-wirkprinzip-gegen-darmkrebs (accessed Jan 23, 2015).

(13) Lehn, J. *Science* **1993**, *260* (5115), 1762–1763.

(14) Crespo, J.; Sun, H.; Welling, T. H.; Tian, Z.; Zou, W. *Curr. Opin. Immunol.* **2013**, *25* (2), 214–221.

(15) Delgoffe, G. M.; Powell, J. D. *Mol. Immunol.* **2015**.

(16) Hulpiau, P.; van Roy, F. *Int. J. Biochem. Cell Biol.* **2009**, *41* (2), 349–369.

(17) Williams, A. F. *Immunol. Today* **1987**, *8* (10), 298–303.

(18) Tamkun, J. W.; DeSimone, D. W.; Fonda, D.; Patel, R. S.; Buck, C.; Horwitz, A. F.; Hynes, R. O. *Cell* **1986**, *46* (2), 271–282.

(19) Sheldrake, H. M.; Patterson, L. H. *J. Med. Chem.* **2014**, *57* (15), 6301–6315.
(20) Hynes, R. O. *Cell* **2002**, *110* (6), 673–687.
(21) Dong, X.; Mi, L.-Z.; Zhu, J.; Wang, W.; Hu, P.; Luo, B.-H.; Springer, T. A. *Biochemistry (Mosc.)* **2012**, *51* (44), 8814–8828.
(22) Takada, Y.; Ye, X.; Simon, S. *Genome Biol.* **2007**, *8* (5), 215.
(23) Vorup-Jensen, T.; Waldron, T. T.; Astrof, N.; Shimaoka, M.; Springer, T. A. *Biochim. Biophys. Acta* **2007**, *1774* (9), 1148–1155.
(24) Sun, C.-C.; Qu, X.-J.; Gao, Z.-H. *Anticancer. Drugs* **2014**, *25* (10), 1107–1121.
(25) Xiong, J.-P. *Science* **2002**, *296* (5565), 151–155.
(26) Xiong, J.-P. *Science* **2002**, *296* (5565), 151–155.
(27) Research Collaboratory for Structural Bioinformatics (RCSB) Protein Data Bank (PDB). Crystal Structure of the Extracellular Segment of Integrin α(V)β(3) in Complex with an Arg-Gly-Asp Ligand http://www.rcsb.org/pdb/explore/explore.do?structureId=1L5G (accessed Feb 13, 2015).
(28) Zhang, K.; Chen, J. *Cell Adhes. Migr.* **2012**, *6* (1), 20–29.
(29) Tadokoro, S.; Shattil, S. J.; Eto, K.; Tai, V.; Liddington, R. C.; de Pereda, J. M.; Ginsberg, M. H.; Calderwood, D. A. *Science* **2003**, *302* (5642), 103–106.
(30) Ruoslahti, E.; Pierschbacher, M. D. *Cell* **1986**, *44* (4), 517–518.
(31) Scarborough, R. M.; Gretler, D. D. *J. Med. Chem.* **2000**, *43* (19), 3453–3473.
(32) Eliceiri, B. P.; Cheresh, D. A. *J. Clin. Invest.* **1999**, *103* (9), 1227–1230.
(33) Shimaoka, M.; Springer, T. A. *Nat. Rev. Drug Discov.* **2003**, *2* (9), 703–716.
(34) Friedlander, M.; Brooks, P. C.; Shaffer, R. W.; Kincaid, C. M.; Varner, J. A.; Cheresh, D. A. *Science* **1995**, *270* (5241), 1500–1502.
(35) Weis, S. M.; Cheresh, D. A. *Cold Spring Harb. Perspect. Med.* **2011**, *1* (1), a006478–a006478.
(36) Haubner, R.; Gratias, R.; Diefenbach, B.; Goodman, S. L.; Jonczyk, A.; Kessler, H. *J. Am. Chem. Soc.* **1996**, *118* (32), 7461–7472.
(37) Tejpar, S.; Prenen, H.; Mazzone, M. *The Oncologist* **2012**, *17* (8), 1039–1050.
(38) Chau, C. H.; Figg, W. D. *Cancer Biol. Ther.* **2012**, *13* (8), 586–587.
(39) Dahmen, C.; Auernheimer, J.; Meyer, A.; Enderle, A.; Goodman, S. L.; Kessler, H. *Angew. Chem. Int. Ed.* **2004**, *43* (48), 6649–6652.
(40) Haubner, R.; Kessler, I. H. *Angew. Chem.* **1997**, *109* (13-14), 1440–1456.
(41) Zanardi, F.; Burreddu, P.; Rassu, G.; Auzzas, L.; Battistini, L.; Curti, C.; Sartori, A.; Nicastro, G.; Menchi, G.; Cini, N.; Bottonocetti, A.; Raspanti, S.; Casiraghi, G. *J. Med. Chem.* **2008**, *51* (6), 1771–1782.
(42) Casiraghi, G.; Burreddu, P.; Manzoni, L. P.; Scolastico, C.; Zanardi, F.; Battistini, L.; Curti, C.; Rassu, G.; Auzzas, L. Integrin

Targeted Cyclopeptide Ligands, Their Preparation and Use.
(43) Rensing, S.; Schrader, T. *Org. Lett.* **2002**, *4* (13), 2161–2164.
(44) Schmuck, C.; Rupprecht, D.; Junkers, M.; Schrader, T. *Chem. - Eur. J.* **2007**, *13* (24), 6864–6873.
(45) Rupprecht, D. Synthese und Optimierung sequenzselektiver künstlicher Rezeptoren für biologisch relevante Oligopeptide, 2006.
(46) Fokkens, M.; Schrader, T.; Klärner, F.-G. *J. Am. Chem. Soc.* **2005**, *127* (41), 14415–14421.
(47) Gersthagen, T.; Hofmann, J.; Klärner, F.-G.; Schmuck, C.; Schrader, T. *Eur. J. Org. Chem.* **2013**, *2013* (6), 1080–1092.
(48) Maehle, A.-H.; Prüll, C.-R.; Halliwell, R. F. *Nat. Rev. Drug Discov.* **2002**, *1* (8), 637–641.
(49) "Jean-Marie Lehn - Nobel Lecture: Supramolecular Chemistry - Scope and Perspectives: Molecules - Supermolecules - Molecular Devices". Nobelprize.org. Nobel Media AB 2014. Web. 11 May 2015. <http://www.nobelprize.org/nobel_prizes/chemistry/laureates/1987/lehn-lecture.html>.
(50) Ma, X.; Zhao, Y. *Chem. Rev.* **2014**, 150317111641003.
(51) *Molecular recognition: receptors for molecular guests*, 1. ed.; Vögtle, F., Lehn, J.-M., Atwood, J. L., Eds.; Comprehensive supramolecular chemistry; Pergamon: Oxford, 1996.
(52) Yu, G.; Jie, K.; Huang, F. *Chem. Rev.* **2015**, *115* (15), 7240–7303.
(53) Lehn, J.-M. *Angew. Chem. Int. Ed. Engl.* **1988**, *27* (1), 89–112.
(54) Schmuck, C. *Eur. J. Org. Chem.* **1999**, *1999* (9), 2397–2403.
(55) Biedermann, F.; Nau, W. M.; Schneider, H.-J. *Angew. Chem. Int. Ed.* **2014**, *53* (42), 11158–11171.
(56) Klemm, K. *Entwicklung neuer polykationischer Rezeptoren zur molekularen Erkennung von DNA und RNA*; Universität Duisburg-Essen, 2011.
(57) Klärner, F.-G.; Schrader, T. *Acc. Chem. Res.* **2013**, *46* (4), 967–978.
(58) Hirose, K. *J Incl. Phenom Macrocycl. Chem* **2001**, *39*, 193–209.
(59) Thordarson, P. *Chem Soc Rev* **2011**, *40* (3), 1305–1323.
(60) Geibel, B. *Biomimetische peptidische Rezeptoren zur Erkennung biologisch relevanter Moleküle -Design, Synthese und Potential-*; Universität Duisburg-Essen, 2013.
(61) Pollard, T. D. *Mol. Biol. Cell* **2010**, *21* (23), 4061–4067.
(62) Hill, Z. D.; MacCarthy, P. *J. Chem. Educ.* **1986**, *63* (2), 162.
(63) MacCarthy, P. *Anal. Chem.* **1978**, *50* (14), 2165–2165.
(64) Lallana, E.; Riguera, R.; Fernandez-Megia, E. *Angew. Chem. Int. Ed.* **2011**, *50* (38), 8794–8804.
(65) *Maestro Version 10.1.013 Release 2015-1*.
(66) Brückner, R. *Reaktionsmechanismen: organische Reaktionen, Stereochemie, moderne Synthesemethoden*, 2., aktualisierte und erw. Aufl.; Spektrum Lehrbuch; Spektrum Akad. Verl: Heidelberg, 2003.

(67) Harfmann, R. G.; Crouch, S. R. *Talanta* **1989**, *36* (1-2), 261–269.
(68) Sunde, C. J.; Erickson, J. G.; Raunio, E. K. *J. Org. Chem.* **1948**, *13* (5), 742–748.
(69) TOMOHIRO, S.; AKIRA, M.; SHOJI, K.; NAOHIRO, U. Preparation of 5,6-benzonorbornene-2,3-dicarboxylic acids. JP2008127311.
(70) Beck, K.; Brand, U.; Hünig, S.; Martin, H.-D.; Mayer, B.; Peters, K.; von Schnering, H. G. *Liebigs Ann.* **1996**, *1996* (11), 1881–1892.
(71) Atasoy, B.; Bayramoğlu, F.; Hökelek, T. *Tetrahedron* **1994**, *50* (19), 5753–5764.
(72) Gersthagen, T. Künstliche ditopische Rezeptormoleküle zur Erkennung von RGD-Schleifen, Duisburg-Essen, 2011.
(73) Klärner, F.-G.; Benkhoff, J.; Boese, R.; Burkert, U.; Kamieth, M.; Naatz, U. *Angew. Chem. Int. Ed. Engl.* **1996**, *35* (10), 1130–1133.
(74) Schmuck, C.; Rupprecht, D.; Urban, C.; Walden, N. *Synthesis* **2006**, *2006* (01), 89–96.
(75) Gawande, M. B.; Shelke, S. N.; Zboril, R.; Varma, R. S. *Acc. Chem. Res.* **2014**, *47* (4), 1338–1348.
(76) Greene, T. W.; Wuts, P. G. M. *Protective Groups in Organic Synthesis*; John Wiley & Sons, Inc.: New York, USA, 1999.
(77) Johnson, D. C.; Widlanski, T. S. *Org. Lett.* **2004**, *6* (25), 4643–4646.
(78) Ben-Ishai, D.; Berger, A. *J. Org. Chem.* **1952**, *17* (12), 1564–1570.
(79) Gröger, G.; Meyer-Zaika, W.; Böttcher, C.; Gröhn, F.; Ruthard, C.; Schmuck, C. *J. Am. Chem. Soc.* **2011**, *133* (23), 8961–8971.
(80) Coste, J.; Le-Nguyen, D.; Castro, B. *Tetrahedron Lett.* **1990**, *31* (2), 205–208.
(81) Al-Warhi, T. I.; Al-Hazimi, H. M. A.; El-Faham, A. *J. Saudi Chem. Soc.* **2012**, *16* (2), 97–116.
(82) Sambiagio, C.; Marsden, S. P.; Blacker, A. J.; McGowan, P. C. *Chem. Soc. Rev.* **2014**, *43* (10), 3525.
(83) Hajipour, A. R.; Mohammadsaleh, F. *Tetrahedron Lett.* **2014**, *55* (50), 6799–6802.
(84) Späth, A.; König, B. *Tetrahedron* **2010**, *66* (10), 1859–1873.
(85) Goriya, Y.; Ramana, C. V. *Tetrahedron* **2010**, *66* (38), 7642–7650.
(86) Peng, H.; Dornevil, K. H.; Draganov, A. B.; Chen, W.; Dai, C.; Nelson, W. H.; Liu, A.; Wang, B. *Tetrahedron* **2013**, *69* (25), 5079–5085.
(87) Gingter, S.; Mondrzik, B.; Ritter, H. *Macromolecules* **2012**, *45* (4), 1753–1757.
(88) Talbiersky, P.; Bastkowski, F.; Klärner, F.-G.; Schrader, T. *J. Am. Chem. Soc.* **2008**, *130* (30), 9824–9828.
(89) Bier, D.; Rose, R.; Bravo-Rodriguez, K.; Bartel, M.; Ramirez-Anguita, J. M.; Dutt, S.; Wilch, C.; Klärner, F.-G.; Sanchez-Garcia, E.; Schrader, T.; Ottmann, C. *Nat. Chem.* **2013**, *5* (3), 234–239.
(90) Xu, Z. *Bioorg. Med. Chem. Lett.* **2015**, *25* (18), 3777–3783.
(91) Shih, H.-W.; Chen, K.-T.; Cheng, W.-C. *Tetrahedron Lett.* **2012**, *53* (2), 243–246.
(92) Klärner, F.-G.; Kahlert, B.; Nellesen, A.; Zienau, J.; Ochsenfeld, C.;

Schrader, T. *J. Am. Chem. Soc.* **2006**, *128* (14), 4831–4841.
(93) Bertini, I.; Pierattelli, R. *Pure Appl. Chem.* **2004**, *76* (2).
(94) Bertini, I.; Turano, P.; Vila, A. J. *Chem. Rev.* **1993**, *93* (8), 2833–2932.
(95) Wienand, W. Ein künstlicher Rezeptor für das Dipeptid D-Alanin-D-Alanin : Konzeption, Synthese und physikalisch-organische Charakterisierung, Köln, 2002.
(96) Kaiser, E.; Colescott, R. L.; Bossinger, C. D.; Cook, P. I. *Anal. Biochem.* **1970**, *34* (2), 595–598.
(97) Dai, X.; Su, Z.; Liu, J. O. *Tetrahedron Lett.* **2000**, *41* (33), 6295–6298.
(98) Bickert, V. *Neue künstliche Guanidiniocarbonylpyrrol-Rezeptoren zur Komplexierung von Oxo-Anionen in Wasser*, 2008.
(99) Vosburgh, W. C.; Cooper, G. R. *J. Am. Chem. Soc.* **1941**, *63* (2), 437–442.
(100) Giessibl, F. J. *Rev. Mod. Phys.* **2003**, *75* (3), 949–983.
(101) Richter, C. Etablierung der Rasterkraftmikroskopie an kardiovaskulär relevanten Zellen, Proteinen und Materialien -Ein methodischer Ansatz-, Charité: Berlin, 2003.
(102) Guzman, H. V.; Garcia, P. D.; Garcia, R. *Beilstein J. Nanotechnol.* **2015**, *6*, 369–379.
(103) Bielefeldt, H.; Giessibl, F. J. *Surf. Sci.* **1999**, *440* (3), L863–L867.
(104) Tamayo, J.; García, R. *Langmuir* **1996**, *12* (18), 4430–4435.
(105) Smith, D. P. E. *Rev. Sci. Instrum.* **1995**, *66* (5), 3191.
(106) Malvern Instruments Ltd. *User Manual Zetasizer Nano Series User Manual*; 2004.
(107) Upstone, S. L. In *Encyclopedia of Analytical Chemistry*; Meyers, R. A., Ed.; John Wiley & Sons, Ltd: Chichester, UK, 2013.
(108) *Organikum: organisch-chemisches Grundpraktikum ; mit 220 Tabellen*, 20., bearb. und erw. Aufl., korrigierter Nachdr.; Becker, H. G. O., Ed.; Wiley-VCH: Weinheim, 1999.
(109) López, A. M.; Scarel, F.; Carrero, N. R.; Vázquez, E.; Mateo-Alonso, A.; Ros, T. D.; Prato, M. *Org. Lett.* **2012**, *14* (17), 4450–4453.

"Der Lebenslauf ist in der Online-Version aus Gründen des Datenschutzes nicht enthalten."